The Nature of Pan Sediments: A case study on dust supply from the Makgadikgadi Pans, Botswana

Thesis Presented By:

Kathryn J. Vickery

Department of Environmental and Geographical Science

University of Cape Town

Cape Town, South Africa

THESIS PRESENTED FOR THE DEGREE OF

Doctor of Philosophy

February 2014

Abstract

Understanding dust sources is essential, as aerosols from arid basins have widespread effects on atmospheric, biological and terrestrial processes on regional to global scales. This thesis presents the results of chemical and morphological analysis for sediments from Sua Pan, Botswana, which forms part of the Makgadikgadi Basin, southern Africa's most productive dust source. The analysis was performed in order to evaluate pan sediment characteristics and erosivity controls including the analysis of weather and climatological conditions. We analysed 41 grab samples consisting of crusts, fluff, and soil from 12 locations within a 144 km^2 grid (centred on 25.959°E and -20.5754°S) as well as 6 airborne samples collected using frisbees, BSNE traps and PI-SWERL exhaust, between July and October 2011.

Dry sieving and laser diffraction for all 41 samples revealed a dominance of uni-modal, sand sized sediments, with the particle size distribution controlled by evaporite minerals, inferred from sample digestion. XRD and ICP analysis on 8 and 22 samples respectively, identified evaporite minerals including halite, thenardite, mirabilite and trona, in addition to carbonate minerals, which represent the young transient mineralogy of the pan. Older metal oxides were also present, originating from parent substrates. The addition of QEMSCAN analyses performed on 5 airborne and 1 surface sample, identified feldspar and pyroxene, along with quartz in its amorphous state, which was further confirmed through SEM analysis. QEMSCAN evaluated 255 minerals, many of which were below the detection limits of the 20 minerals identified through XRD analysis. QEMSCAN further attributed mineralogy and morphological detail to 27 000 individual grains per sample, positively linking airborne samples with their surface source.

Seven years of twice daily MODIS images were analysed to identify the emission signature of the Makgadikgadi complex, revealing a number of synoptic states associated with emissions, peaking in July and driven largely by ridging anticyclones. The emission signature of the pans revealed that they respond to diurnal, seasonal and inter-annual controls, moisture dynamics and crust conditions with anthropogenic stresses also being evident.

This study has interpreted the driving mechanisms and limitations associated with both the micro and macro scale of dust entrainment, advancing the current understanding of the Makgadikgadi as a dust source through interpreting these controls at the local scale.

Acknowledgements

Many friends and colleagues have provided me with support, wisdom, guidance and friendship during the time this project has gone from a dream to a dissertation. To all those in all the countries I am lucky enough to call home, I acknowledge their patience, words of wisdom and continual support, over many cups of tea, coffee, sneaky drinks down at the pub, and hours of combined laughter and friendship provided during the years, the ominous task of thesis writing has been made bearable. I have been taught how to think, beg, borrow and, more importantly ask the right questions. I have travelled many kilometres in pursuit of the elusive dust storm and learnt so much on the way. Throughout this, several individuals have kindly and patiently supported me and for their contributions, deserve special mention.

Firstly, Frank Eckardt, who has been an incredible source of inspiration to me throughout my graduate career, giving me the freedom to run with my ideas and helping find my place in academia. His patience and shared passion for this project has been invaluable.

I would like to acknowledge the full DO4 team, Richard Washington, Dave Thomas, Giles Wiggs, Rob Bryant, James King and Jo Nield for the opportunity to be part of the DO4 project, and for invaluable communications during the field seasons. It was a wonderful experience to work on the pans, and after a long day out in the sun I thank you all for still answering my many questions and for conversations over a couple of beers or gin and tonics. Here I also acknowledge all those who provided data, accommodation, and helped pick up the pieces when things (trailers) fell apart - and make special mention of the trusty Dustin.

I would also like to thank the wonderful staff in the Departments of Chemical Engineering and Geology at UCT. To Megan, Stephanie, Kerryn, Kirsten, Suzana, Helen, Lorraine and Lloyd – thank you for showing me the ropes and trusting me with all the shiny and expensive equipment. Kerryn and Lorraine, special thanks go to both of you, for helping develop the QEMSCAN method and for the many discussions. An additional thanks to Kerryn for sharing your insights into the world of the QEMSCAN software and geochemistry.

To Mike Meadows, thank you for the advice and support during my academic career at UCT and I thank you too for the opportunity to teach and follow my passion. To Bruce Hewitson, thank you for the financial support and to Sharon Barnard for ‘finding the money’ which made it possible for me to pursue this crazy dream. To Pippin Anderson – the best post graduate co-ordinator and support system a post-grad student could ask for – thanks for checking up on progress, listening and providing just the right amount of pressure.

I thank my family – and new family who I gained during this journey – to all of you, thank you. To my Mom, Dad and sister thanks for your support and constant belief in me, for sharing in my achievements and putting the challenges and setbacks into perspective. To my Gran whose passion for geography was contagious I dedicate this to your memory; to you and Grandma, your love and interest in Africa has been my inspiration. To my husband, Vaudin, we took on this crazy journey together (while spending many months apart) – thank you for your love and support.

Last but most certainly not least, I would like to thank Sigrid Kenmuir for bravely editing this thesis. You correctly identified why I chose Science and not English, and helped me make friends with punctuation and grammar.

To anyone I may have inadvertently omitted, thank you! I am forever indebted to everyone involved from near and far, in the excitement, frustration, and so very many rich rewards this project has afforded me, where words are inadequate, you have my heartfelt thanks.

Table of Contents

List of Figures

List of Tables

Extended Abstract

Mineral dusts, or aerosols, impact the Earth's radiation budget through interaction with clouds, and by scattering and absorbing solar radiation. These interactions constitute substantial uncertainty in understanding past and predicting future climate changes. One of the causes of uncertainty is in the lack of understanding of particle size distribution and chemistry of the emitted dust aerosols and regional variations therein.

The aim of this study was to examine the pan surface sediments and dust emission controls on Sua Pan, Makgadikgadi. The aim was achieved through five key objectives; the first is to develop an efficient method of grain size determination of salt rich sediments. The second objective was to determine the chemical nature of pan sediments considering the role of chemistry in erodibility and physical surface conditions. The third objective was to evaluate QEMSCAN as a tool for the mineral and morphological classification of dust in aerosol studies. The fourth objective was to chatacterise the seasonal, annual and inter-annual emission signature of the Makgadikgadi pans, within the context of synoptic drivers of the system. The fifth and final objective was to contextualise the emission signature of the Pan within the literature of global archetypal preferential dust sources, evaluating the proposed controls acting on an ephemeral pan.

While dry and exposed sediments have the potential to become dust, ephemeral pans have been identified as globally important dust sources, due to the physical expanse of sparsely vegetated surfaces comprised largely of unconsolidated sediments. These sources have been identified as a preferential dust source with the nature of the source being an important control on the emission characteristic and limitations on source.

The Makgadikgadi Pans in north eastern Botswana are a prime example of a dusty ephemeral pan, extending over 6 000 km^2 receiving between 400 and 500 mm of annual rainfall. Remote sensing has identified the pans as a persistent dust source in southern Africa; consequently the pans were chosen as a Dust Observation for Models (DO4) study site. The project identified a 144 km^2 site on Sua Pan within which extensive surface sampling occurred, set against the backdrop of atmospheric conditions during the 2011 and 2012 dry season (July-October).This study made use of 41 samples from four vertical profiles – crust, fluff, second crust and soil – representing 12 alpha-numerically referenced sites on the pan surface taken during the 2011 field season. These samples were analysed for particle size distribution using laser diffraction and dry sieving, revealing a uni-modal, sand dominated distribution.

Chemistry was analysed through ICP and XRD, and revealed a mix of evaporites and carbonates, including halite, thenardite, mirabilite, calcite and trona. These minerals were found to be highly

variable within the vertical profile, playing a role in surface crusting and the suppression and promotion of emission. The minerals were observed to be highly stratified in the vertical, creating discernible soil, crusts, and fluff horizons strongly linked to the chemistry and grain size distributions. Digestion of samples revealed a significantly finer distribution centred in the silts with mass loss during the removal of evaporites confirming the high concentration of salts in the crusts.

In addition to traditional mineralogical analysis, QEMSCAN was used to determine the mineralogy of 1 surface and 5 airborne samples. QEMSCAN is able to perform rapid mineralogical and morphological analysis on a small sample size, and therefore affords a significant advance to aeolian researchers. The additional data derived from QEMSCAN confirmed the XRD results, and extended the mineral list from 20 to a comprehensive 255, with the addition of mineralogical maps for 27 000 individual grains. Through QEMSCAN analysis, quartz was observed to contribute a large percentage of the bulk mineralogy of all samples, which was not observed through XRD analysis. Correlation of this finding with SEM revealed the ability of QEMSCAN to detect amorphous minerals which is not possible in XRD. Additionally, QEMSCAN morphological output revealed that grains had a tendency to be round to square shape rather than long or thin, which confirmed the applicability of laser diffraction for particle size analysis. Furthermore, the resolution of QEMSCAN data has attributed locally derived fluff as the likely source of aeolian samples captured in the BSNE traps, while the background signature of dust captured in the frisbee suggests the pans as the dominant source of regional aerosol load.

Analysis of emission frequency revealed a pan surface with considerable local and temporal variability, which could be linked to limitations defined in literature including supply, availability and transport. Additionally, the ephemeral nature of the pan revealed the complexity in associating a single limitation for the whole year; rather, the system transitioned between the various limitations. Consequently, the dust season was associated with the dry winter and spring months, peaking in July, when dry sediments are available and can be transported by numerous synoptic states. However, the pan centre was determined to be less emissive than the pan margins which introduced possible mechanisms for such a response, including saltation, human modification of surface conditions, changes in the local wind regime, and livestock.

Finally, linking the micro-scale mineralogy and morphology data determined in this study with the large scale macro controls of synoptic features, highlighted the intermediate scale as an important dimension required to characterise the complexities of the pan better. This link, developed through the fifth objective, draws the need to consider surface conditions with the synoptic scale drivers to better understand the system. This study has illuminated some of the dust emission mechanisms of ephemeral pan systems and placed the Sua Pan in global dust literature, confirming the applicability of preferential dust units as a classification scheme for dust sources.

Chapter 1: Introduction and Context

1.1 Current Research Question

Windblown dust from natural surfaces has been estimated to account for almost 85% of the global aerosol load (Harrison et al., 2001), of which between 50% and 70% is attributed to natural surfaces, with the remainder associated with disturbed surfaces (Tegen & Fung, 1995). Atmospheric mineral dust has become an important research field in earth systems science, because of the impact that aerosols have on radiation, clouds, atmospheric dynamics, chemistry, air quality and biogeochemical systems (Swap et al., 1992; Jickells et al., 2005; Knippertz & Todd, 2012). The inter-disciplinary nature of aerosol research spans the fields of geology, biology, chemistry and atmospheric science, even integrating the work of the extraterrestrial science community (Muhs, 2013). Despite the observed importance of dust in ecological and radiative cycles, relatively little is known about how the chemical composition of aerosols varies in space and time (Lawrence & Neff, 2009). Therefore, in order to better constrain our estimates and improve our understanding of the geochemical flux associated with both transport and deposition, understanding contemporary dust chemistry, morphology, mineralogy, grain size and particle size distributions; along with deposition rates is required.

Therefore, this study has set out to determine the chemical and morphological nature of sediments from the Makgadikgadi Pans, and to determine how the conditions observed on the surface serve to promote or inhibit emission. In general, literature presents two major aspects of aerosol research. Firstly data derived through remote sensing, and secondly ground based studies. Unifying these two themes is the need for ground based validation where the disparate scales between field analysis and the resolution of remote sensing products and climate models has been highlighted.

In light of these factors, the study aims to:

1.1.1 Aim

Examine pan surface sediments chemically and morphologically and establish synoptic dust emission controls at Sua Pan, Makgadikgadi.

1.1.2 Objectives

In order to achieve this, both methodological and process related objectives have been identified.

1. Develop a method for the efficient and effective analysis of grain size for salt rich sediments and present the results of surface and sub-surface sediments on the Makgadikgadi Pans.

2. Determine the elemental and chemical nature of surface and sub-surface sediments; and their role in surface erosivity.
3. Evalute QEMSCAN as a tool for the mineral and morphological classification of dust in aerosol studies, determining the chemical and morphological nature of surface and airborne samples from a single emission event.
4. Characterise the seasonal, annual and multi-annual emission signature of the Makgadikgadi Pans.
5. Contextualise the emission signature of the Pan within the literature of preferential dust sources and evaluate the proposed controls of emission acting on an ephemeral pan

1.1.3 Thesis Outline

To address these objectives, three key themes were considered, namely:

i. Determining grain size and particle size distributions of samples (Chapter 2)
ii. Evaluating the chemistry of samples using different methods (Chapters 3 and 4)
iii. Determining the availability, supply and transport capacity limitations acting on the pan (Chapters 5 and 6)

Chapter 1 provides an introduction to dust from both a historical and a contemporary perspective. This will be followed by a brief consideration of the dust cycle and dust transport, before addressing detection and presenting the current understanding of global and regional dust. Finally, the chapter will provide the a site decription and reveal the site setup.

This will be followed by Chapter 2, which will begin with a review of literature on grain size analysis and methods of grain size determination. Following the review, this chapter will present differing approaches to grain size analysis, evaluating the relevance of the various methods. The chapter will then present the results of the full suite of DO4 samples in order to reveal trends in grain size.

Chapters 3 and 4 will then consider the mineralogical nature of pan sediments; with Chapter 3 providing an elemental and mineralogical analysis of surface sediments from a number of locations within the DO4 grid. Chapter 3 also contains literature consideration on the importance of different minerals in surface conditions. Following this, Chapter 4 evaluates the methodological advancement provided through the use of QEMSCAN to determine the mineralogical and morphological nature of sediments from a single site within the DO4 grid. Chapter 4 begins with a literature review on the mineralogical and morphological properties of dust as well as a review on the principles of QEMSCAN detection. Additionally, this chapter will analyse both surface and airborne samples and consider similarities and difference.

Chapter 5 contains a comprehensive literature review on dust detection and the identification of pan surfaces in literature before considering the atmospheric circulation over southern Africa. The chapter then revises the current understanding of synoptic drivers responsible for emission, by considering both the temporal and spatial emission signature for the region for an eight year period from 2006 to 2012.

This leads into Chapter 6, which evaluates the conceptual model of the Makgadikgadi Pans as a dust producing system, developing our understanding of the Pans as a dust source within the context of preferential dust sources and limitations to emission.

The seventh and final chapter will summarise the key findings of this study, and evaluate the extent to which the aims and objectives have been achieved. It will further present the limitations inherent in this research and the implications for future research in this field.

1.2 Dust

1.2.1 History of Dust Research

The presence of dust in the atmosphere has been well documented for centuries, from early references in The Iliad attributed to Homer written in the 8th Century BC, to descriptions of dust events by English naturalist Charles Darwin in the 19th Century. Accounts range in their understanding of the phenomenon with Homer's Iliad mentioning "rain of blood events" which subsequent scholars have interpreted to be referencing red, clay laden rain drops. Similar records exist in early Chinese, Korean and Japanese literature (Engelbrecht & Derbyshire, 2010); while in Australia and New Zealand reports of "red rain" are observed in literature by Kidson and Gregory (1930). In Europe dust fallout associated with rain and snow are documented by Seignolis and Arago (1846 as cited in Pye, 1987:5).

However, possibly one of the earliest scientific records of dust was made in 1832 by Charles Darwin, who compiled observations of dust deposition on ships, during the voyage of the H.M.S Beagle (1831-1836). While sailing off the coast of the Africa, near the Cape Verde Islands, Darwin noted that,

> *...the atmosphere is hazy; and this is caused by the impalpably fine dust, which was found to have slightly injured the astronomical instruments. ... I have found no less than fifteen different accounts of dust having fallen on vessels when far out in the Atlantic. From the direction of the wind whenever it has fallen, and from its having fallen always during those months when the Harmattan is known to raise the clouds of dust high into the atmosphere, we may feel sure that it comes from Africa… The dust falls in such quantities as to dirty everything on board, and to hurt people's eyes; vessels even have run on shore owing to the obscurity of the atmosphere. It has often fallen on ships … more than a thousand miles from the coast of Africa, and at points sixteen hundred miles distance in a north and south direction. In some dust which was collected on a vessel three hundred miles from the lands, I was much surprised to find particles of stone above the thousandth of an inch square, mixed with finer matter.*
>
> (Darwin, 1889: 26)

Throughout history, dust and dust movements have been attributed to part of the earth's continual making and unmaking. Desert storms have been recorded to have "filled the skies for thousands of miles and change seasons, vegetation and landscapes" (Amato, 2000: 5). However, nowhere in history is the mention of dust more prolific than in the north-west American Dust Bowl during the 1930s (Worster, 1982; Svobida, 1986). From 1932 to 1938 large expanses of the 150 000 square mile Dust Bowl recorded dust-darkened skies turning days into night and causing respiratory disease

(Amato, 2000). During the drought in the 1930's, millions of acres of ploughed farmlands were exposed to strong winds, creating huge dust storms (Engelbrecht & Derbyshire, 2010); exacerbated by poor agricultural practices and unregulated grazing in an unsustainable area (Amato, 2000).

Despite the long history of reporting dramatic dust transport and depositional events such as those by Darwin and further described by Pye (1987), these were largely descriptive and founded on poor understanding of process and source (Goudie & Middleton, 2006). During the past few decades, aeolian dust has become a major environmental topic and as a result research on aeolian sources and transport has demanded a more structured, systematic and quantitative approach . In recent reviews Harrison et al. (2001), Tegen (2003), Goudie and Middleton (2006), Kohfeld and Tegen (2007), Maher et al. (2010) and Shao et al. (2011) summarise a number of effects of mineral dust on Earth-atmosphere systems. These authors reveal that because dust can have high concentrations in the atmosphere, it can change the overall planetary radiation balance through direct effects on radiation at both solar (shortwave) and terrestrial (longwave) portions of the electromagnetic spectrum (Tegen, 2003). This has lead to the recognition of the dust cycle in global transport mechanics, with the effects of dust being experienced in remote areas, often far from the source regions (e.g. McTainsh & Strong, 2007; Lawrence & Neff, 2009; Shao et al., 2011).

Consequently, there have been numerous methods employed for the study of aerosols from long term stratigraphic records, using ocean and ice cores to archival studies using reports and accounts from varying media (Goudie & Middleton, 2006).

1.2.2 Types of Dust

The dust discussed above is but one of a number of aerosols which are found in the atmosphere. Kommalapati and Valsaraj (2009) present that in addition to the dust mentioned above; water vapour (which has a relatively large size), trace gases, a great variety of liquid and solid aerosols from natural and anthropogenic sources are all found in the atmosphere. Collectively, these are called aerosols, and include, but are not limited to, dust generated by wind erosion from surface soils; agricultural activities; sea salt and wave breaking; volcanoes; forest fires; gas to particulate conversion; and industrial emission (*Figure 1.1*).

Middleton (1997) and Tyson and Preston-Whyte (2000) indicate that the classification of aerosols can be done through a variety of means, including analysis of the grain size, mineralogy and chemical composition. This provides the following broad classification categories: anthropogenically sourced – e.g. urban pollutants and smoke from biomass burning; and naturally sourced – e.g. cosmic dust, volcanic dust, sea salt and soil derived dust (*Figure 1.1*). Modern studies have estimated that

anthropogenic dust sources account for approximately 25% of the global load, with 75% derived from natural dust sources (Hsu et al., 2004; Hsu et al., 2006).

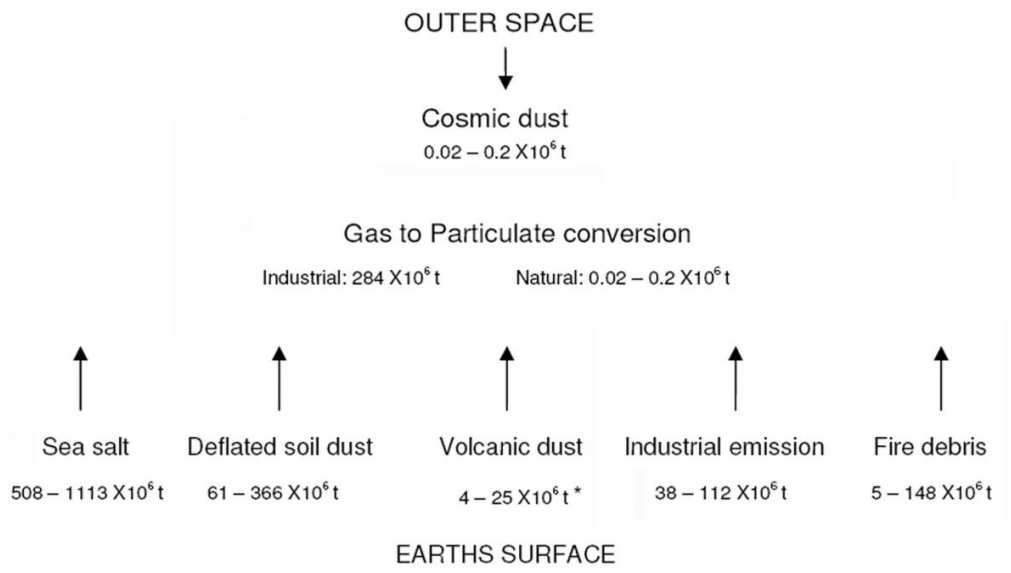

Figure 1.1 Global sources of airborne particles and approximate annual input into the atmosphere - adapted from Pye (1987) (possibly underestimated as not accounting for short range and low level dust).*

1.2.2.1 Aeolian Dust

The above section has considered the full suite of aerosols in the atmosphere as they are not commonly fully differentiated. However this study is largely concerned with the nature of soil derived or mineral aerosols, which were defined by Lawrence and Neff (2009) as: "[aeolian dust is] mineral particulate matter originating from the wind erosion of soils" (Lawrence & Neff, 2009: 46). Additionally Pye (1987) elaborate that while dust is frequently referred to as a mineral aerosol, the term aerosol strictly covers both the particle (dust) and the medium in which it is suspended (atmosphere) (Prospero et al., 1983). For ease of understanding, and in order to conform to a large body of existing literature, the use of the term aerosol will be used simply henceforward in reference to the particulate matter itself. Further, in this study the terms aerosol, dust, mineral aerosol, and aeolian dust will all be used with reference to the particulate matter in various stages of transport.

While the above definitions of dust are largely taken from the 20th century, the study of aeolian sediments in general, and their textural characteristics in particular, began in 1889 when Udden studied grain size of aeolian deposits (Folk, 1966). While many early studies remained focused on dunes, since then the study of aeolian sediments and their processes has shifted to include dry and arid landscapes and landforms globally (e.g. Bagnold, 1941; Folk & Ward, 1957; Prospero et al., 2002; Washington et al., 2003; Bullard et al., 2011; Ginoux et al., 2012).

In addition, aerosols are often rich in nutrients and thus the deposition of such aerosols has the potential to alter the nutrient dynamics at the deposition sites – including oceanic and terrestrial ecosystems (Alpert et al., 1998). Harrison et al. (2001) comment on the highly variable nature of dust in the atmosphere, indicating that changes in climate and extent in the source region, together with anthropogenic and vegetation changes, can all affect the nature of the system. Tegen et al. (1997) indicate that mineral aerosols may be one of the most important aerosols by mass and optical depth in the atmosphere.

As the impact of dust is largely a function of morphology and mineralogy, numerous authors have described the physical properties of dust. An early definition by Bagnold (1941) suggested the cut off to be at 62.5 µm or in relation to the sand silt boundary, while Pye (1987) described atmospheric dust as mostly smaller than 100 µm. In addition, for the particle to be subject to long range atmospheric transport, grain sizes tend to be in the order of 10 µm to 50 µm as larger grains settle during decreased turbulence. Middleton (1997) provided an additional cut off at 80 µm with Prospero (1999) confirming earlier findings commenting that the majority of dust transported over large distances has a median mass diameter of less than 10 µm. Further elaborating that smaller grain size (2 to 5 µm) results in longer residence time in the atmosphere as well as potential for greater transportation – over hundreds of kilometres.

1.2.3 The Dust Cycle

There are a number of recent comprehensive reviews on the dust cycle (e.g. Maher et al., 2010; Ravi et al., 2011; Shao et al., 2011; Shi et al., 2012), which highlight both its importance and its complexity. A review by Shao et al. (2011) defines the dust cycle as the consideration of emission, transport, transformation, deposition and stabilisation. This indicates that, like many Earth systems, the dust cycle involves a number of processes occurring between a range of spatial scales from seconds to millions of years; while temporal scales vary between seconds (emission) to millions of years (formation of the dust source, including weathering, sediment formation) (*Figure 1.2*).

As dust particles are in the size range of a few micrometers and smaller (*Figure 1.2*), once in suspension they can remain in the atmosphere without being affected by gravitational settling and thus can exist in suspension for time periods of up to several weeks (Prospero, 1999). Particles in suspension are therefore subject to distribution by climatic parameters like wind fields and precipitation. Hence they are able to travel thousands of kilometres, with the result that regionalised dust emissions can have a global impact (Middleton & Goudie, 2001).

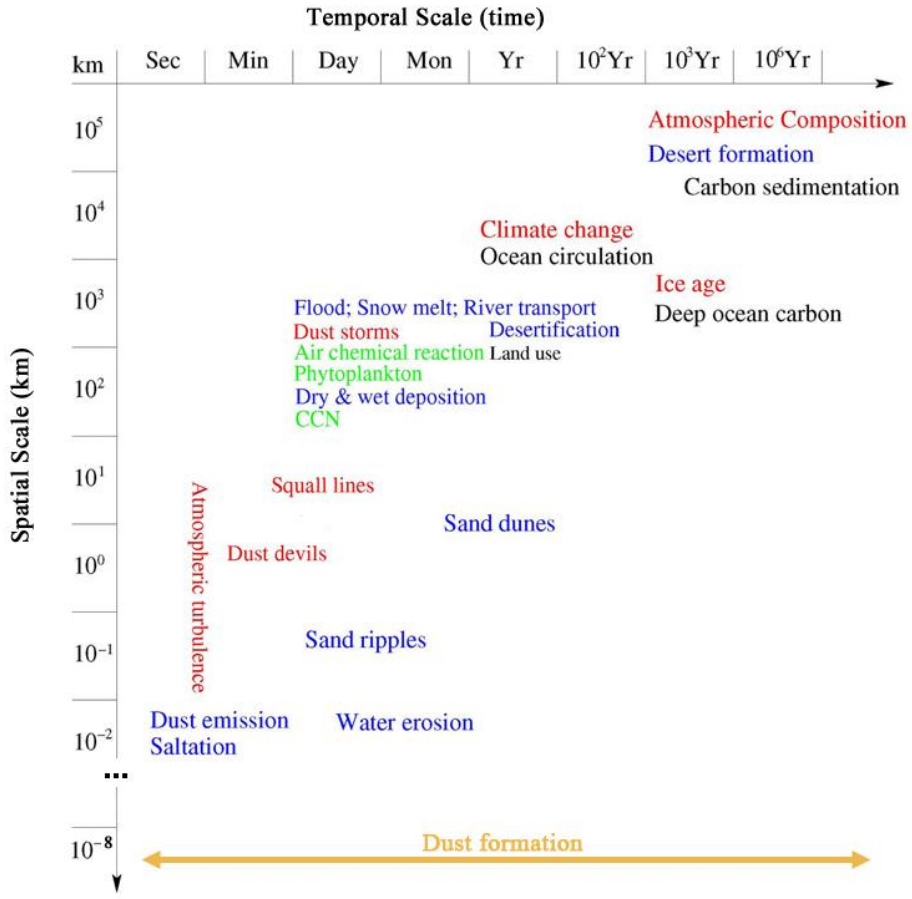

Figure 1.2 Approximate spatial and temporal scales of the processes involved in the dust cycle. Modified after Shao et al. (2011).

Despite the relatively small size of dust grains, Shao et al. (2011) present that each year about 2000 Mt of dust is emitted into the atmosphere, of which, the authors suggest, approximately 75% is deposited onto the land, with the remaining 25% into the ocean. Such volumes of dust transport necessitate the need for substantial research; however, Shao et al. (2011) add that gaps remain in the current understanding of driving processes, interactions and regional fluxes. Combined these explain the global dust cycle and explain many Earth systems (*Figure 1.3*).

Prospero (1999) highlights the truly global scale of aerosol transport, documenting that north African dust contributed to the ambient aerosol concentration in south Florida, affecting geochemical processes and air quality. Numerous studies exists which consider the role of mineral dust in ocean nutrient cycles (e.g. Jickells et al., 2005) and terrestrial ecosystems (e.g. Swap et al., 1992; Prospero et al., 2002; Bryant, 2003; Washington et al., 2003; Jickells et al., 2005; Reason et al., 2006; Soderberg & Compton, 2006; Okin et al., 2011b; Shi et al., 2012), as well as in the modification of snow albedo (Painter et al., 2007) cloud dynamics (Sun & Ariya, 2006) and the biosphere (Ravi et al., 2011).

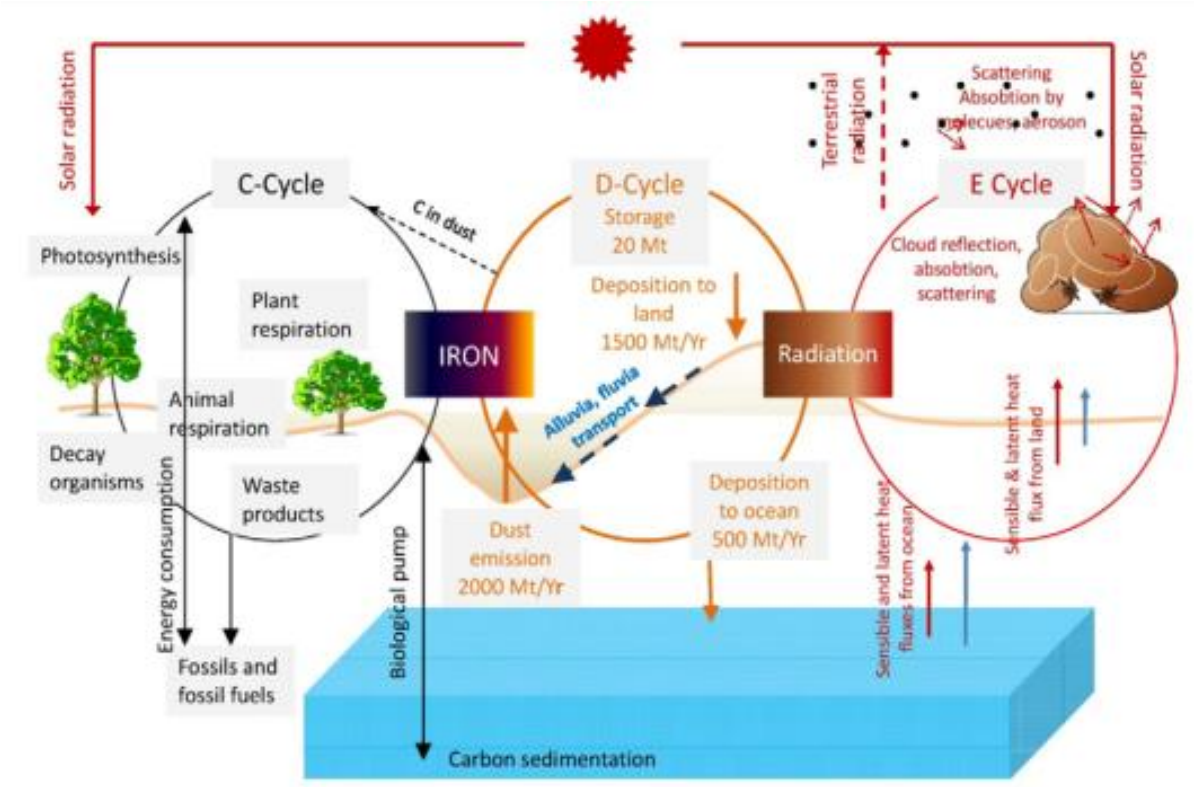

Figure 1.3 Schematic presenting the links between the dust cycle (D-cycle), the carbon cycle (C-cycle) and the energy cycle (E-cycle) as functions of the Earth system (Shao et al. 2011).

Moreover, studies indicate that Saharan dust has an effect on soils in the Canary Islands, the mountains in Cameroon, Barbados, the Bahamas and the Andes (Goudie, 2009) as well as on the ecosystems on the Mediterranean Sea, American coast and Amazon basin, while dust from the Lake Eyre basin (McGowan & Clark, 2008; Goudie, 2009) has been detected in east Antarctica. Another important area of dust research has identified the importance of dust in biogeochemical cycles and soil formation (Yang et al., 2008), with Jickells et al. (2005) commenting on the role of dust in the delivery of iron and phosphorus to the oceans. Within southern Africa, Makgadikgadi aerosols have been linked to the formation of tree islands in the Okavango by Humphries et al. (2013) and Soderberg and Compton (2006) identify the importance of regional aerosols as a nutrient source for fynbos.

A review by Goudie (2014) has considered the effects of aerosols on human health with Prospero (1999) indicating that a substantial proportion of wind-borne soil dust is within the classified "respirable" size range, commonly referred to as PM_{10} and $PM_{2.5}$ (indicating an aerodynamic diameter of 10 µm and 2.5 µm respectively), having potential adverse effect on human health. With Zender and Talamantes (2006) presenting the links between dust outbreaks and respiratory and cardiovascular complaints in the United States of America, while Bennion et al. (2007) found no such links between asthma incidence and aerosols derived from the Aral Sea. Therefore, while dust storms can result in

particulate levels that exceed international standard, not all sources and emissions contain allergens and pathogens including fungi and bacteria (Goudie, 2009) which have the potential to cause disease.

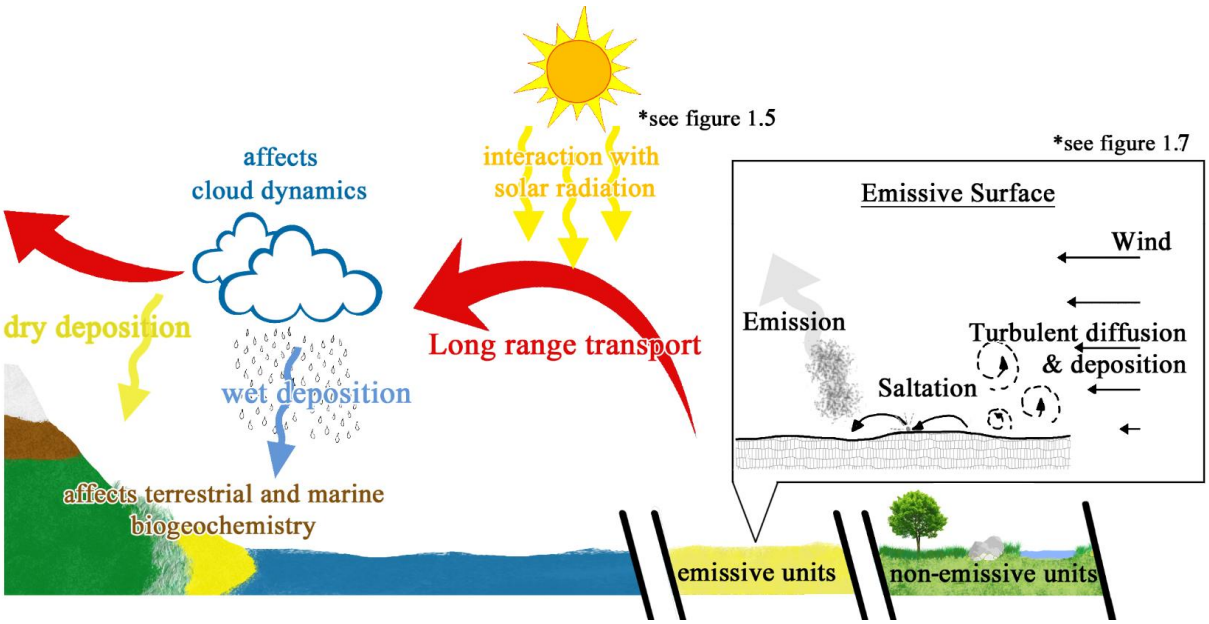

Figure 1.4 Schematic of interactions between mineral dusts, climate and biogeochemistry (modified after Lu, 1999; Mahowald et al., Corrected Proof).

Thus, mineral aerosols can be seen to have a broad spectrum of importance affecting health, weather, climate, and biogeochemistry (Carslaw et al., 2010; Mahowald et al., 2011) as illustrated in Figure 1.3. Additionally Harrison et al. (2001), Hesse and McTainsh (2003), Maher (2010), and Haberlah et al. (2010), discuss the role of dust at differing stages of the Earth's history.

Equally, the role of dust has been considered with regard to the potential to impact the climate system directly by altering the Earth's radiation budget through scattering and absorbing incoming solar radiation, absorbing terrestrial radiation and changing the physical properties of clouds and rainfall (e.g. Prospero, 1999; Harrison et al., 2001; Kaufman et al., 2002; Bryant et al., 2007; Engelstaedter & Washington, 2007a). Due to this, Harrison et al. (2001) indicate that dust is an active component of the climate system, mediating physical and biogeochemical exchanges between the lands surface, ocean and atmosphere. The IPCC Fourth Assessment report (2007) presents the following schematic of the various radiative mechanisms that have been identified to be related to aerosol, cloud and radiation interaction (*Figure 1.5*).

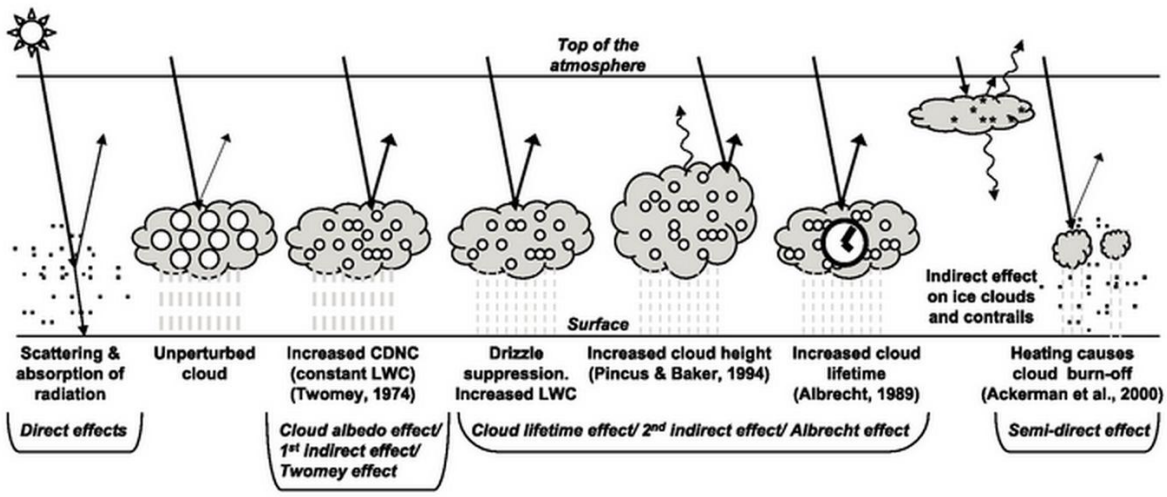

Figure 1.5 Schematic diagram showing the various radiative mechanisms associated with cloud effects that have been identified as significant in relation to aerosols (modified from Haywood & Boucher, 2000). The small black dots represent aerosol particles; the larger open circles cloud droplets. Straight lines represent the incident and reflected solar radiation, and wavy lines represent terrestrial radiation. The smaller white circles indicate cloud droplet number concentration (CDNC). The vertical grey dashes represent rainfall, and LWC refers to the liquid water content (IPCC Fourth Assessment report, (2007)).

From Figure 1.5 it can be observed that aerosols influence the Earth's climate directly by scattering and absorbing the solar and terrestrial radiation and indirectly by modifying the cloud macro- and micro-physical properties (Solomon et al., 2007). Additionally, as described by Goudie and Middleton (2001) and Prospero (1999), aerosols can result in changes in atmospheric temperature through the absorption and scattering of incoming solar radiation and outgoing longwave terrestrial radiation (e.g. D'Almeida, Koepke & Shettle, 1991; Sokolik & Toon, 1996; Alpert et al., 1998; Prospero, 1999; Haywood & Boucher, 2000; Arimoto, 2001). This also affects sea surface temperatures (SST), and the potential for rain through affecting the condensation nuclei and disturbing convective processes and thus cloud formation. Hobbs (2000) adds that aerosols are not only important for the formation of cloud particles (CCN – cloud condensation nuclei), atmospheric radiation, but affect air chemistry and determine visibility, and atmospheric electricity.

As a result of the mechanisms presented above, modelling dust is associated with a high degree of uncertainty (Mahowald et al., Corrected Proof); the Fourth Assessment report of the IPCC (2007) has greater confidence that the Third report regarding their impact, with general agreement on a net cooling effect (Ramaswamy et al., 2001) (*Figure 1.6*). However, possible feedback mechanisms, which can increase or decrease the radiative forcing effect, further decrease the certainty in their radiative effects. Brooks and Legrand (2000) provide evidence of a possible positive feedback mechanism involving rainfall and dust variability as a function of chemistry and source region.

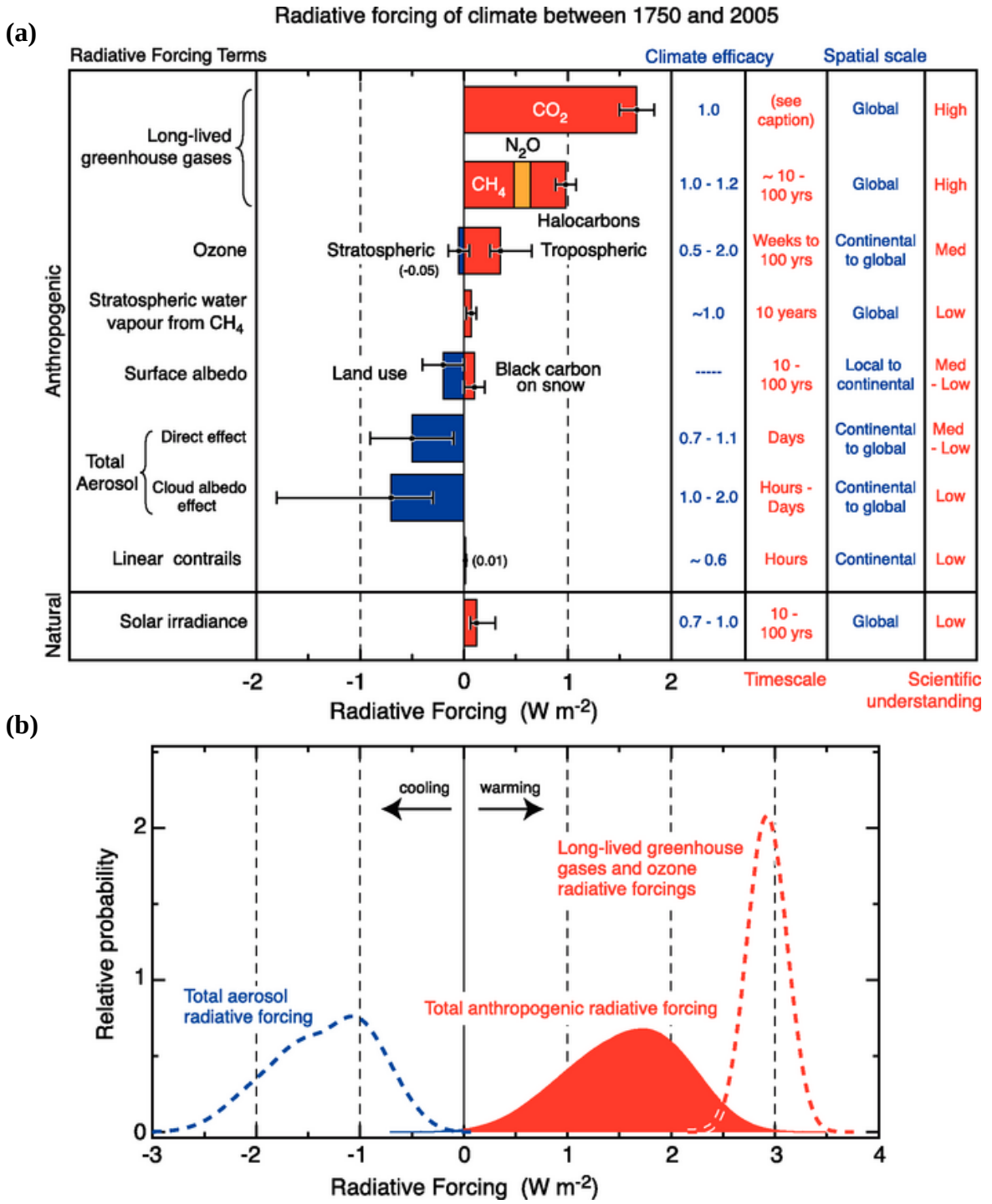

Figure 1.6 (a) Global mean radiative forcing from various components and mechanisms as discussed in the IPCC Fourth Assessment report. Anthropogenic radiative forcings and the natural direct solar radiative forcing are shown. Time scales represent the length of time that a given radiative forcing term would persist in the atmosphere after the associated emissions and changes ceased. (b) Probability distribution functions (pdf) from combining anthropogenic radiative forcings in (a). Three cases are shown: the total of all anthropogenic radiative forcing terms (block filled red curve); Long Lived Green House Gases and ozone radiative forcings only (dashed red curve); and aerosol direct and cloud albedo radiative forcings only (dashed blue curve)(sulphate, fossil fuel organic and black carbon, biomass burning aerosols, surface albedo, contrails and stratospheric water vapour) (Solomon et al., 2007).

An additional complexity in our understanding of dust is associated with long term variability, with Petit et al. (1981) indicating that the amount of dust reaching polar ice sheets has varied by an order of magnitude on glacial and interglacial time scales. More recently Goudie (2013) presents that during the Last Glacial Maximum (LGM) there was increased dust activity with Mahowald et al. (2006) proposing that dust deposition levels were 2-3 times greater than those currently observed. Nevertheless, Petit et al. (1981) add that there is an increased variability being shown for the most recent decade. Sokolik and Toon (1996) and Neff et al. (2008) propose that current land use changes could be causing a substantial increase in the amount of the dust in the atmosphere, providing further supporting evidence for this recent unpredictability. Tegen and Fung (1995) estimate that land surface modification by humans or anthropogenically altered mineral dust emissions could be responsible for between 30 and 50% of the total atmospheric dust loadings, with the potential to alter forcing by 1 $W.m^{-1}$, although uncertainty is substantial. A model of dust potential developed by Harrison et al. (2001) suggests that 30% of the total present continental land area, which translates to 5×10^6 km^2 (Sokolik & Toon, 1996), has the potential to be a dust source. However, of this determined land area, much is presently not active confirming the unpredictability of both the geomorphology and emissive characteristics of these sites and the associated complexity of processes required for emission (Prospero, 1999).

Considering the role that dust plays in affecting climate systems and thus the role it might play in future climate change - through its potential to impact the Earth's ecosystems as well as natural and human environments in the future – it is important to determine where the major dust sources are and how dust concentrations vary in space and time. Schepanski et al. (2007) further suggests that much of the discrepancy, in terms of the degree to which aerosols affect climate, can be attributed to the chemical, physical and optical properties of the particles, which vary due to different source areas and transport paths. In light of this, understanding the source characteristics and climatic controls, including transportation from the site, are of great importance.

1.2.3.1 Dust Transport

While there are a number of definitions for the grains that constitute dust, there are an equal number of definitions for the entrained material. Entrainment is the first of the three stages, defined by Pye (1987: 29), who suggests the simple processes of sediments entrainment is followed by dispersion and deposition. A number of parameters determine the mode of movements, which are a function of both the surface and the sediments (McTainsh et al., 2013). Pye (1987) suggests that windblown sediments are entrained, transported, and deposited by the wind (Zender et al., 2003). As indicated in Figure 1.4, controls include:

i. Atmospheric conditions (wind, precipitation and temperature)
ii. Surface properties (soil texture, composition and aggregation)
iii. Surface characteristics (vegetation, topography, moisture and roughness)

Consequently, dust is presented as being highly variable in space and time. However, assuming an optimal set of conditions are present, sediments will become mobilised, with the degree of mobilisation and mode of transport largely dependent on the sediment size and the power of the wind (Shao, 2000). However McTainsh et al. (2013) indicate that in general, larger particle sizes (e.g. coarse sand; >500 µm) will move by means of creep; where particles are rolled along the surface, while fine to medium sized sand particles (100-500 µm) will undergo saltation, a process whereby sediments are moved in short hops horizontally along the surface. Finally, fine silt and clay (dust, or <100 µm McTaisnsh et al. (2013)) sized particles will undergo suspension, during which the sediments will move with the prevailing flow of air.

The following figure (*Figure 1.7*) from Pye (1987) presents a schematic for the various means of transport, providing an indication of grain size.

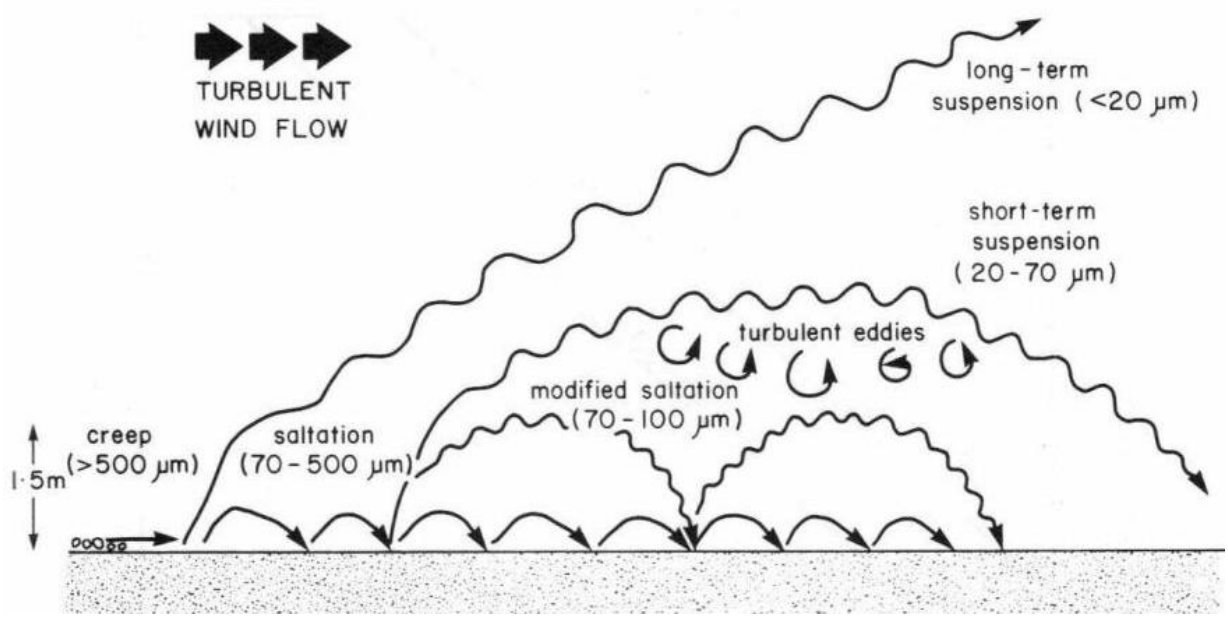

Figure 1.7 Modes of particle transport by wind (Pye, 1987).

Adding to this classification, entrainment can be further defined as a function of visibility, with the following definition based on the World Meteorological Organisation (O'Loingsigh et al. 2014) classification system:

i. Dust storms: The result of turbulent winds raising large quantities of dust into the air and reducing visibility to less than 1000 m
ii. Blowing dust: Aerosols raised by winds to moderate heights above the ground reducing visibility at eye level (1.8 m) but not to less than 1000 m.
iii. Dust haze: The transport of suspended particles which have been raised from the ground by a dust storm prior to observation.
iv. Dust whirls (dust devils): Whirling columns of dust moving with the wind and usually less than 30 m high (but may extend to 300 m or more). These systems have narrow dimensions.

While these classifications are useful they make no reference to the size of grain or the nature of the sediment entrained. Goudie and Middleton (2006) refine the concept of the dust storm, suggesting the use of the terms sand storms or dust storms as more accurate. They elaborate that dust storms have the potential to reach higher altitudes and travel greater distances, as the dominant size of the grains in transport are comprised of silts and clays. However, sand storms are proposed to be more localised and contain sand sized grains. To determine the grain size alone is also not sufficient, with Turner and Colbeck (2008) suggesting that due to the nature of atmospheric particulate matter being from a wide variety of sources a polydisperse (wide range of sizes) distribution would be expected. The authors add that poorly sorted samples tend to be associated with multimodal particle side distributions (psd) and therefore quartiles may be better at revealing trends in grain size.

As aeolian sediments are associated with transport capacity, dust researchers generally regard the clay and silt sized fractions as having the potential to become entrained by suspension in the wind (Goossens, 2001). However, Bagnold (1941) highlights the importance of saltation for dust emission from a soil surface through the effects of sandblasting. It is proposed that the saltation of sand sized particles bombards the soil surface dislodging the finer silt and clay particles, and breaking aggregates. It is this mechanism which is thought to augment the emissive potential of the surface as Livingstone and Warren (1996) present that the entrainment of the silt and clay particles is extremely difficult to achieve with the aerodynamic force of the wind alone, due to the strong cohesive bonds between these small particles (Shao, 2000). While many studies have indicated the importance of saltation for dust liberation (e.g. Shao et al., 1993; Cahill et al., 1996; Rice et al., 1996; Gillette et al., 2004), a number of studies present that emission remains possible in the absence of saltation (e.g. Kjelgaard et al., 2004; Baddock et al., 2011).

Dust emission from an area therefore depends on a complex interplay between the transport capacity of the wind, the supply of appropriate sized sediment and the availability of the sediment to be entrained. As a result Shao (2000) notes that the quantification and simulation of windblown dust is not a trivial task.

1.2.4 Methods of Dust Detection

The presence of dust in the atmosphere has been documented for centuries (Prospero, 1999), with the seminal observations by Darwin forming the foundation upon which subsequent dust studies have been based. However, in contrast to these largely descriptive observations, modern dust studies have evolved from explanatory in nature to quantitative detection and monitoring (Kaufman et al., 2002). Additionally, as our understanding of aerosols has increased during the past two decades, aeolian dust studies have become increasingly prevalent in literature (Stout et al., 2009). The following section will briefly consider *in situ* and remote sensing of aerosols which are considered further in subsequent chapters.

1.2.4.1 In Situ

Due to the origin of dust in arid areas, *in situ* dust observations are limited, resulting in missing and often imperfect records (Goudie & Middleton, 2006). Despite this, Bullard (2010) indicates that there remains the need to perform field sampling which allows for a greater understanding of antecedent conditions and the localised relationship between surfaces and emission events. Additionally, the author indicates that field studies are useful for examining contemporary environments which can better predict or retrospectively predict environmental conditions and changes. Goudie and Middleton (2006) reveal that field sampling can indicate the size, mineralogy, isotopic ratios, fossil content, and plant and pollen content, characteristics which Bullard (2010) reveals are currently poorly detected remotely. Grousset and Biscaye (2005) also present the importance of such variables as they can be used to monitor and 'finger print' source areas.

Responding to the need for *in situ* sampling, to determine the nature of sources, devices have been developed to trap dust and measure dust accumulation and transport rates (Livingstone & Warren, 1996). Traditional passive methods of dust capture and deposition measurement rely on wind to transport the sediment through the intake, and include: inverted frisbee samplers, bowls and buckets with and without a trapping mechanism or device, and Big Spring Number Eight (BSNE) (e.g. Goudie & Middleton, 2006; Goossens & Buck, 2011). These surface based measurement techniques measure properties such as; size distribution, chemical composition, and they continue to be performed, as part of long-term monitoring sites (Rodríguez et al., 2012), or as part of intensive field campaigns (Bullard, 2010). However, they fail to capture the global picture.

Despite the poor coverage of field data, the requirement remains largely in response to the need for data for constraining atmospheric models (Bullard, 2010). However, the comparison of such data against global atmospheric models has revealed a key challenge associated with differences in scale (Solomon et al., 2007) further complicated by the lack of a benchmarked standard for field analysis (Bullard, 2010). Differences in scale are primarily attributed to the *in situ* measurements being

representative of near surface and surface conditions, while models frequently consider the aerosol content in the vertical profile (Solomon et al., 2007). Comparisons introduce biases associated with differences between high resolution surface samples and the spatial resolution of global model grid boxes (typically a few degrees in latitude and longitude).

In order to overcome such biases, the UK National Environmental Research Council (NERC) funded the Quantifying Uncertainties in the Earth System (QUEST) programme, which aimed to develop a geomorphology based preferential dust source map (Bullard, 2010). QUEST aimed to produce a classification scheme where the importance of sediments, process, and landforms were included although not compromised by the global scale required for modelling.

1.2.4.2 Satellite

The challenge of temporal and spatial scale as indicated to be pertinent in the scaling between *in situ* data and modelling is further identified in satellite detection of dust. However, satellite retrieval of aerosol optical depth has improved with the introduction of new generation sensors (Kaufman et al., 2002). O'Neill et al. (2005) state that both passive and active techniques for the identification and quantification of aerosols are evolving due to advances in methodologies and instrumentation.

Such advances are particularly evident in the comparison between the World Meteorological Organisation (WMO) Background Air Pollution Monitoring Network (BAPMoN) (Holben et al., 2001), which failed due to calibration and collaboration issues (O'Neill et al., 2005), with the more successful NASA Aerosol Robotic Network (AERONET) (Torres et al., 2002). Improvements are also observed in the comparison between the earlier TOMS based studies (e.g. Herman et al., 1997; Torres et al., 2002; Prospero et al., 2002) with high temporal and spatial resolution MODIS (Hsu, 2007; Ginoux et al., 2012) (*Figure 1.8*) and Meteosat Second Generation (MSG) (Klüser & Schepanski, 2009; Ashpole & Washington, 2012) studies. These advances have allowed researchers to comprehend the true magnitude of aeolian landscapes and features (Livingstone & Warren, 1996). Additionally, through remote sensing, the extent of arid landscapes and the highly dynamic nature of these surfaces were identified, and as a result, justified further examination of the processes active in these regions.

While these sensors have allowed for truly global data sets, Washington et al. (2003) indicate that the continuous and repeated mapping of dust using remote sensing has been particularly hampered by the detection through clouds, the variable spectral responses of surfaces, and the inability of products to detect low level plumes (e.g. Herman et al., 1997; Hsu et al., 2004; Bryant et al., 2007). The global picture often fails to identify the true nature of systems, with regional studies better identifying information pertaining to dust sources and their activation frequency (e.g. Schepanski et al., 2007; Baddock et al., 2009; Vickery et al., 2013).

Following the shift to remote sensing from ground monitoring, research has shifted back to site based monitoring to augment the globally derived satellite data. However, with this shift, a better understanding of the nature and requirements of surface analysis has been considered (e.g. Bullard, 2010), with the rigorous demands necessary to understand and quantify dust at both a source and modelling perspective, now better understood. Therefore, the requirements of field analysis have changed to encompass the need to quantify frequency, distribution and the precise location of the sources. Bullard (2010) reveals that the sophistication of global models representing dust transport, atmospheric processes and deposition outstrips the level of data with which models are validated and calibrated with respect to the surface conditions. Bryant (2013) adds that source data is often poorly constrained at the scale of both satellite products and model data.

Despite the lack of well constrained data, through advances in satellite detection it has become possible to identify discreet surfaces globally (e.g. Bullard et al., 2011) from which emission occurs. The following section will present our current understanding of global dust sources as determined through field analysis, observation and remotely sensed data.

1.3 Global Sources

Despite the proposal by Bullard (2010) that any terrestrial surface with a supply of suitably sized sediment and an appropriate wind regime can be a dust source, there appears to be a number of preferential sources (Bullard et al., 2011) globally from which dust is both persistently and intermittently emitted. The largest and most persistent source globally is the Bodélé Depression (Washington et al., 2003). This source is found within the northern hemispheres dust belt (Prospero et al., 2002) which extends from the west coast of north Africa, over the Middle East, across central and south Asia, to China.

The presence of dust within this arid belt confirms early indications by Pye (1987) that dominant regions are largely associated with sub tropical desert regions, as well as semi-arid and sub-humid regions where dry soils are exposed to seasonally accelerated winds. These are further classified into more specific terrains, which Pye (1987) indicates to have the potential to act as dust sources (all but the first are associated with arid and semi-arid landscapes):

i. glacial outwash plains and braided fluvioglacial channels
ii. dry wadi beds
iii. dry lake beds
iv. coastal sebkha surfaces
v. alluvial fans
vi. stony deserts with high weathering rates
vii. exposed argillaceous bedrock areas

viii. areas of loess where the vegetation cover has been reduced by climatic change and/or cultivation
ix. deeply weathered regolith where vegetation cover has been reduced by climate change/human activity
x. alluvial floodplain sediments, particularly cultivated regions and
xi. areas of formerly stabilised dunes which are reactivated through a variety of drivers.

Subsequent research by Goudie (1983) advanced this understanding by identifying that most dust source regions were associated with a mean annual rainfall of between 100 and 200 mm; additionally stating that regions receiving below 100 mm were likely to be less dusty. While Chiapello et al. (1999) suggested that dryland surfaces characterised by a reduced vegetation cover and desiccated surfaces would be likely dust sources upon exposure to high velocity winds. Prospero et al. (2002) and Washington et al. (2003) discuss the importance of dry inland basins as dust sources, noting their expanse, dynamic nature, and range of sedimentary environments as central to their highly emissive character.

Remote sensing, primarily through the use of the Total Ozone Mapping Spectrometer (TOMS), has permitted for the development of global dust source maps and therefore the classification of global dust hot spots, with Table 1.1 presenting the rankings as determined by Washington et al. (2003).

Table 1.1 Maximum Mean Aerosol Index (AI) Values for Major Global Dust Sources Determined from TOMS (Washington et al., 2003).

Location	Mean AI Value
Bodélé Depression of south central Sahara	> 3.0
West Sahara in Mali and Mauritania	> 2.4
Arabia (southern Oman/Soudi border)	> 2.1
Easter Sahara (Libya)	> 1.5
Southwest Asia (Makran coast)	> 1.2
Taklamakan/Tarim Basin	> 1.1
Etosha Pan (Namibia)	> 1.1
Lake Eyre Basin (Australia)	> 1.1
Makgadikgadi Basin (Botswana)	> 0.8
Salar de Uyuni (Bolivia)	> 0.7
Great Basin of the United States	> 0.5

Correlation of TOMS findings with basic source region classification has allowed researchers to develop a better understanding of preferential global surfaces. This is particularly evident through the advancements using additional controls (e.g. surface gustiness, Engelstaedter & Washington, 2007b) or higher resolution products (e.g. MODIS, Ginoux et al., 2012) to further inform our current understanding of global dust sources. However, even through the use of these high resolution products

(e.g. Hsu et al., 2004; Hsu et al., 2006; Ginoux et al., 2012), our understanding remains inexact regarding the allocation and quantification of sources (e.g. Zender et al., 2003; Mahowald et al., 2007; Bullard et al., 2011).

Figure 1.8 from Ginoux et al. (2012) presents the advances in our understanding of source regions, through the inclusion of earlier TOMS and OMI (Ozone Monitoring Instrument) contours of aerosol concentration.

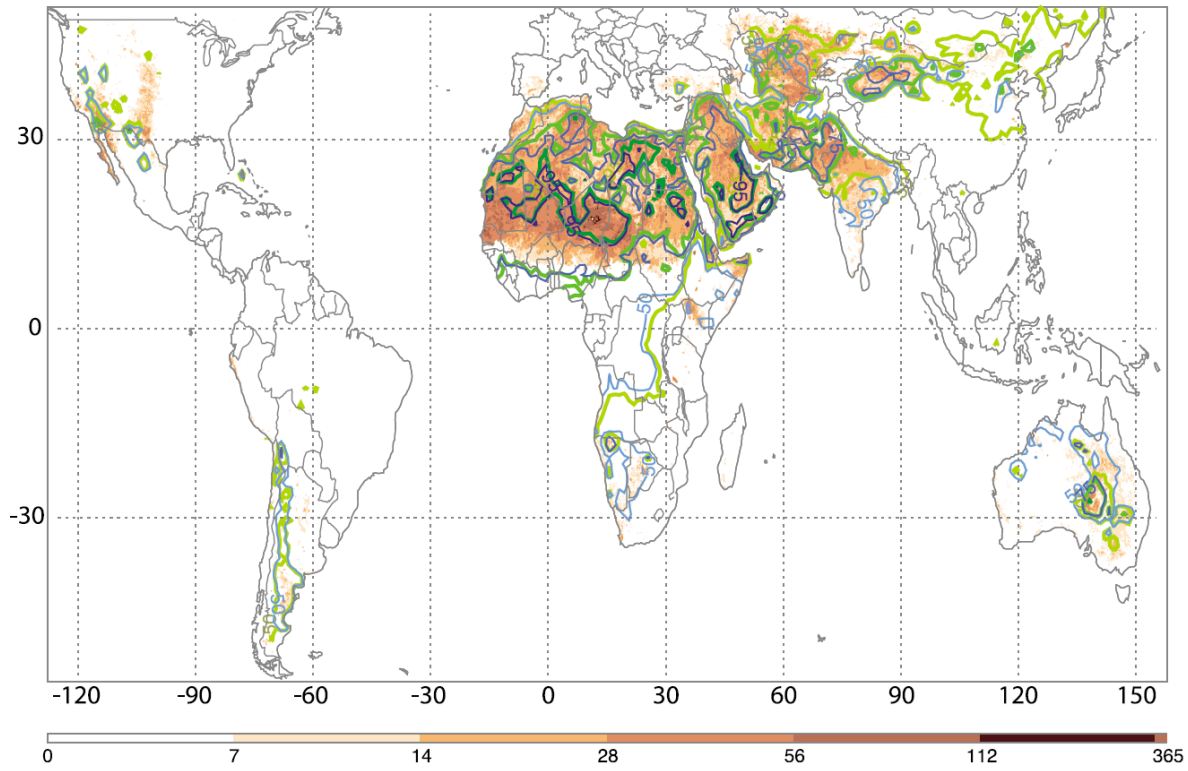

Figure 1.8 Annual mean frequency distribution of MODIS Deep Blue Level 2 (M-DB2)(2003-2009) Dust Optical Depth: DOD >0.2 (red). TOMS (1980-1991) Aerosol Index: AI ≥0.5 (blue), and OMI (2004-2006) Aerosol Index: AI ≥0.5 (green). TOMS and OMI contours have been removed over oceans for clarity (Ginoux et al. 2012).

However, the lack of source specific attribution of plumes remains a challenge when studying dust sources. This was particularly evident in southern Africa where scale and the inherent variations in seasonal and diurnal dust emission variations, combined with the proposed heterogeneity of dust sources (Vickery et al., 2013) result in poor source attribution. However, work by, amongst others Bullard et al. (2011) and Ginoux et al. (2012), have attempted to quantify and classify global sources with geomorphologic units to better understand process and therefore global dust emission (Bryant, 2013). Consequently, global dust source maps are increasingly including surface source types in the classification of dust source regions acknowledging the importance of geomorphology for both the supply of sediment and limitations to emission.

1.3.1 Surface Sources Types

The following section will consider the dominant surface source types associated with dust source regions, using the geomorphological types indicated to be preferential dust sources as presented in Bullard et al. (2011). However, the ephemeral nature of the Makgadikgadi Pans which are central in this study, result in a more in depth consideration of this geomorphic type in the following section.

1.3.1.1 Lakes and Fluvially Linked Systems

Pans, playas and ephemeral systems have been identified to be important global dust sources (Bullard & Livingstone, 2002; Prospero et al., 2002; Yechieli & Wood, 2002; Washington et al., 2003; Bryant, 2003; Mahowald et al., 2003; Washington et al., 2006; Bryant et al., 2007; Bryant, 2013). These, often extensive, sparsely vegetated surfaces are comprised largely of unconsolidated sediments (Shaw & Bryant, 2011), providing the ideal conditions for aeolian activity, with Prospero et al. (2002) and Washington et al. (2003) highlighting the ability of such systems to act as sediment sinks, e.g. the Bodélé, Taoudenni, Tarim, Eyre, Etosha, Makgadikgadi, Uyuni and the Great Salt Lake (Washington et al., 2003). Additionally, they are often located in topographic lows resulting in features that have the greatest potential for dust deflation. These types of geomorphic features and surfaces are often associated with active landscapes (Pye, 1987) and, while they are frequently located in arid regions with annual rainfall under 200 – 250 mm (Washington et al., 2003); the action of water in the region is often evident from the presence of ephemeral streams, rivers, playas and lakes. Bullard and Livingstone (2002) confirm the importance of the interactions between fluvial and aeolian processes adding that in arid environments it is these interactions which result in the high sediment potential of systems. The authors further discuss the natural variability of both aeolian and fluvial processes in dryland pan and playa environments, suggesting that if fluvial systems fail to provide a consistent supply of fine sorted sediments to source areas, the magnitude and frequency of dust events diminishes (e.g. Clarke & Rendell, 1998). The relationship is hypothesised such that sediments are deposited and then exposed through the annual cyclic nature of inundation, followed by deflation through aeolian processes as the waters recede. The periodic renewal of sediments through ephemeral flood inundation events imposes an aspect of supply control on these sources, resulting in a reliance on the flood events to provide the sediment (Shaw & Thomas, 1997). Therefore, where currently active ephemeral streams are a major source of dust, a temporal relationship between the fluvial event and frequency and the dust events can be discerned (McTainsh et al., 1999; Bullard & McTainsh, 2003; Bryant, 2003; Bryant et al., 2007; Vickery & Eckardt, 2013).

The importance of water is further evident as Bullard et al. (2011) divide lake sediments into one of four states dependent on the nature of moisture in the system. The resultant geomorphic classifications are therefore: i) wet; ii) ephemeral; iii) dry, unconsolidated or iv) dry consolidated.

Wet or perennial lakes may contain a supply of fine grained sediments; however, the presence of water serves to inhibit dust emission (availability limited). Dry systems are proposed to have the greatest dust potential, with dry unconsolidated surfaces only limited by transport capacity. However, sediments on dry lake beds are frequently consolidated by salts which can cement the surface and reduce the emissive potential. Therefore, Saint-Amand et al. (1986) suggest that the chemistry of the system is of further importance when considering these sources.

Ephemeral systems, which experience seasonal wetting and drying cycles, were identified as one of the most important dust sources globally (Prospero et al., 2002; Washington et al., 2003; Bryant, 2003; Mahowald et al., 2003; Bryant, 2013) as ephemeral lake systems with disrupted, wind-erodible surfaces are highly conducive to the work of aeolian processes and the creation of dust. Similarly Cooke et al. (1993) and Shaw and Thomas (1997) suggested that ephemeral systems are the primary regional sinks for the dust that settles on them or that is transported into them by fluvial processes. These processes provide a source of fine grained material that can be readily eroded by the wind. Thomas and Shaw (1991) further emphasise the importance of networks of pans and playas, which account for approximately five percent of modern drylands; noting that despite the small spatial coverage they cannot be ignored in global dust literature (Prospero, 1999; Washington et al., 2003). In general, Muhs et al. (2013) add that many ephemeral lakes were perennial at some stage in the past, during which time considerable quantities of fine grained fluvial, groundwater derived and/or biogenic sediments would have accumulated, often holding detailed records of past climatic conditions and dust activity. Bullard et al. (2011) indicate that for perennial sources to become active, the partial or full desiccation of the system is required (Gill, 1996). Possibly the best example of a once perennial source is the Bodélé Depression in Chad, with this system containing an abundant supply of dry, unconsolidated diatomite which is readily entrainable (particularly when activated through saltation (Warren et al., 2007)). Another control on pan emissivity was discussed by Reynolds et al. (2007), who consider the effect of the depth to ground water on the emissivity and chemistry of the pan surface. The authors present the results of observations from both pans with both shallow and deep ground in the Mojave, revealing that wet pans are dynamic with frequent changes in sediment availability in response to rainfall, evaporation and system recharge. Conversely, dry pans were detected to have harder, more stable and less emissive surfaces in the absence of disturbance.

This confirms the importance of water in determining the nature of the system, wet, dry or ephemeral, but also in determining the functionality of the system and the state of the surface. These multiple considerations result in the identification of the arid lakes as highly dynamic environments (Pye, 1987).

1.3.1.2 High and Low Relief Alluvial Systems

Deep alluvial deposits indicative of intermittent flooding are also associated with high deflation potential surfaces (Middleton, 1997; Washington et al., 2003). Bullard et al. (2011) differentiate alluvial systems based on relief or gradient; suggesting that high relief systems are generally associated with a gradient of greater that 3° and comprised of coarser material than low relief systems.

High relief alluvial systems such as fans, piedmont slopes and bajada (Bullard et al., 2011), have a distinctive geomorphologic signature, with largely armoured surfaces comprised of coarse particles (Reheis & Kihl, 1995) which increase the surface roughness and lower the wind erosion potential. In the absence of armouring, these systems are proposed to have a greater dust potential, although they require periodic rains or weathering (Viles & Goudie, 2007) to replenish the system. Bullard and McTainsh (2003) again note the role of fluvial recharge, however in alluvial systems the authors indicate that mechanisms associated with fluvial incision affects the flood plain, inundation frequency and sediments supply. Schepanski et al. (2007) note the importance of topographic channelling in such environments, enhancing regional winds as observed in the Aïr Mountains in the Sahara.

Low relief alluvial systems, including fluvial braided streams, deltas and para- and periglacial outwash plains were documented by McKenna-Neuman and Gilbert (1986) and more recently Muhs et al. (2013) to be significant dust sources. While low relief deposits are sometimes incised, reducing their emissive potential (Eitel et al., 2001; Bullard et al., 2011), dust activity has been linked to the flooding of melt water resulting in the delivery of suspended sediment to the system. Similar to high relief systems, low relief systems can experience armouring or extensive vegetation cover, as in the case of the Okavango delta (Gumbricht & McCarthy, 2003; McCarthy et al., 2012; Humphries et al., 2013) with drought and therefore a decrease in vegetation cover strongly controlling dust emission from the region.

1.3.1.3 Stony Surfaces

Stony surfaces, or desert pavements (McFadden et al., 1987) are low angle, stone mantled surfaces formed by a number of processes (Bullard et al., 2011). Their development is often attributed to deflation, and the erosion of fine grained material or the upwind migration of gravels through a clay-rich, gravel-depleted B-horizon (Cooke & Warren, 1973). In most cases larger gravels cap a store of relatively fine silt and clay sized grains (McFadden et al., 1987), although sand size grains may occur in some locations (Marticorena et al., 1997). Consequently, the coarse upper layer commonly limits aeolian erosion of the finer sediments, associating such regions with availability limitations. These units have, however been detected to produce dust (e.g. the Namibian gravel plains north of the Kuiseb River in Vickery and Eckardt, (2013)); although this is most commonly as a result of

disturbance to the gravels or through additional drivers active within the gravel plains (e.g. Belnap & Warren, 2002; Vickery & Eckardt, 2013).

1.3.1.4 Sand Deposits and Aeolian Loess Systems

Bullard et al. (2011) attributed the geomorphic units of sand sheets and aeolian sand dunes to the 5th geomorphic type, with loess accounting for the sixth type. Sand sheets are areas of low relief with sandy deposits. The authors additionally present that the size and sorting of sediments, results in high susceptibility to wind erosion, with the presence of vegetation and moisture being the primary limitations for emission in such environments. Conversely, sand dunes with their wind sculptured relief (Bagnold, 1941), have highly variable emission potentials, depending on form, sedimentology, grain size, and historical and contemporary setting of the dune (Bagnold, 1941; Fryberger, 1979; Pye, 1987). Bullard et al. (2011) generalise that younger active dunes are less likely to be sources than older more stable dunes, which may accumulate fines or produce silts and clays through weathering. The authors add that dunes in hyper-arid regions are also unlikely to be sources, while semi-arid and temperate regions are more likely to contain fine material, although the presence of vegetated dunes in temperate regions could further limit their emissive potential. Consequently Bullard et al. (2011) suggest dunes are highly dependent on contemporary and palaeo-environmental setting. Both Vickery and Eckardt (2013) and Washington et al. (2003) suggest that in dryland areas with multiple geomorphic units, it is commonly drainage basins and not the dunes which provide the greatest count of emissions, although the supply of mobile dune sediments may provide material for saltation which may enhance the emissivity of the region.

Loess deposits were described by Tsoar and Pye (1987) as mainly medium silt sized grains, with high transport potential, typically associated with short term suspension a few meters above the ground. As a result, loess surfaces often exhibit a strong grain size gradient, with a dominance of coarse grains towards the emission source, fining with increased distance downwind (Tsoar & Pye, 1987; Bullard et al., 2011). Extensive loess deposits are largely formed by topographic obstacles, in areas of moist ground, or vegetated surfaces (Tsoar & Pye, 1987) with subsequent disturbance or change in vegetation cover resulting in highly emissive surfaces. Tsoar and Pye (1987) add that in many arid areas desert loess deposits are poorly developed, with much of the world's loess occurring in mid-latitudes in areas which experienced Pleistocene glaciations. Washington et al. (2003) discuss the importance of pre-Pleistocene dust storms in China, which transported sediments to form the extensive deposit of loess which, through contemporary reactivation, are an important global dust source.

1.3.1.5 Low Emission Surfaces

This seventh and final geomorphological type as presented by Bullard et al. (2011) is essentially the non-emissive geomorphological unit within dust producing regions. These, the authors suggest, include exposed bedrock, steep rocky slopes, duricrusts and areas capped by snow and ice in cold deserts. This low to non-emissive component is associated with either sediment supply or availability limitations.

Common to most of the preferential dust source geomorphologies is their presence in low relief areas. Equally, the role of fluvial activity as a means of sediment transfer into the system is commonly identified. Additionally, many of the sources discussed above have the potential to become dustier through saltation as an initiating factor for liberation and the disaggregation of coarser sediments through ballistic impact (Pye, 1987). Bullard et al. (2011) discuss the applicability of such a scheme in modelling source regions to both predict and retrodict the impacts of climate change on the dust cycle and *vice versa*. The authors acknowledge that even under optimal environmental conditions system response can result in differing temporal behaviours depending primarily on sediment associated limitations.

1.3.2 Southern African Sources

In southern Africa understanding, atmospheric composition and transport patterns has advanced significantly over the past two decades. While early southern African aerosol research was dominated by studies on the industrial Highveld, where mineral aerosols impact was limited (Ichoku et al., 2003), the Southern African Fire Atmospheric Research Initiative (SAFARI)-92 and SAFARI 2000 established a greater understanding of both air-transport patterns and the temporal variability of regional aerosols and confirming the importance of mineral aerosols to the pall that dominates the subcontinent (Reason et al., 2006).

Derived through satellite observation, Abel et al. (2005) noted that the distribution and concentration of the aerosol gradient over southern Africa is reversed between spring and autumn in response to biomass burning. However, throughout this variability, aerosol loadings continued to be dominated by aeolian dust (Piketh et al., 1999). This established the importance of including desert dust in the development of a regionalised aerosol map of southern Africa. Subsequent sub-regional studies on Namibia (e.g. Bryant, 2003; Eckardt & Kuring, 2005) and Botswana (Bryant et al., 2007) revealed the importance of these regions, while the first comprehensive regional study of dust sources in Southern Africa was published by Vickery et al. (2013) (*Figure 1.9*), indicating that dust emission from the region occurs in four key locations centred in the south western Kalahari, the Namibian Coastline, and the Etosha and Makgadikgadi Basins. These four regions were previously identified in

literature as having a dust signature in TOMS (e.g. Washington et al., 2003; Engelstaedter & Washington, 2007b), however specific source locations were not attributed.

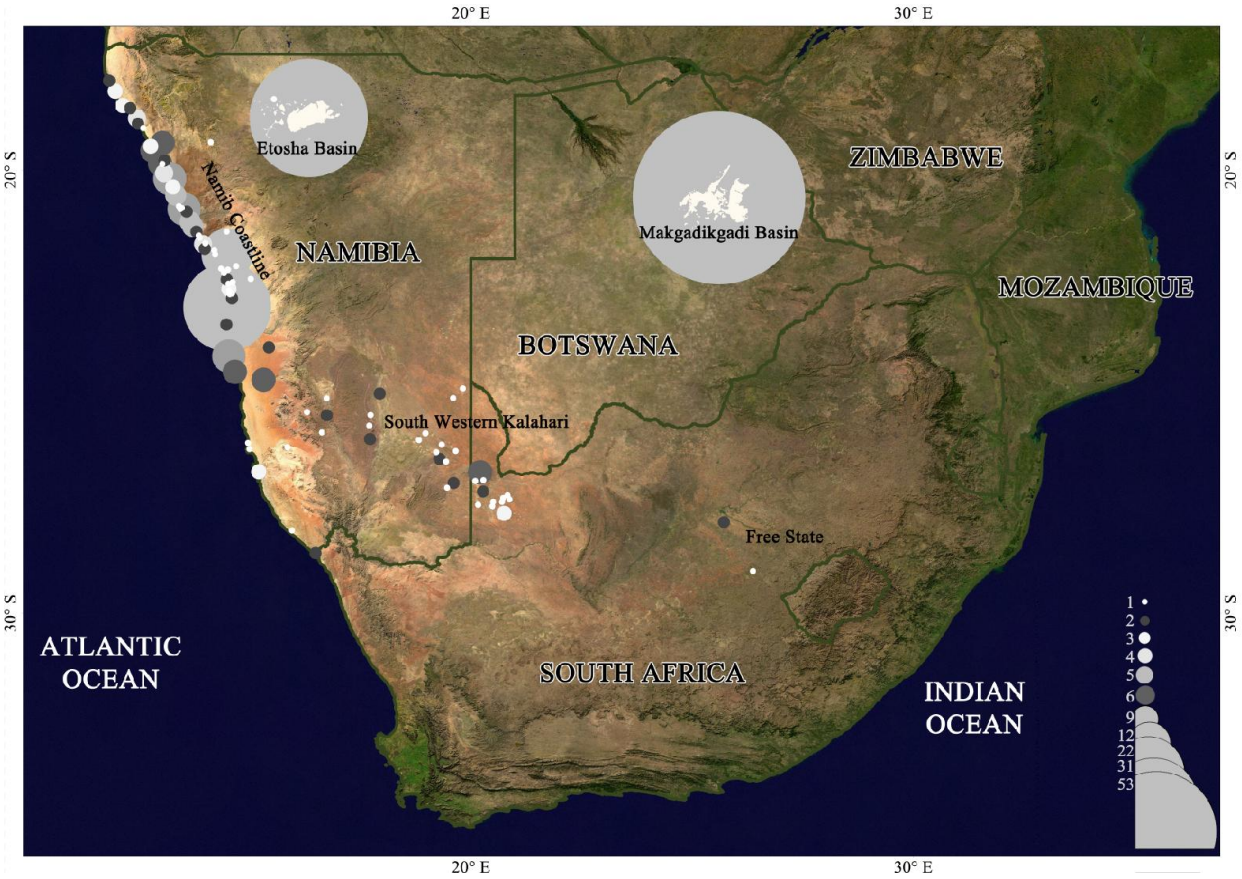

Figure 1.9 Southern African dust plume source locations detected between 2005 and 2008 using a multisensor approach as presented in Vickery et al. (2013). Circles indicated the weighted frequency of the number of dust plumes, clearly indicating the dominance of the Makgadikgadi and Etosha Pans and the Kuiseb Catchment on the Namib Coastline.

Common to studies by Washington et al. (2003), Engelstaedter and Washington (2007b) and Vickery et al. (2013) was the importance of the Makgadikgadi Pans in north eastern Botswana. While Bryant et al. (2007) focussed on this region in a 2007 study which considered the dust emission response from the system in line with large scale climatic drivers, a number of global dust source studies e.g. Prospero et al. (2002), Washington et al. (2003), Zender and Kwon (2005), Ginoux et al. (2012) have considered the role of the Makgadikgadi Pan within both global and southern Africa cycles. Prospero et al. (2002) indicates that the Makgadikgadi is a persistent source, though highly variable from year to year, and add that the precise signature of the region could be affected by biomass burning in central Africa between July and September. Prospero et al. (2002) also state that dust activity can be seen to increase between June and July, peaking between August and October, decreasing during the austral winter. A similar trend was observed by Bryant et al (2007) using TOMS and later confirmed by Vickery et al. (2013). Prospero et al. (2002) also suggest that there was a maximum in dust activity

towards the west, this too was observed in TOMS data by both Washington et al. (2003) and Bryant et al. (2007) although the authors attribute this to transport and detection heights.

Therefore, for several reasons the Makgadikgadi Pans were chosen for this study and the Dust Observation for Models Project (DO4) (see section 1.4). Firstly, it has been identified as a persistent and significant dust source globally and in southern Africa (Prospero et al., 2002; Washington et al., 2003; Bryant et al., 2007; Vickery et al., 2013). Secondly, when trying to quantify emissions from a large inland basin, it is proposed that the Makgadikgadi can serve as an analogue for emission characteristics from large inland pan systems globally. Finally, this region was identified as producing multiple emissions per year from a number of discreet source locations (Vickery et al., 2013) and the region is accessible for field analysis and therefore emission and source region monitoring.

1.3.3 Makgadikgadi Pan Complex

The Makgadikgadi Pans lies in an internally draining basin in north eastern Botswana (*Figure 1.10*). The basin forms part of the larger Lake Palaeo-Makgadikgadi, associated with the Makgadikgadi-Okavango-Zambezi (MOZ) rift, and represents one of the largest palaeo-lakes in Africa (Ringrose et al., 2005; White & Eckardt, 2006; Burrough et al., 2009). Cooke and Verstappen (1984) suggest that during the Pleistocene the Paleo-lake Makgadikgadi was over 120 000 km^2, encompassing much of the Okavango delta and surrounding areas (Cooke, 1979). The system has changed considerably from this proposal of a permanent mega-lake system to the ephemeral nature of the contemporary pan system. With the current 37 00 km^2 (Cooke & Verstappen, 1984) basin representing a range of fluvial, lacustrine and aeolian surface morphologies as defined by Bryant et al. (2007). Eckardt et al. (2008) suggest that the Makgadikgadi are amongst the largest arid zone, saline, inland pan systems in the world.

Occupying the contemporary basin are two large ephemeral lakes, (Thomas & Shaw, 1991; Shaw & Thomas, 1997) most notably the Ntwetwe Pan to the west (~900 m above sea level) and the slightly smaller Sua Pan to the east (~890 m asl) covering ~3 000 km^2. The Sua Pan, which is the lowest point on the southern African inland basin (Wood et al., 2011), results in the Sua Pan being a natural sink for ground water and surface flow (Hulsmans et al., 2006). In addition to seasonal rainfall, the pans are principally fed by a number of rivers which drain into the basin (McCulloch et al., 2008). The Sua Pan largely receives inflow from the Nata river to the north, with its watershed extending into the wetter eastern regions of Botswana and into Zimbabwe; although additional inflow from the Mosupe, Lepashe, Mosetse, Semowana Rivers reach the pan (*Figure 1.10*) (Hulsmans et al., 2006; Setlhogile et al., 2011). Hulsmans et al. (2006) add that the northern basin of the Sua Pan is the deepest part of the pan, in addition, as it is fed by the largest of all the inflowing rivers into the basin, floods are frequent and for longer periods of time. The Ntwetwe Pan is fed by the Boteti River which serves as an overflow for the Okavango Delta (*Figure 1.10*). However Wood et al. (2011) indicate

that flow has largely ceased since the 1990s, although satellite observation of the region revealed that surface flow from Lake Xau and the Mopipi Dam resumed following heavy rains in 2011. Wood et al. (2011) suggest that river inflow from river systems with headwaters in the Angolan and Zimbabwean highlands (where rainfall is in excess of 1 000 mm.yr^{-1} (Bryant et al., 2007; Burrough et al., 2009)) and the location of the Pans within the Makgadikgadi Depression results in shallow ground water, with the water table often only a metre below the pan surface (Wood et al., 2011). Setlhlogile et al. (2011) add that the quality of the shallow groundwater is variable, and in some areas beneath the pans, highly saline.

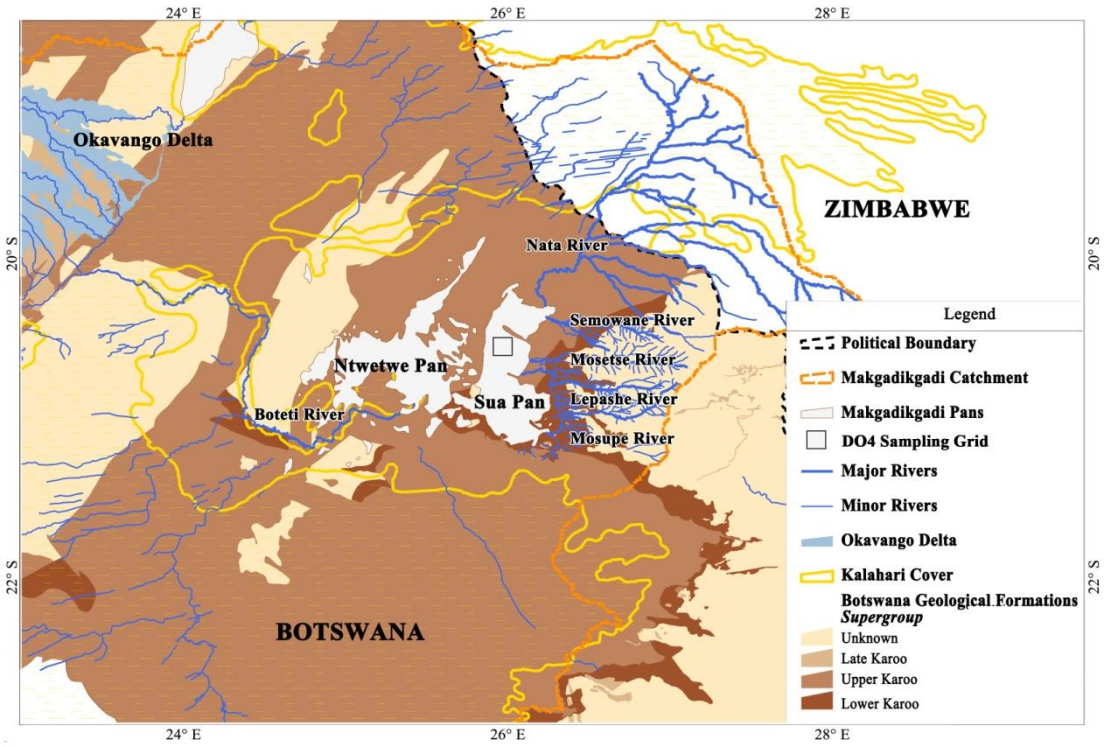

Figure 1.10 Map of north eastern Botswana depicting the major geology and the spatial cover of Kalahari sands in the region, major rivers which drain into the Makgadikgadi and their minor tributaries are also identified. The full extent of the catchment is not shown although can be seen to extend in all directions well beyond the basin boundary.

In addition to the Ntwetwe and Sua Pans there are a number of smaller satellite pans, which, combined with Sua and Ntwetwe Pan account for just over 6 000 km^2 of north eastern semi-arid Kalahari Botswana (Thomas & Shaw, 1991). Goudie and Thomas (1985) reveal that the Makgadikgadi Pans are unlike those of the south west Kalahari due to the absence of lunette dunes, while dunes are common features of the southern Kalahari pans. Consequently, the authors propose that deflation dominated the formation of the southern pans, while an alternative control needed consideration for the Makgadikgadi. Thomas and Shaw (1991) suggest that fundamentally the Kalahari sands are not a homogenous unit, varying in composition, colour and thickness across the vast expanse of the Kalahari. The authors suggest that such differences could be indicative of variations in ages, and therefore multiple pan forming conditions and periods throughout the greater Kalahari permitting such differences.

Eckardt et al. (2008) indicate that much of the contemporary surface of the Makgadikgadi is composed of a mixture of clay minerals and crusting evaporite minerals including halite, mirabilite and thenardite; while Thomas and Shaw (1991) and McCulloch et al. (2008) add trona, and a number of carbonates and sulphates to the chemistry of the pan surface. Helgren (1984) indicate that the thick aeolian sands, evaporites, and relict lake beds that dominate the pan landscape result in few outcrops of the bedrock. Thomas and Shaw (1991) discuss the geology of the region, suggesting that Precambrian granites and Carboniferous to Triassic Karoo Supergroup sediments are dispersed throughout the region. Bailieul (1979) reports on a few observations of bedrock outcrops in the region, indicating the presence of a number of outcrops of Precambrian granites and migmatite on the horst between the Sua and Ntwetwe Pans; additionally noting dikes of terminal Karoo dolerite and Upper Karoo (mid-Mesozoic) sandstones to both the north and south of the basin margin (*Figure 1.10*). While the upper sediments of the extensive basin catchment is comprised of Kalahari sediment based calcisols, luvisols, vertisols and gleysols (Thomas & Shaw, 1991), much of the surrounding soils, particularly close to the pan margin, contain calcrete layers at shallow and moderate depths (McCulloch et al., 2008). Ecologically, Setlhogile et al (2011) comment that the pans are surrounded by grasslands, tree and bush savannah as well as mophane woodlands. These provide a variety of ecological habitats which supports a diversity of fauna and flora (McCulloch, 2003). In addition, the seasonal rainfall supports a variety of water birds including globally severely threatened species such as the water crane, lesser flamingos and the white pelicans (McCulloch, 2003). These same rains flow into the system affecting the surface morphology of the contemporary pan through periodic flow and desiccation, crystal growth and dissolution and aeolian deflations.

1.3.3.1 Basin Climate

The regional climate of the Makgadikgadi basin is semi-arid with rainfall estimated to be between 400 and 500 mm (McCulloch et al., 2008; Setlhogile et al., 2011). Most of the rain falls between November and April (*Figure 1.11*), but large inter-annual fluctuations are characteristic of the climate (Schulze, 1972). Tyson (1987) indicates that 80% of the rainfall for the region falls in high magnitude events during the summer months of October to April. Bhalotra (1987) reveals that most of this rainfall is received through convective processes such as instability showers and thunderstorms. The author adds that these features are several orders of magnitude smaller than the synoptic systems like the Inter-Tropical Convergence Zone (ITCZ) and the Zaire Air Boundary (ZAB), which control the airmasses supplying the moisture. This results in a highly variable spatial distribution of rainfall (Bhalotra, 1987; Thomas & Shaw, 1991). Despite this variability, a strong west/east gradient exists for the isohyets over Botswana, with the north east receiving significantly more rainfall than the drier south west.

During good rainy seasons, Hulsmans et al. (2006) indicate that the pans are transformed into vast shallow salt lakes, with these temporary lakes lasting a matter of months before evaporation returns the lakes to a dry pan.

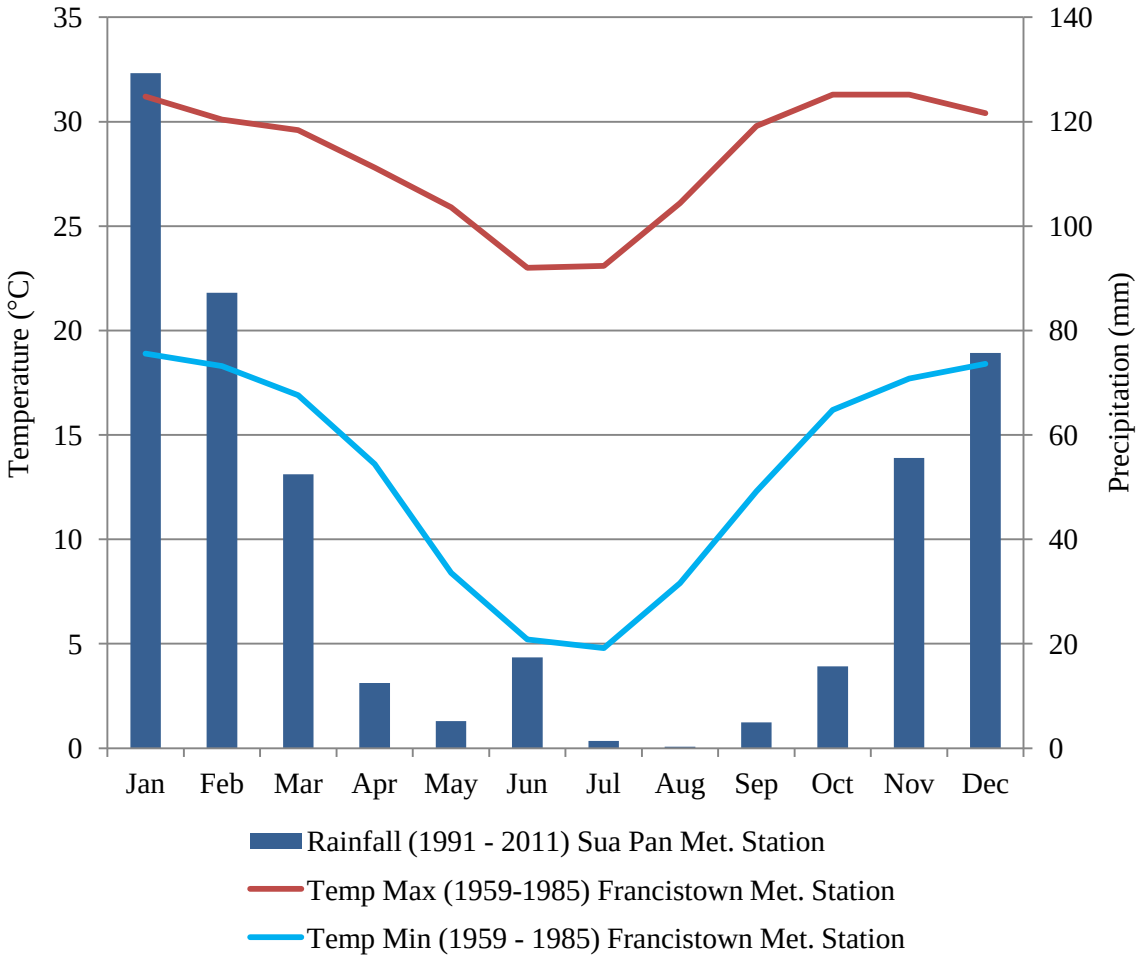

Figure 1.11 Rainfall and Temperature graph for select stations in north eastern Botswana. Temperature for Francistown as reported in Bhalotra (1987) reflecting 26 years of data from 1959 to 1985. Rainfall data is from a meteorological station on the Sua Spit, this data represents 20 years of collection from 1991 to 2011. A peak in winter rainfall in June is partially skewed by high rainfall (252 mm in 2009) and a further high rainfall event in 2000 (59 mm). While temperature and rainfall are from different stations and different time periods, the figure gives an indication of approximate conditions for the north east.

The temperature of the region is associated with cool winters and hot summers, with a summer minimum of approximately 20°C dropping to 5°C in winter, while maximum temperatures in summer can exceed 30°C dropping to 23°C in winter (Bhalotra, 1987) (*Figure 1.11*). According to Thomas and Shaw (1991) these temperatures are lower than other regions at comparable latitudes, suggesting that the altitude of the southern African interior results in lower mean surface temperatures.

1.4 Dust Observation for Models (DO4)

This study was performed as an auxiliary study within the larger Dust Observations for Models – DO4 project. The DO4 Models project is a National Environmental Council (NERC) funded project with the University of Oxford as the lead institution. Other institutions associated with this project include: Imperial College London; The Universities of Sheffield, Cape Town and Southampton; together with the Met Office-Hadley Centre. Further information on the project can be found via the following URL: http://www.geog.ox.ac.uk/research/climate/projects/DO4models/.

The DO4 project set out to generate a new data set for global climate models which characterises surface erodibility and erosivity in dust source areas. This is being achieved through the following objectives:

1. Quantify how erodibility and erosivity influence observed emissions at the climate model grid scale.
2. Assess which component(s) of observed erodibility and erosivity, and at what spatial and temporal scales, make the largest improvement to dust emission simulations in climate models.
3. Development and optimisation of the dust emission scheme for the Met Office regional model (HadGEM3-RA).

1.4.1.1 Grid Set up

Figure 1.12 Alpha-numeric grid set up, for the DO4 Field Site, hereafter referred to as the grid. Met Stations were located at each site (grey shaded) including anemometer mast, pyranometer, soil moisture profile, BSNE, DustTrak, depositional traps, while Automatic weather stations (red shaded) included all Met Station instruments in addition to instrumentation measuring temperature, relative humidity, net radiometer, soil temperature profile.

In order to assess these variables, the project required a 12×12 km (climate model grid scale) field site. The requirements were for an actively emitting, isolated dust source. A 144 km^2 grid (centred on 25.959°S, -20.5754°E, *Figure 1.12*) was selected on the Sua Pan within the Makgadikgadi Basin for two field seasons during the periods from July to October in 2011 and 2012. This site represents an undisturbed pan surface encompassing a range of surface typologies and crust types. For all samples analysed in this study, the alpha-numeric grid reference from the DO4 grid set up was utilised. The following summary table indicates the sample name, what analysis was performed on the sample as part of this study, and in what chapter the analysis can be found (*Table 1.2*).

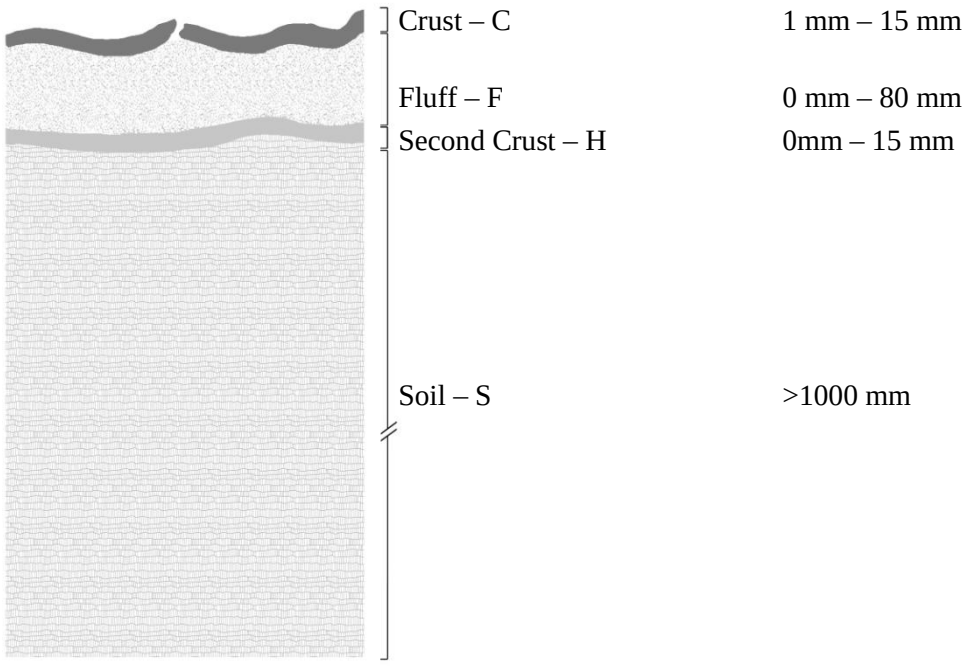

Figure 1.13 Schematic of the vertical structure of the pan indicating the location of the four sampling horizons considered in this study. Approximate measurements given for various depths of the sampling categories. Not all sampling horizons were present at all locations, see table 1.2 (further details can be found in Appendix 1).

Samples were all collected from the central point of each alpha numeric grid in close proximity to the instrumentation. Further information on field set up methodology and research design can be found in articles currently in preparation by the DO4 team.

Table 1.2 (pg 33) Table of all samples analysed in this study indicating the alpha-numeric naming system for samples from the grid. Samples are further labelled with a suffix indicating location within the sampling profile. 'C' indicates the sample is representative of the crust, 'F' the fluff, 'H' the second crust or the horizon crust which was found between the fluff and the wet soil 'S' layer which marks the lowest sampling category.

		Chapter 2 Size			Chapter 3 Chemistry		Chapter 4 Chemistry	Chapter 4 Size
		Screened	Malvern - Ethanol	Malvern - Water	ICP	XRD	QEMSCAN	Malvern - Ethanol
B3	B3 FRISBEE							
	B3C		X	X	X			
	B3F		X	X	X			
	B3H	-	-	-	-	-	-	-
	B3S		X	X				
B7	B7 FRISBEE							
	B7C		X	X	X			
	B7F		X	X	X			
	B7H	-	-	-	-	-	-	-
	B7S		X	X				
D2	D2 FRISBEE							
	D2C		X	X	X			
	D2F		X	X	X			
	D2H		X	X				
	D2S		X	X				
D5	D5 FRISBEE							
	D5C		X	X	X			
	D5F		X	X	X			
	D5H		X	X				
	D5S		X	X				
D10	D10 FRISBEE							
	D10C		X	X	X	X		
	D10F		X	X	X	X		
	D10H		X	X		X		
	D10S		X	X				
G2	G2 FRISBEE							
	G2C		X	X	X	X		
	G2F		X	X	X	X		
	G2H		X	X		X		
	G2S		X	X				
G6	G6 FRISBEE							
	G6C		X	X	X			
	G6F		X	X	X			
	G6H	-	-	-	-	-	-	-
	G6S		X	X				
I4	I4 FRISBEE						X	X
	I4C		X	X	X	X		
	I4F	X	X	X	X	X	X	X
	I4H		X	X				
	I4S		X	X				
I8	I8 FRISBEE							
	I8C		X	X	X			
	I8F		X	-	X			
	I8H		X	X				
	I8S		X	X				
J3	J3 FRISBEE	-	-	-	-	-	-	-
	J3C		X	X	X			
	J3F		X	X	X			
	J3H	-	-	-	-	-	-	-
	J3S		X	X				
J11	J11 FRISBEE							
	J11C		X	X	X			
	J11F	-	-	-	-	-	-	-
	J11H		X	X				
	J11S		X	X				
L5	L5 FRISBEE							
	L5C		X	-	X			
	L5F	-	-	-	-	-	-	-
	L5H	-	-	-	-	-	-	-
	L5S		X	X				
BSNE SAMPLES	SD200						X	X
	SD201						X	X
	SD202						X	X
	SD203						X	X
PiSwirl exhaust	I4PSE						X	X

1.4.1.2 DO4 Grid Instrumentation Overview

In order to understand the nature of the source, 11 sites were set up in the configuration indicated in Figure 1.12. At each site the following instrumentation was set up at each site during the field seasons in 2011 and 2012.

i. Anemometer mast
ii. SW/LW radiation
iii. Soil moisture
iv. Saltation counts
v. Horizontal dust flux
vi. Depositional dust flux
vii. PI-SWERL wind tunnel
viii. Crust properties

While the following were monitored at a selection of sites (see caption for Figure 1.12).

ix. Dust concentration
x. AOD (Cimel photometer)
xi. Terrestrial laser scanner

In addition to this, well measurements, water samples and sediment samples were taken which permitted for the analysis of:

- Shallow water chemistry
- Fluff and Crust chemistry
- Dust chemistry

In this study all samples were taken during the 2011 field campaign and therefore only represent a single season. Figure 1.14 illustrates a typical site set up. Cages were placed over the frisbees to deter birds from tampering with the sponge inserts. While this may affect the wind flow, the frisbee was collecting vertical fall out which should be largely unaffected by the presence of the thin wire cages. No further measures were taken to protect equipment during the two field seasons.

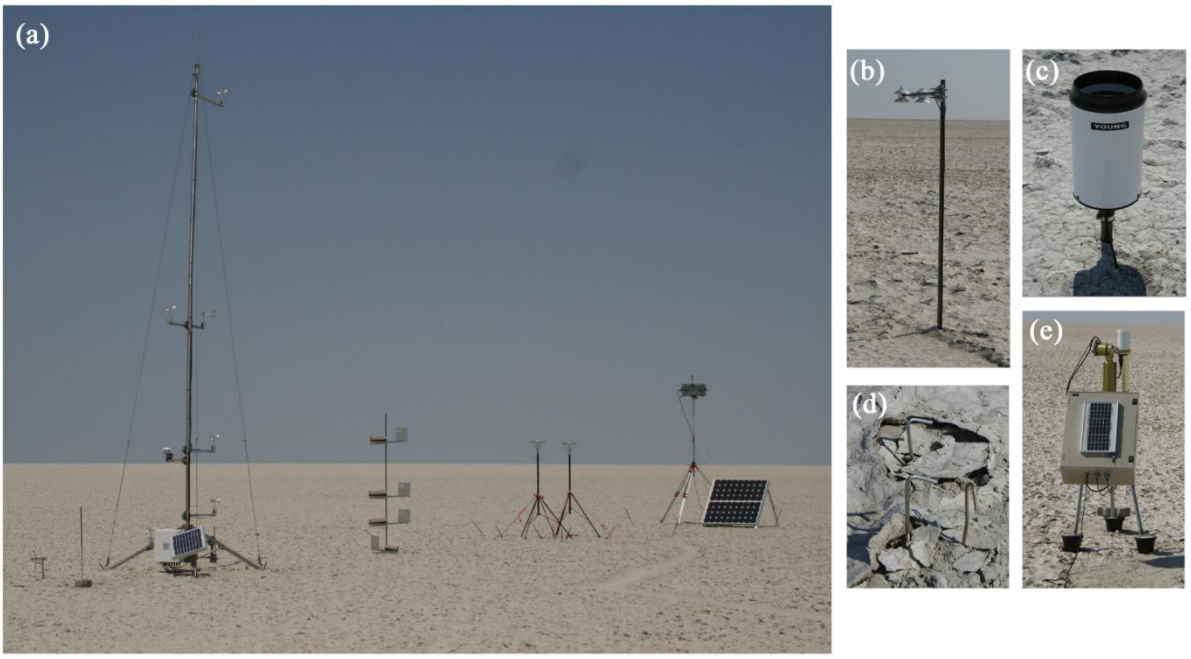

Figure 1.14 (a) Site I4 (Met g) as set up in the 2011 field season. In addition to the instrumentation indicated in the photograph, figure b, shows instrumentation monitoring incoming and outgoing solar radiation, c) shows the rain water gauge, d) the markers indication the location of ibuttons which measured temperature and e) the Cimel Photometer.

1.5 Concluding Remarks

This chapter has presented the aims and objectives of this study and introduced the field of dust research. In addition, this chapter has considered the importance of global and regional studies of dust, and established the location and field context for samples analysed within this study.

The literature review above has further highlighted the necessity of considering the multiple scales of the dust cycle as presented in Figure 1.2. In order to achieve this, it is important to develop an understanding of the nature of the sedimentary body, which includes aspects of particle morphology and mineralogy (Goudie et al., 1990). These structural components of the system develop the micro scale of the dust cycle which extends across a range of temporal scales. Derived through the field analysis of grain size and chemistry, it is at this scale that the dust cycle begins; through sediment formation to transportation either as a function of saltation, liberation or suspension (Pye, 1987). Therefore, these two structural components control the basic emissivity of the surface in the source region.

Assuming surface conditions are optimal for emission, the local scale of the dust cycle needs to be considered. This scale is associated with local transporting wind systems, which are responsible for entrainment (Durán et al., 2011). This local scale further links the micro-scale surface features with the larger scale climatic and radiative effects of dust (Shao et al., 2011). Further, at the intermediate scale, the spatial distribution of surface features can be seen to control emission from within the dust source. Bullard (2010) considered the importance of the intermediate scale when constraining models,

while Shao et al. (2011) indicate that at the local scale atmospheric turbulence and dust devils at shorter temporal scales result in dust storms as a function of days and months.

Integrating local and micro-scale data into global data is a necessary, but challenging, task. Thomas and Wiggs (2008) establish that aeolian research is a function of two disparate scales: small-scale investigations of process and sediments, and large scale landscape, landform and climatic scaled studies. Adding that it is knowledge of the intermediate scale, which integrates the small and large scale understanding of the system. Additionally, local scales can be expressed over a range of temporal periods. Shao et al. (2011) posit that our current understanding of dust at the global scale is primarily through the use of TOMS and other satellite products, adding that at a global scale we have the ability to model the radiative effects of dust (D'Almeida, Koepke & Shettle, 1991) as well as detect large plumes (Brindley et al., 2012) and transport pathways (Ashpole & Washington, 2013 Accepted). Shao et al. (2011) further indicate that micro-understanding is experiencing a resurgence in literature through the need for better quantification. However, it is at the local, intermediate scale where the current need for global data is required.

As indicated in the thesis outline, the following four chapters will all focus on different themes and aspects of Makgadikgadi sediments and emission controls in the region; with each section containing a more focussed literature review. Through the following chapters, aspects of scale, both temporal and spatial, will be considered which will increase our understanding of the dynamic Makgadikgadi Pans as a dust source. Chapter 2, 3 and 4 will consider the micro-scale understanding of the system, while Chapter 5 considers remote detection and associated links to climate systems; this is followed by a discussion at the intermediate scale which attempts to integrate our understanding of the pans as a contemporary dust system. This work is the first of its kind to measure the geochemistry at this resolution of an emissive dust site. In addition, it is the first study in southern Africa considering the geochemistry and morphology of sediments, integrating these findings into the synoptic meteorology of the region. Consequently this study presents both methodological advances and increases our understanding of processese active at the source.

Chapter 2: Grain size, Theoretical and Methodological Considerations

Acronyms used in this chapter:

psd – Particle Size Distribution

MSA – Mechanical Sieve Analysis

LDM – Laser Diffraction Method

PIDS – Polarisation Intensity Differential of Scattered Light

LUE – Laser, Unprocessed, Ethanol dispersant

LUW – Laser, Unprocessed, Water dispersant

LDW – Laser, Digested, Water dispersant

2.1 Introduction:

Grain size is the one of the most fundamental property of sediments, affecting their entrainment, transport and deposition (Blott & Pye, 2001). Therefore, grain size analysis can be used to provide important indicators into the nature of the sediments, their transport history and depositional conditions (Folk & Ward, 1957; Blott & Pye, 2001). Various techniques have been used, including direct measurements, wet and dry sieving, sedimentation, and, more recently, laser granulometry and counters. All these methods have been noted to be descriptive of different aspects of the particle and, in addition to shape, are influenced by density, volume and optical properties. These methods are, however, united by the ultimate aim of organising the observations into size fraction groupings, which allows for the analysis of grain size distributions. The following chapter will consider theoretical and methodological considerations for calculating grain size. This will be followed by a presentation of the grain size results for a single site within the DO4 grid as part of the Makgadikgadi Pan. Using a combination of traditional and modern methods alongside various dispersants on a single sample revealed a number of methodological differences.

2.1.1 Grain Size

The most important starting point for an explanation of many geomorphological processes is through the description of the basic properties of the geomorphologic material in question. Goudie et al. (1990) propose that for a deposited sedimentary body, the material is typically a function of directional properties, geo-technical properties, sedimentary structures and, finally, properties of particles and matrix (*Figure 2.1*).

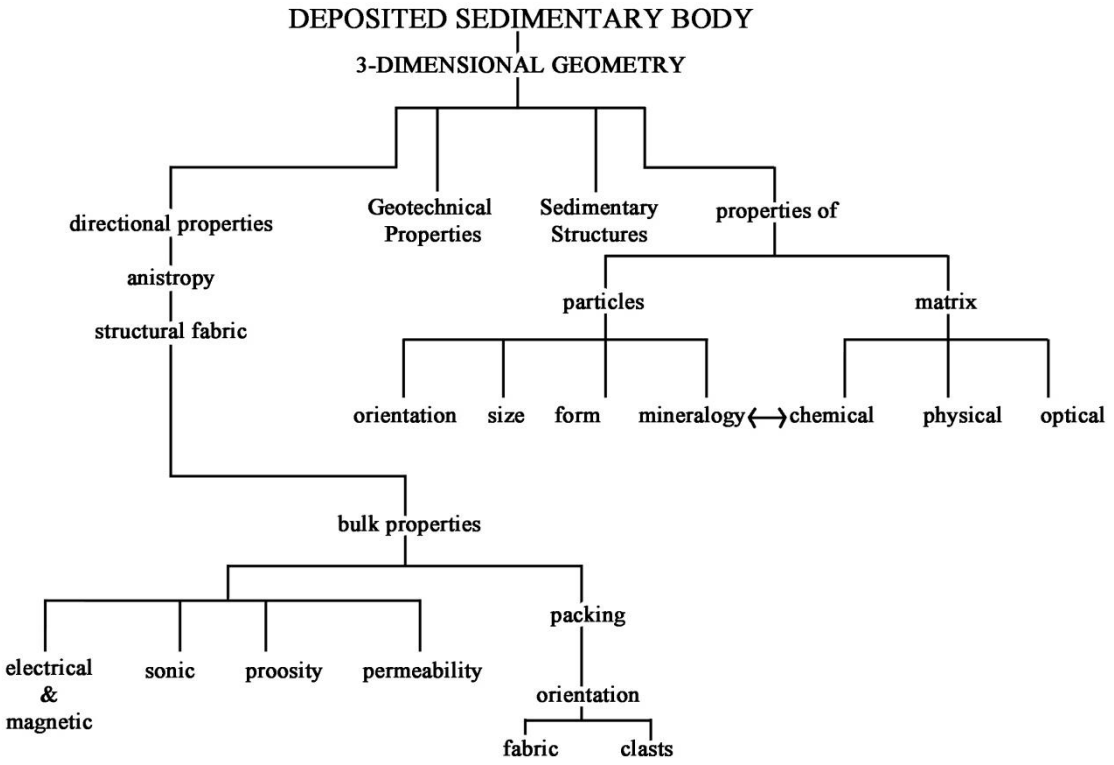

Figure 2.1 Ways of viewing the properties of a sedimentary body, adapted from Goudie et al. (1990).

Blott and Pye (2001) add that the most well considered basic physical property is the measurement of particle size. However, the simple classification of particle size is problematic due to the number of definitions for measurement with particles being complex three dimensional objects. Thus single measurements fail to capture their true nature (Konert & Vandenberghe, 1997). The following definitions for grain size are presented by Goudie et al. (1990):

a) The width of the smallest square or diameter of the smallest circular opening through which a particle can pass;
b) The diameter of a circle whose area is equal to that of the maximum projected area (MPA) of the particle
c) The diameter of a sphere whose volume equals that of the particle
d) The diameter of a sphere whose settling velocity and density in a given fluid equal those of the particle; as well as
e) The longest axis/dimension of the particle

These definitions are based on classical methods of grain size determination and can be seen to relate largely to spherical particles. Spheres are used as they can be unambiguously and quantitatively defined by a single dimension, the diameter (Blott & Pye, 2001). However, spherical grains are not characteristically found in natural soils or clay environments (Goudie et al., 1990). As such, issues of shape and morphology are considered to be important constraints for the determination of grain size.

The measurement methods as presented by Goudie et al (1990) with the exception of the last point transpose the dimensions of the irregularly shaped grain according to the concept of equivalent spheres (*Figure 2.2*). The equivalent sphere of an irregular shape, presents the grain size as a function of, or functions of, the properties of particles and matrix (Allen, 1975). However, it is evident that the equivalent sphere will differ between measurement techniques (Konert & Vandenberghe, 1997). Despite this, the equivalent sphere method is able to produce a single dimensional measurement from which a particle can be described and therefore compared (Allen, 1975).

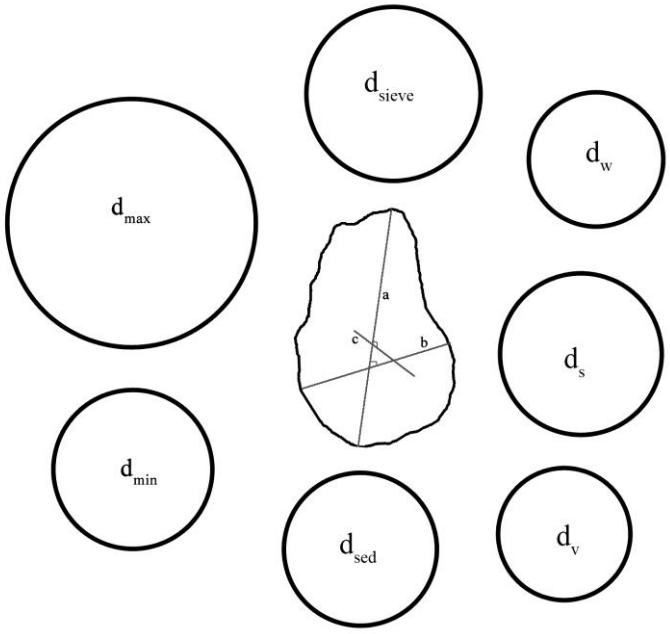

Figure 2.2 Illustration of the concept of equivalent spheres revealing the seven spheres which are proposed for the grain with dimensions a perpendicular to b and c. d_{max}: sphere of same maximum length a; d_{min}: sphere of same minimum length b; d_{sieve}: sphere passing through equivalent sieve aperture; d_w: sphere of same weight; d_s: sphere of same surface area; d_v: sphere of same volume; d_{sed}: sphere having same sedimentation rate (Adapted from Malvern Instruments Limited, 2012).

The Goudie et al. (1990) definitions can then be re-classified using the equivalent spheres as in Figure 2.2 to become:

a) d_{sieve}
b) d_{max}
c) d_v
d) d_{sed}
e) d_{sed}

These definitions are a function of the means of analysis with each technique measuring different aspects of the grain and therefore presenting different equivalent spheres. Allen (1975) comments that the method of analysis should be carefully considered in order to, where possible, measure the most

useful projection for study. Once the best equivalent sphere for the sample has been determined, the particle is represented by a perfect sphere and can be described by its diameter. This measurement can then be represented on the grain size scale which classifies grains based on the division of a continuous range of particle sizes into a series of discrete groups. Several such scales have been devised for the purpose of standardising terms and providing a basis for statistical analysis (Blott & Pye, 2001).

Despite the apparent need for standardisation, the size ranges differ slightly by scientific affinity (Allen, 1975), although there is mostly agreement on qualitative grain descriptions. The various classifications place clay at the finest end of the spectrum, getting coarser through silt and sand to gravel or pebbles, then cobbles and finally classifying boulders as largest descriptor of grain sizes (*Table 2.1*).

Table 2.1 Size scale adopted by Blott and Pye (2001) as used in the GRADISTAT program, compared with those previously used by Udden (1914) and Wentworth (1922) (Adapted from Blott and Pye, 2001).

Grain Size		Descriptive Terminology		
phi	mm or µm	Udden (1914) & Wentworth (1922)	Blott and Pye (2001)	
-11	2048 mm	cobbles	very large	Boulder
-10	1024		large	
-9	512		medium	
-8	256		small	
-7	128		very small	
-6	64	pebbles	very coarse	Gravel
-5	32		coarse	
-4	16		medium	
-3	8		fine	
-2	4	granules	very fine	
-1	2	very coarse sand	very coarse	Sand
0	1	coarse sand	coarse	
1	500 µm	medium sand	medium	
2	250	fine sand	fine	
3	125	very fine sand	very fine	
4	63	silt	very coarse	Silt
5	31		coarse	
6	16		medium	
7	8		fine	
8	4	clay	very fine	
9	2		Clay	

The requirement for a standardised scale was identified by American sedimentary petrologist Udden in 1898, (Udden, 1914) although it was subsequently adapted by Wentworth in the 1920s (Wentworth,

1922). The Wentworth scale, expanded the definitions of the various grades. Table 2.1 presents the Udden and Wentworth size range and grain descriptors together with the terms used in this study as used in Blott and Pye (2001). This classification was adopted in this study as it is focused on the nature of the sediments on the Makgadikgadi Pans since the environment is largely associated with sand and silt sized grains. Meaning that the greatest descriptive resolution was required for these finer grains.

2.1.2 Methods of Grain Size Determination

Over recent decades, various methods for grain-size analysis have been developed. Despite this, traditional sieving, as pioneered by Udden (1898), remains most widely used. The other traditional method that is still largely utilised in the pipette method. Modern methods include: electroresistance particle counting (e.g. Coulter Counter), X-ray attenuation (Sedigraph) and laser diffractrometry (e.g. Malvern Laser sizer) (*Table 2.2*). However, Di Stefano et al. (2010) add that all these approaches define the 'size' of a particle in different ways, utilising various aspects to create the equivalent spheres. As a result, there is an extensive range of literature presenting theoretical considerations as well as comparing various means of psd determination (e.g. McCave et al., 1986; Konert & Vandenberghe, 1997; Beuselinck et al., 1998; Goossens, 2006; Goossens, 2008; Di Stefano et al., 2010).

*Table 2.2: Summary of major methods utilised in similar grain size studies, including the sphere of interest measured. An * indicates the methods considered in this study.*

	Technique		Sphere of interest	Size range	Data resolution
Traditional	Sieving	*	d_{sieve}	20 - 200 µm	Coarse
	Pipette		d_{sed}	< 75 µm	Coarse
Modern	Electroresistance particle counting (e.g. Coulter Counter)		d_{vol}	0.6 - 150 µm [a]	Very high
	X-ray attenuation (Sedigraph)		d_{weight}	1 - 30 µm	Moderate
	Laser diffractrometry (eg. Malvern Laser sizer)	*	d_{max}	0.045 - 2000 µm	Very high

* Indicates approaches considered in this study

[a] set up dependant

Despite the wealth of literature and all the advances in both the methodological and technological determination of psd there remains no consensus on method or classification. Literature classifications of samples range from simple classifications of single grains or grain size groupings, to statistical analysis of grain morphology and associations (Folk, 1966; Livingstone & Warren, 1996; Blott & Pye, 2001; Goossens, 2007).

Due to the number of methods considered in literature, their benefits and shortcomings along with availability were considered before selecting the best means of determining the grain size distribution

of salt rich dust samples from the Makgadikgadi Pans (For further information on the efficiency and reliability of the different approaches see Di Stefano et al. (2010), Goossens (2007) and Buurman et al. (2001)).

While each method of grain size determination has advantages and drawbacks, the choice should depend on the nature of the problem to be solved (Allen, 1975; Goudie et al., 1990). For this reason, a synergy of approaches is presented in order to determine the most appropriate and representative method of surface conditions. Therefore, traditional sieving and modern laser diffraction methods will be considered, along with pre-processing and the effects of dispersants which will be measured which add to the variability of results experienced when presenting the grain size distributions for a sample.

The following section will introduce the principles behind traditional mechanical sieve analysis and modern laser diffraction before a review of different representations of sample processing and preparation.

2.1.2.1 Methods of Grain Size Analysis: Traditional Sieve Analysis and Modern Malvern

i. Traditional Mechanical Sieve Analysis (MSA)

Sieving is probably the easiest, most widely used method of size analysis (Allen, 1975). This traditional method was proposed to be more accurate for measuring larger grain sizes (>75 µm), while the pipette method was used for the finer fraction and the two results combined (Konert & Vandenberghe, 1997). Allen (1975) suggested that it was the cost of producing finer sieves that determined the lower limit, while subsequent research (Konert & Vandenberghe, 1997) indicated that accuracy and calibration are greater limiting factors. For analysis, stacks of sieves in ascending size order are placed over a closed pan. Once the sample is introduced to the stack, manual or mechanical agitation fractionates the sample. This is labour intensive and was often poorly representative of the whole sample (Goudie et al., 1990). Additionally, authors note that the sieve method is particularly affected by the following factors: the calibration of the sieves, the shape of the particles, chemical and mechanical stability and uniformity in density and porosity. Additionally, Konert and Vandenberghe (1997) state that shape and orientation as presented to the sieve mesh will determine whether the particle will pass through the sieve; with sample weight and sampling time being of further consideration for methodological reflection (Allen, 1975).

Sieves are shown to represent finer grains poorly, which were indicated as better represented through the pipette method, an additional limitation of combining the two traditional methods to produce a unified particle size distribution curve can be observed through a comparison of the equivalent spheres measured. While for sieving, maximum breadth and thickness are considered resulting in

d_{sieve}, for the pipette method grain volume is more important (Di Stefano et al., 2010) with the resulting equivalent sphere best represented by d_{sed} or d_{volume} (*Figure 2.2*).

Therefore methodological consideration needs to include the best means to determine a unified curve considering a single equivalent sphere across the whole distribution. Technological advancements and the need for faster and more efficient means of producing such results, have led to the development of modern laser methods. The following section will therefore present the principles and methodological considerations of modern methods.

ii. Modern Laser Diffraction Method (LDM)

The modern Laser Diffraction Method (LDM) for grain size analysis is based on the principle that particles passing through a laser beam will scatter light at an angle that is directly related to their size (Loizeau et al., 2006). Principally based on the Mie Theory and the Polarisation Intensity Differential of Scattered Light (PIDS) (McCave et al., 1986; Lee Black et al., 1996; Ma et al., 2001; Loizeau et al., 2006), the PIDS system measures the light scattering intensity sequentially at two perpendicular optical polarisation angles at multiple angles of detection (Buurman et al., 1997). The difference between the intensities is proportional to the amount of particle material at one third of the wavelength of the light used. Loizeau et al. (2006) add that smaller particles scatter at higher angles then larger grains, therefore, using six angles of detection (Buurman et al., 1997) the lower limit can extend to 0.045 µm, while the upper limit is reached at 2000 µm. This allows LDM to detect fine grains with greater accuracy than traditional methods. However, similar to traditional methods, the output is based on the assumption that the particle is morphologically spherical (Di Stefano et al., 2010). Therefore the further from spherical the grains are the less accurate the detection becomes (Buurman et al., 1997). Although a single representation of an equivalent sphere is applied to the whole distribution.

Most modern laser diffraction methods present the d_{max} of the grain (*Figure 2.2*), meaning that calculations of particle volume are often poor, especially at the finer fraction, as clay grains are rarely spherical. Konert and Vandenberghe (1997) suggest that clays are commonly platy in shape and their orientation results in their size often being over-estimated. In order to reduce the bias of grain morphology on detection, the size distribution is measured while the suspension is continuously pumped around. This is reported to ensure random orientation of most particles relative to the laser beam (Beuselinck et al., 1998).

Despite issues of orientation, LDM is far superior in its ability to detect over a wide range of sizes (Konert & Vandenberghe, 1997) and with greater detail. Like traditional methods, a number of assumptions are made during analysis (e.g. Konert & Vandenberghe, 1997; Di Stefano et al., 2010):

i. The transformation of diffraction patterns to grain sizes is based on matrices, which are calculated for spheres.
ii. Orientation is assumed to be random, but often measurements take place in a continuous flow of particles in which the particle may be orientated, with respect to its shape.
iii. The diffraction pattern to grain size distribution is calculated from diffraction by the particles and differences in absorption and refraction indices have no effect on the calculated grain size distribution (Konert & Vandenberghe, 1997).
iv. Samples are assumed to have homogenous density and to be well flocculated (Buurman et al., 1997).

LDM has the additional advantage of permitting a range of processing environments, both dry (Di Stefano et al., 2010) and wet (Goossens, 2007). With Goossens (2007) commenting that in wet analysis particles can be run in a variety of dispersants ideally when the material has a high refractive index relative to the dispersive medium.

A significant benefit of the modern laser diffraction method is the large range of size fractions which can be determined requiring small sample sizes, relatively quickly (Buurman et al., 1997). However, grain size by laser diffraction cannot replace the classical combination of sieving and sedimentation as correlations between methods have not been established for many populations of samples (Buurman et al., 1997). Buurman et al. (1997) add that comparing medians is problematic between screening and Malvern for two reasons. Firstly the number of size fractions calculated differs greatly, precluding exact calculation of concurrent medians, and secondly, the methods determine differing equivalent sphere of the grain.

This introduces the requirement for understanding not only the properties of an individual grain but of the whole sample. Allen (1975) comments that there are a number of methods for presenting size analysis data, each revealing different aspects of the distribution. Additionally, as many geomorphological processes (e.g. frictional velocity, entrainment and emissivity of surface) require knowledge of not only the mean grain size of the surface sediments, but also statistical parameters of size distribution and contributions of grain classes, these parameters together with the sample distributions, particularly the relative contributions of sand, silt, and clay sized grains, are often required. Therefore, having considered the methods of determination of psd, equal consideration needs to be placed on presenting the results accurately and effectively of the psd through statistical and graphical representations.

2.1.2.2 Methods of Presenting Size Analysis Data: Statistical and Graphical Results

A number of methods exist for the presentation of size analysis results including tabular and pictorial presentations (Allen, 1975). With Folk (1966) expounding that once data has been obtained from the various laboratory methods it becomes possible to represent the results in multiple forms, including:

i) some type of graphical output permitting qualitative and trend analysis of the sample, and
ii) statistical parameters which can be determined creating a numerical representation of the data – namely through kurtosis, skewness, means, modes, medians and quartiles.

Allen (1975) suggests that the significance of distributions is more easily grasped when the data is presented pictorially, the simplest form of which is the histogram (e.g. *Figure 2.4*). While graphical displays of data can reveal trends, the authors confirm tabular data (e.g. *Table 2.6*) as a fundamental means of representing data. Critical to both of these methods is the selection of size grading and class intervals (Folk, 1966; Allen, 1975; Allen, 1985; Konert & Vandenberghe, 1997; Blott & Pye, 2001), with various authors considering both arithmetic and geometric progression. Arithmetic progression will classify sizes with greater size intervals for smaller particles while geometric size intervals are independent of particle size (Allen, 1975). Consequently, arithmetic grain scales are seldom used in sedimentology, favouring geometric scaling which provides equal emphasis to small changes in fines to larger changes in coarser grains (Blott & Pye, 2001).

While the benefits of traditional display methods are known, quantitative analysis of samples has been presented as the best means of trend analysis, revealing key aspects of the sample origin and nature (e.g. Blott & Pye, 2001; Speirs et al., 2008). The two main quantitative statistical methods considered by Blott and Pye (2001) are the method of moments and the graphical method.

The method of moments was described by Folk (1966) to be the most 'mathematically elegant' (Folk, 1966: 78) measurement of frequency distribution. With this method determining distribution from the entire sample rather than using percentiles, thereby identifying a distribution based on the frequency distribution of a class about the mean. However, there are serious shortcomings to this 'elegant' description in its inability to equally weight the finer size fractions in natural, poorly mixed sediments. While the Folk and Ward graphical method produces better statistical results and sorting values on less well sorted sediments (Blott & Pye, 2001), as surface sediment samples are rarely well sorted and with the nature of dust being in the finer size range (Pye, 1987), the mathematical 'elegance' of the method of moments methods was not used instead favouring the graphical method.

Therefore, in this study grain size information will be derived using the graphical geometric methods of Folk and Ward (1957) using the GRADISTAT statistical package (Blott & Pye, 2001). For details on statistical terms used in this chapter see Appendix 2.

2.2 Methods

To compare the psd calculated for the two methods used for analysis, namely laser diffraction (LDM) and mechanical sieve analysis (MSA). The two methods were performed on a sample of fluff sampled from I4. The sample, I4F, represents a surface grab sample of fluff taken in 2011 from the site I4 within the DO4 field site (See Chapter 1, Section 1.4 and Appendix 1), with a total sample mass of 334 g. While every effort was made to ensure that the integrity of the sample was not compromised during transport, temperature and moisture conditions varied from source region which could account for chemical and physical changes through hydration, dehydration and physical destruction.

To allow for the multiple levels of analysis that were proposed for the sample, it was initially split using the PT100 Retsch 10 tube sample divider. Eight out of the ten tubes were combined for traditional sieve analysis. One tube sample was resealed for chemical analysis, while the remaining tube sample, with a mass of 33.4 g was sub-sampled using an 8 tube Rotary Micro Riffler with the components set aside for various pre-treatments for laser diffraction analysis (*Figure 2.3*).

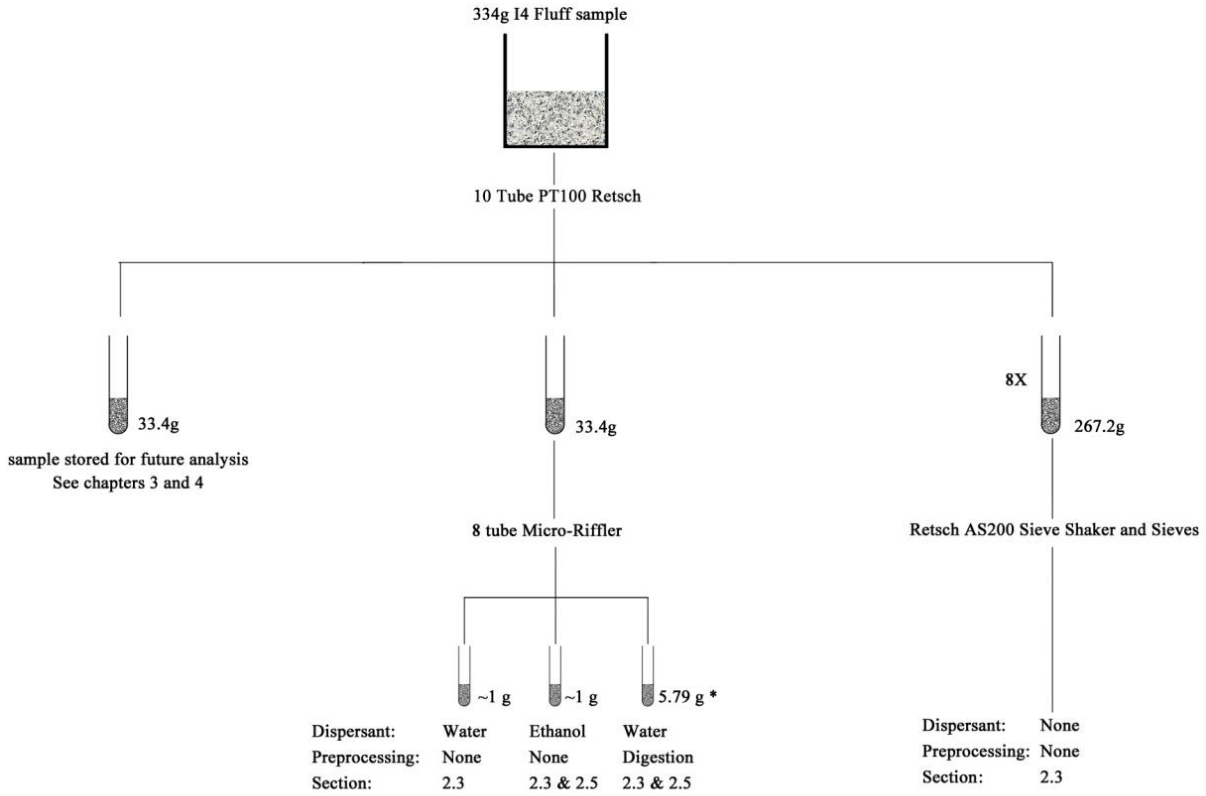

*Figure 2.3: Schematic of the sub-sampling for the sample of I4 fluff. Schematic indicates the methods of splitting, and where details of the sample can be found within this study (indicated by section number or chapter). Dispersants and pre-processing is also indicated for all samples analysed in this chapter. The * indicates the sample mass pre-digestion, following digestion the sample was split with ~1 g of sample being used for grain size analysis.*

Some factors which affect both the LDM and MSA detection were tested before comparing the psd obtained by the two techniques. In particular the following effects were considered:

a. The size of the sample used in MSA analysis

Due to the size of the sieve frame and the assumed fine nature of the sample it was proposed that a sample in excess of 200 g be used to provide statistically significant results (Goudie et al., 1990). Using too large a sample is proposed to limit the accessibility of all samples to the sieve mesh, while too small a sample is proposed to be no longer representative of the original material.

b. The wet or dry sieving in MSA analysis

Dry sieving is known to be less robust then wet sieving below 100 µm (Barth & Sun, 1985), however due to the high salt content of the samples, wet sieving would result in significant changes to the chemical composition and physical properties of the sample and dry sieving was determined to be necessary.

c. The pre-treatment of samples in LDM analysis

Various pre-treatment methods were used in LDM analysis, they will be presented below and the merits of each discussed.

d. The dispersant used during LDM analysis

Like pre-treatments, two dispersants were used: water and ethanol; the results of both will be presented and the merits of each with be discussed.

2.2.1 Mechanical Sieve Method

Traditional sieving was performed using calibrated, sterilised Retsch stainless steel wire gauze sieves and collection trays on the Retsch AS200 vibratory sieve shaker. The manufacturers claim that the throwing motion with angular momentum provides high separation efficiently and the analysis of grains ranging from 20 µm to 2500 µm (Retsch GmbH, 2012).

Eight screens were stacked with a stainless steel catching tray below the smallest screen. Screen sizes measuring 2000 µm, 150 µm, 106 µm, 75 µm, 53 µm, 38 µm and 25 µm were used. Table 2.3 presents the size ranges that could be determined as well as the size range classification contained within each range. The largest screen was used to ensure that no samples contained grain sizes in excess of 2000 µm which is beyond the range of Malvern. As the focus of this study is to determine the psd of sediment with emissive potential, there was an increase in the number of screens measuring the smaller spectrum of samples.

Table 2.3: Grain size ranges as determined by mechanical sieve analysis and the associated size range classifications in accordance with Wentworth (1922) and Blott and Pye (2001).

	Size range classification	
Grain Size Range	Lower limit	Upper limit
> 2000 µm	Very coarse sand	Gravel/boulders
150 µm to 2000 µm	Fine sand	Very coarse sand
106 µm to 150 µm	Very fine sand	Fine sand
75 µm to 106 µm	Very fine sand	Very fine sand
53 µm to 75 µm	Very coarse silt	Very fine sand
38 µm to 53 µm	Very coarse silt	Very coarse silt
25 µm to 38 µm	Coarse silt	Coarse silt
< 25 µm	Coarse silt	Clay

All samples were stored in a drying oven at 20°C for 12 hours prior to screening to reduce contamination from ambient moisture introduced to the sample post sampling. No further pre-treatments or processing was performed on the samples. For analysis, the sample was placed in the sieve for 40 minutes at a sieve vibration height of 40 Hz. This was determined to be the optimal height for sand and silt sized grains (Retsch GmbH, 2012). The longer duration of running was chosen to permit the most accurate determination of psd. Samples were then brushed out of the screens and placed in pre-weighed and labelled sample jars.

2.2.2 Laser Diffraction – Malvern Method

The Malvern Mastersizer 2000 was used for the laser diffraction grain size measurements in this study. The manufacturers claim a working range of 0.02 µm to 2000 µm. All particles give diffraction in all directions using Mie and Fraunhofer scattering with a Reverse Fourier (convergent beam) lens arrangement (Malvern Instruments Limited, 2007). Thus light scattered by particles outside the measured range affects the results over that measured range. For this reason all samples were pre-screened to remove grains over 2000 µm; unless otherwise stated no samples contained grains in excess of this upper limit. Accuracy is quoted by the manufacturer to be better than 1% with less than 1% variation in reproducibility under minimal user error.

Approximately 1 g of the sample was split off using an 8 tube Rotary Micro Riffler and placed in a labelled jar (*Figure 2.3*). A Standard Operating Procedure or SOP was set up using quartz (silica) as the base refractive constituent of the sample with a refractive index of 1.544. This SOP could be used for both water and ethanol processing, with the dispersant conditions set before processing the sample. For ethanol, a refractive index of 1.36 was used while water has a value of 1.33 (*Table 2.4*). Knowledge of the refractive index of the sample and the dispersant are essential as they affect the associated absorption of the laser beam and polarised light and therefore define the optical model used for detection (Malvern Instruments Limited, 2012). As refractive values for both dispersants

significantly differed from that of the base refractive constituent (1.544 silica), with the dispersant values lower (1.33 water and 1.36 ethanol) the readings are proposed to have great accuracy potential (Goossens, 2007).

Table 2.4: Conditions of Standard Operating Procedure and conditions determined for LDM analysis.

Standard Operating Procedure (SOP)		
	Constituent	Refractive Index
Base Refractive Constituent	Silica	1.544
Dispersant	Water	1.33
	Ethanol	1.36
Operating Conditions		
Obscuration	10 - 13 %	
Weighted residual	<1	
Pump speed	1400 rpm	
Number of readings taken	3 per sample and an average	
Time between readings	10 seconds	

For all sampling, an obscuration value of between 10% and 13% was obtained, which allowed results from multiple runs, using various dispersants to be comparable. As obscuration refers to the suspension density within the dispersant, it is dependent on grain size and therefore the sample mass required for analysis varied. Buurman et al. (1997) note that clay contributes strongly to the overall obscuration of the sample and therefore finer samples required less sample mass to obtain the same level of obscuration. It was therefore, essential that samples were added in small increments to ensure a stable and statistically significant obscuration. A weighted residual value of 1 or less was accepted with smaller values being optimal. Three readings were taken with a 10 second time interval between readings for each sample. The results of each reading as well as an average of the three were recorded for all samples. For the Hydro 2000SM a manual sample stirrer speed of 1400 rpm was set as this was determined to be the point at which particle size detection reached a plateau, below this speed the particle sizes were too low suggesting that the pump rate was not fast enough to suspend the larger particles (these values were determined through correlation with MSA analysis). A speed of 1400 rpm was assumed to be the point at which a selection of all particles was correctly presented to the measurement cell for reading (high speeds have the potential to break down the sample). Similar conditions were set for the Hydro 2000G.

Mastersizer output, providing results between user sizes from 0.012 µm and 2000 µm, was extracted for all samples. Due to the resolution required for this study the data was later refined into the 11 size classes in accordance with Blott and Pye (2001) (*Table* 2.5). The classes provided greater resolution to analyse the sample than those extracted using traditional sieve analysis (*Table 2.3*).

Table 2.5: Grain size ranges as determined by GRADISTAT output (Blott and Pye 2001). These classes have the benefit over those shown in Table 2.3 of an increased resolution towards the finer range of grain sizes.

Grain Size Range	Size range
1000 µm to 2000 µm	Very coarse sand
500 µm to 1000 µm	Coarse sand
250 µm to 500 µm	Medium sand
125 µm to 250 µm	Fine sand
63 µm to 125 µm	Very fine sand
31 µm to 63 µm	Very coarse silt
16 µm to 31 µm	Coarse silt
8 µm to 16 µm	Medium silt
4 µm to 8 µm	Fine silt
2µm to 4 µm	Very fine silt
< 2 µm	Clay

2.2.2.1 Ethanol Processing:

For processing with ethanol as the dispersant, the Hydro 2000SM Malvern attachment was linked to the system. This smaller device is manually flushed and refilled and has a dispersant volume capacity of approximately 200 ml. To process each sample, the tank is pre-washed with ethanol and then approximately half filled using 100 ml of ethanol. The sample is then added slowly until the obscuration reading was stable (as displayed on the graphic display on the computer). A wait of three seconds was observed before the analysis was started. For ethanol processing approximately 0.4 – 0.5 g of sample was required.

2.2.2.2 Water Processing:

For processing in water, the standard Hydro 2000G Malvern attachment was used. This larger device has a capacity of 800 ml and was automatically flushed twice between each sample run. The sample was slowly added until the obscuration reading was stable (as displayed on the graphic display on the computer). An automated wait of three seconds was imposed before the analysis was started. For water processing approximately 0.5 – 0.7 g of sample was required to achieve the 10% to 13% obscuration level.

2.2.2.3 Digestion – Pre-processing

For this analysis ~5 g of sample was split out for analysis. The sample was oven dried to measure dry weight for consistency. While pre-treatments are known to remove aggregating agents such as soluble salts, carbonates and organic matter (Soukup et al., 2008b), there exists a trade-off in using pre-treatments. These include the removal of components which are intrinsically constituents of the soil (Buck et al., 2006) and the further risk of altering other minerals within the sample matrix. Despite

these risks it was decided to pre-treat samples to remove soluble salts, carbonates and organics. As the removal of organic matter required acidic conditions (Soukup et al., 2008b) it was determined that this should be the final step with the first process removing soluble salts, followed by carbonates and finally the organics (see Appendix 3).

2.3 Results

The results below will consider various representations of grain size for the sample collected at I4. Firstly, (section 2.3.1) traditional mechanical sieve analysis will be compared with modern laser diffraction methodology using the methods on samples with differing levels of pre-treatment. The second section (section 2.3.2) will consider the effects of pre-treatment in explaining sample grain size distributions.

2.3.1 Laser Diffraction Method vs. Mechanical Sieve Analysis

Two hundred and sixty seven grams of I4F sample were placed in the Retsch sieves and run according to the protocol developed for this study (see section 2.2.1). Weighing the samples from each sieve level revealed that 183.1g or 68.45% of the sample occupied the range greater than 150 µm with no sample greater than 2000 µm. This was the largest contributing size range for the dry sieved, unprocessed sample. Thereafter, the percentage of sample in each size fraction decreased with 13.43% sized between 106 µm and 150 µm, 8.06% between 75 µm and 106 µm, 4.27% between 53 µm and 75 µm, 3.21% between 38 µm and 53 µm, 2.29% between 25 µm and 38 µm and the remaining 0.29% smaller than 25 µm – this final size range weighed 0.785 g (*Table 2.6*).

Table 2.6: I4 Fluff, Sieve and laser results for four methods of grain size distribution methodologies. Statistical results extracted from Blott and Pye (2011) using the Folk and Ward method.

	Sieve	Laser		
Processing	Unprocessed	Unprocessed	Unprocessed	Digested
Dispersant	None	Ethanol	Water	Water
Size ranges	% Contribution to each grain size range			
<25µm	0.29	3.37	19.39	83.67
25 -38µm	2.29	2.17	6.43	10.63
38-53µm	3.21	4.43	8.55	3.90
53-75µm	4.27	8.13	11.31	1.45
75-106µm	8.06	7.79	13.65	0.30
106-150µm	13.43	15.01	13.87	0.05
>150µm	68.45	59.02	26.81	0.00
	Statistical Results (µm)			
mean	>150 µm	191.76	64.13	9.15

This trend was very similar to the results obtained through the LDM method using the unprocessed sample with ethanol as the dispersant (*Table 2.6, Figure 2.4*), where 59% of the sample occupied the 150 µm to 2000 µm size range, with 15% (106-150 µm), 7.8% (75-106 µm) a slightly higher percentage in the 53-75 µm range at 8.1%, again decreasing to 4 % in 38-53 µm and 2% in the 25-38 µm range. Despite the proposed limitations of sieving to detecting fines (Goudie et al., 1990), there was a slight increase with 3% of the sample found to be below 25 µm. Careful consideration of sample size and running time are proposed to have resulted in high sampling efficiency. Both of these methods present a unimodal curve skewed to the larger size range.

The LDM method with water as the dispersant provided quite different results (see *Table 2.6*, *Figure 2.4*). Unprocessed in water, the resultant distribution was nearly bimodal with peaks in both the fine and coarse ranges with almost 20% of the sample in the <25 µm range and 27% in the >150 µm range. Similar to both MSA and the unprocessed ethanol sample, 50% of the sample remained larger than 75 µm.

The processing which resulted in the finest psd was the digested sample. For the digested sample almost 84% was in the finest size range (<25 µm) with less than 2% of the sample greater than 53 µm. This unimodal distribution represents a sample dominated by silt and clay sized grains.

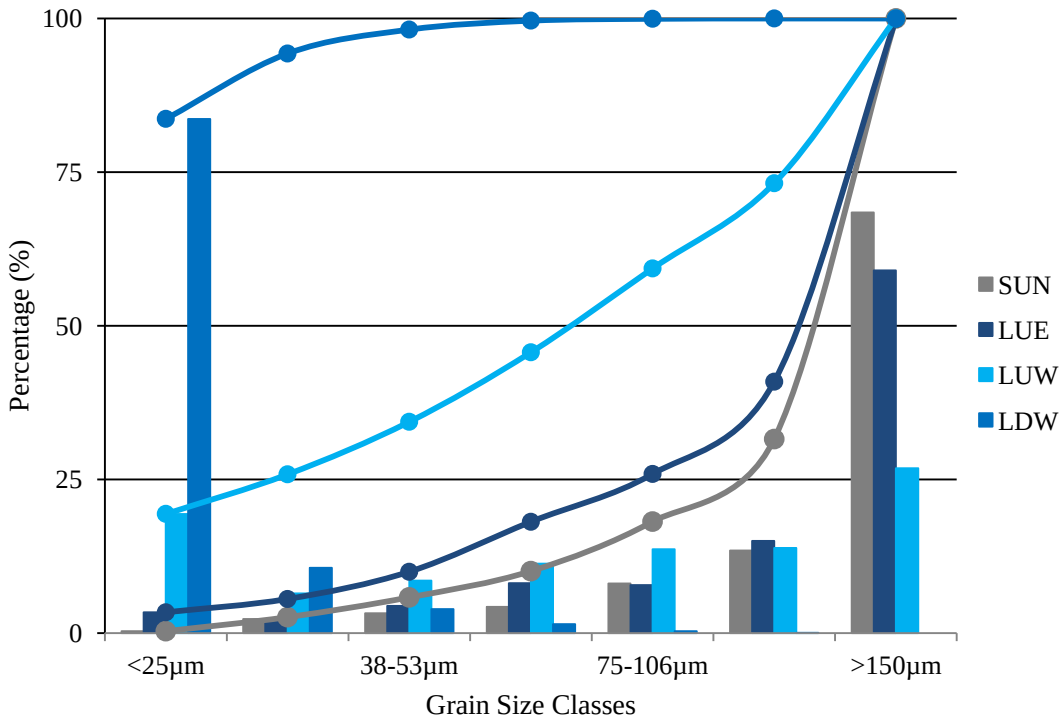

Figure 2.4: Graphical display of sieve and laser results for four methods of grain size calculation for I4 Fluff. Vertical axis values represent percentages while horizontal axis shows sieve size ranges. SUN (Sieve, unprocessed, no dispersant); LUE (laser, unprocessed, ethanol dispersant); LUW (laser, unprocessed, water dispersant); LDW (laser, digested, water dispersant).

As sieve analysis is restricted by the number and availability of sieves to determine bin ranges; it limits statistical analysis that can be performed on sample trends. However, it can be determined that 50% of the sample (the mean) lies above 150 µm. Conversely for the laser methods, mathematical and statistical values can be extracted. The Folk and Ward method (Blott & Pye, 2001) revealed that for the laser unprocessed ethanol the mean was 191 µm while it was significantly smaller for two water processed samples, with means of 64 µm for undigested and 9 µm for digested, run in water.

From the above results it can be seen that while the MSA method can present trends in grain size and produce basic statistical results, LDM provides greater detail. Despite this, the presence of traditional methods continues in literature. The limitations of multiple methods are considered in Blott and Pye (2001) further revealing the difficulties in merging data obtained from different methods. Therefore a single product was determined to best represent grain size. The increased information available on the finer grain sizes using LDM, together with the increased number of grain size classes offered by LDM resulted in the selection of this method. The following section will therefore present the results obtained from LDM using various methods of processing.

2.3.2 Digested, Undigested and Water as a Dispersant for Sample Preparation

Three samples of I4 were run using LDM; the samples were run using different processing levels and dispersants.

Using the LDM with three processing environments revealed differing particle size distributions for the same sample. While clay was not detected in the unprocessed ethanol sample run in water unprocessed there was almost 3% clay while this figure increased to 8.57% when the sample was digested and run in water (*Table 2.7*). A similar trend was observed for the very fine, medium and coarse silts with the digested sample run in water containing a greater percentage of all of these classes when compared to the water run unprocessed sample and the ethanol processed sample (*Table 2.7*). At the 31 µm to 63 µm size fraction (very coarse silt), this trend changes with the unprocessed sample containing the largest percentage of this size range – almost double that of the other two methods (18% compared to 9.37% digested water and 7.43% unprocessed ethanol) (*Figure 2.5*). For the two unprocessed samples, the contribution of very fine sand is nearly consistent (20.71% ethanol and 25.81% water) while there was very little of this size fraction detected in the digested sample (1.17%). For all the sand categories, the unprocessed ethanol has the largest contribution with 21.58% of the sample existing between 250 µm and 500 µm range, while unprocessed water only 8.35% was in this range and no sample of this size was found in the digested sample.

From Figure 2.6, and through the trends visible in Figure 2.4, it is clear that the digested, water run sample was the finest while unprocessed and run in ethanol was the coarsest, relatively. This is mirrored by the statistical output for these samples, with the ethanol run unprocessed sample having a

mean of 191 µm while the unprocessed run in water had a mean 64 µm and 9 µm for the processed sample. These correlate to a mean of fine sand, very fine sand and fine silt respectively. All samples were poorly sorted with a wide range of grain sizes present in the sample. The unprocessed water run sample had the greatest range of size classes and was also the poorest sorted sample with grains detected in all but the coarsest size fraction. Skewness values close to zero (-0.1 to 0.1) suggest near symmetry about the mean, while negative values suggest the curve leans from the mean to the finer sediments, thus both water dispersant curves are skewed towards the finer sediment from the mean, while the ethanol curve was near symmetrical, skewing slightly towards the coarse grains about the mean (*Figure 2.5*).

Table 2.7: Laser results for three methods of grain size calculation for I4 fluff. Statistical results extracted from Blott and Pye (2001) using the Folk and Ward method. Size ranges and the associated grain size classification using the GRADISTAT definitions of Blott and Pye (2001) have been included.

Processing Dispersant		Unprocessed Ethanol	Unprocessed Water	Digested Water
Size ranges	Grain size classification	% Contribution to each grain size range		
< 2 µm	clay	0.00	2.89	8.57
2µm to 4 µm	very fine silt	0.29	2.22	13.09
4 µm to 8 µm	fine silt	0.54	3.27	19.65
8 µm to 16 µm	medium silt	0.95	6.06	25.69
16 µm to 31 µm	coarse silt	2.10	10.72	22.44
31 µm to 63 µm	very coarse silt	7.43	18.00	9.37
63 µm to 125 µm	very fine sand	20.72	25.81	1.17
125 µm to 250 µm	fine sand	30.91	20.99	0.02
250 µm to 500 µm	medium sand	21.58	8.35	0.00
500 µm to 1000 µm	coarse sand	9.11	1.69	0.00
1000 µm to 2000 µm	very coarse sand	6.37	0.01	0.00
		Statistical Results		
mean (µm)		191.76	64.13	9.15
sorting		2.65	3.61	2.84
skewness		0.04	-0.27	-0.14
kurtosis		1.17	1.18	0.94
		Grain size classifications (%)		
Sand		88.68	56.84	1.19
Silt		11.31	40.26	90.24
Clay		0.00	2.89	8.57

Kurtosis or ‘peakness’ of the distribution reveals that all curves are distributed near normally about the mean with a kurtosis value of 1 representing a normal curve. Kurtosis values between 0.9 and 1.1 are indicative of a mesokurtic or moderately peaked distribution and could describe all three methods. While the means varied greatly, the kurtosis and sorting revealed trends that show similar descriptions of the psd of the various methods. Therefore, while all three laser methods produce very different means they do present similar data around a moving mean.

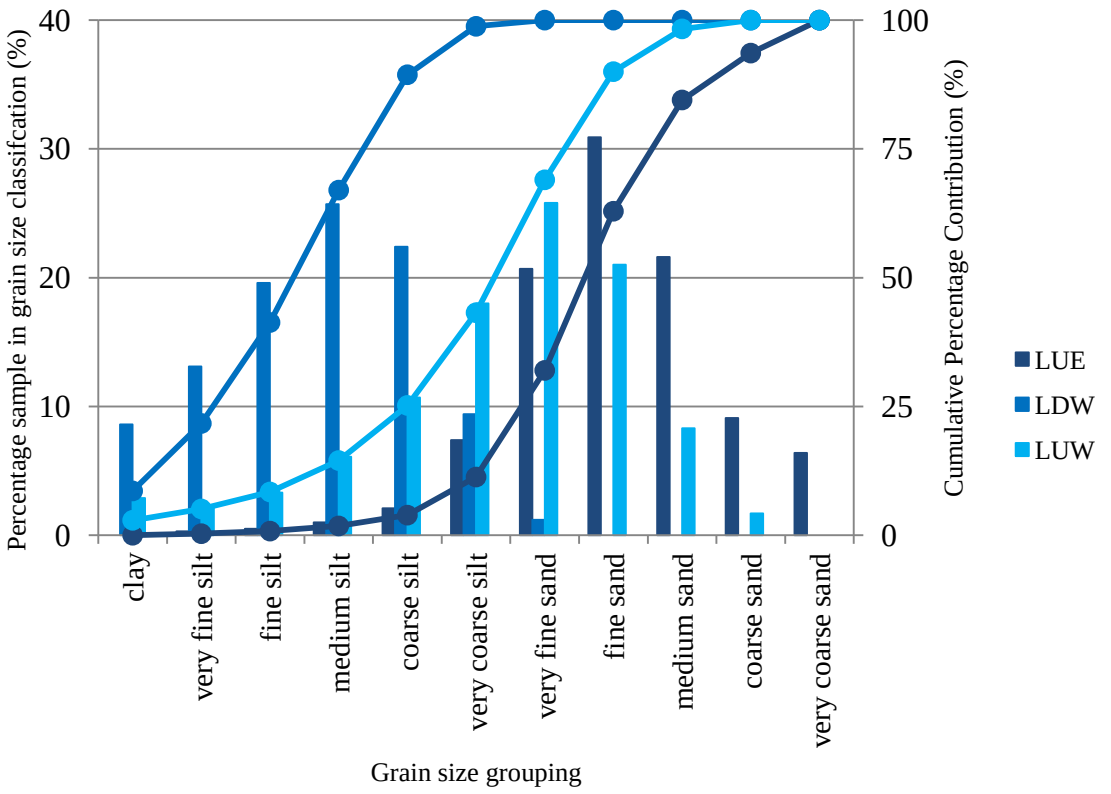

Figure 2.5: Graph of contribution of three samples of I4F to the grain size classification groups using three methods of processing utilizing laser diffraction. LUE (laser, unprocessed, ethanol dispersant); LUW (laser, unprocessed, water dispersant); LDW (laser, digested, water dispersant). Cumulative frequency distribution curves are shown with values on the secondary y axis.

When grouped into the three broad classifications of size distribution, it is evident that levels and different process methodologies can significantly alter the psd that is presented for a sample. Changing the dispersant from ethanol, which due to its polarity does not dissolve salts from the sample; to water, which will dissolve the salts, resulted in a decrease in the sand contribution from 89% to 57% while increasing the silt and clay fractions from 11% to 40% and 0.00% to 2.89% respectively. Processing the sample removing salts, gypsum, carbonates and organics further fined the sample, to contain almost 2% sand size grains with 90% of the sample being in the silt size range and 8.6% being defined as clay.

Additionally through comparing Figure 2.4 and Figure 2.5, the increased detail in size classification is evident. While in Figure 2.4 the unprocessed water and ethanol processed samples appear to have the same peak size range (>150 µm), with a rapid decrease towards the finer spectrum, in Figure 2.5 it can be seen that the peaks are in different size ranges and that the distributions decrease to both the larger and finer size fraction from the peak. This is particularly highlighted in the increased detail available in the finer ranges, while MSA was limited to the finest fraction representing grains to

<25 µm, using the LDM this same size fraction is represented by four size ranges. This reveals trends in the clay and finer silt size ranges, where much of processed water run sample has been detected.

The difference between the results presented in Table 2.6 and Table 2.7, reveal that there is increased resolution possible using the LDM method when compared to the MSA. Additionally, the ability to perform statistical and trend analysis on the samples further motivates for the use of LDM analysis on samples over basic trend and graphical displays obtained from MSA derived results.

2.4 Preliminary Synopsis

Following an in-depth look at the complexities involved in first determining an appropriate method for grain size determination and then how best to present the results, the previous section has presented the results of four methods of determining the particle size distribution of a sample taken from the Makgadikgadi Pans. The results have revealed four very different size distributions for the same sample. Deciding which method and processing level best represents the sample needs to be considered.

As global and regional sources contain sediments with a combination of chemical and morphological compositions there is no 'one size fits all' method of determining the psd for a sample. For the salt rich samples of the Makgadikgadi Pan we have presented the following results:

i. Mechanical Sieve Analysis of a dry unprocessed sample. Presenting 7 bin ranges of grain sizes to an otherwise undisturbed sample.
ii. Laser Diffraction Method of analysis using ethanol which does not dissolve the salts from the sample. This presents a 'least disturbed' representation of chemical conditions.
iii. Laser Diffraction Method of analysis using water as the dispersant which dissolved soluble salts from the sample providing a representation of psd without salts.
iv. Laser Diffraction Method of analysis using water as the dispersant and a fully digested sample. This presents the most disturbed representation of chemical conditions.

The results presented reveal that, using MSA, the sample psd can be determined. For I4F the psd revealed a sample dominated (68%) by coarse grained sediments in the >150 µm range with a rapid decrease in contribution of the smaller size fractions. However, this method is confirmed as being slow and laborious (Di Stefano et al., 2010) and is known to be less effective when working with smaller (mass) samples (Goudie et al., 1990; Chatenet et al., 1996). While this sample was sufficiently large, other samples within the suite to be analysed were notably smaller and would therefore be poorly represented through MSA. Further, the process is fundamentally limited in the number of sieves available and therefore the number of size ranges that can be determined. This

further limits the number of statistical results that can be derived for the traditional method. Despite this, Di Stefano et al. (2010) drew on the importance of utilising traditional methods for psd determination suggesting that combining labour intensive classical methods with modern technologies like LDM would ensure the robustness of the output. While Blott and Pye (2001) suggest that there are difficulties in merging data, despite this it is suggested that traditional mechanical sieve and pipette results can be used to inform the validity of the faster, laser derived results (Konert & Vandenberghe, 1997; Blott & Pye, 2001).

Grain size distribution literature is populated by studies comparing the various methods of grain size determination for the full sample as well as for various size fractions within a sample. Buurman et al. (2001) discuss the ability of LDM to detect clays which are often underestimated, although the authors suggest that this method overestimates the silt size fraction. While he argued that the middle to large size fractions did not experience this error, this over- and underestimation of silt and clay relative to the coarser sands is presented by other authors (e.g. Lee Black et al., 1996; Ma et al., 2000; Ma et al., 2001; Loizeau et al., 2006; Tinke et al., 2008), with Beuselinck et al. (1998) attributing a lot of over/under-estimation to particle morphology. Thus, despite the high reproducibility of results using LDM (Buurman et al., 1997), the method contains a large number of pitfalls. Different approaches are suggested to overcome this, with Beuselinck et al (1998) suggesting that these significant limitations can be overcome by correctly sub-sampling, while Buurman et al. (1997) suggest that using laser methods in conjunction with traditional methods, where possible, is more robust.

However, consideration of equivalent spheres as presented in section 2.1.1, reveals that comparing results derived from different equivalent spheres may introduce further bias into the full distributions. This suggests that sub-sampling is the best means of minimising error, while single method analysis provides the only means of producing a comparable data set. Therefore, when carefully sub-sampled and with proper sample pre-treatment, laser diffraction gives reproducible results that can be used to compare samples and to gain insight into changes within the clay fraction and at the same time variations in coarser fractions (Buurman et al., 1997). Further, while the issue of grain morphology was noted to affect traditional methods (Konert & Vandenberghe, 1997), this problem is not unique to this method, with Tinke et al. (2008) noting that orientation results in significant over/underestimation of grain size in many modern methods. In order to minimise this impact, samples were analysed in triplicate with the average of all runs considered to be the best representation of results, as through repetition and averaging, orientation associated under- and overestimation of grain size should be overcome. A further shortcoming of the laser method is associated with the need to represent the chemistry and density of the sample before processing (Malvern Instruments Limited, 2007). These variables alter the refractive index of the sample, and affect grain detection. However, in this study using sediments from within the Makgadikgadi Pan, which have been determined to be similar in

terms of colour and overall composition (see Chapters 3 and 4 on chemical composition), the variable refractive indices for the samples are similar (Allen, 1985) and therefore more consistent morphological detection is possible.

Knowledge of chemistry and density are also important in determining the pump speed and sampling intervals, as well as ensuring representative presentation of samples to the laser. While higher pump speeds can ensure heavier grains are presented, this needs to be combined with reducing mechanical abrasion associated with faster pump speeds. Konert and Vandenberghe (1997) note issues attributable to flocculation when measuring samples. Here pump speeds were carefully considered, along with densities of the sample and the dispersant, with water sampling of digested samples requiring the addition of a deflocculant during sampling. In line with suggestions by Konert and Vandenberghe (1997) and Blott and Pye (2001) results from MSA were used to inform the validity of results obtained while determining optimum pump speeds and machine conditions.

As previous dust studies reveal, their method of psd has been reliant on pre-treating the sample to remove various constituents, e.g. carbonates, salts, gypsum, organics, iron oxides and aluminosilicate minerals, amongst others (e.g. Soukup et al., 2008b). To conform to literature, and to provide a context in which the samples can be considered, all samples were digested and the psd of the resulting sample was determined.

The use of digestion for samples has been presented in some aerosol studies, e.g. Cattle et al (2009) and Swineford and Frye (1945) although these authors make no claim of altering the chemical composition of the sample. Other authors, e.g. Kriews and Schrems (1998) (15 filter stages), Afeti and Resch (2000) (8 filter stages), and more recently Castillo et al. (2008) (7 filter stages), use various *in situ* high volume impactors with staged filters to collect samples. The filter method is similar to traditional sieve analysis, but uses active sampling to size fractionate and capture grains on inert filter paper to be analysed later. These authors use this method *in situ* as it minimises contamination by using a sterile atmosphere with no dispersants or digesting agents in the determination of grain sizes; yet is faster the traditional mechanical sieve analysis. These two conflicting methods are commonly used in aerosol and other sedimentary studies with very little attention paid to the impact that pre-processing imparts on the sample. Additionally, such disparate techniques complicate the comparative nature of studies. Laurent et al. (2008) present that when considering grain sizes for the inclusion in climate models and associated surface parameters, the dry soil size is used. This value, the authors claim, best reflects the natural state of aggregation in the soil. Laurent et al. (2008) claim that wet sedimentation techniques break down soil aggregates, with the resultant classification revealing relatively large amounts of loose clay particles which are not generally encountered in natural soils as loose particles. The authors additionally present that natural distributions are typically associated with clay aggregates between 50 µm and 100 µm. Figure 2.4 and Table 2.7 confirm this

proposition indicating a significant contribution of this size fraction in the ethanol processed sample, while in the digested sample very little sample exists in the 50 µm to 100 µm, favouring the finer clay fraction. Finally, Chatenet et al. (1996) criticise wet methods as the natural size distribution is destroyed by physical breakage and dissolution of soluble salts, highlighting the use of dry methods which disturb as little as possible of the *in situ* size distribution which need to be considered for valid representation of surface condition.

While in this study the dry method as used in MSA was determined to be laborious, it has been shown that the results from the dry method are comparable to the much more efficient LDM approach using ethanol. As MSA is known to be the least invasive technique, the relationship presented between MSA and the LDM ethanol suggests that they are similar in presenting the natural state of the pan surface.

The challenge of presenting the best representative sphere remains a challenge as samples from the pan would not be assumed to be strongly round as a result of the evaporative nature of the pan environment (Lowenstein & Hardie, 1985). This highlights the importance of the relationship between size, chemistry and form as shown in Figure 2.1. Therefore, unlike the single pathway and definition approach as presented by Goudie (1990), considering multiple physical attributes of the particle will result in better sampling efficiency. Through the understanding of particle form, orientation and mineralogy the appropriateness of the various equivalent spheres can be established, additionally informing the nature of the methodological approach, sampling environment and dispersants.

The overall objective of this chapter was to determine the physical nature of sediments, with the aim of determining the dust potential of the region. It has been determined that using MSA did not provide sufficient detail to discriminate between samples, most notably the finer grained sediments. This therefore did not permit analysis of the dust potential of various samples. Consequently, in terms of research needs, this method was therefore not appropriate. In contrast, the detailed information provided over multiple classes obtained through LDM analysis combined with the high degree of reproducibility and efficiency, resulted in the selection of this method to determine the psd of the samples.

In light of this, the following section will consider samples from a wider area and at various depths within the horizontal pan structure. It should be noted that despite the high resolution provided by LDM using Malvern, it was determined that grouping the samples into silt/sand/clay (Blott & Pye, 2001) was the best descriptor of the sample. Further, to conform to literature and to provide a comparative baseline within which to analyse the dust potential of the region, the digested method will be considered alongside the less invasive ethanol method of processing.

2.5 Results from the DO4 Grid – Grain Size Distributions of Surface and Sub-surface Samples from Dust Source Regions

The following results and discussion will consider 41 samples collected during the DO4 2011 field campaign and will present samples from four sampling categories at 12 sites within a 144 km^2 area on Sua Pan, within the Makgadikgadi Pans complex (*Table 2.8*).

2.5.1 Samples

Samples are initially named by the site at which they were sampled according to the system utilised for the DO4 project (see section 1.4 and Appendix 1). At each sampling site, samples were determined to belong to the following four categories: Fluff, Crust, Secondary crust and Soil, with the suffixes F, C, H and S respectively (see section 1.4 and Appendix 1). All samples are represented by 'grab samples' from the 2011 DO4 field site, with collected samples placed in zip lock bags on site with every effort made to ensure the integrity of the samples was not compromised during transport. Small changes in temperature and moisture conditions were experienced between the source region and the laboratory which could account for chemical and physical changes through hydration, dehydration and compaction.

Table 2.8: Table listing sample ID as used in this chapter as per naming procedure of site ID as developed for the DO4 Project. Samples not present are indicated by '-'.

	Sample Category			
	Crust	Fluff	Horizon-Crust	Soil
suffix	C	F	H	S
Site ID				
	Sample ID			
B3	B3C	B3F	-	B3S
B7	B7C	B7F	-	B7S
D2	D2C	D2F	D2H	D2S
D5	D5C	D5F	D5H	D5S
D10	D10C	D10F	D10H	D10S
G2	G2C	G2F	G2H	G2S
G6	G6C	G6F	-	G6S
I4	I4C	I4F	I4H	I4S
I8	I8C	I8F	I8H	I8S
J3	J3C	J3F	-	J3S
J11	J11C	-	J11H	J11S
L5	L5C	-	-	L5S

Sample preparation, machine set up and conditions for DO4 grid samples (*Table 2.8*) is in accordance with the methods presented in section 2.2.

2.5.2 Ethanol Unprocessed Results

The following section will present the results of ethanol processed LDM samples, for the 41 samples collected as part of the 2011 field campaign (*Table 2.8*).

2.5.2.1 Average Ethanol Unprocessed Results

The average soil sampled from the Makgadikgadi DO4 grid was the finest of the samples (median 236.35 µm, mean 183.84 µm) followed by the average fluff (median 288.44 µm, mean 261.68 µm), average second crust (median 399.03 µm, mean 328.43 µm) and finally average crust (median 423.19 µm, mean 305.23 µm) (*Table 2.9*). Average sand, silt and clay percentages for the soil are 75%, 25% and 1% respectively. This varies from the fluff which has significantly higher contribution of sand sized grains with 86% sand and 13% and 1% for silt and clay respectively. These values are similar to those found for the average crust conditions, with 81% sand, 18% silt and 1% clay; and for the average second crust with 85% sand, 15% silt and no clay.

Table 2.9: Average results for samples from the DO4 grid as a function of the 11 size fractions.

	Sample Category			
	Crust	Fluff	Horizon-Crust	Soil
suffix	C	F	H	S
sample	Average C	Average F	Average H	Average S
	% Contribution to each grain size range			
clay	0.60	0.18	0.37	0.66
very fine silt	1.06	0.49	0.66	1.45
fine silt	1.73	0.88	1.02	2.16
medium silt	2.85	1.53	1.80	3.35
coarse silt	4.95	3.38	3.73	6.51
very coarse silt	7.85	7.18	7.40	11.03
very fine sand	11.23	13.88	12.82	14.47
fine sand	13.03	21.39	17.88	16.01
medium sand	14.10	22.00	16.20	19.91
coarse sand	19.97	18.83	17.91	17.00
very coarse sand	22.63	10.26	20.20	7.45

All samples are dominated by sand size particles (minimum 64%: soil, maximum 99%: fluff) while silts are the next most dominant with values between 1% (fluff) and 35% (soil), silts contribute between 0% and 1% in all samples (*Figure 2.6*).

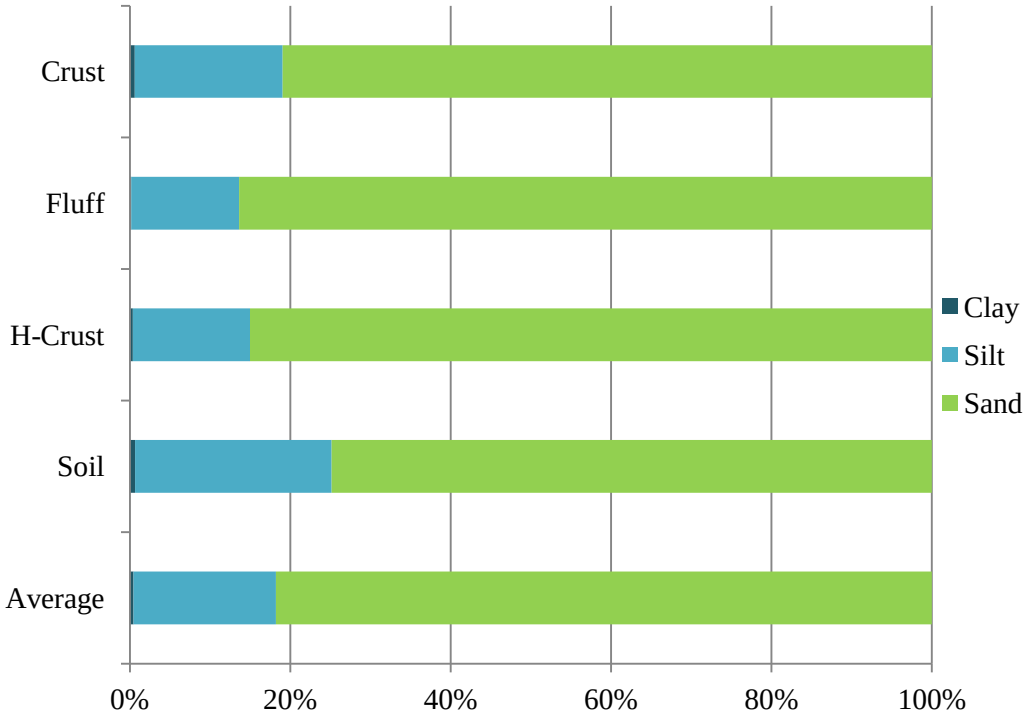

Figure 2.6: Relative contribution of sand, silt and clay to the averaged crusts, fluff, soil and full averaged samples from the DO4 grid. For ethanol processing of all samples.

Trends in grain size distribution for averaged samples from within the DO4 grid reveal that all samples peak in the coarse grain sizes tailing off towards the finer sizes (*Figure 2.7*). When considering the averaged samples as a function of the 11 grain sizes, it becomes possible to break down the sand/silt/clay ratio into finer ranges within the broader sand and silt classifications. The average crust has the largest percent contribution of very coarse sand (23%), while the fluff contains largely medium (22%) to fine sand (21%), the second crust peaks in very coarse sand (20%) with equally large contributions from coarse and fine sand (18%). Soils, like fluff peaked in the medium sand (20%) but contained the smallest percentage of grains larger than this size (*Figure 2.7*).

The distributions (*Figure 2.7*) reveal that average crust, average fluff and average soil have unimodal distributions, while average second crust has a bimodal distribution. All samples are poorly sorted as values exist over a wide range, despite the large percentage of the sample in the larger grain sizes all samples tail off towards the finer sediments and are therefore finely skewed and meso- to platykurtic in their distributions.

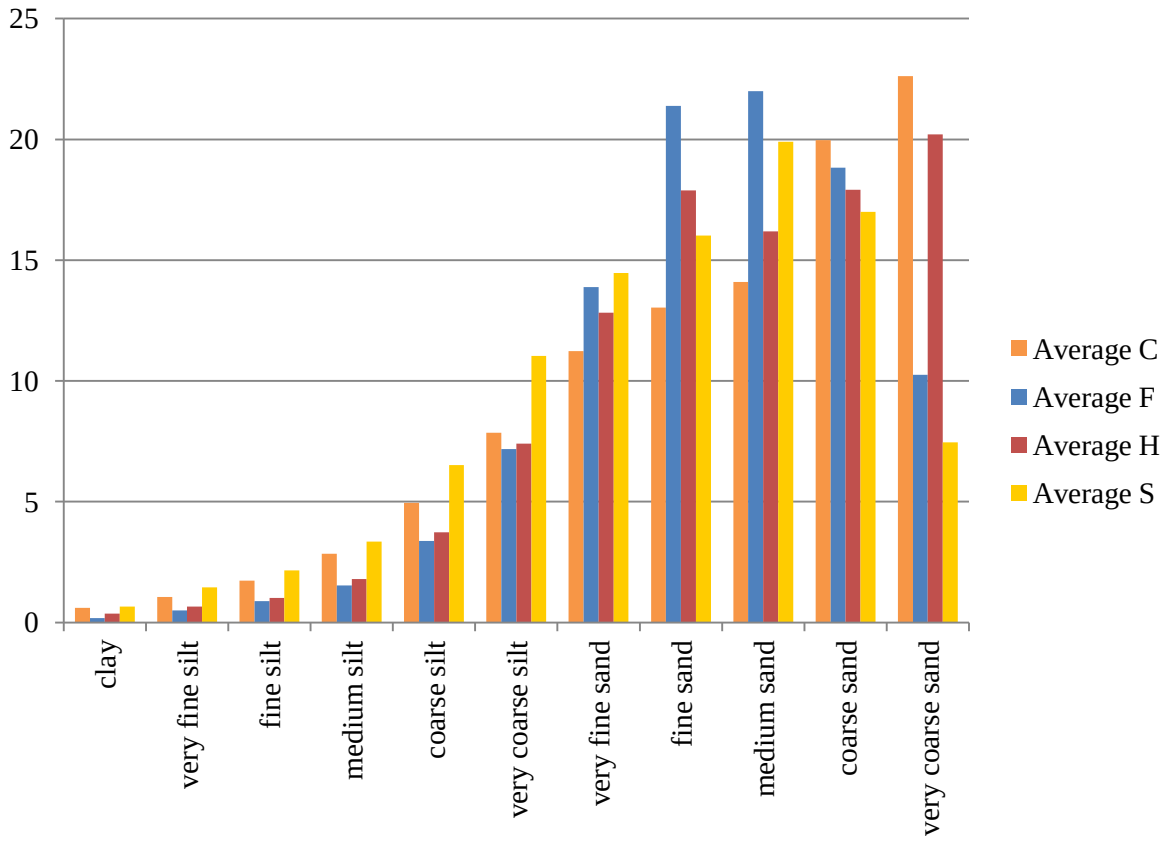

Figure 2.7: Average results for samples from the DO4 grid as a fraction of the 11 size classifications. Average C represents the average crust, while average F represents the average fluff. Similarly average H represents the average second crust and average S the average soil. Further information on location of samples within the vertical and horizontal sampling scheme can be found in Table 2.8 and section 1.4.

Comparison of the clay, silt and sand minimum and maximum values for the samples reveals that there is significant variability between samples even within the sampling category. From Figure 2.8 the variability in clays is evident. Crust, fluff, and H-crust all contain samples with no clay contribution, while the minimum contribution in soils is 0.2%. The range of values of clay contribution between samples is between 0.5% and 1.5%. For silt, the range of values within the sample category is between 19% and 27% with a total range between all samples of 35% and the variability between the means of 11% from 13% in the fluff to 34% in the soil. A similar variability is seen the sand size grains with the variability within sample category of between 19% and 27% with a full range of 35% (minimum of 64% in the soil and maximum of 99% in the fluff). Fluff samples experience the greatest range of values about their mean, while second crust samples experience the smallest range of values.

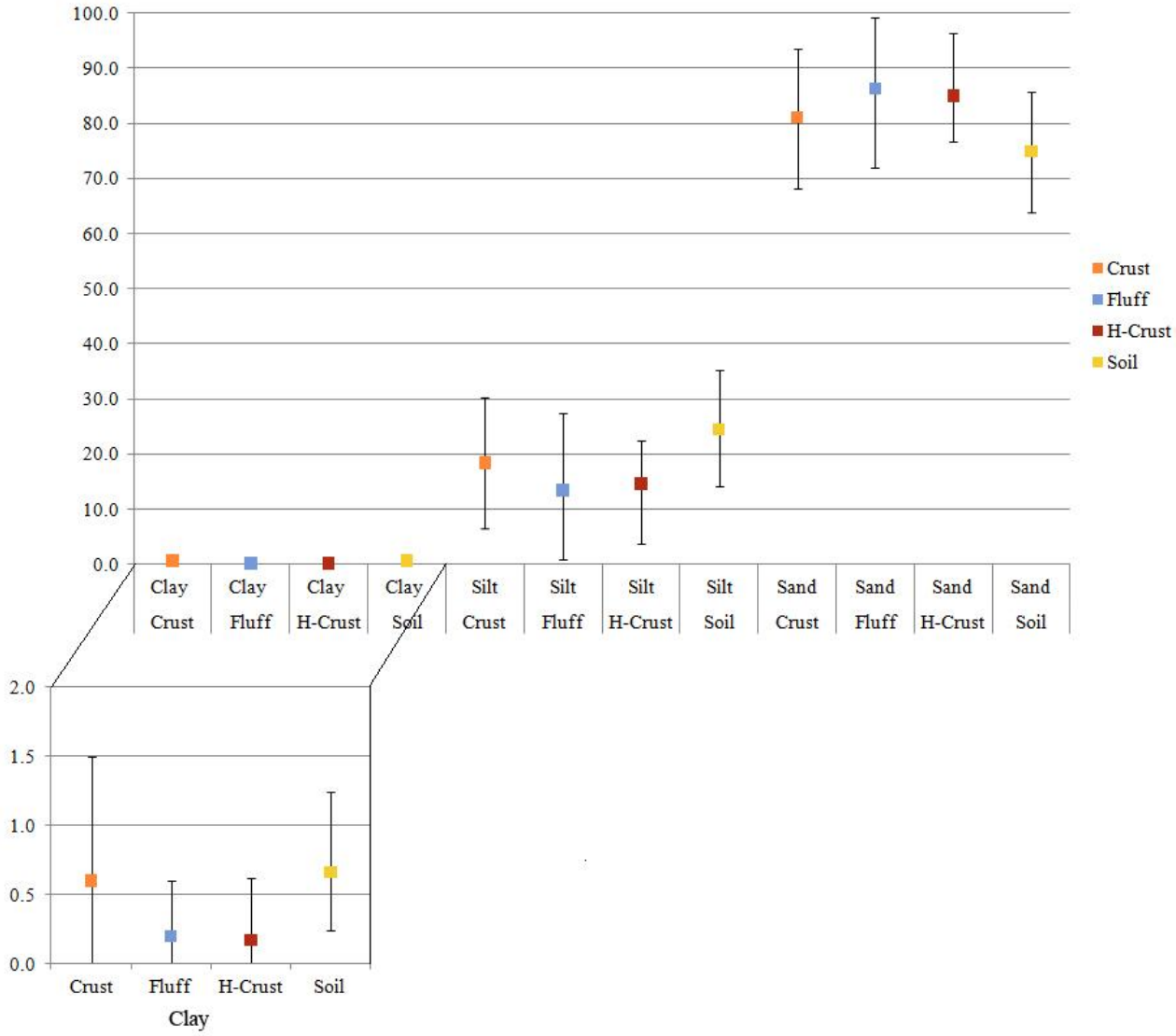

Figure 2.8: Plot of clay, silt and sand minimum, mean and maximum for all samples grouped by sample category (clay inset below).

While presenting the results of sample averages provides information of the standard conditions within the vertical profile, there exists variability between samples as can be seen in Figure 2.8. The following section will present the results of variability between samples within each sampling category, starting at the top of the vertical profile with the crust. This will be followed by the fluff, second crusts and finally the soil.

2.5.2.2 Crust Results

Of the crust samples, B3C was the finest sample containing the greatest percentage of clay (1.5% clay) followed by B7F (0.9%) and J3F (0.8%). All samples contained a contribution of clay, with the smallest being from I8C (0.03%) with the mean contribution being just over 0.5%. Analysis of the silt contribution revealed that B3C was again the finest with 30.3% silt (crust mean 18.4%) while the remaining 68% of the B3C sample was composed of sand sized grains. I8C was the coarsest sample with 93.4% of the sample composed of sand sized grains (mean 81%) with 0.03% and 6.6% clay and silt respectively. Combined clay and silt contributed a maximum of 31.8% at B3C and a minimum of 6.6% at I8C with the mean for crust at 19%.

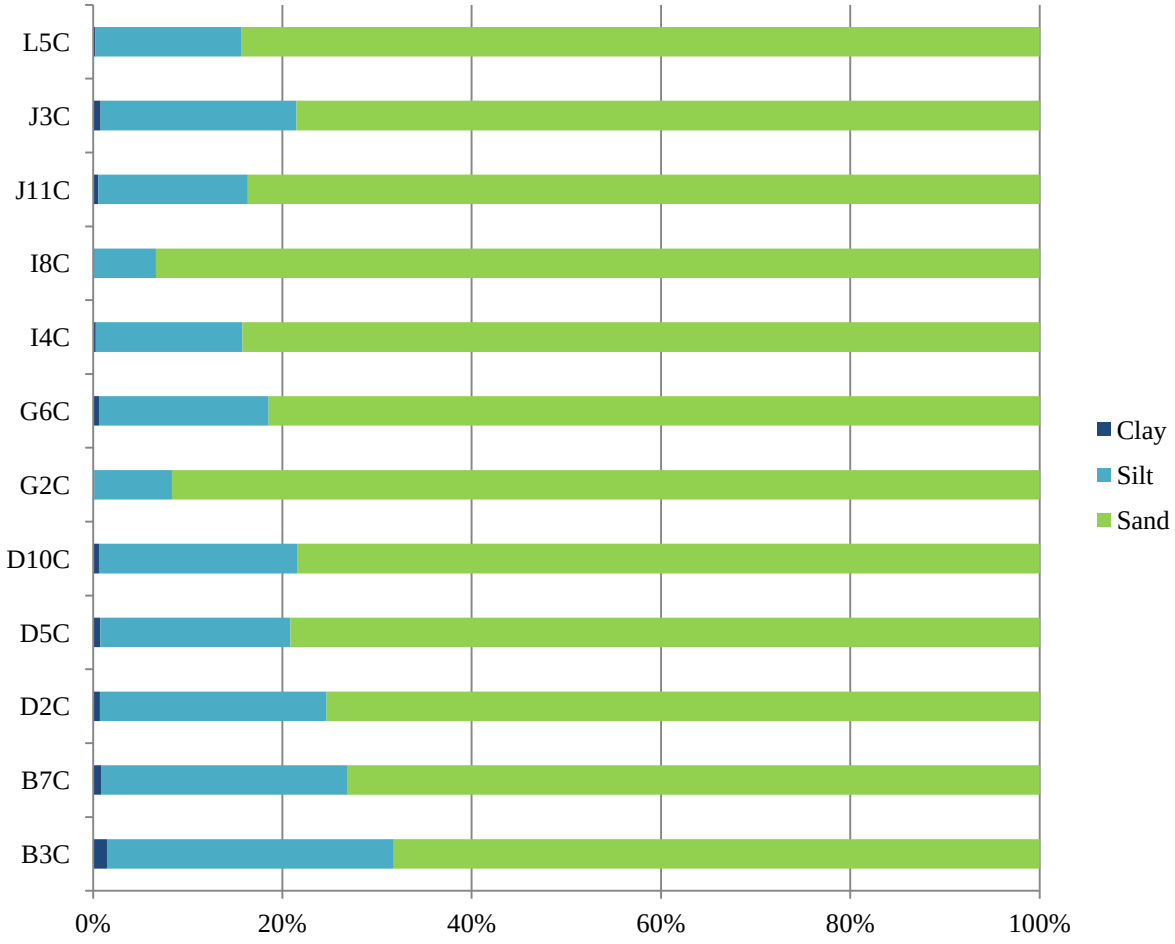

Figure 2.9: Relative contribution of sand, silt and clay to the twelve crust samples from the DO4 grid. B3C can be seen to have the largest contribution of silts and clays, while G2C has the largest contribution of sands. All samples are dominated by sand sized grains.

Table 2.10 confirms the trends shown in Figure 2.9, with B3C having the lowest mean grain size (160 µm) compared with the coarsest mean at I8C (642 µm). I4C is the only other sample with a mean below 200 µm (199 µm). D2C and L5C are the next finest samples with means of 207 µm. I4C, I8C and L5C are all poorly sorted (values between 2.00 and 4.00) while the remaining 9 sites are all

very poorly sorted (values between 4.00 and 16.00) with large grain size distribution ranges. All samples are fine or very finely skewed with a wide range of peakedness, from almost very platykurtic (<0.67) at B7C (0.673) to very leptokurtic (1.5 – 3.00) at G2C.

Table 2.10: Summary of crust results presenting mean and a selection of statistical descriptors for all sites.

Sample ID	Statistical Description					
	Mean	Sorting	Skewness	description	Kurtosis	description
B3C	160.0	6.2	-0.2	Fine Skewed	0.8	Platykurtic
B7C	324.0	5.7	-0.6	Very Fine Skewed	0.7	Platykurtic
D10C	248.8	4.9	-0.2	Fine Skewed	0.8	Platykurtic
D2C	206.7	5.0	-0.1	Fine Skewed	0.8	Platykurtic
D5C	257.0	4.6	-0.5	Very Fine Skewed	0.9	Platykurtic
G2C	632.3	3.2	-0.6	Very Fine Skewed	2.1	Very Leptokurtic
G6C	230.0	4.3	-0.1	Fine Skewed	1.1	Mesokurtic
I4C	199.8	3.2	-0.1	Fine Skewed	1.1	Mesokurtic
I8C	642.2	2.9	-0.5	Very Fine Skewed	1.4	Leptokurtic
J11C	308.3	4.5	-0.3	Very Fine Skewed	1.0	Mesokurtic
J3C	246.8	5.2	-0.4	Very Fine Skewed	0.9	Mesokurtic
L5C	206.8	3.2	-0.2	Fine Skewed	1.0	Mesokurtic

For full results see Appendix 4.

2.5.2.3 Fluff Results

Of the fluff samples, B7F was the finest sample, containing the greatest percentage of clay (0.62% clay) followed by D5F (0.60%). Five sites did not contain any clay sized grains. For silt contribution; B7F was again the finest with 27.4% silt (mean 13.5%) while the remaining 72% of the B7F sample was composed of sand sized grains (sample category mean 86%). Repeat processing of D2F continued to reveal a distribution such that 99.1% of the sample was composed of sand sized grains with the remaining 0.9% of the sample determined to be silt. This sample represents the coarsest of all samples measured in this study. B7F was the finest of the fluff samples with 28% of the sample composed of clay and silt.

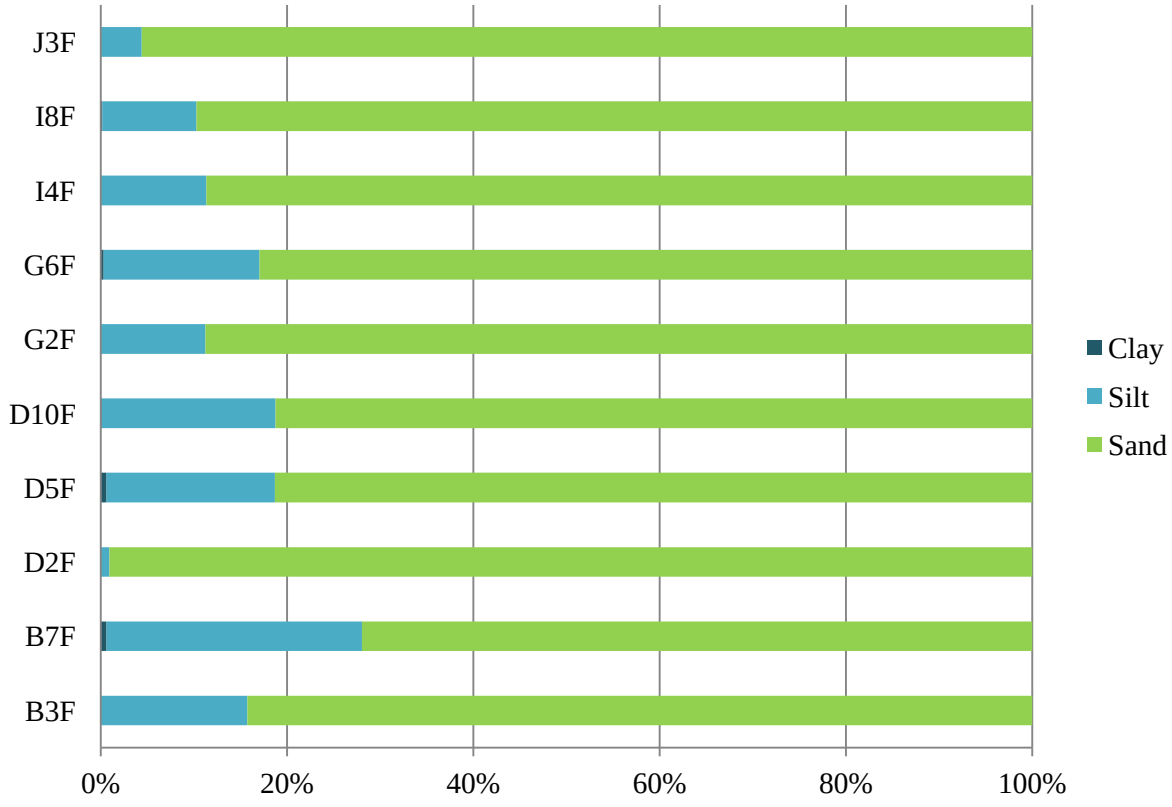

Figure 2.10: Relative contribution of sand, silt and clay to the ten fluff samples from the DO4 grid. B7F can be seen to have the largest contribution of silts and clays, while D2F has the largest contribution of sands. All samples are dominated by sand sized grains.

Table 2.11 confirms the trends shown in Figure 2.10, with B7F having the lowest mean grain size (mean 122 µm) in comparison J3F was the coarsest sample (mean 500 µm). Analysis of means reveal that D10F (mean 187 µm) and I4F (192 µm) are the next finest samples. D2F is the most well sorted of all the samples as 99.1% of the sample is sand sized, all the rest of the samples are poorly sorted with geometric sorting values greater than 2.00. D5F is the most poorly sorted sample, with a value

over 4.00 (very poorly sorted). All samples are between symmetrical and finely skewed with a larger percentage of the sample existing towards the finer range from the mean. Kurtosis values reveal that no sample has a particularly peaked distribution.

Table 2.11: Summary of fluff results presenting mean and a selection of statistical descriptors for all sites.

Sample ID	Statistical Description					
	Mean	Sorting	Skewness	description	Kurtosis	description
B3F	243.7	3.6	0.0	Symmetrical	0.8	Platykurtic
B7F	122.0	3.2	-0.1	Fine Skewed	1.0	Mesokurtic
D2F	307.9	1.9	0.0	Symmetrical	0.9	Platykurtic
D5F	289.8	4.5	-0.4	Very Fine Skewed	0.9	Platykurtic
D10F	187.4	3.4	0.0	Symmetrical	1.0	Mesokurtic
G2F	204.6	2.6	-0.1	Symmetrical	1.0	Mesokurtic
G6F	223.5	3.8	-0.1	Fine Skewed	1.0	Mesokurtic
I4F	191.8	2.7	0.0	Symmetrical	1.2	Leptokurtic
I8F	345.9	3.1	-0.4	Very Fine Skewed	1.3	Leptokurtic
J3F	500.2	2.6	-0.2	Fine Skewed	0.9	Mesokurtic

Fluff represented the coarsest sample category with the lowest clay and silt contributions within samples and the highest sand contribution. For full results see Appendix 4

2.5.2.4 Second Crust Results

Of the second crust samples, I4H was the finest sample containing the greatest percentage of clay and silt (0.7% clay and 22.5% silt), followed by D5H which had the greatest percentage of clay at 0.8% and the second greatest silt contribution at 21.1%. Two samples did not contain any clay (I8H and D2H), while the remaining had small contributions; 0.3%, 0.4%, 0.5%, 0.7% and 0.8% for J11H, D10H, G2H, I4H and D5H respectively. Analysis of silts revealed that second crusts contained the lowest maximum silt contribution, with a maximum of 22.5% at I4H. I8H had the lowest silt concentration amongst second crusts with only 3.8% of the sample in this size range. As I8H contained no clay, the remaining 96.2% was made up of sand size grains, making this the coarsest second crust sample, while I4H was the finest sample with only 76.8% sand.

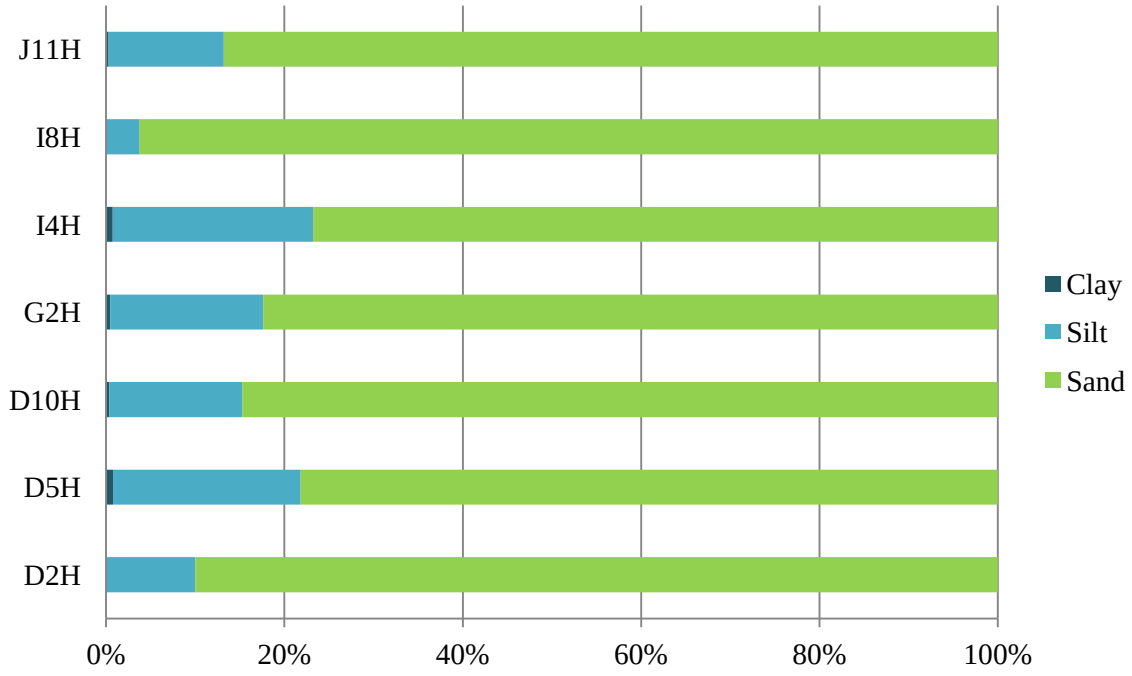

Figure 2.11: Relative contribution of sand, silt and clay to the seven second crust samples from the DO4 grid. I4H can be seen to have the largest contribution of silts and clays, while I8H has the largest contribution of sands. All samples are dominated by sand sized grains.

Table 2.12 confirms the trends shown in Figure 2.11, with I4H having the lowest mean grain size (126 µm) similarly the high silt concentration at D5H resulted in a mean of 162 µm. This is compared with the coarsest mean at I8H (788 µm) with no clay or fine silts, and the finest grains larger than coarse silt. The mean grain size at I8H is more than double the value found at any other site, with the next highest mean found at D2H at 370 µm, which again did not contain any clay or fine silt. D10H had a similarly high mean at 317 µm despite containing a small contribution of fine silts.

All samples are poorly sorted (values between 2.00 and 4.00) while D10H and G2H are very poorly sorted. Other then D5H which peaks in fine sand and contains a nearly equal percentage either side of this peak resulting in this sample being symmetrical, all other samples are fine or very finely skewed. I8H peaking in the largest size range is very strongly finely skewed. There is a wide range of peakedness, from platykurtic (D2H, D10H and G2H), to mesokurtic (J11H), leptokurtic (D5H, I4H) and finally very leptokurtic at I8H.

Table 2.12: Summary of second crust results presenting mean and a selection of statistical descriptors for all sites.

Sample ID	Statistical Description					
	Mean	Sorting	Skewness	description	Kurtosis	description
D2H	370.0	3.4	-0.2	Fine Skewed	0.9	Platykurtic
D5H	162.8	3.9	-0.1	Symmetrical	1.2	Leptokurtic
D10H	316.8	4.1	-0.3	Fine Skewed	0.8	Platykurtic
G2H	267.1	4.2	-0.2	Fine Skewed	0.9	Platykurtic
I4H	125.5	2.9	-0.3	Fine Skewed	1.2	Leptokurtic
I8H	787.9	2.5	-0.5	Very Fine Skewed	1.6	Very Leptokurtic
J11H	268.9	3.4	-0.2	Fine Skewed	1.0	Mesokurtic

The second crust was coarser then the first crust, with similar clay silt and sand values to those found in the fluff. For full results see Appendix 4.

2.5.2.5 Soil Results

Of the soil samples, G2S was the finest sample containing the greatest percentage of clay and silt (0.8% clay and 35.3% silt), followed by J3S, which had the greatest percentage of clay at 1.2% and the second greatest silt contribution at 29.6%. These samples contained the greatest percentage of silt of any sampling category. All soil samples contained clay sized grains, varying from 0.2% in D2S to 1.2% at J3S. The mean for clay was 0.7% which is the largest of all sampling categories. The average silt percentage was also higher than any other sample category with a maximum of 35.3% at G2S, with B7S the only other sample above 30% silt (30.98%). Due to the higher contribution of clay and silt in the soil samples, the resulting sand values were lower. Soil samples contained an average of just under 75%, with only 63.9% found in G2S, 68.4% in B7S up to a maximum of 85.70% in D2S. These values represent the smallest percentage of sand sized grains between sampling categories.

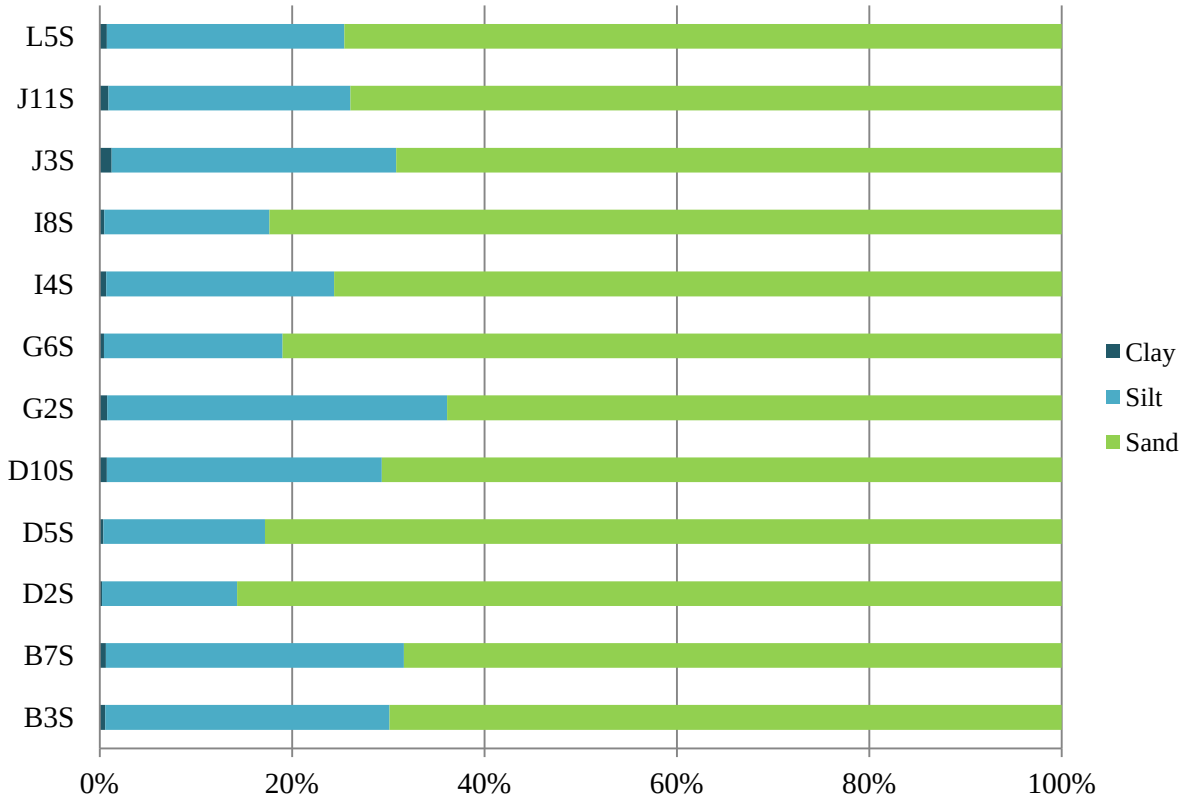

Figure 2.12: Relative contribution of sand, silt and clay to the twelve soil samples from the DO4 grid. G2S can be seen to have the largest contribution of silts and clays, while D2S has the largest contribution of sands. All samples are dominated by sand sized grains.

Table 2.13 confirms the trends shown in Figure 2.12, with G2S having the lowest mean grain size (92.44 µm), with this sample and both B7S and B7F and B3S being the only four samples with a mean grain size below 125 µm (122.05 µm, 121.99 µm and 113.51 µm respectively) and therefore a

mean of very fine sand, close to the sand silt boundary at 63 µm. The relatively low contribution of silt and clay to the samples at D2S and D5S resulted in these two samples having the highest mean of 358.7 µm and 306.9 µm respectively. Half the samples are poorly sorted (values between 2.00 and 4.00) (B3S, D10S, G2S, G6S, I4S, I8S) with the remaining half being very poorly sorted (B7S, D2S, D5S, J11S, J3S, L5S). Other then B7S, which is symmetrical, all other samples are fine or very finely skewed. Sample distributions are all meso- or platykurtic suggesting flat peaked distributions for all samples broadly spread across the full size spectrum and thus confirming the poorly sorted nature of soil sediments.

Table 2.13: Summary of soil results presenting mean and a selection of statistical descriptors for all sites.

Sample ID	Statistical Description					
	Mean	Sorting	Skewness	description	Kurtosis	description
B3S	113.5	3.5	-0.2	Fine Skewed	1.0	Mesokurtic
B7S	122.0	4.0	-0.1	Symmetrical	1.0	Mesokurtic
D2S	358.7	4.0	-0.4	Very Fine Skewed	0.9	Platykurtic
D5S	306.9	4.3	-0.4	Very Fine Skewed	0.9	Platykurtic
D10S	137.5	3.8	-0.2	Fine Skewed	0.9	Platykurtic
G2S	92.4	3.2	-0.2	Fine Skewed	1.0	Mesokurtic
G6S	201.3	3.4	-0.5	Very Fine Skewed	1.0	Mesokurtic
I4S	146.2	3.6	-0.3	Fine Skewed	1.0	Mesokurtic
I8S	241.2	4.0	-0.4	Very Fine Skewed	1.1	Mesokurtic
J3S	134.7	5.2	-0.2	Fine Skewed	0.9	Platykurtic
J11S	183.7	4.9	-0.4	Very Fine Skewed	0.9	Platykurtic
L5S	167.8	4.6	-0.2	Fine Skewed	1.0	Mesokurtic

This sampling category represents the finest of all the samples, with the smallest percentage of sand sized sediments, and therefore the greatest percentage of silt and clay sized grains. For full results see Appendix 4.

2.5.2.6 Summary of Ethanol Unprocessed Samples

- Sand sized grains dominate all samples (64 – 99%), followed by silt (1 – 35%) with the remaining 0 – 1% composed of clay
- The psd for average crust, fluff and soil is unimodal while the second crust has a bimodal distribution.
- Soil was the finest sampling category with the finest mean found at G2 (92.44 µm) with a sample category mean of 183.84 µm.
- The second crust was the coarsest with the largest mean found at I8 (787.87 µm) with a sample category mean of 328.43 µm.

Table 2.14: Mean grain size in (µm) for all samples by sampling category. Mean, maximum and minimum statistical values have been calculated.

	Sampling Category			
	Crust	Fluff	H-Crust	Soil
	Average Grain Size (µm)			
B3	160.0	243.7		113.5
B7	324.0	122.0		122.0
D2	206.7	307.9	370.0	358.7
D5	257.0	289.8	162.8	306.9
D10	248.8	187.4	316.8	137.5
G2	632.3	204.6	267.1	92.4
G6	230.0	223.5		201.3
I4	199.8	191.8	125.5	146.2
I8	642.2	345.9	787.9	241.2
J3	246.8	500.2		134.7
J11	308.3		268.9	183.7
L5	206.8			167.8
	Statistics			
Minimum	160.0	122.0	125.5	92.4
Maximum	642.2	500.2	787.9	358.7
Mean	305.2	261.7	328.4	183.8

While viewing samples on a site by site basis or within the context of the sampling category reveals inter and intra site variability (*Figure 2.13*), by plotting the difference between the observed mean for each sampling category with the mean of a site, the trend in Figure 2.13 can be revealed.

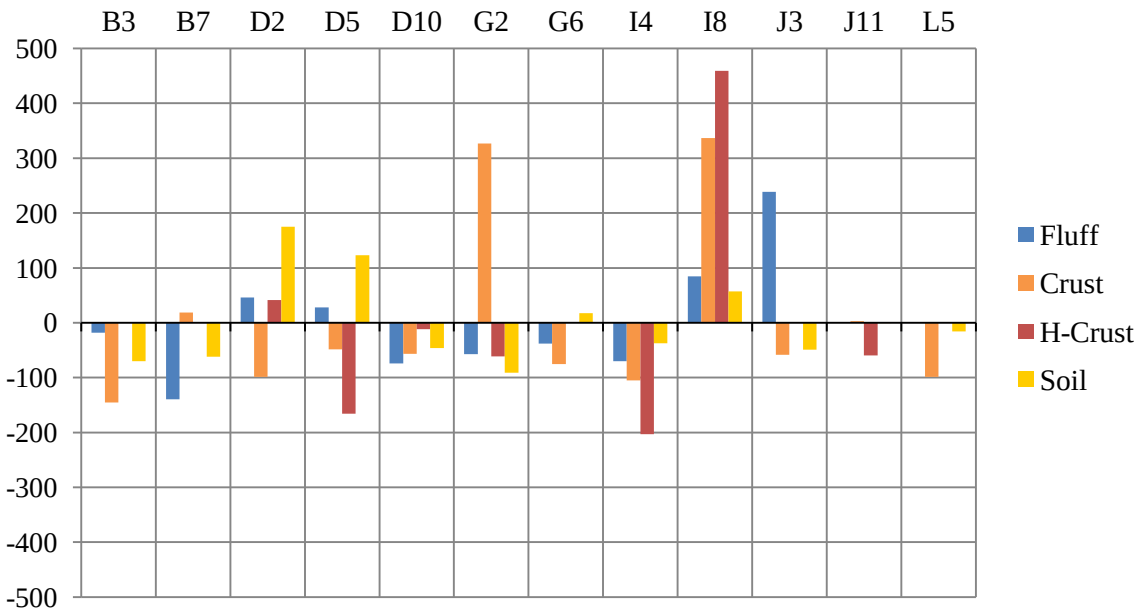

Figure 2.13: Plot of difference between grain size and the mean for the sampling category. Negative values indicate sample values smaller then the mean while positive values indicate averages greater than the mean.

Figure 2.13 reveals that I8 is the coarsest site with all average grain sizes above the mean, while I4 is the finest site with all values below the mean. The crust at G2 was coarser than the mean while all other sampling categories at the site presented values finer than the mean.

While independently these values suggest that I4 would be the finest and therefore the most emissive site by fines alone, the values do not consider soil moisture or the nature of crusting as a factor controlling emission.

2.5.3 Water Digested Results

The following section will present the results of digested water processed LDM samples, for the 39 samples collected as part of the 2011 field campaign. The 39 samples are as per Table 2.8 excluding I8F and L5C as the sample sizes were too small to process. Results of digestion, including the resultant average particle size distributions and mass loss, for the four sampling categories will be presented. As results are not considered to represent natural surface conditions, further information on the samples can be found in section 1.4, while the digestion process can be found in Appendix 3.

2.5.3.1 Average Water Digested Results

Following digestion, fluff was the finest sampling category on average (median 57.9 µm, mean 52.9 µm) followed by crust (median 109.2 µm, mean 62.7 µm), soil (median 137.3 µm, mean 74.9 µm) and then the second crust (median 238.1 µm, mean 187.6 µm). This represents a decrease of the average grain size for soil by 108 µm, 140 µm for second crust, 260 µm for fluff and over 350 µm for the crusts (*Table 2.15 compared to Table 2.9 ethanol processed*).

Table 2.15: Average results for digested samples from the DO4 grid as a function of the 11 size fractions.

	Sample Category			
	Crust	Fluff	Horizon-Crust	Soil
suffix	C	F	H	S
sample	Average C	Average F	Average H	Average S
	% Contribution to each grain size range (digested)			
clay	4.52	5.46	4.68	4.27
very fine silt	6.52	7.77	7.15	5.99
fine silt	8.78	10.44	9.23	7.97
medium silt	10.93	12.42	9.92	9.89
coarse silt	11.62	12.93	8.80	12.54
very coarse silt	9.28	10.46	6.27	14.01
very fine sand	7.60	7.27	5.01	10.58
fine sand	7.09	5.18	5.25	5.43
medium sand	13.26	9.56	12.38	11.20
coarse sand	15.52	11.72	18.87	14.39
very coarse sand	4.89	6.79	12.43	3.73

These changes result in the average fluff and crust changing from being medium sand to being coarse silt, while the second crust went from being medium sand to fine sand and the soil from being fine sand to very fine sand. Average sand, silt and clay ratios also showed noticeable fining (*compare Figure 2.14 and Figure 2.6*). Before digestion, clays were between 0 and 1% of the sample, after digestion values were between 4% and 5%, while silts increased significantly from between 13% and 25% before digestion to 41% to 54% after digestion. Associated with this fining, sand percentages decreased from 75% to 80% pre-digestion to 40% to 54% after digestion (*Figure 2.14*).

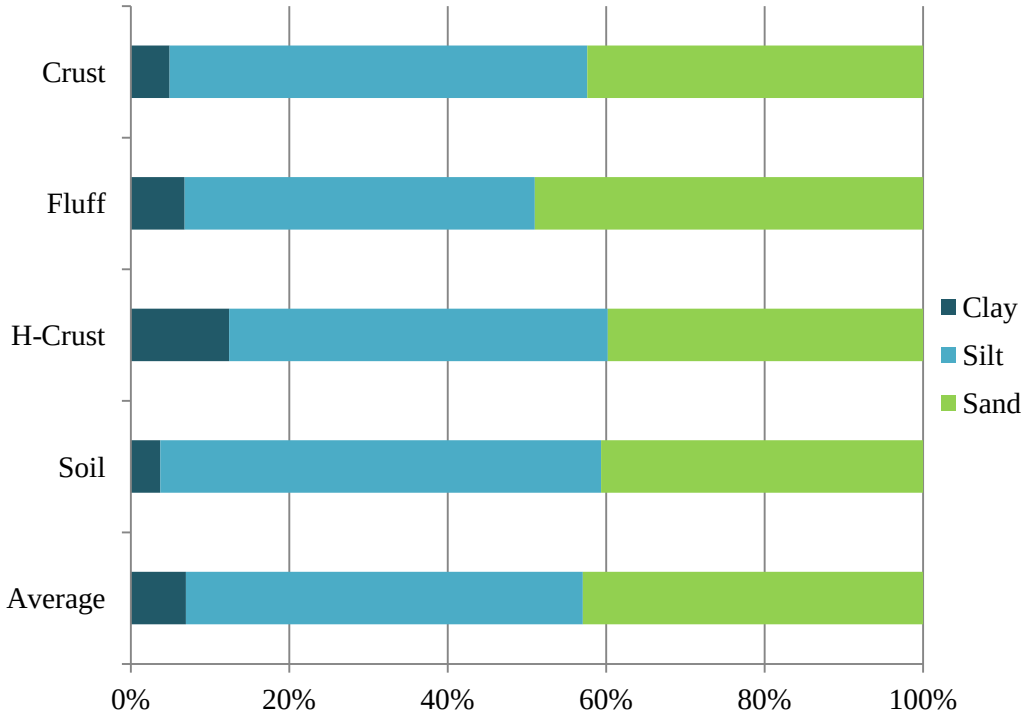

Figure 2.14: Relative contribution of sand, silt and clay to the digested averaged crusts, fluff, soil and full averaged samples from the DO4 grid.

Digesting the samples shows a definite shift between the distribution presented in Figure 2.7 with a distributions peaking in sand and tailing off towards the finer sediments; while digested samples (*Figure 2.15*) all exhibit a bimodal distribution, with a peak in the coarser silt range and a peak in the sand sized range.

Table 2.15 and Figure 2.14 present the results of the contribution of the grain size categories for the digested samples from the four sampling categories. The results reveal the increase in the finer sediments; the bimodal peak for all samples in the medium silt range (8 µm to 16 µm) and the second between 250 µm and 1000 µm, together with a significantly decreased very coarse sand contribution (1000 µm to 2000 µm).

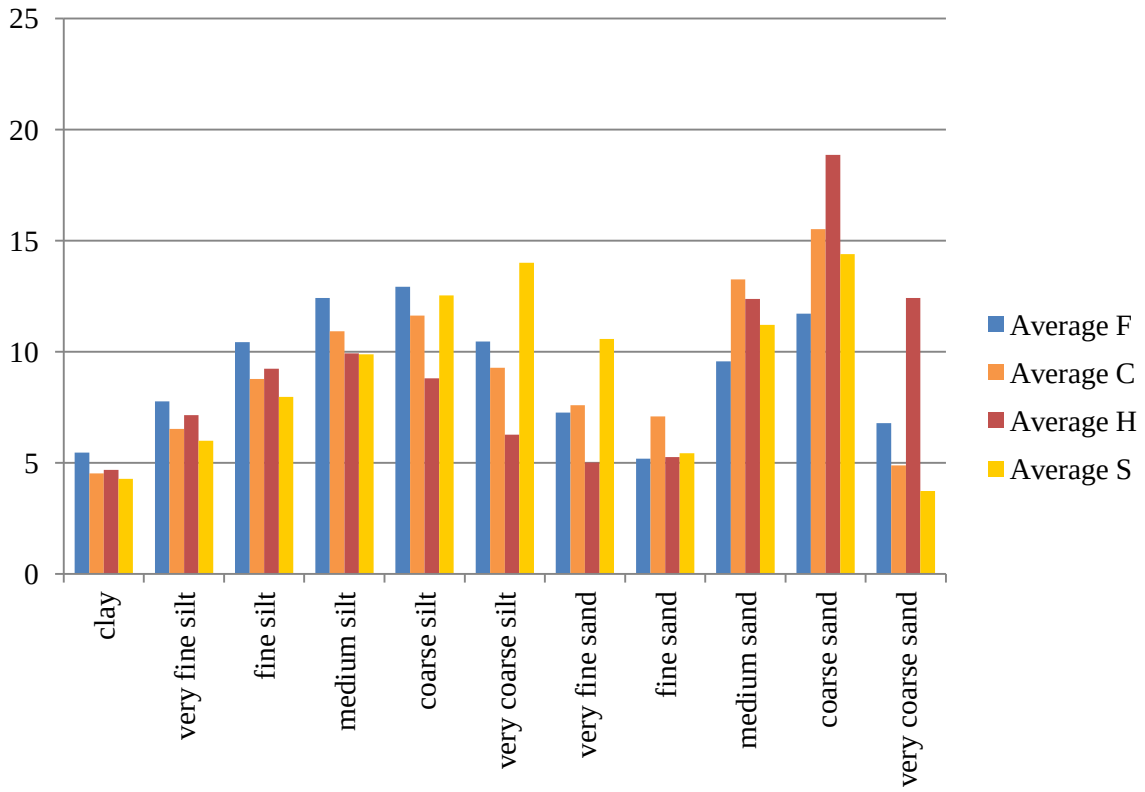

Figure 2.15: Average results for digested samples from the DO4 grid as a faction of the 11 size classifications. Average C represents the average crust, while average F represents the average fluff. Similarly, average H represents the average second crust and average S the average soil. Further information on location of samples within the vertical and horizontal sampling scheme can be found in Table 2.8 and section 1.4.

Table 2.16: Mean grain size in (µm) for all samples by sampling category after digestion. Mean, maximum and minimum statistical values have been calculated

	Sampling Category			
	Crust	Fluff	H-Crust	Soil
	Average Grain Size (µm) Digested			
B3	23.42	69.14		33.32
B7	23.18	52.09		30.64
D2	125.45	43.07	79.63	46.12
D5	46.80	107.30	85.14	25.94
D10	97.74	50.81	897.30	286.62
G2	144.00	38.63	65.99	49.36
G6	47.30	56.29		78.56
I4	73.86	9.15	124.43	42.78
I8	35.65		21.90	45.83
J3	85.96	49.42		107.63
J11	63.68		38.70	33.64
L5				118.46
	Statistics			
Minimum	23.18	9.15	21.90	25.94
Maximum	144.00	107.30	897.30	286.62
Mean	69.73	52.88	187.59	74.91

While presenting the result for grain size after digestion, it can be observed that there was a significant fining when compared with the results presented for undigested samples (section 2.5.2) (*Table 2.16*). From Figure 2.16 it is evident that D10 is the coarsest site, with the crusts and soil significantly coarser than any other sample. Following digestion, samples became increasingly similar with most of the samples being well-represented by the mean. There is the greatest difference observed in the second crusts (H-crust) although this could be in response to the smaller number of samples and being skewed by D10.

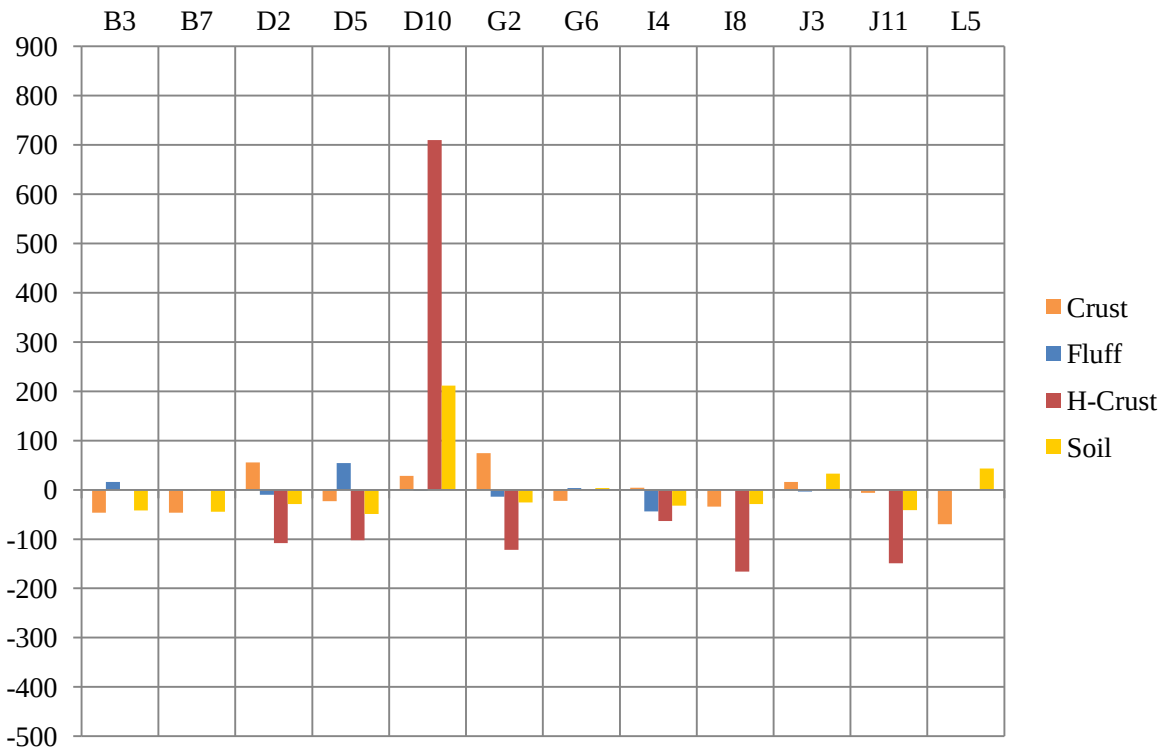

Figure 2.16: Plot of difference between grain size and the mean for the sampling category following digestion. Negative values indicate sample values smaller then the mean while positive values indicate averages greater than the mean

As the results do not represent natural surface conditions, the breakdown of grain size between samples will not be presented (Full results can be found in Appendix 5). However, of interest is the mass loss as determined through digestion, this percentage represents the amount of soluble salts, organics and carbonates in the sample. The following section will present the results of the mass loss through the digestion process for each sample. Decreasing percentages at each stage have been calculated from the mass before each processing step compared to the mass loss after each process.

2.5.4 Mass Loss During Digestion

The greatest mass loss occurred during the removal of soluble salts and gypsum, with the average for all 39 samples being 54%. The greatest decrease in mass occurred for the crust with an average of

76%, followed by the second crust 66%, then fluff 49% and finally 24.6% of soil. Of all the samples, I8C experienced the greatest mass loss with 92%, of which salt and gypsum which accounted for almost 90% of the initial mass lost, with a further 15.8% removed through carbonates and 14.6% through organics. On average crusts lost the most mass during digestion with the greatest losses occurring during the removal of salts and gypsum. Soils maintained their mass the best with losses mostly occurring in the removal of salts and gypsum. I4S was the least affected sample losing only 28.1% of its sample mass through digestion, with 17.9% through the removal of salt and gypsum lower than any other sample. Carbonates accounted for the next greatest decrease varying between 8.6% in G6S to 46% in B7S, with most samples losing around 20% of their mass.

All samples contained a very small amount of organics ranging from 2% to 10%, with an average of 5.1%. Again, crusts lost the most mass during this stage of processing, with 7.2% average removed in the first crust and 6.0% in the second crust, while 4.2% of the fluff and 3.0% of the soil were lost through organics removal.

Table 2.17: Table showing the mass loss through the three stages of digestion for all four sampling categories. The greatest mass loss can be observed for salts in the fluff while all samples contain a relatively small organic component.

	Mass Loss through removal of soluble salts and gypsum												
	B3	B7	D2	D5	D10	G2	G6	I4	I8	J3	J11	L5	Average
Crust	74.7	76.1	63.0	77.7	76.8	75.8	84.5	66.0	88.9	66.0	87.6		76.1
Fluff	50.8	44.6	48.0	53.8	58.6	44.0	52.6	52.2		36.3			49.0
H-Crust			57.7	76.0	72.9	58.9		47.4	66.4		82.7		66.0
Soil	23.6	33.7	19.5	24.6	34.9	18.6	32.2	17.9	23.3	22.0	24.6	20.2	24.6
												average Mass loss	53.9

	Mass Loss through removal of Carbonates											
	B3	B7	D2	D5	D10	G2	G6	I4	I8	J3	J11	L5	
Crust	9.6	46.0	27.3	24.0	41.6	15.8	22.4	15.6	15.8	9.9	15.2		22.1
Fluff	28.4	20.3	16.3	29.1	36.5	14.7	16.8	10.5		10.2			20.3
H-Crust			24.9	31.1	29.3	23.8		11.4	13.9		15.5		21.4
Soil	15.2	13.8	11.3	15.0	12.8	12.4	8.6	10.4	14.9	10.7	15.1	12.0	12.7
												average Mass loss	19.1

	Mass Loss through removal of Organics											
	B3	B7	D2	D5	D10	G2	G6	I4	I8	J3	J11	L5	
Crust	4.9	7.4	7.1	6.3	9.6	3.6	6.1	4.4	14.6	4.9	10.7		7.2
Fluff	3.2	2.8	4.5	4.7	5.8	3.9	3.9	4.4		4.4			4.2
H-Crust			4.6	9.9	4.8	5.0		2.3	6.0		9.2		6.0
Soil	2.9	2.4	2.9	2.7	3.8	2.4	2.5	2.2	3.2	3.2	3.8	3.6	3.0
												average Mass loss	5.1

	Total Mass loss from initial sample												
	B3	B7	D2	D5	D10	G2	G6	I4	I8	J3	J11	L5	
Crust	78.2	88.0	75.0	84.1	87.8	80.4	88.7	72.5	92.0	70.9	90.6		82.6
Fluff	65.8	57.1	58.5	68.8	75.2	54.1	62.1	59.1		45.3			60.7
H-Crust			69.7	85.1	81.7	70.3		54.5	72.8		86.8		74.4
Soil	37.1	44.3	30.7	37.7	45.4	30.4	39.6	28.1	36.9	32.7	38.4	32.3	55.7
												average Mass loss	68.3

Table 2.17 presents the results of all stages of mass loss through digestion. Soluble salts and gypsum as well as carbonates can be seen to be concentrated in the crusts, while they are less prevalent in the soils. The fluff contained approximately 50% soluble salt and gypsum, while soils contained only 25% soluble salt with decreasing mass loss experienced through the removal of carbonates and organics.

2.5.4.1 Summary

i. Removal of soluble salts and gypsum contributed to the greatest mass loss
ii. Soluble salts and gypsum were found in the high concentrations in the crust
iii. Carbonates were the next most important chemical contribution, resulting in on average 20% mass lost with the second crust containing the highest percentage of carbonates
iv. Samples were low in organics accounting for between 2% and 10% of the sample

2.6 Discussion and Conclusion on Makgadikgadi Sediments Considering Methodological Bias in Result Determination

Observation of the data set has confirmed the results of previous studies, which has identified trends in grain size distributions for dust producing regions. Here, the analysis of Sua Pan samples using laser diffraction with ethanol as the dispersant, presented the opportunity to use a modern method while maintaining the integrity of the sample and presenting the natural state of the sediments. While there are many known limitations inherent in determining particle size both through traditional sieving (Buurman et al., 1997) and in the use of modern laser methods (Di Stefano et al., 2010), section 2.4 has presented important conclusions regarding the effects of different techniques in determining grain size distribution. Conservative analysis of samples using ethanol as a dispersant in the Malvern Instruments was therefore determined to be the best means of obtaining a particle size distribution of salt rich sediments.

2.6.1 Discussion of Makgadikgadi Sediments within the Global Setting:

Comparative studies on dust source regions and their surface characteristics are not prevalent in literature. Further, there are a limited number of studies which present data using non-invasive techniques (Laurent et al., 2008; Lawrence & Neff, 2009). Three studies were found with results presented on surface characteristics in dust producing regions, and will be used to provide the context within which Makgadikgadi sediments can be considered.

Mei et al. (2004), Khalaf (1989) and Chatenet et al. (1996) present results for Chinese, Kuwaiti, and Saharan and Sahelian soils respectively. Chatenet et al. (1996) revealed that Saharan and Sahelian soils are a function of four dominant categories namely: alumina-silicated-silt (clay mineral dominant: mean 125 µm), fine sand (quartz dominated: mean 210 µm), coarse sand (quartz dominated: mean 690 µm) and salts (salt and clay minerals: mean 520 µm). The authors acknowledge that statistical

analysis using only eight sieve classes produces a risk of "over fitting" (Chatenet et al., 1996: p904). However, they classify sediments statistically as a function of the four classes using the traditional log-normal distribution, fitting samples with XRF chemical analysis. Using similar categories, Khalaf (1989) describes samples as being a function of a number of categories which can reveal the nature of sediment origin and suggest that modes are indicative of underlying sediment chemistry. Evans et al. (2004) add to this, commenting on the bimodality of size being a function of the "Tanner Gap" which reflects the mechanisms involved in weathering and *in situ* processes.

This link between sediment characteristics and chemistry is well known, with the nature of salt and saline chemistry considered in aeolian studies (Nickling & Ecclestone, 1981; Lowenstein & Hardie, 1985; Saint-Amand et al., 1987; Reheis & Kihl, 1995; Buck et al., 2006; Soukup et al., 2008a; Cattle et al., 2009; Buck et al., 2011). Further, the importance of pans or playas as global dust sources is recognised (Prospero et al., 2002; Bullard et al., 2011), with the surface chemistry of these units synonymous with evaporite salts (Shaw & Thomas, 1997; Prospero et al., 2002). This saline nature of pans has an effect on both the emissivity of the pan surface and the grain size distribution, with the role of salts within the soil profile discussed as by Gillette et al. (1979) to be of greater importance in clay rich locations. Gillette et al. (1979) determined that in soils with high clay contents, there is a higher cation exchange capacity and therefore greater potential for salt-clay aggregates. Through chemical analysis, Chatenet et al. (1996) revealed that samples with a mode between 450 µm and 600 µm were rich in salt. This is confirmed in the dominance of the 450 µm to 600 µm size range in both Owens Lake (Chatenet et al., 1996) and Sua sediments. For Owens Lake sediments, this is in response to salt efflorescence increasing the size through aggregating and salt crusting of finer grains. Modal values from Sua Pan fluff and crusts samples presented a primary or secondary mode within this range. Additionally, crusts samples showed the strongest mode peaks in this range, which is confirmed by a 75% mass loss in crusts during soluble salt removal through digestion. Soils which contained modes in either finer categories (70 - 90 µm) or coarser (>600 µm) experienced an average of only 25% mass loss. This would confirm the role of salts efflorescence in aggregating the finer grains within the Sua samples. Full digestion also increased the percentage of clays and fine silts while decreasing the percentage of medium and coarse sands where salt aggregates were proposed to occur.

This fine modal category of clays was particularly evident in the soil samples; which, on average, were the finest of the Sua sediments. This sampling category presented results with a nominally bimodal distribution with one mode in <125 µm and a second >600 µm. This confirms the relationship between the hydrated soil samples and the drier upper sediments. Reynolds et al. (2007) suggest that the salt saturated clay rich soils will principally form salt-clay crust aggregates during evaporation and crystallisation. This is confirmed by Chatenet et al. (1996) who observed that dried salty-clayey samples were dominated by grains in the range from 450 to 600 µm, while sand

dominated samples were less likely to exist in this range in the presence of salt. Mei et al. (2004) identify similar trends in the Taklimakan and Gobi deserts in China. In 88 surface soil samples, none of the samples contained a mean below 90 µm, as Mei et al. (2004) found that salt rich aggregations cemented the finer sediments resulting in a shift of the median grain size towards the coarser sediments. These authors found that despite the relatively large median grain size, deserts and farmlands with sand dominated soils were the major dust sources (Mei et al., 2004).

While Makgadikgadi and Owens Lake sediments had modal values between 450 µm to 600 µm, a number of Saharan, Sahelian and Chinese soils were associated with a mode greater than 600 µm. This range is proposed to be associated with (i) dune (or similar) sands transported into the source (ii) from localised sand seas or (iii) representative of *in situ* weathering (Chatenet et al., 1996). These coarse samples were often rich in large quartz grains. None of the Sua Pan fluff or crust sediments were found with modes in this range, while half of the 12 sampled soils existed in this range. It can therefore be proposed that while the lower sediments are dominated by weathered materials with the salts in solution and therefore not aggregating the finer sediments, the drier upper layers are dominated by saltier evaporite aggregated fine sediments. Khalaf (1989) presented similar results for 334 samples from the Kuwaiti desert, with a quartz dominated coarse sand mode (or lag) at 750 µm with a finer quartz mode at 250 µm. The Kuwaiti samples also contained a mineralogically variable finest mode at 125 µm.

However Khalaf (1989) did not observe a modal mean between 450 and 600 µm, therefore using the assumption of Chatenet et al. (1996) that the domination of this size range can be attributed to the presence of salt, it can be proposed that there is likely an absence of salty soils in Kuwaiti desert; a proposal that is confirmed through chemical analysis of Kuwaiti sediments in a study by Hadi and Al-Ruwaih (2008). The authors confirm the relatively low concentrations of salt and therefore further verify the role salt rich conditions have in the dominance of this size range. In further confirmation of this mineralogically derived modal mean, following digestion, samples from the Sua Pan did not contain this mean instead values shifted to finer sample sizes.

While definitions of surface conditions, most particularly in dust producing regions, are not prevalent in the literature, the classifications of sediments which are associated with dust (see section 1.2 and further discussed in Chapter 4, Section 4.1.1.2) are considerably finer then the results presented here. Bullard et al. (2011) attribute this discrepancy to selective entrainment associated with wind erosion, while Cahill et al. (1996) add that mechanisms associated with saltation are often responsible for the differing conditions between the surface and the airborne material from sources. Bullard et al. (2011) suggest that wind erosion is responsible for the removal of fine particles (usually <100 µm in diameter) from the land surface leaving behind a lag of coarser grains. Wang and Jia (2011) propose that these lag sediments are exposed to wind stresses, which imparts momentum on the larger grains,

typically between 100 and 1500 µm, leading to saltation and surface sandblasting. This sandblasting and/or saltation liberates smaller sediments through exposing or disaggregating finer sediments (Bagnold, 1941; Cahill et al., 1996; Chatenet et al., 1996; Mei et al., 2004; Wang & Jia, 2011). Therefore, the absence of dust sized grains from the surface does not determine the dust flux potential of the surface. This confirms work by, amongst others, Khalaf (1989), Chatenet et al. (1996) and Mei et al. (2004), who state that sediments in dust source regions are significantly coarser then the dust they emit. Further surface sediments become coarser towards the end of the dust season in supply limited systems. While the Makgadikgadi samples revealed a sample in this coarse range, the results represent a single sampling period during the early stages of the dust season and therefore are not considered to be representative of a late season lag surface and therefore more likely indicate the nature of the pan structure.

Despite the indication that the samples analysed in this study are only representative of a single season, Mahowald et al. (Corrected Proof) suggest that the accurate representation of dust particles in the atmosphere begins with a precise parameterisation of dust at the source. The authors further indicate that few studies exist which fully characterise source regions, while fewer still extend the particle size distributions to the coarser sizes. Despite the lack of data the authors indicate that results of field campaigns appear to present that the aerosol load from emissive surface is relatively consistent for the 1-5 µm size fraction regardless of the surface state. Thus supporting the hypothesis (Mahowald et al., Corrected Proof) that the emission of this size fraction is unaffected by the soil type, state and wind speed. However Kok (2011) suggests that while the fine grains may be similar between sites and sources, the larger aerosols (>5 µm) vary substantially. Therefore, using this assumption, the sediments from the Makgadikgadi can be assumed to contain a similar amount of fine sediments (<5 µm) to global sources despite the surface containing less than 1% clay sized grains and a similarly low percentage of fine silts. While surfaces are known to be highly variable, Mahowald et al. (Corrected Proof) note that the size distribution of transported aerosols are often found to be log normal, although add that this is unlikely to be observed close to the source as with transport, the larger size fraction will be disproportionately removed in response to gravitation settling. Kok (2011) add that while this coarse fraction may not be subjected to significant transport, coarse fraction aerosols are important for longwave radiative interactions as well as local biogeochemical systems. While chapter 5 will further consider the nature of transport from this region, the relatively coarse nature of the surface, suggests a high potential for coarse fraction aerosols, even if just in the local aerosol load.

While analysis of clay, silt and sand percentages within samples revealed that regionally values of silt, clay and sand are comparable to studies of Saharan, Sahelian and Chinese soils (Chatenet et al., 1996; Mei et al., 2004) these regions are known to be significantly more emissive than the Makgadikgadi (Washington et al., 2003). Mahowald et al. (Corrected Proof) suggested that regardless

of source conditions, the fine fractions from all these regions is likely to be similar however no such statement can be made for the coarser fraction. However it was in the coarse fraction that much of the Makgadikgadi sediments were detected to occur, with noteworthy variability found between sites and within the vertical structure of the pan. Much of this discrepancy can be attributed to the chemistry of the pan, thus confirming the role of salts in affecting the emissive nature of surfaces (Nickling & Ecclestone, 1981) and highlighting the importance of salts in the measured grain size distribution of natural surfaces. An important signature within the psd of all undigested Makgadikgadi samples was the peak in 450 µm to 600 µm range indicative of a saline environment. The absence of this in the digested sample further reveals the changes in the nature of the sample imposed through digestion.

While trend analysis in grain size of surface samples is possible, there remains the problem of directly comparing these studies with Sua sediments, as sampling strategies, methods and laboratory techniques can produce vastly different results for the same sample under differing conditions (as in section 2.3). Further, many literature studies did not appear to discriminate between the different surfaces types present, sampling mainly the upper few centimetres of the surface, while in this study a clear vertical structure existed on the pan surface with crusts, fluff and soil being sampled independently. It is unlikely that this will significantly affect the trends determined above, but it does introduce caution to the relatively fine nature of Sua sediments compared with other source regions.

While comparison of this surface within the global literature drew strong links with similar large inland, saline ephemeral systems, the true sub-basin variability is not considered and can provide further insight into the spatial variability of the system. The following section therefore presents the results of the Sua sediments within the 144 km^2 array and considers the nature of the pan sediments within the context of the Kalahari sands.

2.6.2 Discussion of Sua Sediments within the Grid and Regional Context

The results presented in this study reveal a strongly heterogeneous pan surface at the sub-basin scale. This confirms findings by Vickery et al. (2013) that the Makgadikgadi Pan is not a large homogenous playa surface, but is instead comprised of variable surfaces and therefore has emissive characteristics. Figure 2.13 presents grain sizes as relative to the mean, and while this cannot be viewed independently of the moisture content and crust characteristics (strength, depth and completeness), it does present these sites with consistently finer sediments than others. For example, all samples taken from I4 are finer than the mean, while I8 samples are all consistently coarser than the mean. These sites are within 4 km of each other and therefore confirm a spatially heterogeneous pan surface, which could account for the spatially discreet nature of emissions from the pan surface.

An additional factor that controls the emissive nature of the pan is the chemistry and composition of the surface (see section 2.5). Through digestion, a difference in the chemical composition between I4

and I8 could reveal why I8 sediments are consistently coarser. Earlier discussion considered the importance of salts in agglomerating finer clay particles into the medium sand range. Through the removal of salts alone, I8C lost 88.9% of its mass compared to 66.0% at I4C, with similar trends for I8H (66.4%) and I4H (47.4%), and I8S (23.3%) and I4S (17.9%). Similarly, I8 samples lost more mass during the removal of carbonates and organics than their I4 equivalents. When presenting values as a function of the mean, before digestion I4 was finer than the mean, while after digestion, other than a very fine fluff sample, it was only slightly finer than the mean (*Figure 2.13, Figure 2.16*). Conversely, I8 was significantly coarser than the mean before digestion, while following digestion it became finer in all sampling categories. The fining observed at I8 is therefore likely to be due to the removal of agglomerating salts and carbonates thereby presenting the finer particles for detection.

Correlation of mass loss and fining revealed a near zero correlation (R^2=0.09) for soils with a slightly positive correlation observed for the crusts (R^2=0.24). This suggests that while digestion results in sample fining, the poor correlation could reveal that there are spatial differences in the grain size distribution irrespective of the effects of chemistry. Further, while fining was observed in all sampling categories following digestion, the effects were most notable for the crusts which, on average, lost 83%, compared with only 56% in soils and 61% and 74% in fluff and second crusts respectively. This high mass loss in the crust confirms the findings of Gillette et al. (2001) who indicate that the soluble salt content is higher in the crust than in the subsurface, because evaporation concentrates the salts near the surface. The proposal of 'saltier' upper layers does not manifest itself in a highly salty fluff, nor to the second crust which lost less mass in all stages of digestion. Therefore, the presence and location of salts within the vertical profile of the pan sediments along with the distribution of the various grain sizes can both be deterministic of *in situ* conditions and can reveal further information on the nature of the capillary zone (Reynolds et al., 2007) and associations with ground water proximity.

While grain size was initially proposed to be prescriptive of emissivity (Bagnold, 1941; Pye, 1987), it is essential that the sediment is sufficiently exposed to the wind shear in order to be entrained (Nickling & Ecclestone, 1981). In light of this, the soil samples that were detected to be the finest are an unlikely source in the absence of significant deflation and drying, as they are trapped beneath crust(s) and in many cases fluff and are in a hydrated state.

The importance of soil moisture is confirmed through the difference between wet and dry sample masses, with drying accounting for between 20% and 30% mass lost in soils compared to between 2% and 5% for fluff and crust samples. Therefore the moisture content in the upper soils is significant and can be considered to result in negligible dust potential from soils.

While neither the soil nor the cemented crust(s) can be assumed to be the source of significant sediment, it is proposed that the emissive material on the Makgadikgadi Pans originates from the fluff. The composition of the fluff, and more importantly the relative contribution of clays and silts within the fluff, can give a rough estimate of the amount of aeolian dust potential between sites. From Table 2.14 it can be proposed that I4 has the greatest potential to be emissive as it has the finest mean composition. Additionally, assuming these results occur in the absence of the crust and other environmental factors, including moisture conditions, B7 is an equally likely source of dust, while J3 is the least likely.

Table 2.18: Comparison of soil samples from the Sua Pan and the Mega Kalahari, data adapted from Thomas (1987).

		clay	silt	sand
Sua Digested Soil Samples from within the D04 sampling grid	B3	4.3	60.8	34.9
	B7	3.7	67.8	28.5
	D2	4.1	54.5	41.3
	D5	5.8	64.8	29.3
	D10	1.7	20.3	78.0
	G2	3.7	59.9	36.4
	G6	3.7	41.0	55.4
	I4	4.3	56.6	39.1
	I8	5.7	52.7	41.6
	J3	4.5	35.2	60.3
	J11	6.5	60.4	33.1
	L5	3.3	30.6	66.1
	Average	4.3	50.4	45.3
Thomas (1987) Mega Kalahari sand samples from landform elements	Ridge Crest	1.0	4.6	94.4
	Trough	3.5	11.4	85.5
	Pan	6.4	22.4	71.8
	Pan Surround	5.6	10.3	80.5
	Palaeolake	10.4	19.6	71.2
	Fossil Channel	2.2	14.7	82.1
	Unclassified	1.96	7.14	89.86

In determining the emissive potential of the Makgadikgadi Pans within the regional setting, comparing results obtained here to studies on grain size of Kalahari sediments can reveal further controls highlighting the importance of pan sediments. Thomas (1987) presents the results for Kalahari sediments within the context of determining the different depositional environments of the Mega Kalahari. Samples were taken from a depth of 30 cm using a 12 cm auger (to avoid surface sediments) (Thomas, 1987). As samples were taken from depth, comparison with Sua soil samples could indicate the nature of sub-surface pan sediments within the regional context. As the results described by Thomas (1987) are on digested samples, comparison of digested soil samples reveal that Sua sediments contain a significantly higher contribution of silt (average 50% vs. 12%) than samples presented by Thomas (1987) (*Table 2.18*). While clay contribution remains fairly consistent with Sua

Pan samples containing relatively similar percentages of clay to those of the Mega Kalahari 'Pan' and 'Pan Surround' samples, the percentage of sand is significantly higher in all Thomas (1987) samples. While soil cannot be assumed to representative of the surface sample it can indicate that there is significant variability experienced throughout the Kalahari beneath the surface. In addition, the data suggests that sub-surface sediments in the Makgadikgadi and other Kalahari Pans are similar and therefore does not exclude other pans in the region from present or future emissions.

Similarly, a study by Ringrose (1999) presents results for the western margin on the Makgadikgadi Pan complex using traditional sieve methods and pipette settling for the finer grains (*Table 2.19*). Results reveal that relative to the Gidikwe ridge and Boteti, Sua sediments contain significantly higher silt contributions, but lower sand and clay percentages. Methodologically the Ringrose (1999) results are comparable with the ethanol results presented here and therefore cautious comparison is possible. It can be assumed that on a regional level the Sua samples contain on average 11% less sand sized grains than those described by Ringrose (1999) and just over 1% fewer clay sized grains, these discrepancies result in silt values on the pan being 13% higher. Therefore, as finer sediments are present on the pan than on the periphery, given a uniform wind over both surfaces, pan sediments will preferentially be entrained.

Table 2.19: Comparison of Sua Pan samples with upper grey sands to the west of the Makgadikgadi Pan complex, data adapted from Ringrose (1999).

		clay	silt	sand
Sua Digested Soil Samples from within the D04 sampling grid	Sua Crust	0.6	18.4	81.0
	Sua Fluff	0.2	13.5	86.4
	Sua H-Crust	0.4	14.6	85.0
	Sua Soil	0.7	24.5	74.8
	Sua Average	0.5	17.8	81.8
Ringrose (1999) Textural characteristics of upper grey sands by Geomorphological unit	Gidikwe ridge - crest	2.0	5.1	84.6
	Gidikwe ridge - lower slopes	1.3	4.0	94.6
	Northern Plains	1.0	2.5	96.4
	Southern Plains	2.7	6.0	91.2
	Recent dunes	3.3	6.5	90.2
	Boteti Riverbed	0.9	1.0	98.2
	Boteti Floodplain	1.6	3.4	95.0

While viewing pan sediments in the context of the Thomas (1987) and Ringrose (1999) studies can increase our understanding of the nature of the pan sediments, it also allows for the sediments to be presented in the regional context. It can therefore be proposed that while the Makgadikgadi Pans are indeed a function of the Mega Kalahari in a base geological setting, the system and associated evaporite salts, create an environment with sedimentalogical properties unlike those of its surroundings. On a large scale this is supported by Thomas (1987) who noted that, on the whole,

Kalahari sediments were exposed to a similar environmental history with spatially discreet modification of sediments by subsequent processes and systems.

The results presented above have implications for the interpretation and inclusion of accurate field data into climate models. Typically models include data provided from global databases (e.g. Zobler, 1986), however these results are not comparable with the resolution of those presented above. Lawrence et al. (2010) claim that these database values are useful in locations where soil conditions are not known. Further, field data often presents results of partially digested samples; this would present conditions finer than those of the natural surface. The surface of the pan is further complicated by surface crusts and therefore, the results presented here could have a significant impact on the skill in the modelling of the Makgadikgadi Pans.

2.7 Concluding Summary for Determining Grain Size Trends for the Makgadikgadi Pan:

Through the above discussion it is evident that considering grains independently of context is too simplistic. This was particularly evident when grain size was viewed through digestion, as aspects of chemistry were revealed, presenting valuable insight into the nature of the sample, confirming the proposal by Grousset and Biscaye (2005: 153) that "dust aerosols do not exist as individual grains, but as aggregates of particles within a range of grain sizes." Despite this, Blanco et al. (2003) suggest that single particle studies are essential in environmental atmospheric chemistry, since they allow for the identification of the various processes involved in the formation and evolution of atmospheric aerosols. This is particularly relevant in the consideration of particle morphology which is better understood on a grain by grain basis. It is essential to understand both the bulk and single mineral dimensions of the sample in order to determine transport, radiative and ecological impacts.

In order to determine the nature the nature of,Makgadikgadi sediments, samples were run in both water and ethanol revealing that:

a. Samples run in ethanol had a uni-modal distribution centred at medium sand (40%) (250 – 500 µm) – confirming the proposal by Chatenet et al. (1996) that salt rich samples will aggregate finer grains to produce a modal peak in this range.
b. Samples run in water had a bi-modal distribution located at silt (40%) (3.9 – 62.5µm) and very fine sand (20%).

Therefore, additional consideration needs to be placed into the means of analysis for samples, particularly in comparing grain size thresholds. The main findings of this chapter can be summarised as follows:

i. A number of methods exist to evaluate the grain size of samples, the aim here was to present the least disturbed representation of surface (*in situ*) conditions. This was determined to be through the use of ethanol.
ii. Despite the absence of ethanol processed data in the literature, in this study it was determined to be a significant contribution to the literature on how to determine the psd of salt rich samples.
iii. Analysis of grain size trends and the observed mode in the 450 to 600 µm range, suggest that this region is associated with salt-clay agglomerates. This is confirmed by measuring mass loss during digestion.
iv. The digestion process found that crusts lost on average 76% through the removal of salts and gypsum, with fluff, second crusts and soils losing 49%, 66% and 25% respectively. Combined with further losses through the removal of carbonates and organics, resulted in between 36% (soils) and 83% (crusts) being removed from the sample.

The relatively fine nature of Makgadikgadi sediments also confirmed that there is sufficient fine grained sediment to result in the pan being a significant source of mineral aerosol. The vertical structure of the pan revealed that the most probable source of dust is associated with the fluff which is in line with other studies globally. A fundamental assumption is that while Sua sediments were consistently presented as similar to global dust region sediments, this cannot be viewed in the absence of the nature of the surface which includes the crust and chemistry which are important determinants for quantifying and categorising the emissivity of the pan surface. The following chapter will present the chemistry of the pan surface in order to further detail the heterogeneity of the pan surface.

Chapter 3: Surface Chemistry of the Makgadikgadi Pans

3.1 Introduction

The Makgadikgadi Pans, covering approximately 6 000 km^2 found within the Makgadikgadi Basin, are situated in the semi-arid north east of Botswana (Thomas & Shaw, 1991). The 37 000 km^2 basin represents a range of fluvial, lacustrine and aeolian surface morphologies, as defined by Bryant et al. (2007). The Pans have been identified as an important evaporitic basin in southern Africa due to their highly emissive nature (Bryant et al., 2007; Vickery et al., 2013). Similar large pans are widespread features of many of the world's drylands; a substantial proportion of these are closed basins (Goudie & Wells, 1995). There are a number of authors who have attempted to define pans or playas, most of which include comment on their location, hydrological context and morphology (Eugster, 1980; Shaw & Bryant, 2011). Shaw and Bryant (2011) define pans (or playas) as:

> *"...arid zone basins of widely varying size and origin which, although generally above the present groundwater table, are subject to ephemeral surface water inundation of variable periodicity and extent. Their basal and marginal sediments often display evidence of evaporite accumulation, aeolian deflation and accumulation, and/or lacustrine activity."* (Shaw & Bryant, 2011: 375)

The context, as outlined by Shaw and Bryant (2011), results in such environments existing in orographic or inland basin floors, with many of these associated with tectonic initiation (Eugster, 1980; Shaw & Bryant, 2011). Due to the hydrologically closed nature of these systems, inflow most frequently occurs from perennial rivers and springs, ephemeral streams (Shaw & Thomas, 1997) and occasionally through storm run-off. However, many of these systems experience evaporation levels up to ten times that of the inflow (Shaw & Thomas, 1997), resulting in highly saline supersaturated water (Eugster, 1980). This high level of evaporation further concentrates the solutes present in the groundwater. When the environment is characterised by shallow ground water this evaporation results in rich evaporite crusts (Saint-Amand et al., 1987; Shaw & Bryant, 2011), which are ubiquitous features of inland basins (Eugster, 1980).

Prolonged standing water is rarely experienced, although seasonal flood waters, which dissolve efflorescent crusts, are important for solute recycling within systems (Eugster, 1980), with the extent and frequency of inundation dependant on climatologic and hydrological setting (Shaw & Bryant, 2011). Mineral stability often creates conditions such that sodium chlorides, carbonates and sulphates will be dissolved, while alkaline earth carbonates and silica will remain in the crust (Eugster, 1980). These processes maintain the solute load of the system and create a seasonal response to surface crusting and chemistry. In closed systems evaporation will act to concentrate the solutes present,

whereas in open systems, inflow serves to both dilute and bring a replenishing solute load (Yechieli & Wood, 2002).

The nature of these solutes and the associated evaporites is highly variable. While marine environments are often constrained by the chemistry of sea water, there is no such constraint for continental saline lakes and their evaporites. It is noted by Hardie et al. (1978) that catchment lithology, weathering rates and system age are important determinants of the types of salts expected. Further, airborne salts and regional transport cannot be negated for mineral input into systems (Field et al., 2010). Despite this variability, Eugster (1980) and Shaw and Bryant (2011) suggest that continental brines can be represented by the following ions: Na^{+}, K^{+}, Ca_2^{+}, Mg_2^{+}, Cl^{-}, SO_4^{-}, SiO_2 and HCO_3^{-}-CO_3^{-}, all commonly derived from surface and groundwater catchments. Eugster (1980) suggested that, mineralogically, these ions will create one of four brine types (a) Na-CO_3-Cl; (b) Na-CO_3-SO_4-Cl; (c) Na-SO_4-Cl; (d) Na-Mg-SO_4-Cl; and (e) Ca-Mg-Na-Cl. The author has considered the presence of these minerals and their relative abundance in an effort to predict the nature of the associated systems. Eugster and Hardie (1978) looked at Ca/Mg and HCO_3 to determine brine types, further developed by Eugster (1980) into the mineral groupings presented in Table 3.1 (Eugster & Hardie, 1978; Eugster, 1980). The author notes that rates of evaporation and mineral presence are controlled by temperature and the stability of minerals, leading to variations on diurnal to seasonal scales (Yechieli & Wood, 2002).

Given the above variance and the range of solute sources in arid environments, there is potential for geochemical variability within and between basins. Therefore, using mineralogy alone, it is not always possible to differentiate the nature of the source. Additionally, differentiating marine versus non marine origin is complicated, as halite and gypsum are common in both environments (Eugster, 1980), while carbonates (e.g. trona, gaylussite, burkeite) are exclusive to continental evaporites and therefore their detection indicates a non-marine origin.

Buck et al. (2011) notes the importance of mineral evaporites in pan environments, particularly those associated with shallow water. In these systems, the continual replenishment of minerals occurs through the drawing of solute rich ground water through the capillary zone, providing a near infinite supply of salts. However, it is noted by Mees (2003) that the factors and processes that determine the distribution and morphology of evaporite minerals in saline environments are poorly understood. With Mees (2001) proposing that mineral evaporites form exclusively after the development of pan depressions through interactions with groundwater, while clays and silicaceous minerals represent the base minerals associated with the system.

Table 3.1: Saline minerals of non-marine environments (Eugster, 1980)

Brine Type		Primary Minerals		Authigenic Minerals	
(a)	$Na - CO_3 - Cl$	Halite	NaCl	Gaylussite	$Na_2CO_3.CaCO_3.5H_20$
		Nahcolite	$NaHCO_3$	Prissonite	$Na_2CO_3.CaCO_3.2H_20$
		Natron	$NaCO_3.10H_20$	Shortite	$Na_2CO_3.2CaCO_3$
		Thermonatrite	$Na_2CO_3.H_20$	Northupite	$Na_2CO_3.MgCO_3.NaCl$
		Trona	$NaHCO_3.Na_2CO_3.2H_2O$	Hanksite	$9Na_2SO_4.2NaCO_3.KCl$
				Aphthitalite	$K_3Na(SO_4)_2$
				Tychite	$Na_2CO_3.MgCO_3.Na_2SO_4$
				Dawsonite	$NaAlCO_3(OH)_2$
(b)	$Na - CO_3 - SO_4 - Cl$	Burkeite	$Na_2CO_3.2Na_2SO_4$		
		Halite	NaCl		
		Mirabilite	$Na_2SO_4.10H_2O$		
		Nahcolite	$NaHCO_3$		
		Natron	$NaCO_3.10H_20$		
		Thenardite	Na_2SO_4		
		Thermonatrite	$Na_2CO_3.H_20$		
(c)	$Na - SO_4 - Cl$	Halite	NaCl	Glauberite	$CaSO_4.Na_2SO_4$
		Gypsum	$CaSO_4.2H_20$		
		Glauberite	$CaSO_4.Na_2SO_4$		
		Thenardite	Na_2SO_4		
		Mirabilite	$Na_2SO_4.10H_2O$		
(d)	$Mg - Na - SO_4 - Cl$	Halite	NaCl		
		Bischofite	$MgCl_2.6H_2O$		
		Glauberite	$CaSO_4.\ Na_2SO_4$	Glauberite	$CaSO_4.Na_2SO_4$
		Gypsum	$CaSO_4.2H_20$	Bloedite	$Na_2SO_4.MgSO_4.4H_2O$
		Epsomite	$MgSO_4.7H_2O$		
		Hexahydrite	$MgSO_4.6H_2O$		
		Kieserite	$MgSO_4.H_2O$		
		Thenardite	Na_2SO_4		
		Mirabilite	$Na_2SO_4.10H_2O$		
		Bloedite	$Na_2SO_4.MgSO_4.4H_2O$		
(e)	Ca – Mg – Na - Cl	Halite	NaCl		
		Sylvite	KCl		
		Antarticite	$CaCl_2.6H_2O$		
		Bischofite	$MgCl_2.6H_2O$		
		Carnallite	$KCl.MgCl_2.6H_2O$		
		Tachyhydrite	$CaCl_2.2MgCl_2.12H_2O$		

Understanding the nature of the parent materials, the age of the system and the context of the samples is essential in the interpretation of chemical results. Furthermore, the presence of minerals or ions can be used as tracers, with continental sodium ions often associated with prolonged weathering of feldspar, while gypsum and mirabilite are common features of brine rich environments (Eugster, 1980). The natures of many evaporite deposits are reliant on the climatic, hydrologic, geochemical, biologic and sedimentological aspects, with the deposits representing very brief records of these conditions and subject to change on seasonal, annual and decadal time scales. Changes in ground water saturation levels, system recharge and climate variability can have dramatic effects on both the nature of the minerals and the surface of the system.

While this chapter does not attempt to determine the factors and processes that have led to the conditions present in the Makgadikgadi system, nor to determine the precise composition of locally derived aerosols. It will examine the compositional variations of the Makgadikgadi Pan surface and determine the spatial and chemical variability of sediments within the vertical pan structure.

3.2 Field and Laboratory Methods

3.2.1 Field Procedure:

Samples are initially named by the site at which they were sampled according to the system utilised for the DO4 project (see site details in Chapter 1 and Appendix 1). At each sampling site, samples were determined to belong to the following four categories: fluff, crust, secondary crust and soil. All samples are represented by 'grab samples' from the 2011 DO4 field site. Crust samples represent the hardened pan surface (crust) that was found at most sites with varying thickness from a few millimetres to over a centimetre in thickness (Figure 3.1), below this, a dry powdery layer was found varying in thickness from zero to almost 8 centimetres – this represents the fluff. At some sites a second hardened layer was found between the fluff and the wet sediment layer below, again in the order of a few millimetres to a centimetre in thickness – this is described by the second crust or horizon crust. The wet sediment layer which represents the lowest sampling horizon, extended relatively homogenously over a meter below the pan surface, and has been classed as soil.

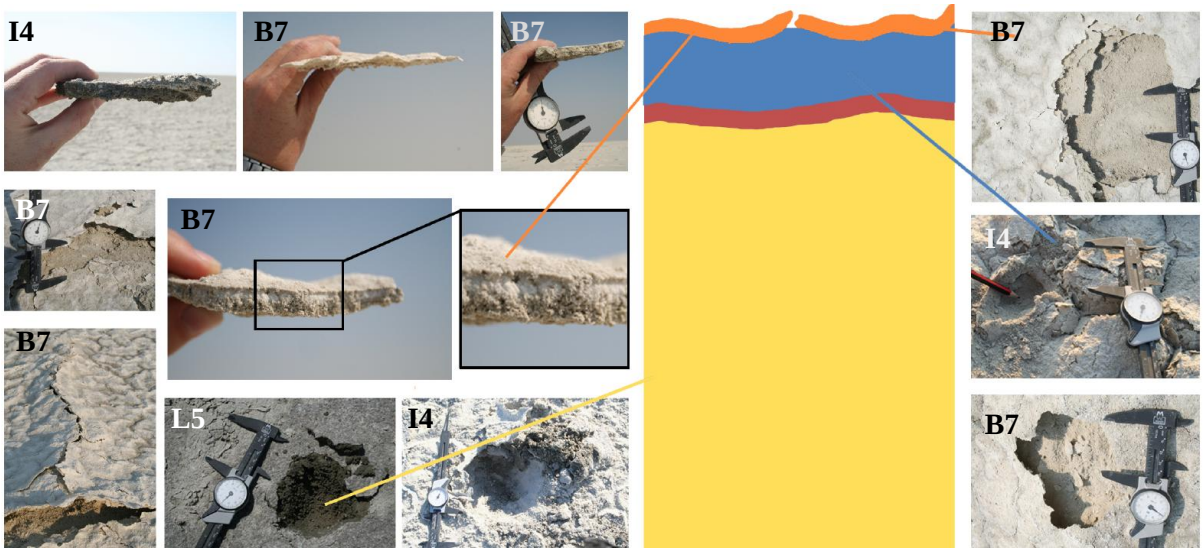

Figure 3.1 Vertical profile of the pan indicating a surface crust of varying thickness (orange), below which lies the fluff (blue) then the second crust (red) with damp soil (yellow) present at the base of the profile. The second crust was only occasionally present between the fluff and soil layers. Additionally, at a number of locations no fluff or discernible crusts were observed – see Table 3.2. Callipers on the pan surface and revealing fluff characteristics indicate 5 cm. While crust callipers, where present, indicate 1 cm. Alpha-numeric site identifications have been included for each location, presenting the within site variability observed for three sites within the grid (Photographs by author taken during Makgadikgadi DO4 2011 field season).

Fluff samples were then given the suffix F, while **C**rust samples were given the suffix C, **S**oil was given S, with the secondary crust layer which lay beneath the primary crust (C) given the suffix H, (representing the **H**orizon crust). Samples were collected and sealed within zip lock bags on site. Every effort was made to ensure the integrity of the samples was not compromised during transport, despite variations in temperature and moisture conditions between source region and laboratory working conditions. This could account for chemical and physical changes through hydration, dehydration and compaction. The following analysis only considers samples from the upper three sampling categories and did not include an analysis of soil samples.

Table 3.2: Table listing sample ID as used in this chapter as per naming procedure of site ID as developed for the DO4 Project. Samples not present are indicated by '-'. Table 3.2a) indicated samples considered for ICP analysis (section 3.3.1) while 3.2b) presents samples considered for XRD analysis (section 3.3.2).

a)

	Sample Category	
	Crust	Fluff
suffix	C	F
Site ID	Sample ID	
B3	B3C	B3F
B7	B7C	B7F
D2	D2C	D2F
D5	D5C	D5F
D10	D10C	D10F
G2	G2C	G2F
G6	G6C	G6F
I4	I4C	I4F
I8	I8C	I8F
J3	J3C	J3F
J11	J11C	-
L5	L5C	-

b)

	Sample Category		
	Crust	Fluff	Horizon-Crust
suffix	C	F	H
Site ID	Sample ID		
D10	D10C	D10F	D10H
G2	G2C	G2F	G2H
I4	I4C	I4F	*

* sample present but too small for XRD analysis

3.2.2 Laboratory methods

Collected samples were prepared and processed for chemical and elemental composition, through the use of X-Ray Diffraction (XRD) and Inductively Coupled Plasma – Optical Emission Spectrometry (ICP-OES). These two methods are capable of identifying trends in the chemical and elemental nature of the samples. All samples were screened such that grains under 2000 µm were analysed for bulk chemistry.

3.2.2.1 ICP-OES

Twenty two samples un-sized fluff and crust samples accurately weighing 0.1g were digested in a Mars 5 Express CEM Microwave digestion unit with the following operating conditions:

HNO_3	2 ml
HCl	6 ml
HF	4 ml
Max Temp	210°C
Max Pressure	1600 W

The samples are then analysed in a Varian ICP-OES 730 Series for the required elements. The concentrations of 16 elements (Cd, Co, V, Cr, Zn, Cu, Mn Ni, Ti, Fe, Mg, S, K, Al, Ca, Si, Na,) were determined by Inductively Coupled Plasma Optical Emission Spectrometry (ICP-OES) (Olesik, 1991). Samples were run and prepared in the Department of Chemical Engineering at the University of Cape Town.

3.2.2.2 XRD

Eight un-sized samples representing fluff, crust and second crust from three sites on the Makgadikgadi Pans were split until a 3 g sample was achieved (for details on splitting see Chapter 2 section 2.2). The samples were then micronized in a plastic sampler with 48 beads (A1203) in 7 ml of ethanol and placed in the shaker for 10 minutes. The jars and sample were then washed out with ethanol into dishes and placed in an oven to dry. Dry samples were analysed with powder XRD spectra obtained by using a Bruker D8 Advance powder diffractometer with a Vantec detector and fixed divergence and receiving slits with Co-Ka radiation. The phases were identified using Bruker Topas 4.1 software and the relative phase amounts (weight %) were estimated using the Rietveld method. Samples were prepared and processed at the Department of Chemical Engineering at the University of Cape Town.

3.3 Results and Discussion

Mineral dust samples from the upper three categories; crust, fluff and second crust (Figure 3.1), were examined in this chapter (*Table 3.2*).

The 12 sites selected for ICP-OES analysis (section 3.3.1) represent a range of pan surface conditions, from dry, well crusted surfaces through to wetter, efflorescent sites and broken crusts with exposed fluff. These observed structural differences extended to variability in colour and texture of the samples. Of the 12 sites, all sites contained a differentiable crust varying in thickness (*Table 3.2*). Beneath these crusts 10 sites contained a loose, fluffy layer, below which the wetter sediments lay. Three sites were selected for XRD analysis (section 3.3.2) representing the top three sampling categories presenting the results for the two crusts and fluff for D10, G2 and I4 (*Table 3.2*).

The following section will first present the average elemental composition of samples within the vertical column, before presenting the results of bulk sample chemistry at three discrete locations within the DO4 grid. The compositions derived through analysis are represented as percentages of the total sample, as determined by the two methods.

Mineral dust in the atmosphere is assumed to be in the micron size range (>100 μm) and in Chapter 2, samples were found to occupy a wide range of size fractions. As such, the results presented here represent surface conditions from which selective entrainment would result in differential composition between surface and airborne samples. Samples were pre-screened to remove any sample larger than 2000 μm as these exceeded the size range of morphological studies. As no samples were affected by this process, it can be presented that the following analysis represents the full un-sized sample.

3.3.1 ICP-OES: Elemental Characterisation

The results of the 16 elements tested using ICP-OES revealed, on average, less than half of the composition of Sua Pan samples, with J3F showing the highest overall concentration of the 16 elements, and 71% of the sample described. Most of this was found to be associated with calcium (*Table 3.3, Figure 3.2*) with silicon and sodium accounting for much of the remaining explained chemistry. The crusts were found to be relatively sodium enriched, with up to 34% found in G6C down to 9.4% in I4C with an average of just over 26%. This can be compared with fluff values of between 25.8% at I8F and 8.0% at I4F, with an average of almost 18%, highlighting the spatial variability experienced across the pan surface. Silicon was the next most dominant element accounting for between 3.0% at B7C and 16.5% at L5C, while only accounting for 1.6% of B3F yet 21.3% at G2F. Silicon was found to be more abundant in the fluff compared to the crust, with the exception of B3 and D2 where the crust contained over 5% more silicon than its fluff sample.

The prevalence of these sodium and silicon minerals in the sample confirms the context of these results in the global literature as presented by Krueger et al. (2004). However, the sodium values are notably higher than the 2% recorded for Saharan values and both inland and coastal Saudi values. Saint-Amand et al. (1987) propose that high salt concentrations can be expected on alkali playas with shallow ground water, like this system. Bing et al. (2009) present results for saline emissions from north-eastern China, revealing seasonal trends in the dominant element composition. The authors also found that sodium enriched periods coincided with spring time conditions and the associated increase in pedogenic salt formation. Bing et al. (2009) comment that the airborne samples contained up to 10% sample mass of sodium; a value considerably higher than the surface sample. These values remain below those of the Sua samples, reaffirming the high saline concentration and strongly natric nature of this system. While sodium values were notably higher, the Sua silicon values were detected to be less than half of those reported for Saharan dust samples, averaging 10% ranging from 2% to 21% compared with Saharan values at 46%. Both Saharan and Sua silicon values were lower than

both coastal Saudi (69%) and inland Saudi (53%) (Krueger et al., 2004). While conforming in terms of dominant minerals to other dust producing source regions; the Sua sediments will have differing ecological and radiative effects to other aerosols.

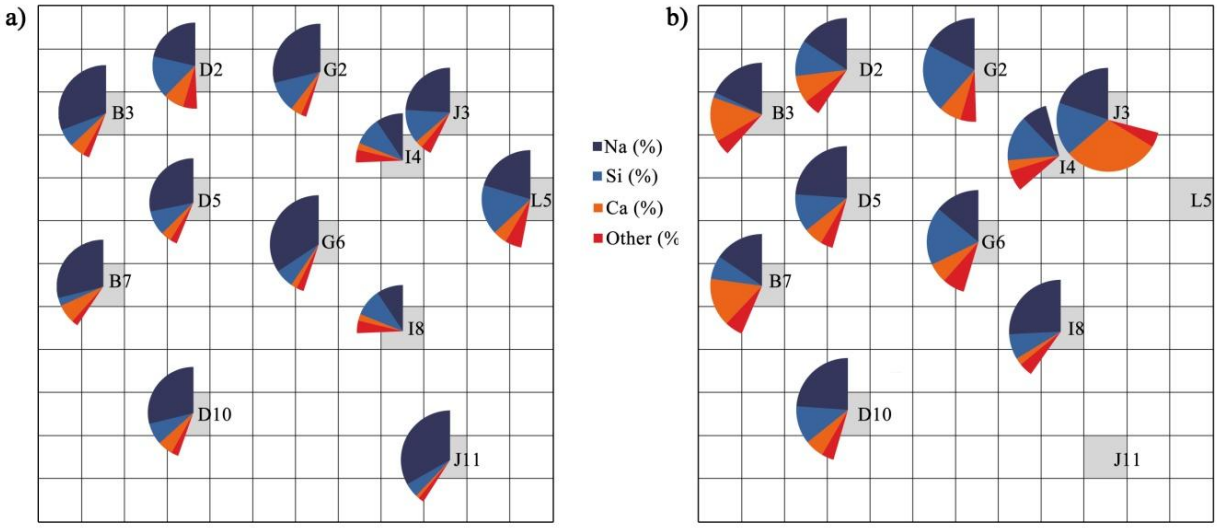

Figure 3.2: Results of ICP analysis as represented by sample location on the grid. Figure a) represents the crust samples, with figure b) representing the fluff. The three dominant minerals are indicated, (Na: Sodium; Si: Silicon; Ca: Calcium), with the remaining 13 minerals, which occur in trace amounts, indicated by 'other'. The remaining unaccounted for fraction of the pie represents the proportion of mineralogy of the sample not-identified by the 16 mineral analyses. Fluff was not present at J11 or L5 and is therefore not included in the analysis.

Additionally, Sua samples contained higher amounts of calcium in the fluff (average 10.3%) compared to the crust (3.8%) with values ranging from 1.0% in I8C to 30.0% in J3F. These ranges result in the samples being similar to Saudi (2-3%) all the way up to Saharan (17%) with J3F extending up to values similar to Chinese loess (39%) (Bing et al., 2009). Other elements appear, although with lesser contributions, including aluminium, potassium, sulphur, magnesium and iron.

The presence of sodium, potassium, calcium, magnesium, chlorine, sulphur and silicon (*Table 3.3*) all confirm the continental nature of the elements present in the system as determined in Eugster (1980) and Shaw and Bryant (2011).

The results presented through ICP-OES can reveal information on the bulk elemental composition of the samples, and confirm the origin of the samples. It is not possible to determine the mineralogical composition of the samples. Arimoto (2001) comments on the weakness of elemental studies, noting that elemental methods often fail to reveal mineralogical tracers which can link airborne samples to terrestrial sources. Arimoto (2001) adds that ICP results often fail to detect sufficient diagnostic characteristics, preferring mineralogical analysis or the use of elemental ratios to determine the nature of sample, while trace or rare earth elemental analysis on samples could reveal more detailed information which can be used to track and trace aeolian samples. Despite claims by Arimoto (2001),

knowledge of elemental characteristics is integral in understanding conditions as elemental ratios are largely unaltered during longer periods associated with transport (Castillo et al., 2008). Bing (2009) presents results of both airborne and crust samples and reveals that with changes in seasonality and wind the direction, airborne sample can be more or less enriched in various elemental constituents.

Table 3.3: Results of ICP-OES for Fluff and Crust samples examined in this study. Percentage of sample explained represents the percentage of sample represented by the 16 elements interrogated in this study.

	B3C	B7C	D2C	D5C	D10C	G2C	G6C	I4C	I8C	J3C	J11C	L5C	B3F	B7F	D2F	D5F	D10F	G2F	G6F	I4F	I8F	J3F
Elements	% Contribution to bulk mineralogy																					
Cd (%)	0.0	0.0	0.0	0.0	0.0	0.0	0.0		0.0	0.0	0.0	0.0	0.0	0.0	0.0	0.0	0.0	0.0	0.0		0.0	0.0
Co (%)								0.0												0.0		
V (%)	0.0	0.0	0.0	0.0	0.0	0.0	0.0	0.0	0.0	0.0	0.0	0.0	0.0	0.0	0.0	0.0	0.0	0.0	0.0	0.0	0.0	0.0
Cr (%)	0.0	0.0	0.0	0.0	0.0	0.0	0.0	0.0	0.0	0.0	0.0	0.0	0.0	0.0	0.0	0.0	0.0	0.0	0.0	0.0	0.0	0.0
Zn (%)	0.0	0.0	0.0	0.0	0.0	0.0	0.0	0.0	0.0	0.0	0.0	0.0	0.0	0.0	0.0	0.0	0.0	0.0	0.0	0.0	0.0	0.0
Cu (%)	0.0	0.0	0.0	0.0	0.0	0.0	0.0	0.0	0.0	0.0	0.0	0.0	0.0	0.0	0.0	0.0	0.0	0.0	0.0	0.0	0.0	0.0
Mn (%)	0.0	0.0	0.0	0.0	0.0	0.0	0.0	0.0	0.0	0.0	0.0	0.0	0.0	0.0	0.0	0.0	0.0	0.0	0.0	0.0	0.0	0.0
Ni (%)	0.0	0.0	0.0	0.0	0.0	0.0	0.0	0.0	0.0	0.0	0.0	0.0	0.0	0.0	0.0	0.0	0.0	0.0	0.0	0.0	0.0	0.0
Ti (%)	0.0	0.0	0.1	0.0	0.0	0.0	0.0	0.0	0.0	0.0	0.0	0.1	0.1	0.1	0.1	0.0	0.1	0.1	0.1	0.1	0.0	0.1
Fe (%)	0.2	0.2	0.4	0.4	0.3	0.2	0.2	0.5	0.2	0.3	0.2	0.7	0.5	0.6	0.5	0.4	0.6	0.4	0.8	0.8	0.4	0.5
Mg (%)	0.3	0.3	0.5	0.4	0.4	0.3	0.3	0.6	0.3	0.3	0.3	0.8	0.7	0.9	0.7	0.6	0.8	0.6	1.2	1.0	0.5	0.5
S (%)	0.5	0.5	1.3	0.4	0.4	0.1	0.5	0.9	0.1	1.0	0.3	0.4	0.7	0.6	0.7	0.7	0.9	0.7	0.8	1.0	1.1	0.8
K (%)	0.6	0.6	1.3	0.7	0.7	0.5	0.8	1.2	0.4	1.1	0.6	1.5	1.4	1.6	1.6	1.1	1.5	1.5	2.0	1.8	1.3	1.3
Al (%)	0.6	0.6	1.7	0.7	0.8	0.8	0.7	1.1	0.5	1.1	0.5	2.0	1.5	1.9	1.6	1.1	1.5	1.7	2.1	1.8	1.0	1.5
Ca (%)	5.0	6.6	7.8	3.8	5.4	3.8	2.0	2.3	1.0	2.7	1.1	4.6	13.9	15.1	8.6	5.9	9.9	7.0	6.2	3.4	2.2	30.0
Si (%)	6.3	3.0	16.2	9.2	7.8	10.7	6.2	9.5	4.4	12.2	4.7	16.5	1.6	7.3	11.2	11.8	11.3	21.3	18.1	14.2	7.9	16.6
Na (%)	30.7	28.8	21.4	28.2	28.8	28.8	34.3	9.4	32.3	24.1	33.2	20.4	18.0	15.5	15.7	23.9	18.8	17.2	14.1	8.0	25.8	19.7
% Explained	44.2	40.6	50.7	43.8	44.6	45.2	45.0	25.6	39.2	42.8	40.9	47.0	38.4	43.6	40.7	45.5	45.4	50.5	45.4	32.2	40.2	71.0

Therefore, despite the transient nature of elemental and mineralogical conditions, the chemical character of the surface is required in order to understand the system better, and predict dust load and associated impacts. This requires that the analysis move beyond elemental characterisation; consequently, the following section presents the results of XRD analysis for a select number of sites.

3.3.2 XRD: Mineral Characterisation

While a full suite of XRD analysis was not performed, crusts and fluff from three sites with differing surface conditions were prepared for analysis. These crust (C and H) and fluff (F) samples from G2, D2 and I4 were processed for 20 mineral phases. The composition of all 20 minerals examined in this study is presented in Table 3.4.

The mineralogy of surface and sub-surface samples has been extensively considered in literature (e.g. Nickling & Ecclestone, 1981; Nickling, 1984; Gill et al., 2002; Buck et al., 2006; Buck et al., 2011). These authors suggest that the location and concentration of soluble components are remnants of older, weathered base geology and proximity to ground water which are integral in determining the structure of the pan surface and for the soil profile. Analysis of samples at differing locations in both the vertical and horizontal structure of the pan along with a selection of mineral components permits the analysis of spatial variability of the pan environment, which can be used to predict the nature of the surface.

Table 3.4: Mineralogy and chemical formulas for minerals found in this study.

Mineral	Chemical Formula
Biotite 1M Mica	$K(Mg,Fe)_3[AlSi_3O_{10}(OH,F)_2]$
Chlorite IIb	ClO_2
Hornblende magnesian iron	$(Ca,Na)_{2-3}(Mg,Fe,Al)_5(Al,Si)_8O_{22}(OH,F)_2$
Kaolinite (BISH)	$Al_2Si_2O_5(OH_4)$
Phlogopite 1M Mica	$KMg_3AlSi_3O_{10}(F,OH)_2$
Anorthite	$CaAl_2Si_2O_8$.
Bronzite	$(Mg,Fe)SiO_3$
Calcite	$CaCO_3$
Chromite	$FeCr_2O_4$
Diopside	$MgCaSi_2O_6$
Epidote	$Ca_2Al_2(Fe;Al)(SiO_4)(Si_2O_7)O(OH),$
Gypsum	$CaSO_4\ 2H_20$
Halite	NaCl
Illite	$(K,H_3O)(Al,Mg,Fe)_2(Si,Al)_4O_{10}[(OH)_2,(H_2O)]$
Ilmenite	$FeTiO_3$
Mirabilite	$Na_2SO_4\ 10H_2O$
Quartz	SiO_2
Rutile	TiO_2
Thenardite	Na_2SO_4
Trona	$Na_3H(CO_3)_2\ 2H_2O$

Various chemical analytical methods reveal different aspects of the sample, with direct comparison of results obtained by different means impossible. However, using the results to infer similarities or correlations is recommended. For example, the link between the abundance of sodium determined through ICP-OES and the dominance of sodium based salts can be drawn. Silicon is less indicative and could be associated with the silicate based minerals or the micaceous minerals. Through ICP-OES, sodium was determined to be the most descriptive element, while silicate based minerals were determined to dominate samples through XRD analysis. This could be in response to the differing sensitivities of the various methods (Olesik, 1991). Additionally, through ICP analysis between 26% and 71% of the sample was explained (average 44%) and therefore much of the samples elemental composition remained unclassified.

Attributing elements into their mineralogical groupings confirms of presence of the sodium detected in ICP-OES with the nitric salts, halite, trona, thenardite, gypsum and mirabilite, all of which were all identified in the XRD results. The silicon detected in ICP-OES can be attributed primarily to illite and quartz and to lesser degree to the presence of biotite. Finally, metal oxides, namely chromite, ilmenite and rutile, which through XRD are detected to only contribute a small fraction in samples is confirmed, with the relatively low percentages of titanium and iron observed in ICP-OES. Thus linking the results of ICP-OES to minerals detected in XRD can reveal trends in samples where XRD

was not run, but cannot attribute precise mineralogy to the samples. The absolute and relative abundance of these minerals varies significantly between samples and within the sampling profile (*Table 3.5* and *Figure 3.3*).

Table 3.5: Results of XRD analysis on three sites and at different locations within the vertical sampling profile of the pan. Samples have been grouped into the four classes discussed in this study. Chemical formulas for minerals can be found in Table 3.4.

	Crusts			Fluff			Second Crusts	
	G2C	D10C	I4C	G2F	D10F	I4F	G2H	D10H
	% Contribution to bulk mineralogy							
MINERAL EVAPORITES								
Halite	16.55	37.98	43.92	7.16	8.81	38.43	11.49	14.43
Gypsum	0.12	0.50	0.31	0.12	0.11	0.26	0.09	0.06
Trona	0.40	5.22	4.29	1.35	0.86	7.23	0.92	0.75
Thenardite	0.04	0.91	0.46	0.14	0.31	0.00	0.06	0.18
"Chlorite IIb"	0.30	0.43	1.19	0.33	0.31	0.97	0.29	0.38
Mirabilite	3.16	0.00	0.00	20.77	0.00	0.00	26.18	0.00
Calcite	1.92	4.00	4.95	4.16	6.92	2.52	2.31	3.38
SILICATE BASED								
"Hornblende magnesian iron"	1.10	3.18	2.38	0.25	0.72	0.80	0.33	0.64
"Kaolinite (BISH)"	0.24	0.35	0.56	0.19	0.08	0.22	0.23	0.23
Epidote	0.05	0.00	1.30	0.00	0.00	0.44	0.00	0.00
Anorthite	0.60	0.84	6.12	1.31	0.95	3.99	0.53	0.51
Bronzite	0.30	0.51	0.00	0.28	0.31	0.20	0.15	0.11
Diopside	0.57	3.06	0.38	0.19	0.89	0.45	0.27	0.87
Quartz	3.63	2.16	11.82	6.08	2.33	5.79	2.69	1.38
micaceous mineral								
Illite	69.79	38.27	19.73	56.35	75.85	36.75	53.51	75.29
"Phlogopite 1M Mica"	0.00	0.00	1.82	0.00	0.52	1.38	0.00	0.71
"Biotite 1M Mica"	1.15	2.16	0.47	1.09	0.79	0.35	0.85	0.87
METAL OXIDES								
Chromite	0.00	0.00	0.07	0.00	0.02	0.01	0.00	0.00
Ilmenite	0.04	0.34	0.17	0.15	0.12	0.28	0.11	0.15
Rutile	0.09	0.08	0.03	0.08	0.10	0.06	0.01	0.06

In order to reveal trends in the data, the 20 mineral phases analysed through XRD were grouped to represent mineralogical categories, these can be broadly classified as (i) evaporite minerals, (ii) silicate based minerals, (iii) micaceaous silicates and (iv) metal oxides. This grouping follows the proposal by Mees (2001; 2003) who considers the analysis of functional groupings to be the best means of revealing trends in mineralogical analysis.

Due to the known importance of salts and evaporites in determining the structure of the pan surface, the results of these will be considered before examining the nature of silicates and finally metal oxides (Figure 3.1). Additionally, from Figure 3.3, mineral evaporites can be seen to be both noteworthy and highly variable constituents of the samples.

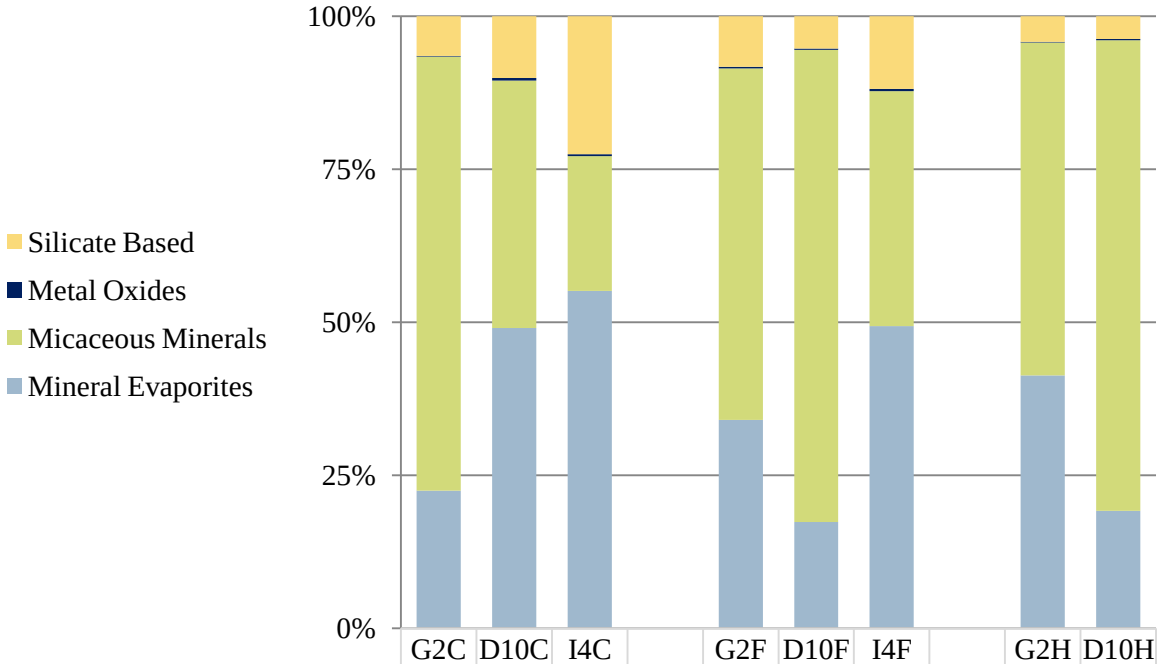

	G2C	D10C	I4C		G2F	D10F	I4F		G2H	D10H
Silicate Based	6	10	23		8	5	12		4	4
Metal Oxides	0	0	0		0	0	0		0	0
Micaceous Minerals	71	40	22		57	77	38		54	77
Mineral Evaporites	22	49	55		34	17	49		41	19

Figure 3.3: Chart representing the results of XRD for the four dominant mineral groups, considering the results for crust, fluff and second crust for three sites.

3.3.2.1 Salt Evaporites

While every effort was made to preserve sampling conditions, temperature and moisture changes can alter the hydrous/anhydrous phases of minerals out of the balance of the natural state. Further, as evaporite minerals are dependent on temperature and moisture for their stability (Reynolds et al., 2009), time of sampling within the diurnal cycle and transport could affect the balance between the minerals. Despite this, there was a visual difference observed between the sites (*Figure 3.4*), which can largely be attributed to the combinations and concentrations of minerals (Gillette et al., 2001).

There were noteworthy variations in the contribution of mineral evaporites between samples, ranging from 55% of I4C down to 22% in G2C. For both samples, halite was the dominant contributor accounting for 44% of I4C, while only 17% of G2C. D10C was similarly rich in mineral evaporites, explaining 49% of the sample of which 38% was determined to be halite (*Figure 3.3*, *Table 3.5*). Equally, fluff from I4 was found to be composed of 49% mineral evaporites, with 38% of the sample comprised of halite.

However, for D10C the remaining evaporite contribution was from trona (5%) and calcite (4%); while I4F had a greater contribution of trona (7%) with only 2.5% of calcite. Halite concentrations were considerably lower in both G2F and D10F with values of only 7% and 9% respectively.

Therefore, while in terms of evaporite concentration the crust at D10 and fluff at I4 had similar compositions, namely halite, trona and calcite, they represented very different physical surface conditions. Visually, this difference in evaporite mineral composition can be seen in the differing response on the surfaces (*Figure 3.4a, b, c*). At I4 the sample was a light, fluffy emissive material, while at D10 a harder crusted material was found. Therefore, the relative contributions of evaporites and other minerals together with the location of the sample to either the surface or ground water strongly control the nature of the material.

The importance of evaporites in determining pan structure, crusting and emissivity is indicated by the abundance of studies focusing on them (e.g. Nickling & Ecclestone, 1981; Nickling, 1984; Rice et al., 1996; Joeckel & Clement, 1999; Compton et al., 2003; Gillette et al., 2004; Langston & McKenna Neuman, 2005; Buck et al., 2011; Shaw & Bryant, 2011). Reynolds et al. (2009) note that the evaporative loss of large quantities of sub-surface water produces fluffy sediments composed of loose aggregates of evaporite minerals. Slower rates of evaporations or lower ground water salinity levels produce more compact "puffy" sediments (Reynolds et al., 2007). This relationship is complicated by the understanding that evaporite minerals form, leaving void space, and the potential that further crystallisation of minerals can occur within these voids. Therefore, through changing temperature, stability and chemical setting, these gaps may be filled by additional minerals reducing the porosity and cementing the evaporite crusts, or displacing the original crust. This secondary period of crystallisation results in the formation of complex mixed crusts of multiple minerals (Eugster, 1980). Buck et al. (2011) indicate that these complex mixed crusts would have varied responses to temperature fluxes and moisture conditions determined by individual mineral stabilities and tendencies.

From Figure 3.4 it can be observed that D10, G2 and I4 present very different surface conditions, with polygon shaped broken crusts exposing fluff at I4, while at D10 and G2 larger ridges dominate. Mineralogically, G2 contained 3% mirabilite in the upper crust, 21% in the fluff and 26% in the lower crust, while no mirabilite was detected at I4 and D10. Thenardite was present in very small percentages in all samples with a maximum of 0.9% found in the crust at D10. This small percentage is greater than the stated error and can therefore not account for a possible sampling bias. Therefore while G2 contained mirabilite, the absence of this mineral in I4 and D10 was not observed to be associated with a relative enrichment of the less voluminous anhydrous form, thenardite.

There is an additional proposal that due to the similarity in the reflective nature of halite and thenardite spectra, there is the possibility of poor differentiation of these two minerals (Corin, K. 2011, *pers. comm.*., 30 November). However, even combining mirabilite, thenardite and halite values remains inconsistent between sites and the differences can be attributed to an underlying control in evaporite chemistry between these sites rather than a detection limit or error.

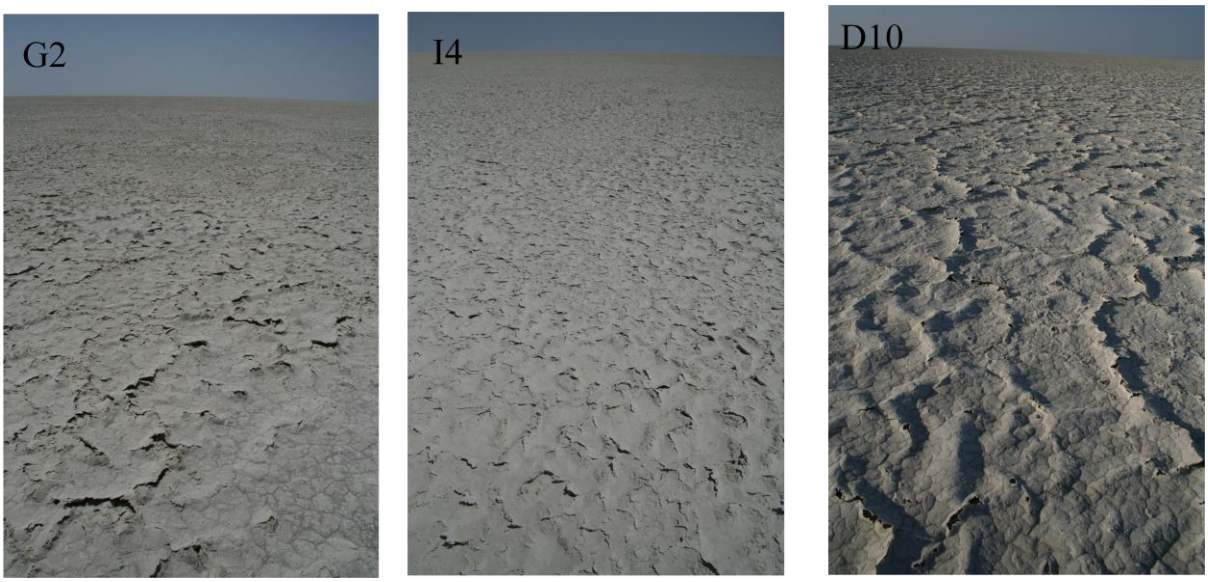

Figure 3.4 Photographs of a) G2 b) I4 and c) D10 sites during the 2011 field campaign, the visible difference in crust can be considered to be a function of different mineralogical composition. Figures Figure 3.4a, b and c represent surface conditions taken during the 2011 field campaign at the time of sampling. The images represent G2 (Figure 3.4a), I4 (Figure 3.4b) and D10 (Figure 3.4c) and show different amounts of crusting, ridges and broken crust exposing fluff. Figure 3.4b, presents a broken crust dominated by the exposed fluff patches at I4, D10 (Figure 3.4c) was relatively more crusted over, while at G2 (Figure 3.4a) there were broken ridges on the crust exposing the fluff beneath (Photographs by author taken during Makgadikgadi DO4 2011 field season).

The presence of mirabilite at G2 and its absence at other sites is important as Nield et al. (in prep.) discuss its role in the formation of different crust types as determined from field observation (*Figure 3.4*). The authors note that mirabilite is an important trace mineral for understanding source and crystallisation conditions. Saint-Amand et al. (1987) propose that for nitric salts, 18°C is the threshold above which trona, thenardite and halite form, while below this temperature mirabilite formation is favoured over thenardite. Reynolds et al. (2009) confirm this temperature dependence for these minerals, noting that the relationship is reliant on ambient conditions, further commenting that these minerals are not mutually exclusive in their presence. Laboratory experiments (Shahidzadeh-Bonn et al., 2010) have shown evidence to support the possibility of co-existence of mirabilite and thenardite through a partial phase change, whereby thenardite crystals are partially dissolved with mirabilite forming on a thenardite structure. For this phase change numerous conditions are known to be important, often existing within a diurnal cycle which can result in changing surface environments over short time periods Nield et al. (in prep.). Further, the cyclicity of these systems is noted through

the role of precipitation and high relative humidity in dissolving crystals, meaning the presence or absence of mirabilite, thenardite, halite and trona can be seen as important diagnostic minerals for soil conditions and evaporation controls as observed in the pan system.

As halite was present at all sites, along with the appearance of trona, it can be assumed that crystallisation on the surface largely occurred when temperatures exceeded 18°C. The field season and therefore sampling occurred between August and November when day time temperatures were considerably higher than this threshold. Additionally, these months are associated with the dry season which would suggest that additional moisture to the surface salts is likely to occur through the capillary zone or ambient moisture (humidity), rather than through rain or surface flow. Therefore, the co-existence of mirabilite and thenardite is likely to be associated with partial phase changes in response to large diurnal temperature fluxes and the associated changes between the hydrous and anhydrous phases of salts within the soil column.

Another evaporite mineral found in all samples was calcite, with calcium detected in all samples through ICP analysis. Yechieli and Wood (2002) associate carbonates to fluffy sediments, while Goudie and Middleton (2006) suggest that calcium carbonate can increase the threshold wind speed required for deflation. Therefore, while there is a proposal that carbonates produce fluffy sediments, the association with calcium in calcite is proposed to produce a hardened surface. Thus, the precise mineralogy and ionic association can be assumed to have a control over surface emissivity, further highlighting the need for mineralogical analysis alongside elemental analysis for the correct attribution of the chemistry of the pan system response.

Figure 3.5 Thick crust (1.1 cm) from B7 clearly indicating a pale salt rich horizon just below the surface (Photographs by author taken during Makgadikgadi DO4 2011 field season).

Here, the detected calcite found in all samples, could be providing cementation and surface hardening, increasing the threshold wind speed required for emission and reducing the emissive potential of the surface. Additionally, calcite showed significant spatial variability both horizontally and within the vertical profile, with greater percentages of calcite found in the fluff at D10 and G2, while the crust at

I4 experienced the highest contribution at that site. This variation in calcite is in contrast with findings by Gillette et al. (2001) who present results for Owens Lake revealing calcite content to be consistent between crusts and sub-layers due to the poor solubility of the mineral. However, on the Etosha Pan, core sampling by Buch and Rose (1996) revealed that calcite was found in its highest concentrations on the pan surface decreasing rapidly with depth, while dolomite levels were enriched below the surface with a highly variable distribution on the pan surface. The authors note that on the wetter eastern margins of the Etosha Pans, calcite values were considerably lower, with dolomite absent from the sampling profile. Inferred values for calcite in the Etosha samples ranged from 1 – 2% while Makgadikgadi samples were notably higher, as Buch and Rose (1996) indicate that calcite has a greater dominance in wetter regions, this could indicate a greater moisture content or availability in the Makgadikgadi system compared with Etosha.

Despite being slightly higher in calcite than the Etosha pans, globally carbonate concentrations were detected to be significantly higher than those presented here. Goudie and Middleton (2006) indicate that Saharan dust transported to the Pyrenees had carbonate values between 20 and 30%, while Saharan dust transported to the Canaries had between 6 and 9%. These values are still greater than the 2 – 7% found in the Sua samples. The depleted levels of carbonate based minerals in the Makgadikgadi (and Etosha) is confirmed by Wang et al. (2007) who suggest that in the Kalahari, with increased drying, carbonate rich sediments are found at greater depth. Ringrose et al. (1999) also note the relatively low concentration of carbonates in the Makgadikgadi basin suggesting calcite to quartz ratios of 1:4 or less. Ringrose et al. (1999) add that calcium carbonate was not particularly abundant, but that it was highly variable across the basin increasing to almost a 1:1 ratio with quartz towards the Boteti Gorge. In this study, an average of all samples revealed a 1:1 ratio between quartz and calcite (values ranged from 1:0.3 to 1:2.4) suggesting little change between background Kalahari sediments and pan sediments when considering carbonate based minerals. Therefore, while there were clear links to the background signature, there remained variability between sites within the pan. This is also noted by Eckardt et al. (2008) who, through analysis of sub-surface brines, confirm variability at low levels throughout the system. Thus confirming the relatively low, but significant, contribution of carbonate sediments to the pan and therefore the potential aeolian load.

3.3.2.1.1 Evaporites as surface crusts

The lateral variations in evaporite mineralogy are likely in response to the variations in ground water depth across the pan, further compounded by sub-surface ground water flow. Buck et al. (2011) add that due to the high solubility of salts, they can be added to or removed from the system in very short time periods with climate, slope, water table, soil type and texture determining their spatial coverage. Thus, many variables can result in a spatially heterogeneous pan surface with regard to chemistry and morphology.

The seasonality experienced on the Makgadikgadi, together with the shallow, highly saline ground water (White & Eckardt, 2006), correspond well to the optimal conditions outlined for evaporation and therefore salt crystallisation in saline environments. During the hot, dry winter and spring months, shallow ground water can evaporate through the capillary zone, which is seasonally recharged by summer rainfall. In the presence of these high temperatures, the minerals in solution have the propensity to evaporate within minutes, further drawing additional solutes through the capillary zone from the shallow groundwater. This process forms distinctive surface crusting with diurnal and seasonal cycles serving to promote subsequent phase changes in the minerals (Reynolds et al., 2009). Temperature and moisture cycles operating on daily cycles, can further enhance the formation of raised ridges in the crusts which breaks when under stresses, exposing the finer sediments for deflation.

Through heating and drying, and diurnal fluxes certain minerals are favoured over others. For example, the cooler night conditions favour the formation of mirabilite (Saint-Amand et al., 1987), while warmer conditions favour thenardite. The relationship and relative concentrations of these salts varies across the pan and the precise controls for these cannot be known without extensive analysis of temperature fluxes and moisture conditions in both in the soil and atmosphere. The presence or absence of mirabilite and/or thenardite together with trona and halite presenting the greatest concentration in the crust, confirms the proposal by Saint-Amand et al. (1987) that alkali efflorescent crusts form on playas where there is a shallow water table. Further, the authors propose that the chemistry of the fluff is varies between seasons as a function of temperature and precipitation, a process known as the Soret effect (Saint-Amand et al., 1987: 115). A similar process is proposed for the ephemeral Makgadikgadi. Gillette et al. (2001) add that the soluble salt content could be expected to be higher in the crust than in the subsurface as evaporation concentrates salts near the surface. The relative concentration of salts in the crusts is confirmed with the crustal concentration of salts being on average 42% while the fluff resulted in an average of 33% further decreasing in the second crusts with an average of 30%. Such high values of evaporites is not unusual with Blank et al. (1999) commenting that desiccated surfaces on salt lakes will produce surfaces and therefore dust which is rich in soluble salts, while Kiefert (1994) suggests that values could be as high as 50%.

Buck et al. (2011) add to this, noting that mineralogy affects both the surface environment and its emissivity. As such Yechieli and Wood (2002) add that it is important to consider the ratios between different minerals, as while samples may contain fluffy mineral components, the relative contribution of cementing minerals could result in less emissive surfaces than single mineral analysis would suggest. They further propose that sodium chlorides have a strong cementing effect, while sodium sulphates and sodium carbonates produce finer, fluffier surfaces. Therefore, assuming that calcite ($CaCO_3$) (Goudie & Middleton, 2006) and halite (NaCl) (Yechieli & Wood, 2002) are cementing and that thenardite (Na_2SO_4), mirabilite ($Na_2SO_4.10H_20$) and trona ($Na_3H(CO_3)_2.2H_20$) (Yechieli & Wood,

2002) are fluffy, it can be assumed that I4C would be the hardest crust with a ratio ('fluffy to cemented') of 1:10 while G2C will have a fluffier crust 1:5. While D10F would be the most cemented (1:14) and G2F would be the fluffiest (1:0.5). Similar 'fluffy to cemented' ratios existed for the second crusts at G2 and D10. Removing trona and mirabilite, which are hydrated crystals which decrease the emissivity of surfaces (Goudie & Middleton, 2006) result in surfaces which are even more cemented and less likely to be emissive, however as dust is known to come from these surfaces this cannot be entirely descriptive of surface processes. Upon considering 'fluffy to cemented' ratios for the fluff samples, D10F is presented as being the least fluffy with a ratio of 1:13, while 14 has a ratio of 1:6 however G2F is the fluffiest with a ratio of 1: 0.5 which would suggest that G2 contains the least cemented fluff. However, as crusts cap the fluff, this alone cannot be viewed as deterministic of surface emissivity.

The evaporite mineralogy described here for Sua sediments is similar to those found in the Salton Sea Basin with Buck et al. (2011) indicating that halite, thenardite, mirabilite and gypsum were all present in crust samples from the region. Saint-Amand et al. (1987) reveal a similar geochemical composition of Owens Lake crusts, including halite, trona and thenardite/mirabilite. Further, these authors reveal a number of other sodium, carbonate and sulphate containing salts which, along with results presented here, confirm the natric nature of these systems and the proposed similarities in chemistry. However, the physical surfaces of these three systems differ greatly, largely in response to the ambient conditions of the different source locations.

The above discussion has largely considered evaporite minerals, but the rich and diverse mineralogy of the pan surface is not limited to evaporite minerals. Considering functional groups independently is in line with Mees (2001; 2003), who considers the analysis of salt minerals separately from the clay and silicate based minerals, commenting that the relative youth of the salts when compared with the older base material clays and silicates require independent analysis. The following section will consider the presence and possible origin of the silicates which dominate the mineralogy of samples as determined through the use of XRD analysis.

3.3.2.2 Silicates

Silicates are found in all samples, with silicate abundance mostly attributable to the presence of quartz. The relative abundance of silicon based minerals is unsurprising, when more than one-quarter of the Earth's crust is made up of this element (Turekian & Wedepohl, 1961). Quartz is the most abundant silicon based mineral (Turekian & Wedepohl, 1961) and would therefore be assumed to be readily found in most terrestrial samples. Additionally, this dominance was found by Engelbrecht and Derbyshire (2010) to extend to dominance in global dust mineralogy. Although Chudnovsky et al. (2009) note that when considering bulk concentrations, quartz and feldspar may dominate although the mineralogical content of dust is highly variable containing a complex mix of minerals.

Even with its proposed widespread dominance, quartz was not found to dominate in the pan samples. This could be due to the relatively fine nature of Sua sediments, further confirming the findings of Wang et al. (2007) who suggested that, within the regional context, quartz dominates the coarser fraction of Kalahari sediments. Additionally, the abundance of evaporites serves to reduce the dominance of quartz in this highly saline environment. The detected quartz was found to vary, likely in response to salt dominance, with I4 crust containing almost 12% quartz with less than half this amount found in the fluff at the same site. The opposite relationship was observed for G2, where quartz accounted for 4% of the crust while just over 6% of the fluff, decreasing to 2% of the second crust. For D10, values of quartz were similar at all sampling horizons varying by less than 1% between all three sampling horizons. While the evaporite dominance could account for some of the observed trend, a further underestimation of quartz could be associated with the abundance of amorphous quartz as observed in SEM analysis (Appendix 6).

Another factor which could explain the relatively depleted levels of quartz in Makgadikgadi sediments relative to other large dust producing regions, is the pan setting, with large sand seas assumed to be significant sources of quartz. Therefore, as a result of the sedimentary environment, Sua samples are likely to be relatively depleted in quartz compared to north Africa and other sand sea dominated sources. Additionally, the relatively depleted nature of the Sua Pan sediments, when compared with Kalahari sediments, could confirm the findings of Mees (2001) who suggests that evaporite formation occurs after the development of the pan. Therefore, the clays and silicaceous minerals indicate the background of the younger, evaporite dominated system.

While quartz was not found to dominate, the high percentage of detected silicon can be associated with illite which was present in all samples as determined by XRD analysis. Goudie and Middleton (2006) comment that clay minerals like illite, smectite and kaoline, can be strong indicators for source regions. Similar to global studies (Goudie & Middleton, 2006), sheet silicates (micaceous minerals), most commonly illite, dominated all samples. Illite and the presence of micas indicate that sediments within the pan surface are not entirely allogenic with local Kalahari sediments exhibiting similar dominance of illite and micas (Thomas & Shaw, 1991). The detection of kaolinite and illite in the sample, and thus in the potential aerosol load, confirms the similarity of the Makgadikgadi system within the global setting with Moreno et al. (2006) indicating the presence kaolinite and illite in Saharan and Sahelian samples. Additionally, Buck et al. (2011) link the movement of salts to the surface with the vertical movement of silicates, due to the displacive nature of salt crystallisation. This, according to the authors, results in a surface rich in both salts and fine silicates for emission, with this vertical movement providing mineralogical transports between the old base minerals and the surface.

Mineralogically, quartz, illite and other micaceous minerals in the sediments link the contemporary pan environment with the Precambrian granites, which are known to exist widely in the region (Thomas & Shaw, 1991). The presence of igneous rock intrusions within the Pan (e.g. Kubu Island) (Wright, 1978; Thomas & Shaw, 1991), and the identification of other igneous minerals can give an indication of the relative age of the pan sediments. Quartz, muscovite and potash feldspar are more stable than olivine, pyroxene and calcic plagioclase, which are formed at earlier stages of crystallisation. In light of these factors, the presence of olivine and pyroxene, amongst others, could be an indicator of either immature sediments or could indicate continuous active erosion of basal lithologies.

The final mineral groupings that will be considered are the metal oxides, which are lesser minerals within common igneous rocks and are proposed to link with the granites that dominate the basal geology and rocky outcrops throughout the pan complex.

3.3.2.3 Metal Oxides

While metal oxides are not found in great abundance, their presence is indicative of weathered igneous rocks and therefore contextualise the sediments with their base geology. Metal oxides (commonly magnetite and ilmenite) are often found in relatively old landscapes, commonly associated with continental rifts (Reid & Frostick, 1985). While Reynolds et al. (2006) note the use of magnetite as an important mineral tracer for aeolian transport in the Colorado Plateau, the authors note that the presence of ilmenite, which is a common igneous mineral is less prescriptive of conditions or age. Therefore ilmenite, while not prescriptive of source regions, does serve to further confirm the links between pan chemistry and deeply weathered base geology. The identification of rutile in the samples, even if in low concentration, confrims the findings of Nash et al. (1994) who indicates the presence of rutile in both Kalahari and Cape Coastal silcretes. The authors suggest that, through geochemical analysis, $Ti0_2$ provides the greatest variation between samples, with the noticeably low level in Kalahari samples being attributed to differences in host mineral rather than climatic controls. Therefore, the low levels detected in the pan sediments confirms the links between deeply weathered Kalahari sediments in which the pan complex lies. Rutile and chromite could both be considered as important minerals for downwind tracers, with chromite and ilmenite being potential sources of downwind iron fertilisation. However, the contribution of metal oxides within the samples is relatively low even when compared to the low concentrations found by Frostick and Reid (1990) in Lake Turkana, northern Kenya.

The above discussion has considered four functional mineralogical groups, whose minerals dominate Makgadikgadi sediments. The combinations reveal that both authigenic and allogenic processes are active on the pan and present the dominance of young evaporites on the pan surface.

3.3.3 Mineralogical Synopsis

In line with findings by Shi et al. (2012) who acknowledge the need for detailed assessments and the inclusion of mineralogical composition of dust in atmospheric models, this study has presented the results for surface samples from the DO4 Grid on Sua Pan. Evans et al. (2004) comment that samples taken from the source will result in the best approximation of the dust load, and it is noted that for pan systems, the source is best represented as a function of the underlying geology and regional setting. For the Makgadikgadi Pan system, these are a function of i) the young evaporite minerals of the pan complex and ii) the deeply weathered Precambrian Kalahari sediments along with a contribution of regional aeolian introduced sediments. Within these two dominant compositions, the evaporite rich efflorescent fluff and crust sediments dominate the upper sampling categories, while base minerals dominate in the wet soils where younger minerals remain in solution in the ground water capillary zone.

On the Makgadikgadi Pans, the importance of ground water and capillary transport were confirmed through the mineralogical similarity between the shallow, solute rich ground water (Eckardt et al., 2008), and the surface. Transport in the capillary zone between shallow ground water is particularly pronounced in this region where the evaporation rate is proposed to exceed that of precipitation by a factor of three (Bhalotra, 1987). The similarity between the minerals presented in this study and those presented by Eckardt et al. (2008) for Na-Cl concentrations in Nata River flood waters, reveals the importance of the capillary transport of solutes from the ground water up to the pan surface. Additionally, the seasonal inflow of Ca-HCO_3 dissolved into rivers and ground water which enters the system, presents the likely source of calcite addition for the system. However, the levels assumed to be introduced through the Nata flood waters exceed the levels of calcite detected in the samples; this could be due to the presence of Mg^{2+} ions which are known to retard the formation of calcite (Berner, 1975). More directly linked to the surface mineralogy is the presence of SO_4^{2-} in subsurface brines, the sulphate ions, proposed to be derived from bedrock, can be seen to respond to seasonal drying and present numerous sulphate containing evaporites on the surface. These sulphate containing minerals link the pan surface to the Eugster (1980) continental brine type b strongly, while the relatively depleted nature of carbonates in the system relative to the hydrochemistry could also be determined as a response to the high nature of saline evaporites (Eugster, 1980).

The distribution patterns of evaporite minerals formed through ground water evaporation can be explained by considering the mechanisms of water and solute movement through the soil profile. In addition, the spatially variable surface mineralogy can be observed to be a function of the lithological differences between sites (see Chapter 2) – differences which are known to affect the solute pathway and, therefore, the evaporite distribution at the pan surface. Further, continual reworking of minerals

through the system by seasonal inundation may also be responsible for the lateral variations experienced.

Results of XRD analysis presents crusts and fluff containing trona, thenardite and halite as well as mirabilite. The coincident appearance of both these minerals could be in response to the sampling and transporting conditions or could represent the transient nature of mineral phase changes proposed by Shahidzadeh-Bonn (2010). It is understood that re-sampling through different seasons will support the importance of temporal induced phase changes most notably in the anhydrous/hydrous phase of some minerals. Similarly, it is proposed that seasonal inundation events will return the crystalline structures to solution and move the solutes through the capillary zone until warmer conditions return. Therefore, the samples and results presented here represent the transient nature of sediment conditions on the pan, which can further be affected by selective entrainment of minerals during emission events.

Even with the differences between sites presented above; all sites contained illite, halite, quartz, calcite, biotite and to a lesser degree, trona, gypsum and various silicate minerals. This list is similar to that outlined by Middleton (1997) who indicated that the dominant minerals in desert dust include: quartz, calcite, dolomite, micas, chlorite, kaolinite, illite, smectite, mixed layer clays, palygorskite, heavy oxide and silicate minerals, along with gypsum, halite, opal and amorphous inorganic and organic material. This confirms the statement by Krueger et al. (2004: 6254) which states that "...to assume desert dust to be a homogenous entity is a gross oversimplification of the rich mineralogy and varying chemical composition of dust." This study has verified both assumptions confirming many of the minerals presented by Middleton (1997) to dominate, and highlighted the validity of Krueger's (2004) statement. Additionally, the detection of trona and thenardite in Makgadikgadi sediments reveals mineralogical similarity to the Etosha basin in Namibia. Buch and Rose (1996) note that, despite limited geochemical studies on the Etosha sediments, the commercial exploitation of trona, thenardite, sulfohalite and prissonite on Otjivalunda salt pan give some indication of the nitric nature of this system. These findings indicate that the Sua system is largely predictable within both the global and regional literature, with bulk mineralogy linked to that outlined by Middleton (1997), and the evaporite minerals akin to type b as grouped by Eugster (1980).

Despite the large scale predictability within the system, variations were observed at the sub-basin scale, with D10 and G2 being dominated by quartz, while halite dominated both samples taken from I4. Visual comparison of the sites revealed that, unlike G2 and D10, I4 exhibited a largely broken crust surface with a large percentage of the surface existing as fluff (*Figure 3.4a, b, c*). This confirms the proposal of Buck et al. (2011) on the importance of salt forming processing in the creation of fluff and emissive surfaces. While Gill et al. (2002) indicated that composition alone was not an indicator for the crust appearance, Buck et al. (2011) add that, mineralogically, with increased temperatures and the associated dehydration of hydrous minerals like mirabilite to thenardite, more emissive surfaces

will result in visibly loose crystals or smaller aggregates. Therefore, it can be said that warmer conditions associated with lower humidity and the dehydration of salts creates optimally emissive surfaces. However, optimal conditions for salt formation may also have a cementing effect, through multiple crystallisation processes of additional minerals, filling void spaces, forming cemented complex mixed crusts (Eugster, 1980) with reduced porosity and thus lowering emissive potential.

Despite the importance of grain size for emission schemes, there was no size differentiation prior to XRD and ICP analysis, rather presenting the bulk mineralogy of the sample. This sampling strategy could explain the relatively depleted nature of the sample with respect to quartz and calcite which Livingstone and Warren (1996) and Castillo et al. (2008) attribute to the larger size fraction of desert sediments. As Sua sediments are relative fine when compared to the Kalahari Desert sands (Thomas, 1987) (and Chapter 2), clays and silicate minerals, which are ordinarily finer, have been determined to dominate.

3.4 Concluding Remarks

The results of high resolution sampling of mineralogical work augments previous studies which have considered the bulk chemistry of the region (Ringrose et al., 1999; White & Eckardt, 2006; Eckardt et al., 2008; Wood et al., 2011) by adding detail in terms of the location of minerals within the vertical structure of the pan as well as detailing the spatial variability within the pan system. This work presents the dual nature of pan sediments as being both a function of allogenic and authogenic sediments alongside chemical evaporites. These findings have served to determine the elemental and chemical nature of surface and sub-surface sediments; and consider their role in surface erosivity thereby adressing the second objective. The key findings of this chapter can be summarised as follows:

i. The role of the capillary zone and relatively shallow ground water were confirmed through the presence of thenardite, mirabilite, trona and halite. These minerals and their proximity to the ground water together with the climatic controls of temperature and diurnal fluctuations can be determined to be crucial in shaping the surface and sub-surface environment and the pan.
ii. The recognition of multiple evaporites, as well as silicate based and metal oxide functional groups, presents deeper insight into the composition of the pan surface. Despite not considering the size fractionation of samples, it was possible to determine the bulk chemistry of the region.
iii. While there appeared to be no geographic trends in bulk elemental composition of pan sediments, links between elemental and mineralogical composition suggest all sites to have a chemical signature indicating young evaporite minerals alongside the older base geology of the region strongly influenced by the pan environment.

iv. The combination of ICP and XRD has confirmed the presence of dominant salts and minerals, while presenting the base mineralogy of Makgadikgadi sediments.

v. Mineralogy is not prescriptive of the dust potential of the surface nor is the mineralogy if the surface prescriptive of the dust composition. Buck et al. (2011) confirm this, indicating that it is the crystal habits rather than the precise mineralogy which provide the greatest determinant of emissive potential. Thus, neither the availability of suitable sediment nor the mineralogy alone is sufficient to result in a dust plume.

vi. A detailed understanding of source and surface conditions along with a complex number of surface and atmospheric interactions need to be optimised in order to result in aeolian transportation.

The primary goal of this study was to evaluate the chemical variations and trends in physical and chemical properties of the pan surface and, within the vertical structure of the pan, attempt to reveal clues as to the origin and supply of minerals to the environment. Although this study does not allow for the identification of the precise controls of mineral variability across the pan surface, it does indicate the spatial variability and suggest possible controls. The following chapter, utilising high resolution QEMSCAN data, will consider both the sized geochemistry and morphology of the surface conditions, as well as entrained material, and will reveal further insight into the nature of aeolian sediments from this source.

Chapter 4: QEMSCAN of Surface and Airborne Samples from I4

4.1 Introduction

In this study, four aeolian samples were collected during a local dust storm on the 5th of October 2011 during the extensive DO4 field campaign. Samples were analysed using QEMSCAN, which allows the relationship between chemistry and particle size, shape and composition to be made. Additionally, the analysis of a surface sample, from which entrainment was proposed to have occurred, permits for the analysis of the representative nature of the surface with the airborne plume.

Few studies have synthesised results from such samples and even fewer have combined grain mineralogy and morphology in a single study with focus on a single event. This is also evident on the Makgadikgadi Pans, as existing studies have considered either the mineralogical analysis of source surfaces (Eckardt et al., 2008) and downwind soils (Wood et al., 2011) or considered the grain size of source conditions (Ringrose et al., 2005). While these approaches were capable of determining information on bulk surface chemistry as well as particle size distribution, none of these previous studies have been able to examine particle by particle correlations considering morphology, size and chemistry. Recent advances in understanding the radiative, chemical and human health impacts of mineral aerosols have shown that a unified understanding of the chemical and morphological character is essential for assessing their role and impact on local and regional scales. Therefore this chapter aims to determine the applicability of QEMSCAN as a multi-parameter tool for the chemical and morphological analysis of aeolian and surface sediments from the Makgadikgadi Pans.

4.1.1 Dust

Within the earth's atmosphere there exists a myriad of airborne particles termed aerosols, including dust, smoke from biomass burning, and anthropogenically produced air pollutants (e.g. Prospero, 1999; Piketh et al., 1999; Kaufman et al., 2002; Kohlfeld & Tegen, 2007; Engelbrecht & Derbyshire, 2010; Ravi et al., 2011). Of particular importance in this study are mineral aerosols, or dust, which, through its origin in arid and semi-arid regions globally, experiences a high degree of variability both spatially and temporally.

Aerosols are emitted into the atmosphere through a range of drivers both climatic and geomorphologic. They have the potential to modify the earth's climate (e.g. Ramanathan et al., 2001; Kaufman et al., 2002; Engelstaedter & Washington, 2007a; Kommalapati & Valsaraj, 2009; Washington et al., 2009; Mahowald, 2011; Shao et al., 2011) through both the direct and indirect effects of radiation as well as nutrient dynamics and ecosystem functions (Prospero, 1999; Harrison et al., 2001; Soderberg & Compton, 2006). The magnitude and direction of the potential impact is a function of particle morphology and composition, which is determined by, amongst other factors, the source region. Thus, knowledge of dust source regions and site characteristics is of the utmost importance in increasing our understanding of their potential impacts.

As Sokolik and Toon (1996) ascertained, regional scale knowledge is of further importance due to the fact that the regional radiative effects of mineral aerosols can potentially exceed those of sulphur and other anthropogenic aerosols, and may even be comparable to those of clouds. Therefore, the study of dust requires high spatial and temporal resolution to be able to capture source region and emission characteristics of the various sites. Ideally, these should be augmented by accurate and well constrained source region information and field data. Such strict requirements have meant that, both globally and regionally, dust region and frequency maps fall short of what is needed.

While there is much variability associated with source regions, arid and semi-arid soils are the primary source of dust globally (Prospero et al., 1983; Middleton, 1997; King et al., 1999; Ridgwell, 2002; Washington et al., 2003; Goudie & Middleton, 2006). Within these arid regions, a number of geomophological sub-units are considered to be significant dust sources. These include large, inland saline lakes; areas of alluvial outwash; ephemeral rivers and streams; and deltas and floodplains (Lawrence & Neff, 2009; Thomas, 2011).

The Makgadikgadi Pans in Botswana are a large inland ephemeral salt pan and are recognised as the most significant dust source in southern Africa (Vickery et al., 2013) as well as the 8th most significant global source (Washington et al., 2003; Bryant et al., 2007). Despite this observed significance, studies on the surface chemistry and grain size morphology of this system remain largely absent in current literature. According to previous studies, the Makgadikgadi may be one of the largest single sources of mineral dust released into the atmosphere per unit area in southern Africa (Vickery et al., 2013). The transport and deposition of these fine particles has great potential to affect visibility, public health, and the downwind ecological and geological environments (Cahill et al., 1996; Reheis et al., 2002; McTainsh & Strong, 2007; Okin et al., 2011a). Pye (1987) adds that dust infiltration into surface soils can alter the texture and nature of the soil, affecting both the development of landscapes as well as the soil fertility and hydrology. Further, due to the widespread transport of entrained materials, aeolian dust can influence ecology and landscape geochemistry heavily over large areas, up to several hundred kilometres from the source.

As dust is fundamentally a function of surface conditions, the precise nature of the emitted aerosol can be highly variable on both geographical and temporal scales. Additionally, the differing reactivity of various minerals (Krueger et al., 2004: 6254) highlights the importance of including dust mineralogy in atmospheric chemistry and climate models.

While our understanding of dust remains rudimentary (Harrison et al., 2001), a deeper understanding is dependent on the use of high resolution global climate models. While such models are becoming increasingly sophisticated (Bullard, 2010: 496), surface validation, observations and reliable *in situ* data remain as limiting factors in the accuracy. Existing studies have relied on the approximation of

aerosol load through sampling of source conditions (Evans et al., 2004), however this only yields the best approximation of immediate proximal source conditions. Therefore, in order to fully identify the signature of a region, sampling of the dust in transport is required.

While Chapter 3 considered the chemistry of the pan surface and, through analysis of various functional groups, determined the bulk chemistry of the pan; selective entrainment is likely. In order to fully understand the system, comparative analysis between entrained samples and the surface from which it is most likely sourced could provide a better indication of the emissive nature of the surface. Size fractioned analysis is also required to determine the chemistry of the aerosol load and associated impacts.

4.1.1.1 Mineralogy of Dust

Generalising on the composition of dust is problematic, due to the dependence of mineralogy on source location, seasonality and local conditions. Pye (1987) indicates that the precise composition of any given dust plume is dependent on the nature of the source material and source location. Meanwhile, the links between arid and semi-arid regions and dust sources globally (Prospero et al., 2002) presents that the likely dominant constituents of dust will include quartz, feldspars, calcite, dolomite, micas, chlorite, kaolinite, illite, smectite, clays, metal oxides, and silicate minerals (Middleton, 1997). In addition there is present a number of mineral evaporites in ephemerally active systems, including halite and gypsum, along with amorphous inorganic material, organic matter and bacteria, pollen, seeds, ash and stem tissue (Pye, 1987; Goudie & Middleton, 2006; Carslaw et al., 2010; Engelbrecht & Derbyshire, 2010).

While some minerals can be viewed as diagnostic of source region or source conditions, other minerals, like quartz, feldspar and mica are ubiquitous and can be found in most sources and plumes. Goudie and Middleton (2006) add that, at times, even the relative contribution of various elements can be similar from sources with large geographic separation. The authors note that SiO_2 and Al_20_3 concentrations in Harmattan, European, North American and Saharan dusts are all similar; incidentally, the concentrations are similar to values determined for global rocks (Goudie & Middleton, 2006). Blank et al. (1999) add that surfaces which are associated with soluble salts will produce plumes with high soluble salt contents, with Australian plumes containing up to 50% soluble salts by weight. Therefore while bulk mineralogy may give an indication of source region, differences in smaller trace minerals and the inclusion of trace minerals and evaporites or pollens, may further the attribution of dusts to source regions.

Thus, as the mineralogy of dust is known to be linked to the surface conditions of source regions, extensive field work has been undertaken in the past decade to collect data for the large deserts on Earth. The precise mineralogy between locations within large systems can be quite different.

Lawrence and Neff (2009) suggest that using global soil data bases provide bulk crustal conditions (Turekian & Wedepohl, 1961), which, while not ideal, are a suitable approximation for evaluating the chemical composition of regional dust. They add that upper continental crust values may not be highly representative of dust chemistry, as regions which are significant dust sources have often undergone considerable and prolonged physical and chemical weathering. However, despite the often poor correlation, in the absence of ground based information, global scale products are able to provide a good approximation of mineralogy.

4.1.1.2 Morphology of Dust

While determining mineralogy is possible through the use of global databases, determining the morphology of samples remotely is less accurate. An additional challenge exists when classifying dust, as many authors present differing values for grain size cut-offs, from simple early definitions by Pye (1987) who merely state that dust largely occupies size categories smaller than 100 μm. He adds that for the particle to be subject to significant atmospheric transport; grain sizes tend to be in the order of 10 μm to 50 μm, since larger grains settle during decreased turbulence. Bagnold (1941) defines the cut-off using the silt-sand boundary at less than 62.5 μm with Middleton (1997) suggesting local and regional dust are smaller than 80 μm, elaborating that smaller grain size (2 to 5 μm) results in longer residence time in the atmosphere. Prospero (1999) comments that the majority of dust transported over large distances has a median mass diameter of less than 10 μm (*Table 4.1*). Therefore, while Pye (1987) and Middleton's (1997) thresholds can be proposed for local and regional aerosols, Prospero's (1999) definition can be assumed to hold for aerosols with greater transport potential as Middleton (1997) suggests that smaller grain size (2 to 5 μm) can result in longer residence time in the atmosphere as well as potential for greater (continental) transportation – over hundreds of kilometres. Rodriguez et al. (2012) suggest that sampling proximity can serve to define dust as significantly coarser/finer than is truly representative, due to preferential deposition of larger grains closer to source. This is a shortcoming as confirmed by Krueger et al. (2004) who suggest that representing dust as a function of grain size alone without consideration of sampling location and source context, can provide questionable results and provide a poor representation of source and entrainment conditions.

Table 4.1: Different classifications of dust by grain size (Bagnold, 1941; Pye, 1987; Middleton, 1997; Prospero, 1999).

Size Range	Additional Classification	Reference
< 62.5 μm	Sand Silt boundary	Bagnold (1941)
10 – 50 μm	Strictly < 100 μm, although smaller results in greater transport distance	Pye (1987)
< 80 μm	2-5 μm results in longer residence time	Middleton (1997)
< 50 μm	< 10 μm will result in longer residence time	Prospero (1999)

As many of these definitions vary (*Table 4.1)* it is evident that even classifying dust is complicated. Despite the considerable variation presented in these definitions, there is general consensus that dust sized grains are towards the finer end of the grain size spectrum existing in the clay and silt ranges as defined by Wentworth (1922). Due to the limitations of grain size determination in analysis, in this study the cut-off will be at 53 µm (Pye, 1987) with 75 µm (Middleton, 1997) marking the upper limit of short range transport.

Through an understanding of grain sizes that have dust potential, determining the grain size distribution of the source can predict the emissive potential of a surface as well as present the potential to determine transport distances. However, due to the complexities of entrainment processes (Nickling, 1984; Komar, 1987) and chemistry, grain size alone cannot be viewed as prescriptive of source emissivity.

While the theoretically, grain sizes typically transported by wind under standard conditions is confined to a smaller range than those associated with aqueous transport (Kocurek, 1996), the range remains large as a function of wind capacity. Livingstone and Warren (1996) suggest that dust exists as a function of a range between 1 µm and 200 µm, which is further defined by a bimodal distribution (Tanner Gap - Tanner, 1958)) with a coarse size fraction (between 10 and 200 µm) and a finer size fraction (between 1 and 20 µm). This large range is a trend that, according to the authors, is not an aerial control but rather a ground control on dust production processes at site (Kocurek, 1996; Livingstone & Warren, 1996). Evans et al. (2004) add that the trend exists in response to the mechanisms involved in the shaping of clastic sedimentary particles. While the mechanisms behind the formation of the coarser fraction are better understood, the processes behind the formation of the finer silt size particles in such environments is less definitively known (Middleton, 1997). In confirmation, global trends reveal that natural surfaces are not a simple continuum of sizes, but rather demarcatable families of sizes determined by mechanisms of transportation and mineralogical properties. Khalaf (1989) indicates that skewness and kurtosis can be indicative of the chemical nature of the sediments, noting that different minerals within a sample can produce definite signatures within the psd.

Kruger et al. (2004) suggest that viewing samples as function of psd alone should be viewed with caution indicating that it reveals questionable results in threshold monitoring. Rodriguez et al. (2012) developed the idea that preferential deposition of larger particles during atmospheric transport modifies the original size distribution, enhancing the relative contribution of smaller dust particles, skewing the psd. The authors suggest that classification of grain size for aerosol studies can merely provide a time slice on aerosol conditions. They also suggest that the highly variable temporal and depositional structure of samples may influence the aerosol dust mineralogy (e.g. small clays versus large quartz, with regards to preferential deposition).

Many current methods of grain size determination are further classified based on 2D representations of 3D grains. Goudie et al. (1990) suggest measurements of the longest, intermediate and shortest axis best represent grains size, although manual measurements are restricted by size range with smaller grains falling below the threshold for manual measurements. Similarly, Ried et al. (2003) indicate that ratios of these variables can be important in determining morphology characteristics. They note that major and minor axes, maximum and minimum dimensions, surface area, circumference and many others can be used to categorise morphology (*Figure 4.1*).

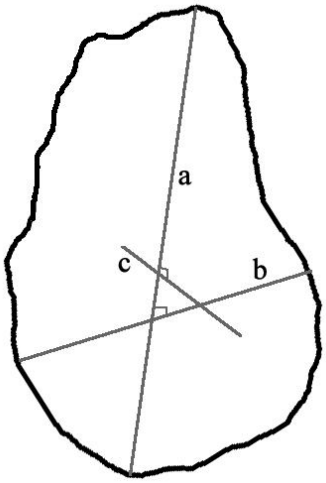

Figure 4.1 The three dimensions of an irregular sedimentary particle (Adapted from Allen (1985)). Dimensions present such that the area is calculated using product of 2 perpendicular lengths, with the shape factor defined by the Perimeter^2/Area. While the Aspect ratio is calculated using the quotient of the shortest to longest perpendicular lengths.

Such measurements are rarely taken (Reid et al., 2003) and the real character (Goudie et al., 1990) of grains remains hidden. Further, Goudie et al. (1990) suggest that the rather limited use of particle form in literature is further compounded by "both the ill definition of the often illusive nature of particle form, and the concomitant persistent inability of deriving simple measurements by which to characterise form efficiently at all scales of particle size." (Goudie et al., 1990: 121). These issues translate into inconsistencies in the definition of shape, sphericity, roundness/angularity and surface texture. Inconsistencies are further complicated by the dependence of shape on roundness or shape on sphericity, with Goudie et al. (1990) suggesting that to consider any single variable or subsume a mixture of these elements without context does not do justice to the description of particulate form.

Despite this, work by Powers (1953) was seminal in developing grain angularity as a functional method of analysis. Figure 4.2 presents the roundness scale as developed by Powers (1953); however, Reid et al. (2003) suggest that, even in contemporary research, the laborious nature of sediment classification remains a limiting factor in determining particle morphology. Goudie et al. (1990) add that visual descriptions, comparisons and measurements are often impractical on bulk samples.

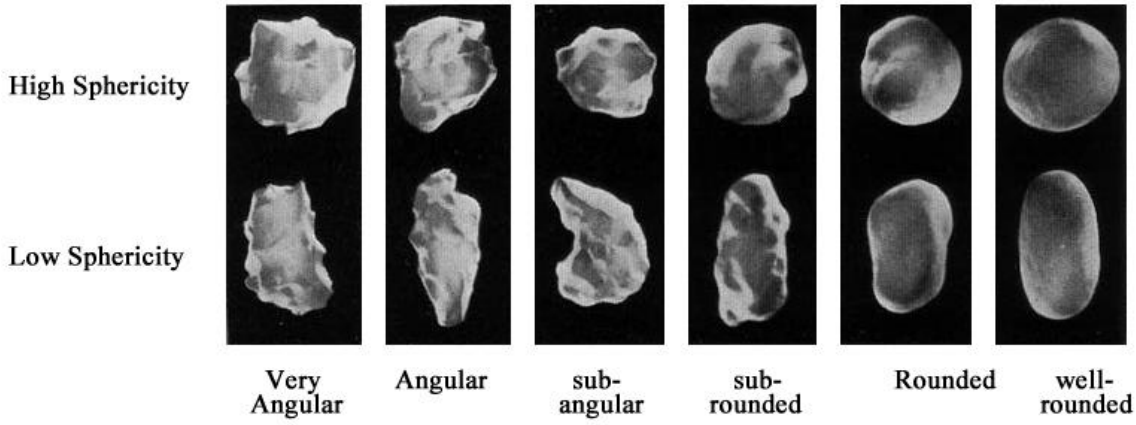

Figure 4.2 Particle form, roundness and sphericity scale as defined by Powers (1953) (Adapted from Powers (1953)).

As a result, very few formal definitions and discussions of dust shape are made in literature. Existing literature is largely based on the generalisation that aeolian samples that have been actively transported would be assumed rounder due to mechanisms associated with transport (Bagnold, 1941). Pye (1987) adds that younger and mechanically weathered grains would be characteristically angular, whilst grains that were associated with fluvial (and aeolian) processes would be notably rounder. Daniels and Hammer (1992) argue that sharp edges, conchoidal surfaces and striations are common weathering features on larger grains and may not indicate the nature of the current sedimentary environment. They also note that well rounded and spherical grains would be more likely features of fluvial environments, while well sub-angular to sub-rounded grains would likely populate aeolian environments. However, these definitions fail to consider the mineralogy of the sample and the nature of the process at source region.

However, methodological advancements and automation of classical methods has seen resurgence in the computing and analysis of grain form; this is particularly evident through the capabilities of QEMSCAN (Speirs et al., 2008).

4.1.2 QEMSCAN

Traditionally, mineralogists identified mineralogy using optical microscopy manually, however samples were often highly complex (Gottlieb et al., 2000) and could not always be adequately quantified by manual quantitative microscopy. This led to the development of QEMSCAN (earlier QEM*SEM - (Gottlieb et al., 2000)) which is an automated scanning electron microscopy (SEM) system that provides quantitative and qualitative elemental, mineralogical and morphological data on a sample. The technology was developed in the 1970's by the Commonwealth Scientific and Industrial Research Organisation (CSIRO) in Australia for the minerals industry to complement bulk chemical analysis (Ayling et al., 2012). Subsequent refinements and modifications of both the technology and software programmes has broadened its application to other sectors including, oil and

gas (e.g. Edwards & Butcher, 1999), geosciences (e.g. Speirs et al., 2008) and geothermal systems (e.g. Ayling et al., 2012).

The SEM system is fitted with four light-element Energy Dispersive X-ray (EDX) spectrometers (Ayling et al., 2012). It utilises the EDX-ray spectra together with Backscattered Electron Imagery (BEI) information from each measurement point to identify the minerals using the chemical composition, from X-ray information preferentially over backscattered electron brightness. Each identified mineral species represents either individual minerals or groups of minerals with similar chemical compositions. Using a database of mineralogical composition, minerals are differentiated based on elemental ratios using either the EDX-ray spectra or BEI in both real time processing and off-line post processing (Gottlieb et al., 2000). The measured spectra are automatically compared against a database of known spectra and a mineral or phase name is assigned to each measurement point by the QEMSCAN computer software programme. In this way, the near-surface qualitative elemental composition of each particle is systematically mapped, assigned to a mineral name or chemical compound/species, and digital pixel maps of each particle are created (*Figure 4.3*).

This fully automated analysis system enables quantitative chemical analysis of high resolution mineral maps and images (Gottlieb et al., 2000). Currently, three measurement modes exist for analysis, these include: bulk mineralogical analysis (BMA), particle mineral analysis (PMA) and specific mineral particle analysis (SMPA). BMA uses linear scans to characterise the sample, identifying mineral intercepts, transitions and intercept lengths to determine mineral abundance, surface areas, mineral association and particle size. PMA provides more detailed mineralogical classification of particles, scanning the full particle, revealing similar data but on a particle by particle basis (e.g. *Figure 4.3*). Finally, SMPA is performed based on a specific mineral search of trace minerals using a similar mode to PMA; this process is typically used where minerals are present in 0.5 vol % or less (Gottlieb et al., 2000). The EDX-ray spectra are used to create digital grain images with mineral maps at a user defined resolution based on sample size and detail required, using either PMA, BMA or SMPA (Martin et al., 2008; Speirs et al., 2008).

The error associated with the automated sampling method depends largely on representative sampling and the validity of sampling preparation methods (Gottlieb et al., 2000). For this study, a similar dry mounting technique as used by Martin et al. (2008) was adopted, splitting of sufficiently large samples to provide representative subsamples, which were then dry mounted on tape and carbon coated prior to analysis. This is in contrast to the methods presented elsewhere in literature whereby samples were mounted into resin or wax blocks, polished and then carbon coated prior to analysis (e.g. Gottlieb et al., 2000; Speirs et al., 2008; Ayling et al., 2012). The softer evaporite minerals were found to be destroyed through polishing producing a pitted resin block, which resulted in a poorly representative sample.

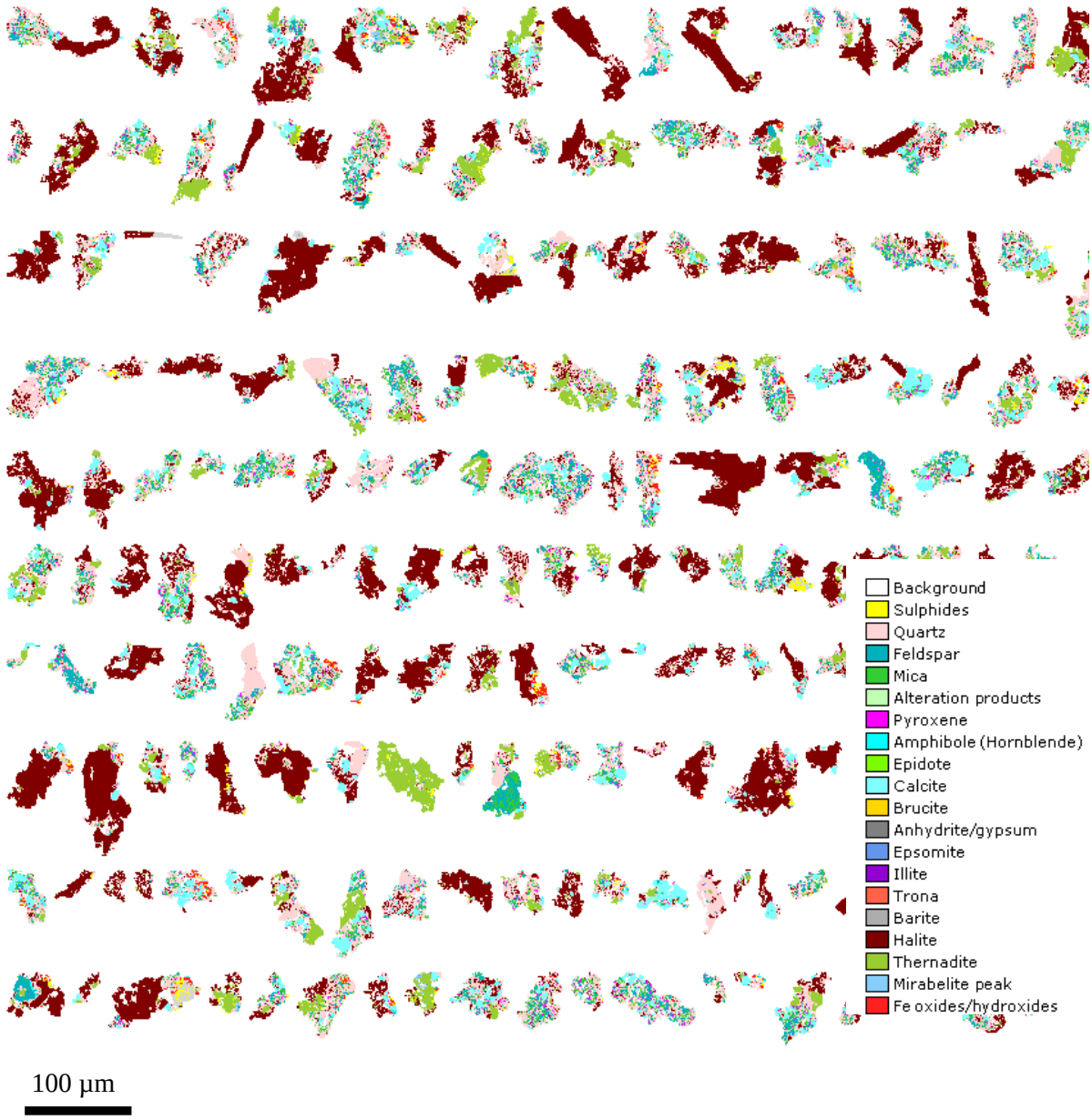

Figure 4.3 QEMSCAN graphical display output for grains from I4 fluff from the largest size fraction (75 µm to 106 µm). The colour key/legend has been included along with a scale bar for reference. This excerpt is only a small subset from a single disc of one size fraction and may not be fully representative of the sample.

In addition to providing a qualitative elemental analysis and mineralogical or phase assignment for each particle, data relating to particle size, shape and calculated specific density is also generated. Previous comparative studies demonstrate that QEMSCAN determined mineralogy is comparable to standard techniques (Speirs et al., 2008). Additionally QEMSCAN has been determined to detect all minerals presented through XRD analysis along with a wide range of minor minerals below the detection limit of XRD and other standard techniques (Krueger et al., 2004; Goodall et al., 2005; Speirs et al., 2008)

The purpose of this study was to use QEMSCAN to determine the particle morphology and mineralogical composition of aeolian dust samples collected during a single dust event located within the DO4 grid on Sua Pan in October 2011. Through this high resolution analysis, it becomes possible to identify the degree of preferential entrainment experienced on the pan surface and thereby better represent the properties of the plume that is likely to be transported from this region. This study also investigates how the particle size distributions (psd) of the sample varied between the surface and the height of sample collection above the pan surface. Additionally, it presents the psd of a long term frisbee sample, which can indicate composition of both the local and regional aerosol load. It is hypothesised, based on field work by Cahill et al. (1996), that the seasonality of the storm and the height of the sample trap above the pan all influence the composition and morphology of the dust sample.

As yet, there are not many publications that deal with the subtleties of trace element variation with different grain sizes (Castillo et al., 2008). This is largely because the analysis of the physical attributes of aeolian sediments, including the size, shape and mineralogy, were typically time consuming due to the manual nature of identifying samples using optical microscopy, XRD and fluorescence (Speirs et al., 2008). Therefore, much literature which attempts to characterise aeolian samples typically presents either the chemistry or the grain size. In a limited number of locations including the Sahara (Prospero et al., 1987; Zender et al., 2003; Moreno et al., 2006; Laurent et al., 2008; Crouvi et al., 2012), a considerable amount of work has been undertaken in an attempt to indentify the multiple signatures of dust from this region, including identification and characterisation of both the aerosols and the surface chemistry. These studies have shown that the addition of sized geochemistry of source dramatically increases our understanding of source regions. Therefore, the purpose of this study is to examine compositional variations of mineral dust using data on samples collected from the Makgadikgadi Pans. Additionally, these samples serve to illustrate the relationship between airborne samples and the mineralogy of the surrounding crusts and soils. These findings are all placed within the context of exploring the capabilities of QEMSCAN for rapid high resolution mineralogical and morphological analysis of samples.

4.2 Field and Laboratory Methods

In October of 2011, a major dust storm broke out on the Makgadikgadi Pans. Four BSNE traps on a single mast set up as part of the DO4 field season captured dust entrained during this event at four heights, while two frisbee traps collected passive fallout from this and localised transport. These samples, together with a surface fluff sample and the exhaust from PI-SWERL analysis, were analysed for both grain size and chemical compositions, revealing both the morphology and mineralogy of the samples. Collected samples were processed for chemistry using QEMSCAN PMA analysis and size-resolved through the use of Malvern.

4.2.1 Field Sites and Sampling:

The grain size and mineralogical characteristics of seven samples collected from the site I4 on Sua Pan, Makgadikgadi during 2011 were analysed using QEMSCAN. One of these samples represents a surface grab sample of local fluff (*Figure 4.3, Table 4.2*), four represent passive sampling traps at differing heights (BSNE traps, (see Goossens, 2001) – *Figure 4.4a, b*), the final sample represents long term deposition at the site collected through passive sampling (Frisbee – *Figure 4.4c, d*) (see Goossens, 2007 for sampling efficiency information). The four aeolian samples were collected from a single set of four wedge-shaped BSNE traps based on the design by Fryrear (1986). The pivoting traps represent four heights from near surface (0.25 m) to a height of 1.68 m representing a vertical profile of transported sediment (*Figure 4.4a, b*). This trap design and set up was similar to that presented by Shao et al. (1993) who tested the configuration, and indicated an overall sampling efficiency of 90±5% for aeolian sand sized grains, although no comment was made of clay and silt sized sample. Two frisbee samples located at I4 were combined to allow for a significant sample size for analysis, the samples collected from 1.68 m, represent just under two months worth of passive collection.

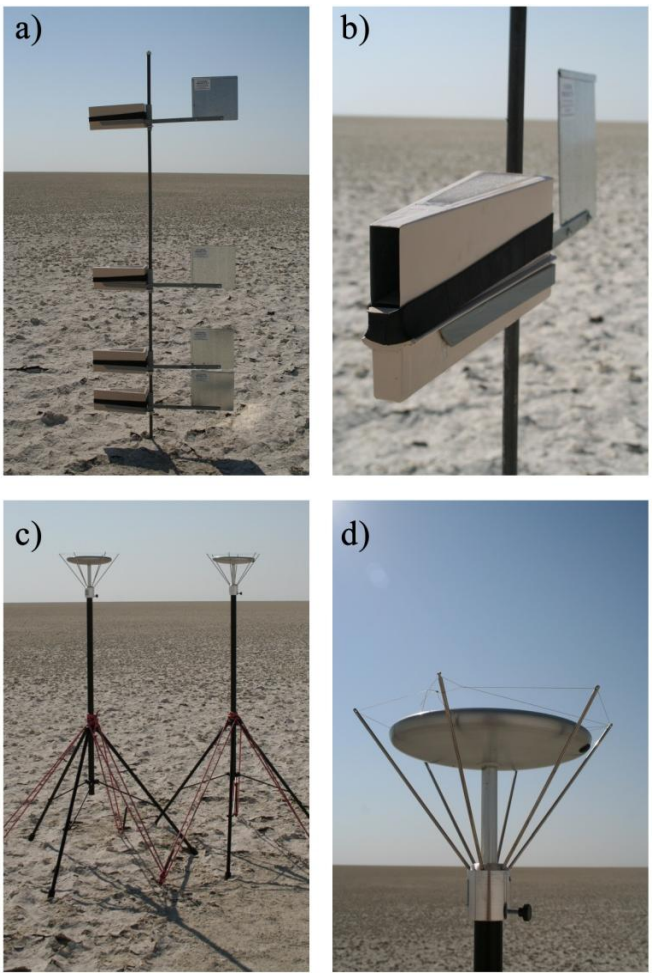

Figure 4.4 Sampling equipment on the Makgadikgadi Pans. Figure a) the four BSNE traps on a single mast located at I4,samples taken from lowest trap, SD200 to highest, SD203 b) looking into the BSNE trap. Figures c) and d) show the passive frisbee sampler, with the cage visible in figure d) added to prevent birds from disturbing the sponges (Photographs by author taken during Makgadikgadi DO4 2011 field season).

Table 4.2: Sample description and nature for samples analysed using QEMSCAN.

Sample Source	Sample ID	Sample Collection Date	Sample Description
Fluff Sample	I4F	30 August 2011	Approximately 3 cm of fluff directly below the crust
BSNE at 0.25 m (BSNE 1)	SD200	5 October 2011	9.2 g of sample collected from BSNE 1
BSNE at 0.47 m (BSNE 2)	SD201	5 October 2011	6.3 g of sample collected from BSNE 2
BSNE at 0.89 m (BSNE 3)	SD202	5 October 2011	4.6 g of sample collected from BSNE 3
BSNE at 1.68 m (BSNE 4)	SD203	5 October 2011	3.1 g of sample collected from BSNE 4
Frisbee Sample (Frisbee 1 and 2) (1.68 m)	I4FRISBEE	16 October 2011	1.3 g of sample collected from two Frisbee's (0.49 g and 0.81 g)
Pi-Swerl Exhaust	I4PSE	23 September 2011	9.06 g of exhaust sampled at 53 000 RPM at I4

The four BSNE samples were collected following a dust event in October 2011, representing this event and 8 full days prior, while the fluff was sampled in late August, earlier in the field season. The frisbee samples represent just under two months (28th August – 16th October) of passive collection. The final sample is exhaust captured from the PI-SWERL (for more information on PI-SWERL see Sweeney et al., 2008) at 53 000 rpm on the I4 surface.

4.2.2 Grain Size Analysis

Analysis was performed on representatively split samples of between 0.4 g and 0.5 g using an 8 tube Rotary Micro Riffler, before being analysed on the Malvern Mastersizer 2000 instrument with the Hydro 2000SM attachment. Samples were processed using ethanol with three readings per sample taken and the average used unless significant variation existed between samples (for more information on sampling procedure, methodology and justification see Chapter 2, for further information on procedure see Appendix 7). The Malvern machine determined grain size using modern laser diffractrometry, presenting the distribution of the sample in 200 grain size classes between 0.012 µm and 2000 µm. However due to the required resolution these were grouped into the 11 size fractions as used in Blott and Pye (2001) (see Chapter 2 for a detailed analysis of methods and statistical processing).

4.2.3 Sediment Preparation and QEMSCAN Analysis:

Surface and BSNE trap samples were placed into labelled and sealed sediment bags in the field, while the frisbee samples were transported to the laboratory in the sampling device before being extracted into sample bags. On return to the laboratory, samples were oven dried for 12 hours at 35°C. Samples were screened, according to the method outlined in Chapter 2, into three size fractions representing 0 – 53 µm, 53 – 75 µm, and 75 – 106 µm, these ranges approximating clays and silts, very fine sand, and fine sand to coarse sand respectively. These three size ranges were then split using a spinning microriffler to obtain samples of approximately 0.1 g for each fraction of each sample. The samples were then screened onto QEMSCAN discs pre-covered with a layer of double sided sticky tape, before mechanically removing the poorly adhered particles using compressed air (see Appendix 7). This ensured a single layer of sample on the disc to minimise obscuration and machine error. The covered discs were then coated with graphite before analysis and kept in an oven set to 40°C to ensure

that ambient moisture was not drawn into the sample. Three discs were prepared for each size fraction with 3 000 grains counted per disc, (*Figure 4.5*) attributing grains to a customised mineral list of 255 known minerals.

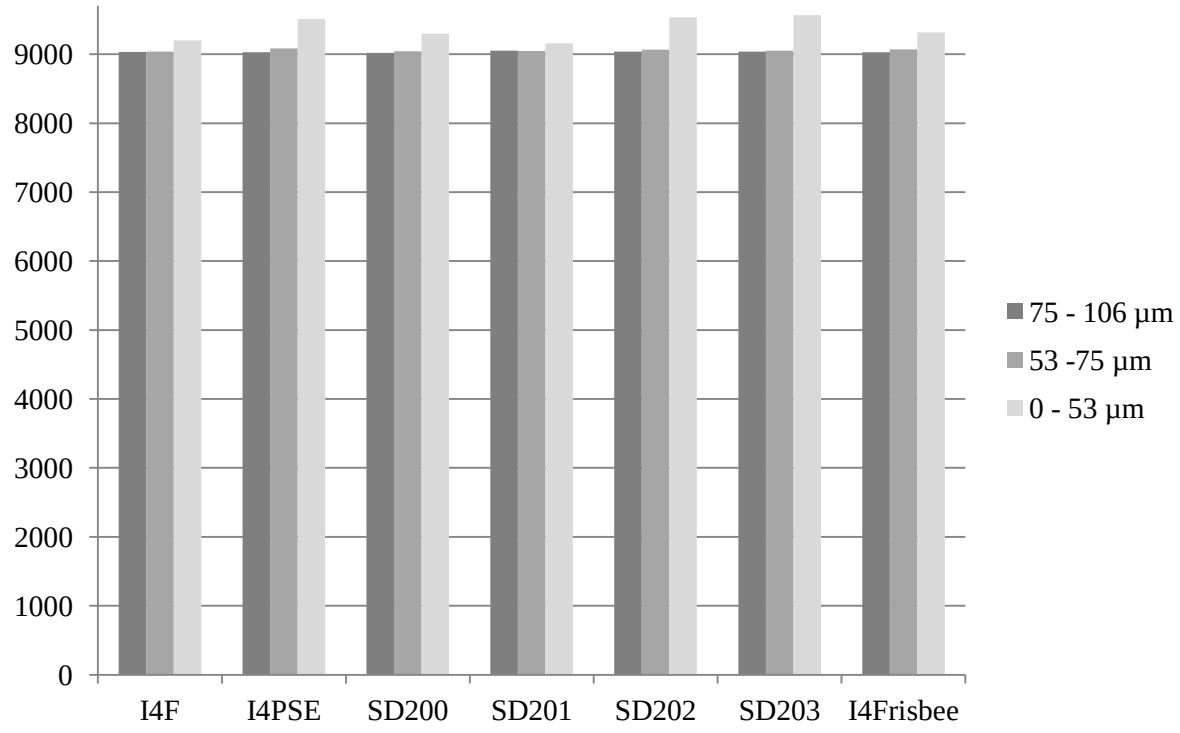

Figure 4.5: Plot of number of grains counted (and accepted) per size fraction. Partial grains are excluded from the count, with a minimum of 3 000 complete grains requested per disc to be counted. The smaller grain size had a higher density of grains per unit area and as a result more grains were fully included in the count area and a slightly higher grain count resulted.

Along with chemistry, QEMSCAN permits the analysis of a number of grain morphology characteristics. Grain shape, using a 'shape factor', which is defined by the software to represent the grain perimeter squared, is one useful indicator of transport and origin and was used in this study. The resultant shape factor value can be compared to a perfect sphere giving an indication of sphericity of the grain, with a sphere having a shape factor of 4π or 12.56. Therefore grains with 'shape factor' values <15 were determined to be well rounded, 15-16 rounded, 16-17 as sub-rounded, 17-18 sub-angular, 18-19 angular and >19 angular in accordance with ranges used in Speirs et al. (2008) developed by Powers (1953) (*Figure 4.2*). Aspect ratios were also calculated; this value represents the smallest length divided by the longest perpendicular length, and indicates whether the grain is round/square (values ~1) or long and thin (~0). Mineral associations were also calculated, and determined using the count of the co-occurrence of multiple minerals in a grain, such that low counts indicate a mineral most commonly occurring as a pure grain with higher association indicating a grain comprised of multiple minerals.

4.3 Results

The results presented represent the three size fractions, 0 – 53 µm, 53 – 75 µm, 75 – 106 µm, and a weighted combined value for the sample. They present the mineralogy and morphology results of the QEMSCAN analysis on the four types of samples – surface fluff, passive dust, airborne dust and PI-SWERL exhaust – before presenting the differences in chemistry, morphology and associations.

Grain size results as determined from QEMSCAN are biased by orientation, so the results of grain size determined through Malvern will be presented to reveal the trends in grain size for the various samples.

4.3.1 Mineralogical Results:

4.3.1.1 Results of the Chemical and Morphological Characteristics of Surface Fluff (I4F)

i. Mineralogical Results

Results from the QEMSCAN analysis of I4F reveals the presence of 58 out of the 255 test minerals. Table 4.3, the 20 mineral summary of the sample, presents the results of the three size fractions as well as the weighted combined bulk chemistry. Quartz was found to dominate at all size fractions (35% combined), with the greatest percentage to be found in the finest size range at 38%, with only 34% found in the largest size fraction. Halite was the next most commonly occurring mineral found to strongly decrease with sediment fining (*Table 4.3*); similarly, thenardite was present, with lesser dominance in the finest category. Mica, feldspar, calcite and pyroxene were all found to increase with decreased grain size. These seven minerals account for over 90% of the I4 fluff sample and correspond well to results presented in Chapter 3. As the largest size fraction accounts for 68% of the sample, the dominant minerals in this size fraction are the best representation of the bulk mineralogy of the sample.

Table 4.3: Summary of mineralogical results for surface fluff from I4.

Mineralogical results	Combined	75 - 106 µm	53 - 75 µm	0 - 53 µm
Quartz	35.1	34.0	35.7	38.5
Halite	18.2	20.5	14.1	12.4
Thenardite	10.3	10.6	10.8	8.7
Mica	9.9	8.9	11.6	12.1
Feldspar	9.6	8.9	11.7	10.3
Calcite	4.8	4.4	5.4	5.5
Pyroxene	3.8	3.0	4.7	6.2
Others	3.0	3.1	2.2	3.2
Sulphides	2.3	2.8	1.1	1.1
Amphibole (hornblende)	1.3	1.3	1.3	1.1
Fe oxides/hydroxides	1.3	1.7	0.6	0.2
Mirabilite Peak	0.2	0.2	0.2	0.2
Alteration products	0.2	0.1	0.2	0.4
Epidote	0.1	0.1	0.2	0.1
Anhydrite/gypsum	0.1	0.1	0.1	0.1
Barite	0.0	0.0	0.0	0.1
Brucite	0.0	0.0	0.0	0.0
Epsomite	0.0	0.0	0.0	0.0
Illite	0.0	0.0	0.0	0.0
Trona	0.0	0.0	0.0	0.0
% Mass size distribution		68	14	18

ii. Morphological Results

Morphological results using aspect ratio reveal that grains in I4 fluff are more rounded to square than needle-like; this trend is true for all size fractions and all minerals. In order to determine the significance of the 'roundness' of the grains, shape factor needs to be considered. Shape factor results presents that the round to square shaped grains are highly angular. For the unsized sample 69% of the sample can be classified as very angular, almost 80% of the sample being composed of values greater than 17. While the remaining 21% of grains can be considered round, with 11% of the sample classified as well rounded. Considering the dominant six minerals (quartz, feldspar, halite, thenardite, mica and calcite) and the three size fractions processed, it can be seen that there is a trend of rounding with decreased grain size. For the largest size fraction 76% of the sample is very angular decreasing to 40% of the sample in the finest fraction (*Figure 4.6*).

Along with the trend in becoming more rounded with decreasing grain size, there is also an increased fraction of the sample existing in the angular, sub-angular, sub-rounded and rounded classifications. Between minerals, halite is the most angular with 75% of the mineral irrespective of size having a value >19, while calcite and quartz are the least angular with 65% of the mineral classified as having a value greater than 19.

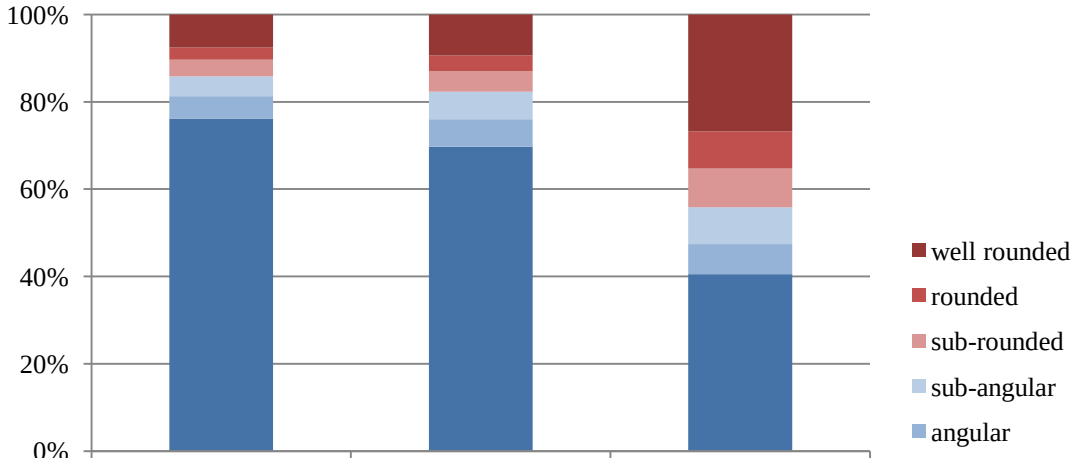

	75 - 106 µm	53 - 75 µm	0 - 53 µm
well rounded	7.6	9.4	26.8
rounded	2.8	3.6	8.5
sub-rounded	3.8	4.7	8.8
sub-angular	4.5	6.3	8.5
angular	5.2	6.3	6.9
very angular	76.1	69.7	40.6

Figure 4.6: Results of shape factor analysis on I4 fluff sample indicating the angularity of the dominant six minerals.

iii. Mineral Associations

Mineral association analysis of I4 fluff sample revealed that 25% of all grains were single mineral grains with the remaining occurring as compound grains. Of the base minerals, quartz was associated with feldspar (14%), mica (18%), pyroxene (4.8%) with almost 28% of quartz grains associated with evaporites of which halite accounted for 20%. The remaining quartz found minor associations with lesser minerals with 31% found as pure quartz grains. Feldspar was also found to be associated with quartz (44%), with almost 22% of all grains found alongside mica and 8% with pyroxene; very few evaporite minerals were associated with feldspar (>2%) while only 17% of the feldspar occurring as pure grains. 60% of halite grains were found as pure halite, while just over 29% of grains were associated with quartz. The remaining halite was found to be associated with thenardite and sulphides. Thenardite and mirabilite were common associations with these minerals being detected to co-occur on a single grain on almost half of all counted mirabilite grains, while only 3% of thenardite grains were found as pure grains in just over 52% of all counts, while 20% of grains were associated with quartz. Only 22% of mirabilite grains were pure, with common grain associations being sulphides, quartz, feldspar and mica.

4.3.1.2 Results of the Chemical and Morphological Characteristics of Passive Frisbee Sample (I4FRISBEE)

i. Mineralogical Results

The frisbee sample contained 75 minerals from the extensive 255 mineral list. Table 4.4 presents the 20 mineral summary, of which only 16 minerals were identified. Quartz was found to dominate once again; halite was the second most commonly occurring mineral decreasing in abundance with decreased grain size (20% in 75 µm to 106 µm, 4% in 0 µm to 53 µm), while the inverse was true for thenardite which increased from 11% in the 75 µm – 106 µm range to 13% in the 0 µm – 53 µm range. Mica, feldspar, pyroxene and calcite all had minor variations between the size fractions; these minerals together with quartz, thenardite and halite accounted for approximately 92% of the sample. Lesser amounts of amphibole, iron oxides and sulphides were all present with trace amounts of alteration products, anhydrite/gypsum, epidote, wollastonite and mirabilite completing the major mineralogy of the sample.

Table 4.4: Summary of mineralogical results for the combined frisbee traps from I4.

Mineralogical results	Combined	75 - 106 µm	53 - 75 µm	0 - 53 µm
Quartz	43.9	41.5	47.4	46.7
Thenardite	11.8	11.4	12.2	12.6
Halite	11.3	15.8	7.4	3.9
Others	7.2	6.9	6.7	8.3
Mica	6.0	5.5	5.4	7.3
Feldspar	5.4	5.6	4.8	5.5
Pyroxene	5.3	5.1	5.4	5.5
Calcite	4.7	3.9	5.9	5.7
Amphibole (Hornblende)	2.0	1.3	2.6	2.9
Fe oxides/hydroxides	1.1	1.3	1.2	0.5
Sulphides	0.7	1.1	0.5	0.2
Alteration products	0.4	0.4	0.3	0.7
Anhydrite/gypsum	0.1	0.1	0.1	0.2
Epidote	0.1	0.1	0.1	0.1
Mirabilite peak	0.0	0.0	0.0	0.0
Barite	0.0	0.0	0.0	0.0
Brucite	0.0	0.0	0.0	0.0
Epsomite	0.0	0.0	0.0	0.0
Illite	0.0	0.0	0.0	0.0
Trona	0.0	0.0	0.0	0.0
% Mass size distribution		56	19	24

The sample was again dominated by the coarse fraction accounting for 56% of the sample, although the finest fraction contained a larger proportion than the intermediate size (24% in 0 µm – 53 µm;

19% in 53 µm – 75 µm) (*Table 4.4*). Evaporite minerals were more dominant in the coarsest fraction (35%) than in the finest (23%) with quartz and feldspar accounting for 54% of the finest category and 48% in the coarsest.

ii. Morphological Results

Analysis of aspect ratio revealed that combined there is no apparent difference between the aspect ratio of minerals with all minerals presenting similar counts in all categories (*Figure 4.7*). However, when considering the results by grain size for the six dominant minerals, it can be observed that the largest grains are the most rounded while the smaller grain size has the a greater contribution of needle-like grains, from 1% in the largest grain size up to 5% in the smallest. Six percent of halite grains in the finest category were proposed to be needle-like compared to only 1.4% in the 75 µm – 106 µm size fraction. To determine the effect of angularity on frisbee samples, shape factor results were analysed.

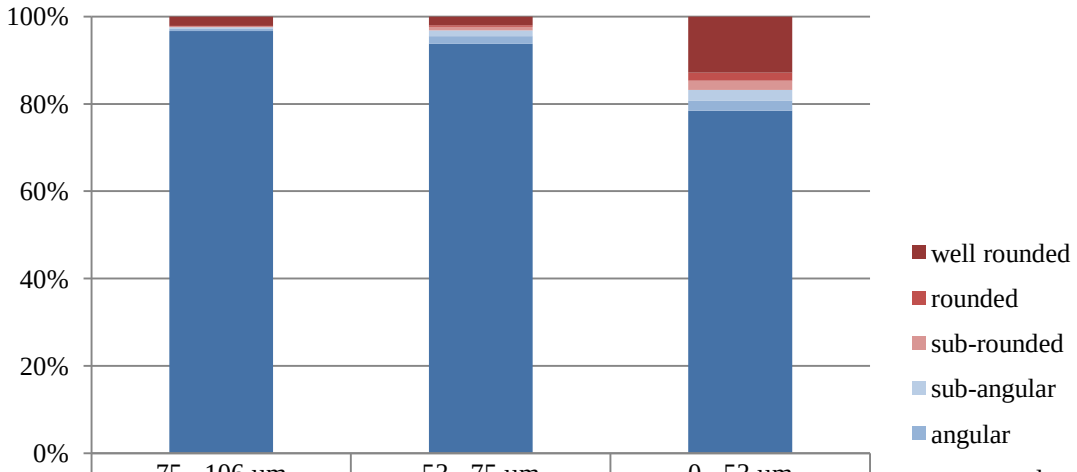

	75 - 106 µm	53 - 75 µm	0 - 53 µm
well rounded	2.16	2.00	12.84
rounded	0.16	0.37	1.88
sub-rounded	0.14	0.78	2.08
sub-angular	0.25	1.31	2.41
angular	0.58	1.82	2.35
very angular	96.71	93.72	78.44

Figure 4.7: Results of shape factor analysis on I4 frisbee samples indicating the angularity of the dominant six minerals.

Considering the results of the frisbee sample, using an average of the six main minerals it can be observed that grains are dominantly very angular with over 90% of the larger two size fractions being represented by a shape factor >19 (*Figure 4.7*). Further, these two size fractions represent 75% of the sample meaning that their shape strongly influences the overall composition of the sample. The three angular categories account for 81% - 96% of the sample with the remaining represented by the

rounded categories. By weighted sample average, only 4% of the frisbee sample is represented by <15 or well rounded. This sample is therefore representative of highly angular sediment.

iii. Mineral Associations:

Twenty-seven percent of counted grains for the frisbee sample occurred as single mineral grains, with a further 27% associated with quartz. Analysis of mineral association revealed that of the I4 frisbee samples 40% of quartz grains were found as pure grains. A further 30% of quartz was found to be associated with evaporites, 22.5% of this associated with halite. Quartz and mica was also a common association with 11% of all quartz grains association with mica, which was presented as over half of all mica grains (55%) associated with quartz. Of the evaporites, halite was found more commonly associated with quartz (61%) with only 20% occurring as pure halite. Halite and thenardite was another common association, accounting for 5% of halite associations and 11% of thenardite associations. Thenardite was found to present pure crystals 44% of the time, with 35% occurring coincidentally with quartz. Almost 60% of mirabilite occurred coincidentally with thenardite, with a further 20% of mirabilite occurring as pure crystals. Calcite occurred as pure crystals 55% of all counts, with only 5% of all calcite crystals occurring alongside other evaporite minerals, while more commonly found with quartz (12%), amphibole (11%), pyroxene (6%) and mica (3%).

4.3.1.3 Results of the Chemical Characteristics of Airborne Samples (SD200-SD203)

The same minerals dominate all four BSNE samples: quartz, halite, thenardite, mica, pyroxene, feldspar and calcite, which have slightly differing contributions between the samples. The following section will present the results of the BSNE traps from the lowest to the highest trap sample.

4.3.1.3.1 Results of SD200

i. Mineralogical Results

SD200 was sampled from the lowest trap (0.25 m above the pan surface) and was the heaviest (9.23 g) and coarsest with 48% of the sample existing in the 75 µm – 106 µm size range, decreasing to 38% and finally 13% in the 0 µm – 53 µm range. Mineralogically, 15 of the 20 minerals were present with similar trends to that of the fluff with quartz accounting for the bulk of the sample (see *Table 4.5*), while halite was the second most abundant mineral. This evaporite mineral accounted for almost 25% of the largest size fraction, while only 9% of the smaller, indicating the halite dominance in the coarser size fraction. Thenardite showed a similar trend, while mica, pyroxene, calcite and feldspar all decreased with decreased grain size. These seven minerals characterise approximately 93% of the sample.

Table 4.5: Summary of mineralogical results for SD200.

Mineralogical results	Combined	75 - 106 µm	53 - 75 µm	0 - 53 µm
Quartz	43.7	40.3	46.2	48.8
Halite	19.0	24.7	15.3	9.0
Thenardite	9.1	10.1	9.0	6.1
Mica	6.3	5.2	7.0	8.0
Pyroxene	5.0	3.5	5.9	8.2
Calcite	4.9	4.2	5.5	6.2
Feldspar	4.3	3.7	4.8	5.1
Others	2.6	2.3	2.1	4.7
Amphibole (hornblende)	1.7	1.5	1.8	1.7
Fe oxides/hydroxides	1.3	2.0	0.8	0.3
Sulphides	1.3	1.9	0.8	0.6
Alteration products	0.2	0.2	0.3	0.5
Epidote	0.1	0.1	0.2	0.3
Mirabilite Peak	0.1	0.1	0.1	0.1
Anhydrite/gypsum	0.1	0.1	0.1	0.1
Barite	0.0	0.0	0.0	0.0
Brucite	0.0	0.0	0.0	0.0
Epsomite	0.0	0.0	0.0	0.0
Illite	0.0	0.0	0.0	0.0
Trona	0.0	0.0	0.0	0.0
Zn trap	0.2	0.1	0.2	0.5
% Mass size distribution		48	38	13

ii. Morphological Results

The aspect ratios for SD200 revealed a dominance of round and square shaped grains (80%), while only 1% of the sample was considered to have a long or thin aspect ratio. Shape factor analysis further

revealed that the coarsest fraction was largely angular, becoming increasingly rounded with fining for the six dominant minerals (*Figure 4.8*). Very angular grains accounted for almost 73% of the coarsest fraction decreasing to 63% and finally 38% in the sub-53 µm size fraction, while well rounded grains increased from 9% to 11% up to 25% with decreasing grain size.

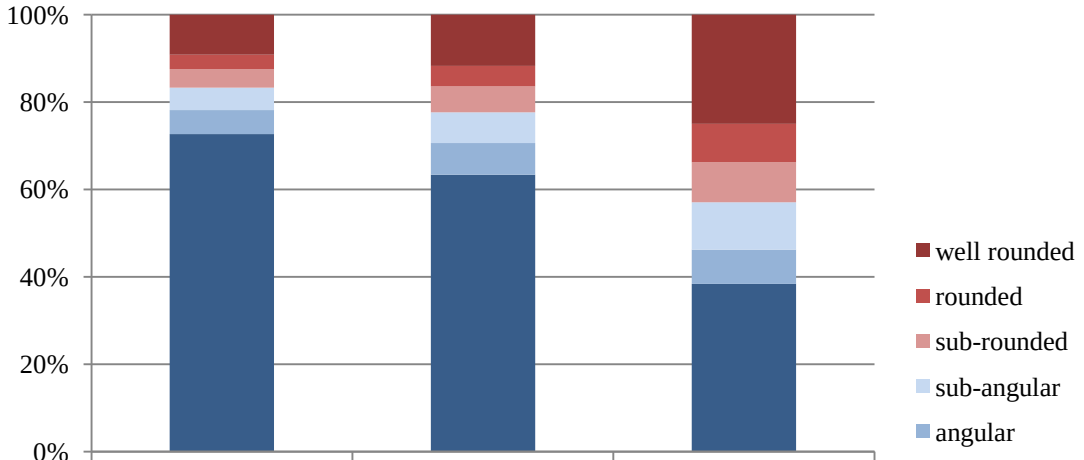

	75 - 106 µm	53 - 75 µm	0 - 53 µm
well rounded	9.2	11.7	25.0
rounded	3.3	4.7	8.8
sub-rounded	4.3	5.9	9.2
sub-angular	5.2	7.0	10.8
angular	5.4	7.2	7.8
very angular	72.7	63.4	38.4

Figure 4.8: Results of shape factor analysis of SD200 indicating the angularity of the dominant six minerals.

iii. Mineral Associations:

One quarter of the SD200 sample occurred as individual mineral grains, with the remaining occurring as compound minerals. A third of all quartz grains occurred as pure mineral grains, with a further third associated with halite, the remaining third associated with mica (11%), feldspar and pyroxene (6% each), then calcite and thenardite (3% each) and lesser amounts of amphibole and iron oxide. Over half (54%) of halite was found as pure crystals with 39% of halite associated with quartz and the remainder with calcite and thenardite. Similarly, 45% of thenardite occurred as pure, while 24% was associated with quartz, and 6% occurring with halite and a further 13% coinciding with a quartz halite interface.

4.3.1.3.2 Results of SD201

i. Mineralogical Results

SD201 was captured from a trap 0.5 m above the pan surface and this sample contained 43% in the coarsest fraction, 33% in the 53 µm – 75 µm range and 24% in the finest size range (*Table 4.6*). The sample weighed just over 6 g and had 15 minerals of the 20 minerals in the list present. Quartz dominated this sample, contributing 47% of the 75 µm – 106 µm and the 0 µm – 53 µm size fractions, with 42.5% in the 53 µm – 75 µm. Halite values vary with 15% in the largest range, increasing to 18% in sediments sized between 53 µm – 75 µm, then decreasing to 9% in the finest category. A similar trend was observed for thenardite which peaked between 53 µm – 75 µm decreasing in both the larger and finer sediments, while mica, pyroxene and calcite increased with decreasing sediment size. These seven minerals characterise over 90% of the sample with the remaining eight minerals existing in small and largely similar percentages between sample sizes.

Table 4.6: Summary of mineralogical results for SD201.

Mineralogical results	Combined	75 - 106 µm	53 - 75 µm	0 - 53 µm
Quartz	45.6	47.2	42.5	47.1
Halite	15.0	15.9	18.1	9.1
Thenardite	8.4	7.8	9.7	7.5
Mica	6.2	4.7	6.9	8.1
Pyroxene	6.0	5.2	5.6	8.0
Calcite	4.6	3.8	4.8	6.0
Feldspar	6.3	7.0	5.8	5.9
Others	2.7	2.5	2.1	4.1
Amphibole (hornblende)	1.6	1.8	1.5	1.5
Fe oxides/hydroxides	1.1	1.7	1.0	0.2
Sulphides	1.2	1.6	1.1	0.6
Alteration products	0.3	0.2	0.3	0.6
Epidote	0.1	0.1	0.1	0.1
Mirabilite Peak	0.1	0.1	0.1	0.1
Anhydrite/gypsum	0.1	0.1	0.1	0.1
Barite	0.0	0.0	0.0	0.0
Brucite	0.0	0.0	0.0	0.0
Epsomite	0.0	0.0	0.0	0.0
Illite	0.0	0.0	0.0	0.0
Trona	0.0	0.0	0.0	0.0
Zn trap	0.5	0.3	0.4	0.9
% Mass size distribution		43	33	24

ii. Morphological Results:

In the aspect ratios for SD201, almost 80% of the sample could be categorised as round to square with only 2% of the sample being categorised as long and thin. Shape factor analysis further revealed that

the coarsest fraction contained the highest percentage of very angular grains, while the 53 µm to 75 µm was the most angular overall (83%) decreasing to only 61% in the finest fraction, or concluding that 39% of the finest fraction was rounded (*Figure 4.9*). Twenty three percent of the finest fraction could be considered well rounded, double that of the coarsest fraction which was determined to be 10% well rounded.

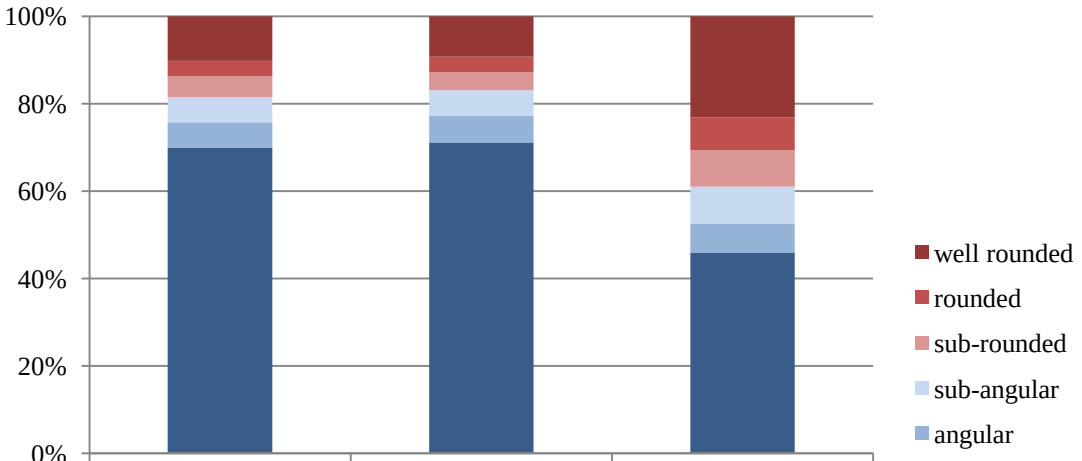

	75 - 106 µm	53 - 75 µm	0 - 53 µm
well rounded	10.2	9.3	23.1
rounded	3.5	3.5	7.5
sub-rounded	4.7	4.2	8.4
sub-angular	5.8	5.9	8.4
angular	5.9	6.0	6.7
very angular	69.8	71.2	45.9

Figure 4.9: Results of shape factor analysis of SD201 indicating the angularity of the dominant six minerals.

iii. Mineral Associations

The SD201 sample presented 25% of all counted grains to be a single mineral with the remaining presenting as composite grains. Quartz was found as a single mineral grain in 37% of all counts, with 7% and 9% associated with feldspar and mica respectively. The co-occurrence of halite and quartz was found to account for 27%. For halite, 50% of all grains were a single mineral, with a further 43% associated with quartz, coincident detection with calcite, iron oxides and thenardite account for a further 6% of associations. Thenardite was detected as a single mineral on 46% of all occurrences with a further 30% occurring with feldspar. The co-occurrence of thenardite, halite and quartz accounts for a further 7% of thenardite mineral associations. Mica was found to be a single mineral grain 15% of occurrences, with the mineral most commonly associated with quartz (51%) and feldspar (41%). Mica was also associated with pyroxene (7%) and calcite (5%) but rarely with sodium based evaporites, less than 0.1% with halite and 1.2% with thenardite.

4.3.1.3.3 Results of SD202

i. Mineralogical Results

The SD202 sample from a trap at 0.85 m above the pan surface contained 41% in the coarsest fraction and in the 53 µm – 75 µm range, with the remaining 19% in the finest size range (*Table 4.7*). The sample weighed just over 4.5 g and had 15 minerals of the 20 mineral list present. The sample was largely composed of quartz with a combined percentage of 41%, with 37% in the 75 µm – 106 µm range, increasing to 42% in the 53 µm – 75 µm, further increasing to 47% in the 0 µm – 53 µm size fractions. A similar trend was observed for mica, pyroxene, calcite and feldspar all of which experienced increasing percentage contributions with decreasing grain size. The inverse was found for thenardite and halite which were found in the greatest abundance in the coarsest size fraction. These seven minerals characterise over 90% of the sample with the remaining eight minerals existing in small and largely similar percentages between sample sizes.

Table 4.7: Summary of mineralogical results for SD202.

Mineralogical results	Combined	75 - 106 µm	53 - 75 µm	0 - 53 µm
Quartz	41.3	37.9	42.0	46.9
Halite	18.8	24.3	16.9	10.4
Thenardite	9.8	10.4	10.1	7.9
Mica	7.1	6.2	7.1	8.7
Pyroxene	5.3	4.4	5.8	6.4
Calcite	4.9	4.0	5.3	6.0
Feldspar	6.0	5.4	6.4	6.5
Others	2.2	2.2	1.9	2.9
Amphibole (hornblende)	1.4	1.3	1.5	1.6
Fe oxides/hydroxides	1.0	1.5	0.7	0.2
Sulphides	1.1	1.7	0.9	0.5
Alteration products	0.4	0.3	0.4	0.5
Epidote	0.1	0.1	0.1	0.1
Mirabilite Peak	0.1	0.1	0.1	0.1
Anhydrite/gypsum	0.1	0.1	0.1	0.1
Barite	0.0	0.0	0.0	0.0
Brucite	0.0	0.0	0.0	0.0
Epsomite	0.0	0.0	0.0	0.0
Illite	0.0	0.0	0.0	0.0
Trona	0.0	0.0	0.0	0.0
Zn trap	0.6	0.1	0.7	1.2
% Mass size distribution		41	41	19

ii. Morphological Results

Aspect ratio analysis for SD202 revealed a dominance of round and square shaped grains, with only 1% of the sample tending towards a long and thin in shape. Shape factor analysis revealed that the coarsest fraction was largely angular (70% very angular) becoming increasingly rounded (39% very

angular) with fining for the six dominant minerals (*Figure 4.10*). The two larger size fractions were similar with regard to the distribution of round and angular grains, while the finest size fraction contained twice as many rounded grains as the larger two fractions, 26% rounded in 0 µm – 53 µm compared with 11% and 13% in the 75 µm – 106 µm and 53 µm – 75 µm respectively.

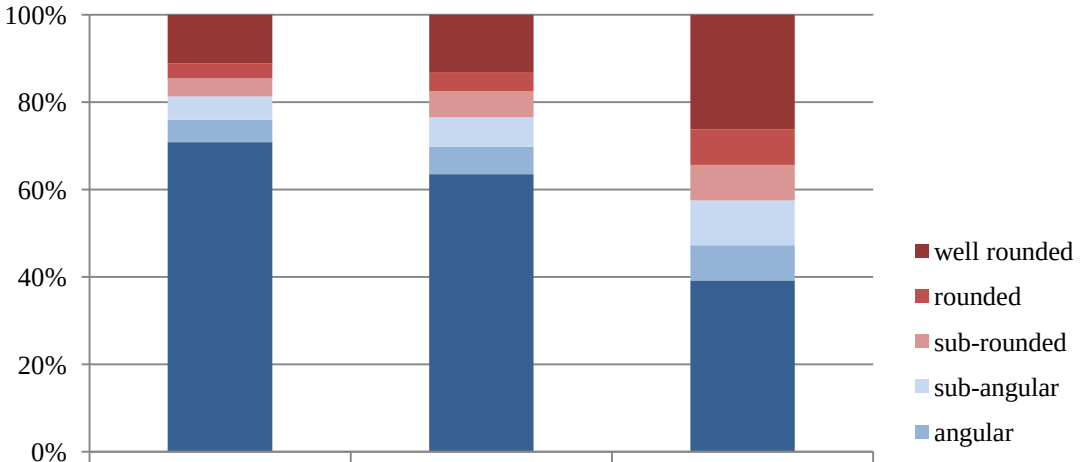

	75 - 106 µm	53 - 75 µm	0 - 53 µm
well rounded	11.2	13.1	26.2
rounded	3.4	4.4	8.1
sub-rounded	4.1	6.0	8.2
sub-angular	5.4	6.8	10.2
angular	5.1	6.3	8.1
very angular	70.8	63.5	39.2

Figure 4.10 Results of shape factor analysis of SD202 indicating the angularity of the dominant six minerals.

iii. Mineral Associations

For grains analysed for sample SD202, 28% presented pure grains of single mineral, the remaining grains were composite minerals. Again, quartz minerals were found to be associated with halite (28%), feldspar (8%), mica (11%) and pyroxene (6%). Over half (57%) of halite was found as single mineral grains, while 35% was associated with quartz and 1.8% and 1.99% with calcite and thenardite respectively. Similarly, thenardite was most commonly found as a single mineral grain (50%), with other common associations including quartz (24%), halite (5%) and sulphides (2%) while the co-occurrence of quartz, halite and thenardite explained 10% of associations.

4.3.1.3.4 Results of SD203

i. Mineralogical Results

SD203 was captured in the highest of the BSNE trap samples (trap height 1.65m), the sample weighing 3g, contained 28% of the sample in the 75 µm – 106 µm, 36% in the 53 µm – 75 µm size fraction and the remaining 37% in the finest fraction (0 µm – 53 µm) (*Table 4.8*). Fifteen minerals again represented the sample, with quartz accounting for the majority of the sample with increased contribution in the finer size fractions. Halite and thenardite were the next most abundant minerals, with these evaporites decreasing in their abundance with decreased grain size. Halite was found to characterise 28% of the 75 µm – 106 µm size range, decreasing to 20% in the 53 µm – 75 µm fraction and finally 10% in 0 µm – 53 µm, with thenardite values decreasing from 11% to 10.9% down to 7% in the same size fractions order. Mica, pyroxene, feldspar and calcite were found with increasing contribution with sediment fining. These seven minerals characterise over 90% of the sample, with amphibole, hydroxides, sulphides, epidote, mirabilite and anhydrite/gypsum accounting for the remaining 10%.

Table 4.8 Summary of mineralogical results for SD203.

Mineralogical results	Combined	75 - 106 µm	53 - 75 µm	0 - 53 µm
Quartz	42.4	35.8	41.5	47.9
Halite	18.6	28.1	19.6	10.1
Thenardite	9.7	11.1	10.9	7.5
Mica	6.4	4.9	6.3	7.5
Pyroxene	4.7	3.1	4.5	6.1
Calcite	5.0	4.0	4.8	6.0
Feldspar	4.9	3.6	5.0	5.6
Others	2.8	2.9	2.2	3.3
Amphibole (hornblende)	1.3	1.2	1.3	1.4
Fe oxides/hydroxides	1.2	2.0	1.2	0.5
Sulphides	1.4	2.2	1.3	0.7
Alteration products	0.3	0.1	0.2	0.5
Epidote	0.1	0.1	0.1	0.1
Mirabilite Peak	0.1	0.1	0.1	0.1
Anhydrite/gypsum	0.1	0.1	0.1	0.1
Barite	0.0	0.0	0.0	0.0
Brucite	0.0	0.0	0.0	0.0
Epsomite	0.0	0.0	0.0	0.0
Illite	0.0	0.0	0.0	0.0
Trona	0.0	0.0	0.0	0.0
Zn trap	1.5	0.8	0.8	2.6
% Mass size distribution		28	36	37

ii. Morphological Results

Analysis of aspect ratio revealed that SD203 was largely composed of round to square shaped grains with 2% of the sample tending to long and thin (*Figure 4.11*). Shape factor analysis revealed that these grains were largely angular, becoming increasingly rounded with decreased grain size. Sample roundness increased from 10% in the 75 µm - 106 µm size fraction, to 11% in the 53 µm – 75 µm fraction up to 26% in the 0 µm – 53 µm range.

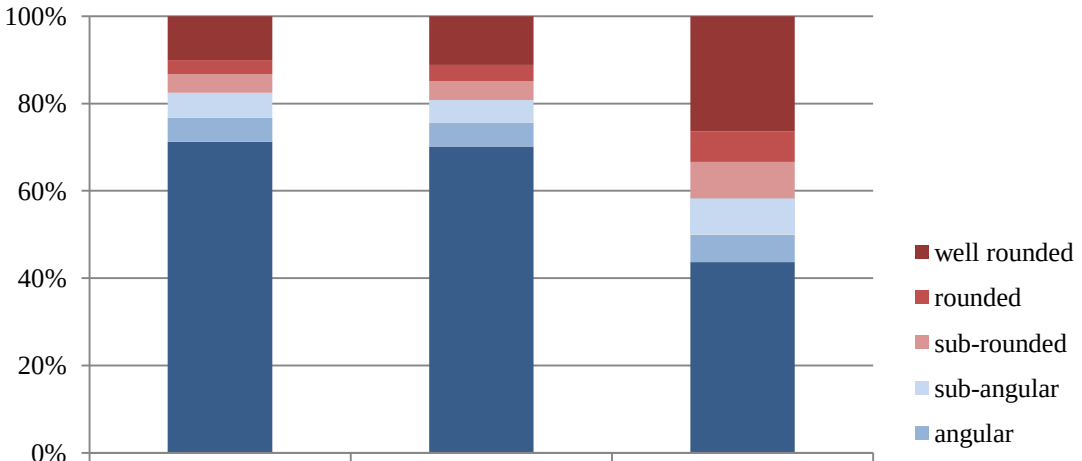

	75 - 106 µm	53 - 75 µm	0 - 53 µm
well rounded	10.1	11.2	26.4
rounded	3.2	3.7	7.0
sub-rounded	4.3	4.3	8.4
sub-angular	5.7	5.2	8.2
angular	5.5	5.4	6.3
very angular	71.3	70.2	43.7

Figure 4.11 Results of shape factor analysis of SD203 indicating the angularity of the dominant six minerals.

iii. Mineral Associations

For grains analysed for sample SD203, 27% presented pure grains of single mineral; the remaining grains were composite minerals. Quartz was found to be a single mineral grain 35% of all occurrences, with 33% of the remaining occurrences associated with halite. The final third of quartz was associated with mica (11%), feldspar (6%), pyroxene (5%) and thenardite (4%). Further, mica was found to be associated with quartz in 56% of all associations, with 16% of mica detected as single mica grains, with other significant associations including feldspar (9%) and calcite (4%). Fifty-seven percent of halite detections were associated with single mineral grain, with a further 35% associated with quartz. The remaining thenardite associations include sulphides (3%), calcite (2%) and mirabilite (1%).

4.3.1.4 Results of the PI-SWERL Exhaust (PSE) experiment (I4PSE)

i. Chemical Results

Results from QEMSCAN analysis reveal the presence of 15 minerals presented in Table 4.9. The table presents the results of the three size fractions as well as the weighted combined bulk chemistry. Quartz was found to dominate at all size fractions (36% combined), with the greatest percentage to be found in the finest size range at almost 40%, with 34.5% and 34.7% found in the largest size fraction and intermediate size fractions respectively. Halite was the next most commonly occurring mineral, in the larger two size fractions the contribution was found to be identical, at 27% decreasing to 19.5% with sediment fining (*Table 4.9*).

Table 4.9 Summary of mineralogical results for I4PSE.

Mineralogical results	Combined	75 - 106 µm	53 - 75 µm	0 - 53 µm
Quartz	35.7	34.5	34.7	39.7
Halite	25.5	27.1	27.1	19.5
Thenardite	9.4	10.3	9.1	9.1
Mica	7.3	7.0	7.1	7.8
Feldspar	6.4	6.4	6.4	6.3
Calcite	5.2	4.5	5.3	5.8
Pyroxene	4.6	4.0	4.7	5.2
Others	2.3	2.0	2.0	3.2
Amphibole (hornblende)	1.4	1.3	1.4	1.5
Sulphides	1.0	1.4	0.9	1.0
Fe oxides/hydroxides	0.6	1.0	0.6	0.4
Alteration products	0.3	0.2	0.3	0.3
Mirabilite Peak	0.1	0.1	0.1	0.1
Epidote	0.1	0.1	0.2	0.1
Anhydrite/gypsum	0.1	0.1	0.1	0.1
Barite	0.0	0.0	0.0	0.0
Brucite	0.0	0.0	0.0	0.0
Epsomite	0.0	0.0	0.0	0.0
Illite	0.0	0.0	0.0	0.0
Trona	0.0	0.0	0.0	0.0
Zn trap	0.0	0.0	0.0	0.0
% Mass size distribution		21	57	21

Thenardite was also found to be in equal percentages but in the finest two size fractions (9.1%) with slightly more than 10.3% found in the largest fraction, while feldspar was found in nearly equal percentages in all three size fractions. Calcite and pyroxene were found to present with greater dominance in the finest category. Mica, feldspar, calcite and pyroxene were all found to increase with decreased grain size. These seven minerals account for over 94% of the I4 exhaust sample with the remaining 6% attributable to amphibole, sulphides, hydroxides, alteration products, mirabilite, epidote

and gypsum. As the largest size fraction accounts for 68% of the sample, the dominant minerals in this size fraction are the best representation of the bulk mineralogy of the sample.

ii. Morphological Results

Results of analysis on I4PSE samples reveal that samples are generally round or square, with only 1% of grains tending to be long and thin (*Figure 4.12*). Aspect ratio revealed that grains were generally angular, with 75% of the largest size fraction classified as angular, with almost 60% of these being very angular while only 12% were classified as well rounded. With fining, grains became rounder, with only 61% of the finest size fraction considered very angular while 25% was now classified as well rounded.

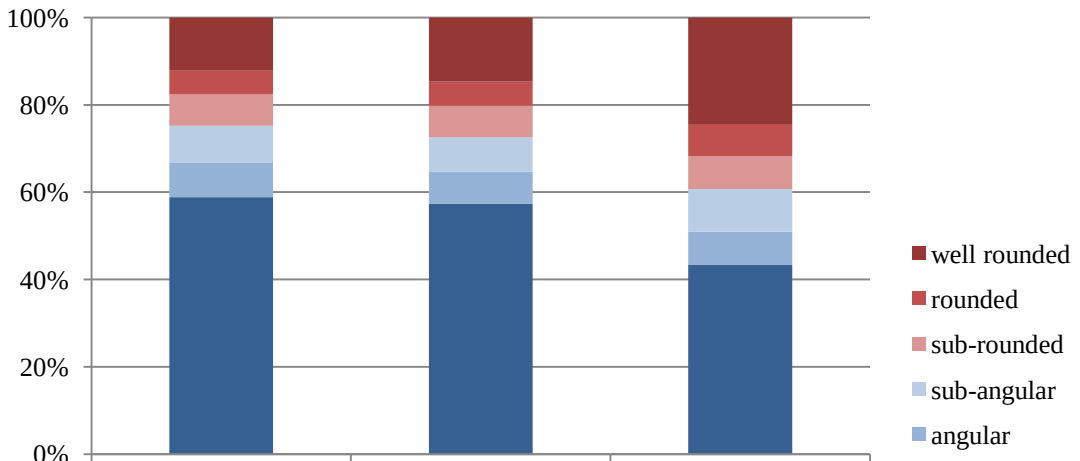

	75 - 106 µm	53 - 75 µm	0 - 53 µm
well rounded	12.2	14.7	24.6
rounded	5.4	5.5	7.1
sub-rounded	7.2	7.3	7.6
sub-angular	8.5	7.9	9.7
angular	7.9	7.4	7.6
very angular	58.9	57.3	43.3

Figure 4.12 Results of shape factor analysis of I4PSE indicating the angularity of the dominant six minerals.

iii. Mineral Associations

For grains analysed for the PSE sample, 28% presented pure grains of a single mineral, the remaining grains were composite minerals. Quartz was found to be a single mineral grain in just over one third of all quartz detections (34%), with simultaneous detection of a grain with halite occurring on 28% of all grains, with the remainder associated with mica (13%), feldspar (10%), pyroxene (6%) and calcite (4%). Single mineral halite were detected in 65% of all halite occurrences with simultaneous halite quartz detection contributing a further 27% of detections. Thenardite and calcite were found with 2% of all halite detections.

4.3.2 Summary of Results

4.3.2.1 Mineralogical Results

From the 20 mineral list, the same 15 minerals were found in all BSNE samples. While barite was only included in the finest size fraction of SD200, I4 fluff and all frisbee samples, quartz, thenardite, halite and mica were found to be the top four dominant minerals in all samples.

Minor differences exist between BSNE samples. SD201 had a higher quartz values (45.6% compared with 44% at SD200, 41% at SD202 and 42% at SD203) and a slightly lower weighted average halite value (see *Figure 4.13*). The remaining minerals were all present within a 1% to 2% range between all BSNE samples.

I4Frisbee presented similar results to those of the BSNE samples in terms of quartz, while containing considerably less halite and more thenardite. Again, mica concentrations were similar to BSNE samples although lower than those presented for the surface fluff and exhaust sample. The exhaust sample is relatively enriched in halite (25.5%) compared to all other samples (range 15 to 19%).

The I4 fluff sample contained almost 10% feldspar, higher than any other analysed sample by 4% to 6%, although it was relatively depleted in pyroxene compared to other samples and enriched in sulphides. The five airborne samples all contain more quartz than the fluff and exhaust samples by approximately 5%, with airborne sample values ranging from 41 to 45%, while I4F and I4PSE have values of 35.1 and 35.7% respectively. Thenardite values are consistent between samples, with mica found in greater abundance in the fluff sample.

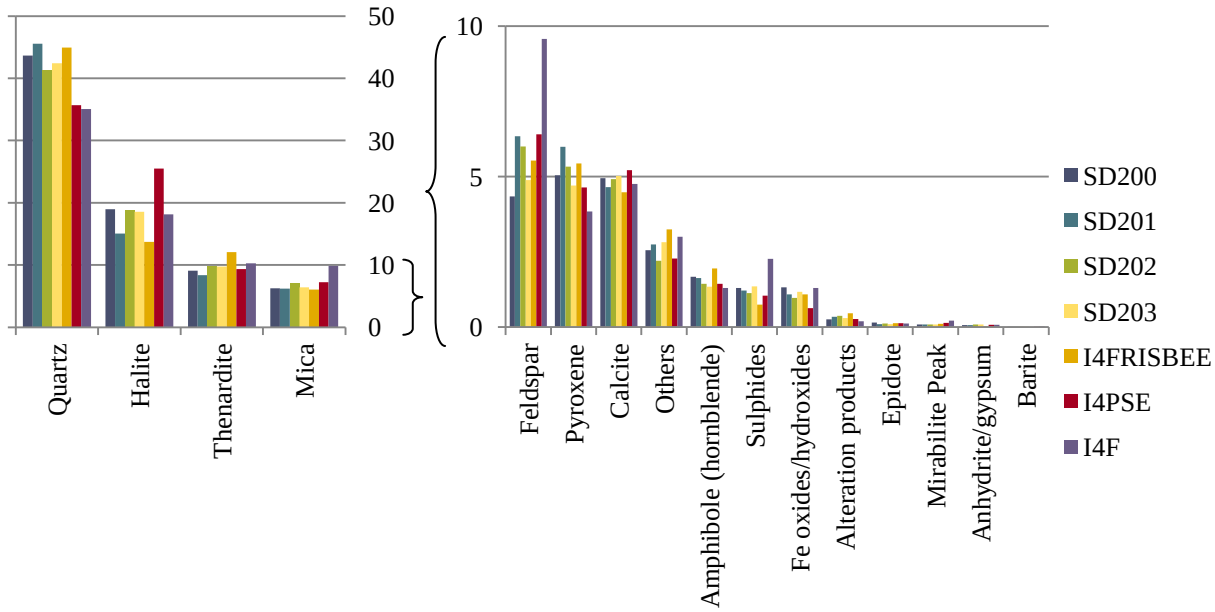

Figure 4.13 Mineralogical results of QEMSCAN analysis on the weighted combined samples, the inset figure presents the results of the minor minerals with a different axis to reveal trends in mineralogy.

Halite was found to be most abundant in the coarsest size fraction for all samples decreasing with decreasing grain size, a similar trend was observed for thenardite, although the decrease was less pronounced. While quartz, mica, pyroxene, calcite were found to be most abundant in the finest size fraction, feldspar was most abundant in the 53 µm – 75 µm range decreasing with a minimum in the coarse size fraction.

4.1.1.1. Summary of Morphology Results

All samples and all grain sizes presented largely round or square shaped grains values over 0.5, while smaller grains had a slightly increased percentage of being long and thin compared to their larger counterpart (*Figure 4.14*). Samples had, on average, 1% of grains exhibiting long or thin tendencies, with the exception of I4Frisbee which had 2% in the 53 µm – 75 µm up to 5% in the 0 µm – 53 µm range. The I4Frisbee sample was the only sample which had more long and thin grains with decreased grain size. As a result, I4Frisbee contained the least grains with rounder aspect ratio.

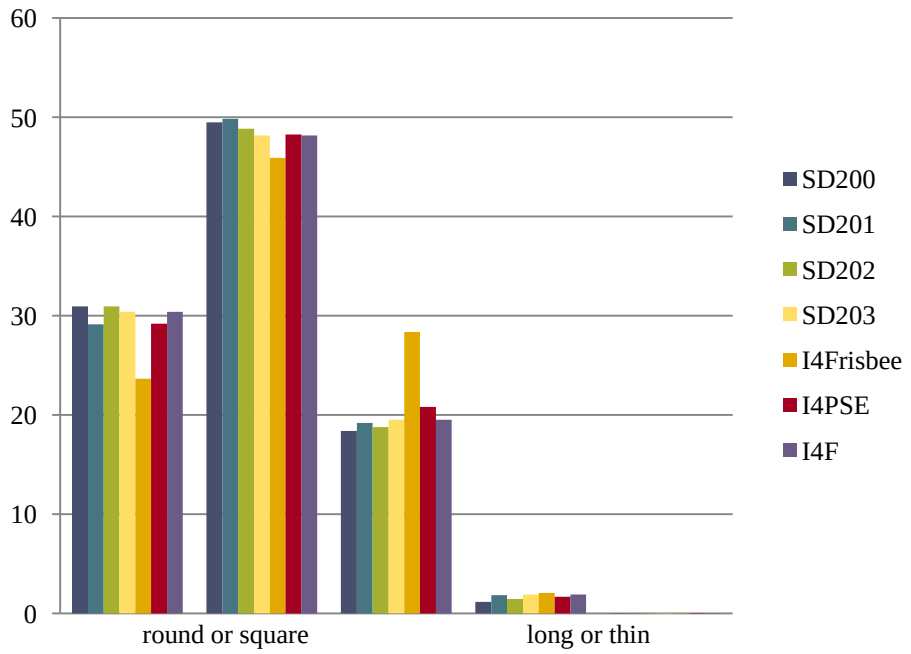

Figure 4.14 Standardised data presenting the results for the aspect ratio of six dominant minerals for all unsized samples (represented by weighted combined average).

When considering the shape factor of samples, the frisbee sample is the most angular with the top BSNE sample (SD203) having a similar percentage of the sample described by the well rounded category. I4PSE is the most well rounded sample with the lowest percentage of the sample being described by angular categories. There is a trend of increasing roundness or decreasing angularity with increased height up the BSNE tower. I4F is more angular than the trap samples while being less

angular than the frisbee sample, exhibiting the lowest percentage of well rounded grains for all samples (*Figure 4.15 and see Figure 4.2 for definition of shape).*

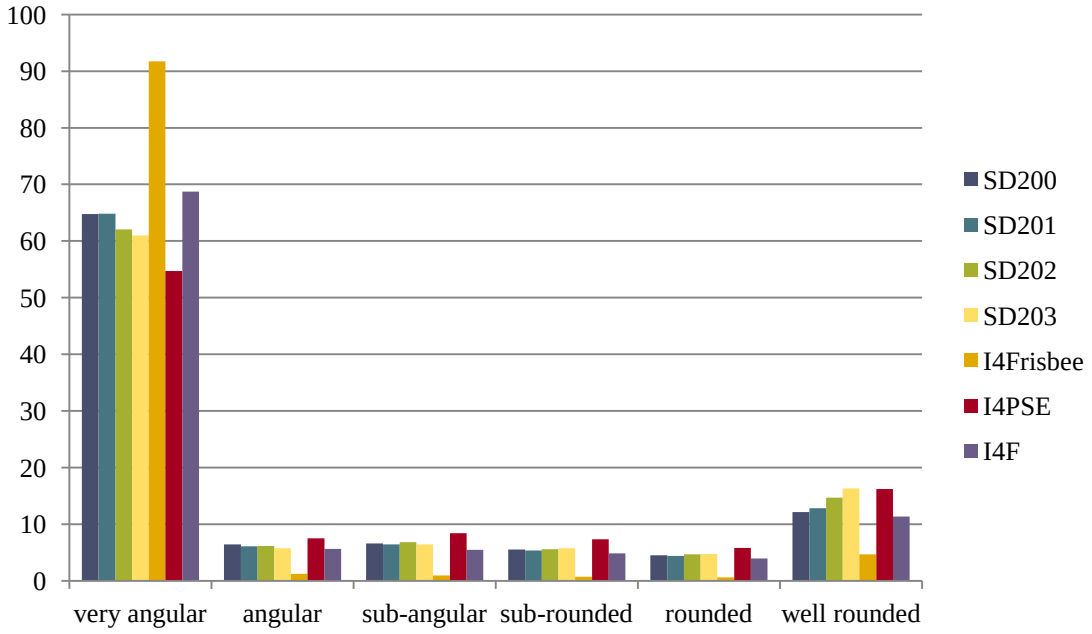

Figure 4.15 Standardised data presenting the results of shape factor analysis of six dominant minerals for all unsized samples (represented by weighted combined average).

Smaller grains presented increased roundness with all samples irrespective of height or sample type. The percentage of well rounded grains increases from almost 9% to 23.5% with this value increasing to just over 25% with the exclusion of the highly angular frisbee sample. With the increase in very round grains there was a decrease in the very angular grains, while the angular and sub-angular grains increased. This suggests a general shift towards roundness for all grains with decreased grain size.

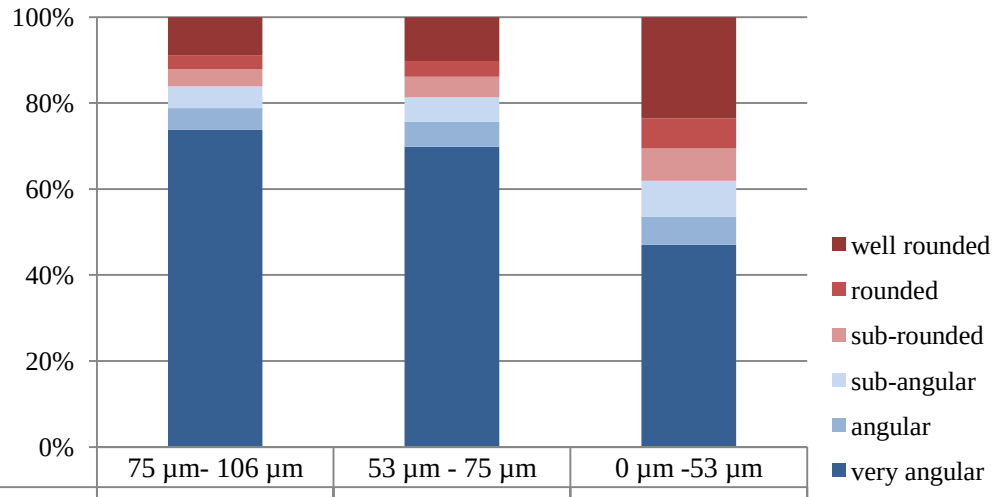

	75 µm- 106 µm	53 µm - 75 µm	0 µm -53 µm
well rounded	8.94	10.20	23.57
rounded	3.11	3.67	6.98
sub-rounded	4.08	4.74	7.52
sub-angular	5.04	5.77	8.33
angular	5.08	5.77	6.54
very angular	73.76	69.85	47.06

Figure 4.16 Average of standardised results of shape factor analysis of six dominant minerals for all sized samples.

4.3.2.2 Summary of Mineral Associations

Comparison of results reveal that the fluff and PSE samples exhibit similar values for associations and single mineral grains for halite and thenardite, which are higher than those detected for the airborne samples. The fluff and PSE samples presented that 61% and 65% of halite was found as individual grains compared to between 50% and 58% for the BSNE (SD200 to SD203) samples. Similarly, thenardite in the fluff sample was found as individual grains in 53% of all detections, increasing to 55% in the PSE sample, down to 45%, 47%, 50% and 49% in the SD200, SD201, SD202 and SD203 samples respectively.

The frisbee sample was composed of significantly more composite grains with only 41% of quartz detections, 26% of halite detections and 44% of thenardite detections occurring as single grains.

The association of quartz with halite was consistent throughout all samples, however due to the relatively lower number of single mineral grains in the frisbee sample, these values were markedly higher. Five to ten percent of all quartz detections were associated with halite for fluff, PSE and BSNE traps while this value was 23% for the frisbee. Similarly, 18% to 36% of detected halite was found to be associated with quartz while this number increased to 61% in the frisbee sample.

From visual observation during analysis, the bigger the grains, the more composite they became, while smaller grains had a tendency to be a single mineral. Additionally, the BSNE samples contained trace amounts of zinc which was determined to be from the galvanising of the BSNE traps. Further

analysis of mineral associations of zinc within the SD samples revealed association with halite, wollastonite and sulphides, with the addition of zinc/iron oxide association in SD202 and zinc/calcite in SD203.

The following section will present the results of grain size analysis for all samples.

4.3.3 Grain Size Analysis:

4.3.3.1 QEMSCAN Size Fraction Results:

Based on the percentage of sample within the three categories used for QEMSCAN analysis, the fluff sample was the coarsest, containing 68% of the sample in the 75 µm to 106 µm size fraction. SD203 was the finest with only 28% in this coarse size fraction (*Figure 4.17*). There was a general fining of samples with increased height up the BSNE trap with a decrease in the contribution of the coarsest size fraction. The lowest BSNE trap sample (SD200) contained the smallest percentage of sample in 0 µm to 53 µm fraction (13%), with the top trap sample (SS203) containing the most (37%). Relative to the fluff sample from which the PSE sample was generated, the sample contained less of the coarsest fraction, while a significantly higher percentage of the 53 µm to 75 µm size fraction, and a slightly higher percentage of the finest size fraction.

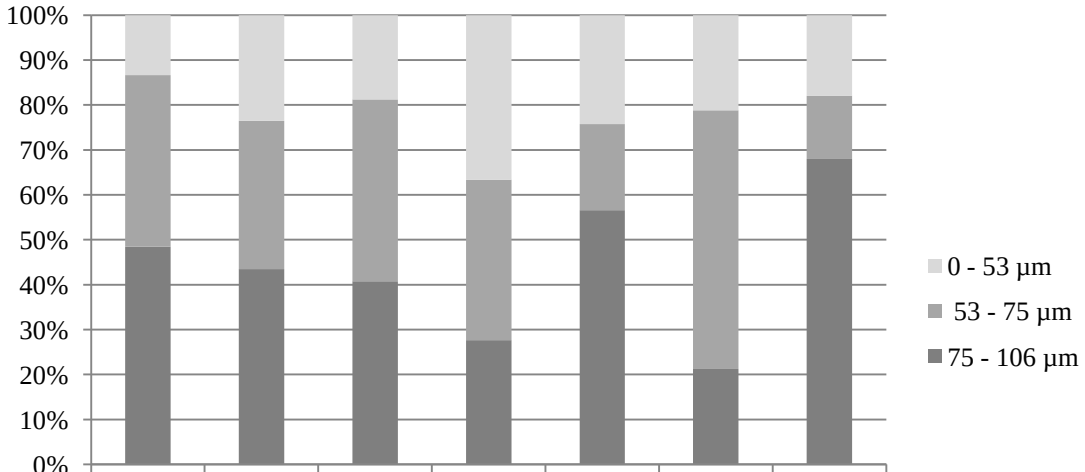

	SD200	SD201	SD202	SD203	I4Frisbee	I4PSE	I4F
0 - 53 µm	13	24	19	37	24	21	18
53 - 75 µm	38	33	41	36	19	57	14
75 - 106 µm	48	43	41	28	56	21	68

Figure 4.17 Size fractions as determined through dry sieving of samples in preparation for QEMSCAN analysis and determination of weighting for combined values.

SD201 had an increase in overall grain size along with an increase in angularity of the finer sediments. With the exception of SD200, all samples contained a higher relative percentage of fines

(0 µm to 53 µm) than the surface from which they are proposed to be entrained, with preferential entrainment of the 53 µm to 75 µm observed in all samples.

4.3.3.1.1 Malvern Grain Size Results:

The size distributions of the samples from I4 display markedly different patterns. The surface sample was categorised as symmetrical, poorly sorted, fine sand, while the frisbee sample was defined as fine skewed, poorly sorted, fine sand (*Table 4.10*). The PSE sample was also fine skewed, although moderately sorted and considered as very coarse silt. The top and bottom (SD200 and SD203 respectively) were poorly sorted with SD200 presenting as very coarsely skewed fine sand, while SD203 was coarsely skewed very fine sand. SD201 and SD202 were both moderately well sorted very fine sand with SD201 being described by a symmetrical distribution while SD202 was finely skewed.

The results of grain size analysis for I4F present a sample about a mean of 192 µm (fine sand). The fluff sample contained trace amounts of clay (>0%) with 11% silt of which 7% exists at the silt sand boundary, the remainder of the sample (89%) is attributable to sand sized grains. The poorly sorted fluff sample was symmetrical about a leptokurtic distribution. The I4Frisbee sample presented a mean at 156 µm (fine sand). The sample was dominantly composed of sand (78%) while 0.8% of the sample classified as clay, with the remaining 22% of the sample described as silt, of which 10% was presented at the sand silt boundary. Less than 0.5% of the sample was very coarse sand, resulting in a poorly sorted, finely skewed mesokurtic distribution. The PSE sample had a mean of 59 µm making it the finest sample with a mean in the very coarse silt range. The sample contained 49% silt, with a further 49% sand and the remaining nearly 2% as clay. This contribution of clay is the greatest for all of the I4 generated samples.

Table 4.10 Results of grain size analysis using the geometric statistical methods of Folk and Ward (1957) on all samples taken from I4.

Sample ID	I4F	I4Frisbee	SD200	SD201	SD202	SD203	I4PSE
Grain size classification	% Contribution to each grain size range						
clay	0.00	0.75	0.04	0.25	0.10	0.62	1.42
very fine silt	0.29	1.19	0.38	0.37	0.56	0.51	0.90
fine silt	0.54	1.94	0.53	0.47	0.67	0.73	1.16
medium silt	0.95	3.46	1.30	1.25	1.71	1.68	3.17
coarse silt	2.10	5.15	1.76	1.85	2.60	3.12	9.68
very coarse silt	7.43	10.06	14.27	20.21	18.46	20.08	34.32
very fine sand	20.72	17.72	38.96	51.43	46.07	42.41	40.32
fine sand	30.91	19.53	24.41	23.11	29.26	20.11	9.03
medium sand	21.58	23.52	3.34	1.06	0.58	0.60	0.00
coarse sand	9.11	16.18	5.62	0.00	0.00	0.44	0.00
very coarse sand	6.37	0.51	9.38	0.00	0.00	9.68	0.00
	Statistical Description						
Mean (µm)	191.76	156.809	132.18	87.92	91.62	92.89	58.67
Sorting	2.65	3.558	2.71	1.66	1.78	2.57	1.99
Skewness	0.04	-0.242	0.34	-0.07	-0.14	0.19	-0.23
description	Symmetrical	Fine Skewed	Very Coarse Skewed	Symmetrical	Fine Skewed	Coarse Skewed	Fine Skewed
Kurtosis	1.17	1.011	1.58	1.06	1.08	1.99	1.27
description	Leptokurtic	Mesokurtic	Very Leptokurtic	Mesokurtic	Mesokurtic	Very Leptokurtic	Leptokurtic

The BSNE samples contained increasing contributions of clay with increased height up the BSNE stack from 0.04% at SD200 to 0.62% at SD203, with 0.25% at SD201 and a slight decrease to 0.10% at SD201 (*Figure 4.18*). Despite this drop in clay content, SD201 presented the finest mean at 88 µm, with 132 µm in SD200, 92 µm in SD202 and 93 µm in SD203. All samples were dominated by sand sized grains varying from 81% of the sample in SD200 to 73% in SD203 with 76% in SD201 and SD202. The percentage contribution of silt sized grains increased from 18% (SD200), 24% (SD201 and SD202) to 26% (SD203).

Results of Figure 4.18, show that the sample size decreases with increased height up the BSNE device. The I4 fluff sample can be seen to be coarser than any of the BSNE trap samples, while the relative contribution of very fine sand and fine sand can be seen to increase from the surface sample to the BSNE samples, yet still decrease with increased height. The relative mass of silt is relatively consistent decreasing slightly with height. There is an inclusion of very coarse sand in the highest trap with very little present in the lower traps.

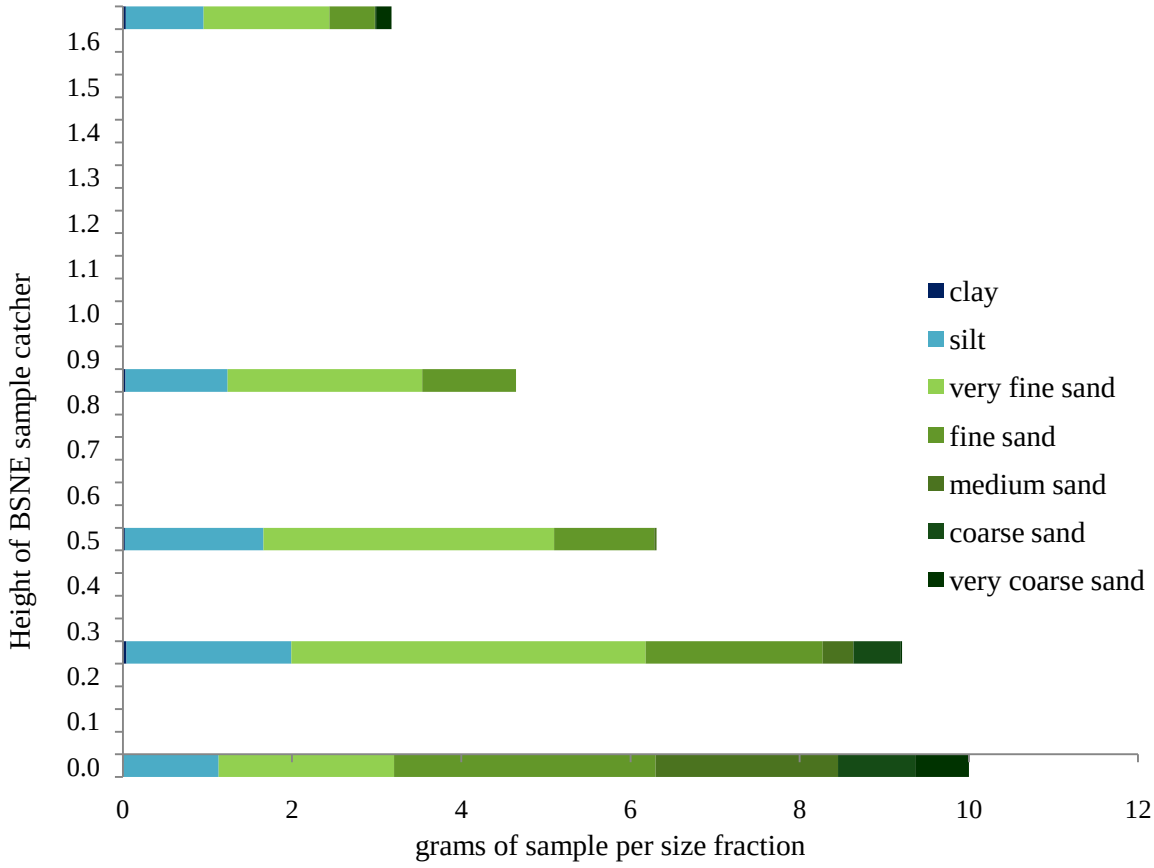

Figure 4.18 Presenting Malvern results for the mass of each sample represented by the 7 grain sizes. Samples are displayed as a function of the total mass of the sample and are presented at the height above the pan surface in the vertical. The horizontal axis marks the pan surface, with the lowest sample representing the surface fluff with, SD200, SD201, SD202 and SD203 sequentially higher up the BSNE device.

4.3.4 Synoptic Setting of the BSNE Sample

While 2011 was not a particularly dusty year, (see Chapter 5), on the 5th of October 2011 surface winds from the north-west led to the deflation of surface material from I4. The synoptic setting for this event, was associated with a ridging anticyclone, accounts for almost one third of all significant plumes in the region between 2006 and 2012. On this occasion, while this feature did produce dust, it was not visible on satellite imagery (*Figure 4.19*). Therefore, this event which was captured through ground observation was not observed on satellite imagery and is proposed to be highly localised in nature. As no plume could be mapped, an air transport climatology was mapped through the use of HYSPLIT trajectory modelling (see Chapter 5). Through this, it can be seen that the plume could be expected to travel in a south westerly direction from the pan, in line with the significant transport route for the region. As this event was detected at ground level but not on satellite imagery, it can be assumed that this localised event transported sediment at a low altitude locally.

Figure 4.19 MODIS Aqua image of the 5th of October 2011 a day on which dust was detected on the pan surface yet no visible plumes can be seen in the imagery.

4.4 Discussion

The above results have presented the mineralogical composition and morphology of five airborne samples and two ground based samples using the high resolution capabilities of QEMSCAN. Additionally, the particle size distributions of the samples have been presented using laser diffraction. Combined, this data reveals trends in entrainment as well as fining with increased height associated with vertical shear.

The following discussion will first compare the surface sample and the trap samples in an attempt to understand entrainment and morphological or mineralogical differences. This section will also consider the difference observed between samples collected through the frisbee and the BSNE traps in an attempt to quantify horizontal and vertical transport dynamics. The discussion will then consider

how it is possible to determine the likely chemistry of the dust from the region through the capabilities of QEMSCAN.

Grain size and chemistry characteristics of the flux sediments transported locally by winds, revealed that the eroded sediments are strongly influenced by the conditions of the parent material and therefore the local conditions. This is in line with findings by Leys and McTainsh (1996), who studied the links between sediment fluxes and surface conditions in south eastern Australia. Similarly, in this study on the Sua Pan, it was observed that while surface conditions can indicate the nature of the airborne sample, there were significant deviations in conditions. These were experienced most notably with sample trap height.

4.4.1 Morphology, Grain Shape

The first aspect that will be considered will be morphology, which was, for much of early grain shape research, determined to be solely indicative of sedimentary environments (Doornkamp, 1974). It was suggested that angular grains were associated with mechanical processes while rounded grains were associated with fluvial (and aeolian) processes (Pye, 1987). However, with the advance of microscopic analysis for grain morphology, a greater number of shape classifications became possible. It was also noted that through combined analysis of shape and texture, it was possible to distinguish between authigenic and allogenic sediments.

In light of this, it was observed that the frisbee sample was the most angular, however this was most likely in response to significant mineral reworking *in situ* in response to the duration of exposure. Additionally, in agreement with Pye (1987), the BSNE traps samples were all more rounded than the surface sample. Thus, the general proposition of aeolian processes is that increasing roundness can be seen to relate to the underlying controls on grain size. Further, QEMSCAN revealed that highly angular authigenic evaporites occupied all size fractions, with the greatest contribution in the largest size fraction, with angularity increasing with increased grain size. An earlier study by Thomas (1987) in the Kalahari found that, regardless of landform associations, there was a propensity for increased grain roundness with increasing grain size. However, this was not observed here, which could be as a result of the Thomas (1987) study being focused on old weathered Kalahari sands, where the effects of evaporites is assumed to be negligible. Therefore while this trend was not observed to hold for Sua sediments, the older weathered Kalahari sediments, which have likely been exposed to prolonged weathering, both allogenic and *in situ* (McFarlane et al., 2007), could provide background roundness to some of the sample. Consequently, despite the inclusion of base Kalahari sediments into the sedimentary environment, the observed trends revealed that grains were found to be increasingly round with decreasing grain size regardless of mineralogy. Even though there was increased roundness, the resultant classification remained that approximately 60% of grains 0 – 53 µm and ~80% of the 53 – 75 µm and 75 – 106 µm were classified as angular. However, there was the

additional trend that samples were increasing well rounded on average with increasing height up the BSNE sampler, this conforms with findings by earlier researchers (e.g. Doornkamp, 1974; Shao et al., 1993; Leys & McTainsh, 1996).

The exception to this trend was found in SD201 which was notably more angular. Mineralogical differences could explain this, as SD201 contained almost 3% less halite, along with the lowest thenardite concentration amongst trap samples, while containing the most quartz. Distribution of the quartz between the grain sizes shows that it was largely in the 75 – 106 µm range. As quartz was observed to become increasingly angular in the largest size fraction, this can therefore be assumed to be a significant contributor to the detected angularity of the sample.

While very few studies present morphological results of samples, Reid et al. (2003) present SEM derived morphology results for African derived airborne samples collected during the Puerto Rico Dust Experiment. The SEM microscopy derived results revealed a mean aspect ratio of 2.12 with a large standard deviation (1.5). This high standard deviation is contextualised by Ried et al. (2003) to be as a result of the skewness of the distribution with only 8% of samples presenting aspect ratio values above 3. Despite this, such values for aspect ratios indicate highly rounded grains. For samples from the Sua Pan, an aspect ratio of between 0.6 and 0.8 was found; this mean value presents grains which are significantly longer and thinner than north African dust samples. Additionally, the mean value of 2 as presented by Reid et al. (2003) is in line with findings presented in Mishchenko et al. (1997) as typical of African dust determined through spheroid light scattering computations. Despite the indication that sediments in this study are notably less round than those detected in both the Reid et al. (2003) and Mishchenko et al. (1997) studies, sampling location, transport distance and evaporite mineralogy can account for much of this discrepancy. Additionally, the samples collected in both north African studies had been subject to significant transport, were captured in transport and were considerably finer than Makgadikgadi aerosols.

While aspects of grain roundness and morphology confirm the suggestion of various authors with regards to the relationship between increasing roundness with transport, the angularity provided an additional complexity. Angularity was found to correlate to the number of mineral associations, with high angularity associated with complex minerals and lower angularity with single mineral grains. Consequently, the high concentration of evaporites and their associated cementing effect could decrease roundness and increase angularity.

While the results of angularity suggest that the samples are not well rounded, analysis of the aspect ratio of the samples suggested that these highly angular grains remain more round or square than long and thin. This finding justifies the use of laser diffraction for grain size determination as laser diffraction determination of grain size is limited by the assumption that grains are spherical (Chapter

2). Therefore, the sphericity of the samples as detected through QEMSCAN analysis serves to validate the results presented for grain size as representative of the sample.

4.4.2 Grain Size

In line with findings by Speirs et al. (2008) there was an overall decrease in mean grain size with height above the pan surface. Leys and McTainsh (1996) present a similar relationship, additionally suggesting that the size of the eroded sediment closest to the ground surface strongly reflects the conditions of the parent material. In confirmation of this, the surface sample was found to be the coarsest (191 µm) with the lowest sample SD200 (132 µm) presenting a similarly large mean, further up the sampler, SD201 presented a finer mean (88 µm) however the subsequent traps did not produce linearly finer samples. Following SD201 there was an increase towards the highest two samples SD202 (92 µm) SD203 (93 µm).

The inversions in the grain size distribution with height could be in response to low level transport or through saltation, such as transport of coarser grains into SD200. The inclusion of coarser grains in the upper sediment catchers could be in response to mineralogical reworking of the sample post capture or represent a poorly mixed boundary layer. Nickling (1983) suggests that the grain size distributions of the sediments transported in suspension and surface creep are characterised by strong positive skewness. This is as a result of selective removal of surface particles small enough to be transported by the wind at a given velocity. Conversely, the grain-size distribution of samples associated with saltation are negatively skewed.

Due to the likely localised nature of this transport event and therefore early stage boundary layer mixing and turbidity, this cannot be considered as prescriptive of the transport mechanics. However, it was observed that SD200 was coarsely skewed or positively skewed which would indicate that this sample was not collected through saltation. The lack of sensit hits (Wiggs *pers. comm.*) confirms this assumption, while SD201 and SD202 were observed to be symmetrical to finely skewed (negatively skewed). At these heights, the effects of saltation are thought to be less significant (Cahill et al., 1996) and therefore additional mechanisms are required to determine the origin of sediments. These include turbulence, vertical shear and wind strength (Nickling, 1983; Zender et al., 2003; Cattle et al., 2009), which will change the boundary layer conditions. These variables are all considered to result in both semi-logarithmic and parabolic variability (Goossens, 1985) of grain size with height. As a result of the highly localised nature of this event, the sediment transport detected here is best represented by a highly mixed, poorly sorted un-stratified transport environment.

While there was observed to be sediment fining with the contribution of clay and silt sized grains increasing with height up the sample trap, from 0.4% to 1.1% clay, with silt increasing from 21% to 29% (*Figure 4.20*). The major variations existed between the sand sized grains. Coarse and very

coarse sand was only found in the top (SD203) and bottom (SD200) traps, while the coarsest size found in SD202 was fine sand. As no saltation was detected, a localised event associated with a poorly stratified boundary layer can explain the trend observed in SD200.

However, the addition of zinc to the mineralogy of the BSNE samples could be an alternative mechanism which explains the trend observed in SD203. The detected presence of zinc, which was determined to be a contaminant from the galvanising process of the traps, could be an indicator for mineral reworking within the trap. This could explain the deviation from the proposed fining trend. Analysis of mineral associations further confirms this proposal, revealing high mineral associations between zinc and halite, confirming that crystallisation occurred post capture and thereby produced larger grain sizes through the agglomerating effect of salts. Morphologically, this expresses itself in the inclusion of some needle like (or long and thin grains) within the upper sample catchers indicative of slow and undisturbed crystal growth.

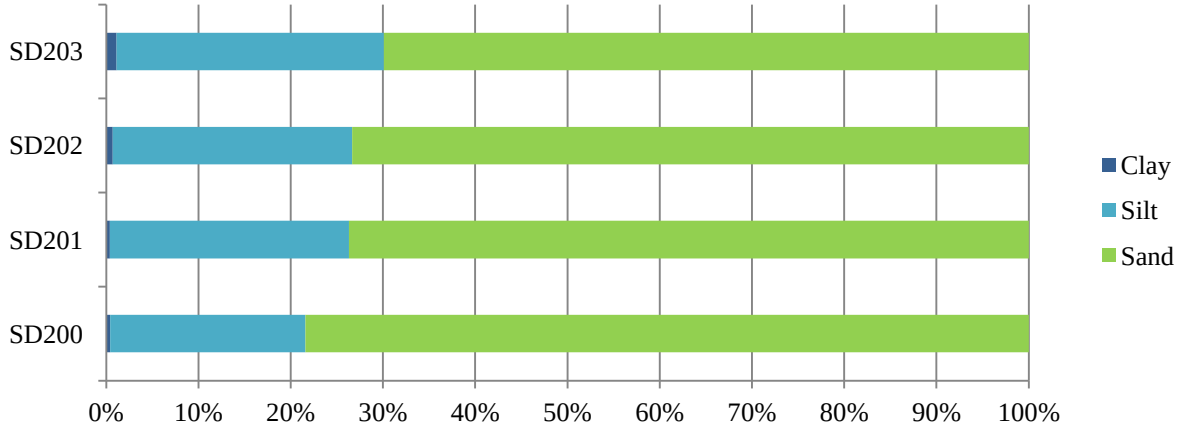

Figure 4.20 Clay, silt, and sand contributions for airborne samples indicating fining with increased height.

As recrystallisation would result in changes to the grain size distribution and associated morphological results, these results can be assumed to contain significant variation from the actual conditions of the original sample. Despite this, underlying fining trends remain evident. Leys and McTainsh (1996) suggest that, like sample fining with increased height, samples are likely to express increased sorting with increased height. Analysis of Malvern results using the Folk and Ward method (Folk, 1966; Blott & Pye, 2001) revealed that the lowest sample was poorly sorted (σ_G 2.7) with the middle two samples presenting as moderately sorted to moderately well sorted (σ_G 1.6 and 1.7), while the top sample deviates and again presents as poorly sorted (σ_G 2.5). Similarly, the surface fluff sample was poorly sorted (σ_G 2.7) although it was dominated by fine sand; all trap samples were classified as very fine sand. This confirms that there was at least some sorting and stratification

occurring in the boundary layer. Therefore, the inversion in both grain size and sorting, which is likely attributable to re-crystallisation, may not represent the true nature of the entrained plume.

Morphologically, it can be seen that there are differences between the surface sample and the BSNE trap samples, although it remains evident that the surface composition played a significant role in the characteristics of the aeolian sample. Additionally, while authors have attempted to link morphology and shape with environments and transport, given the complex nature of the pan setting and lack of mineral stability, most particularly the evaporites, these proposals are too simple to represent the observed trends.

As morphology alone cannot reveal trends, the following section will consider the representative nature of the mineralogy of the samples.

4.4.3 Mineralogical Differences:

As the same 15 minerals were found to dominate all samples, with only minor deviations found to exist, it can be confirmed that the fluff sampled and transported locally is the likely origin of the trap sediments. Additionally, many of the variations observed are within the natural variations for minerals within the upper continental crust (Lawrence & Neff, 2009) and therefore much of the low level variability is not significant. For example, calcite values determined here are in line with those proposed by Claquin et al. (1999). However, there was variability identified above the tolerances stated for the upper continental crust (Lawrence & Neff, 2009) observed for the more dominant minerals namely: quartz, halite, mica and feldspar and, to a lesser extent, thenardite and pyroxene. These minerals can be used to determine if there is selective entrainment and consequently predict the likely differences between the surface chemistry and the possible aerosol load.

While halite was found to vary only slightly between surface and trap samples, the trap samples were relatively depleted in thenardite and mica, and significantly depleted in feldspar (*Figure 4.21*). Conversely, the airborne trap samples contained notably higher quartz and pyroxene concentrations. The relatively quartz enriched BSNE samples, contained values almost 10% higher than the surface. Overall the concentration of quartz remained relatively consistent with the changing height above the pan surface, which is similar to the observation of Speirs et al. (2008). For the surface, concentrations ranged from 34% in the largest size fraction to 39% in the finest size fraction, while BSNE trap samples contained 36% to 49%. The greater abundance of quartz in the finest size fraction is in direct contrast to the findings of Hardy and Cornu (2006) who suggest that quartz content increases with increasing particle size. The finest size fraction revealed that while on the surface quartz accounted for 39% of the sample, in the trap 25 cm above the ground surface this number increased to 49%, before stabilising at 47% in the higher three traps. This discrepancy between quartz concentrations in surface and trap samples extended to all size fractions.

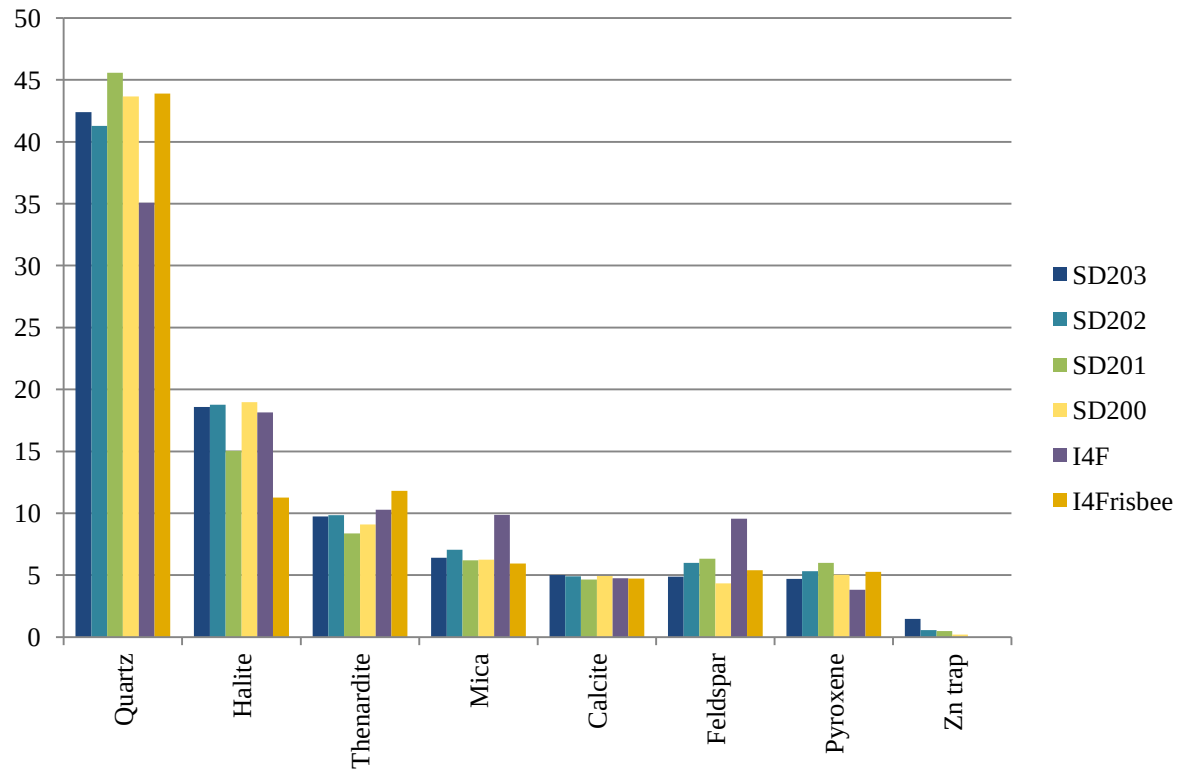

Figure 4.21 Minerals displaying significant variability between surface and airborne samples using the combined weighted average derived from QEMSCAN analysis.

This dominance of entrained quartz supports the findings of Speirs et al. (2008), however, unlike Victoria Valley Antarctica, feldspar was not found to be preferentially entrained. Hardy and Cornu (2006) proposed that due to the nature of feldspar weathering, it often dominates the finer size fractions. Sized mineralogical analysis revealed that feldspar was found to be more prevalent in the finer two size fractions and therefore supports the proposal of Hardy and Cornu (2006). This would suggest that feldspar would be readily entrained due to its fine nature, as Lawrence and Neff (2009) and Bullard et al. (2011) indicate that wind erosion preferentially removes fine textured particles. However, surface samples contained more than double the percentage of feldspar than was contained in the trap samples. Similarly, mica, which was found to be more dominant in the finer size fractions, was found to be slightly more abundant in the surface samples than in the BSNE and frisbee samples. This could be in response to the increased speeds required for finer grains, as determined by Bagnold (1941). Despite the apparent decrease relative to the surface, feldspar concentration was found to increase with height, which is likely a function of boundary layer mixing.

Through the advanced capabilities of QEMSCAN, it is possible to correlate these findings with mineral associations and thus determine if composite or single mineral grains are more readily entrained. These results reveal that on the pan surface single mineral quartz grains occur 31% of the

time, while showing a relative increase in the traps (34% to 37%). Therefore, the single mineral grains, which are unlikely to be cemented with evaporites or carbonates, are likely to be entrained. Despite both the frisbee and the uppermost BSNE trap being at the same height (1.68 m), the sampling devices captured very different samples. While the BSNE trap was capturing horizontal transport the frisbee trap was dominantly capturing vertical fall out. Despite this, for both the BSNE and frisbee samples single mineral quartz grains accounted for almost 40% of all captured quartz, while the remainder of the quartz was associated with halite, mica and feldspar. While quartz-halite and quartz-mica values are consistent between surface, BSNE and frisbee samples, the preference for single mineral quartz in the trap samples exceeds the surface values. Therefore, samples containing a greater percentage of single mineral quartz are likely to be airborne samples. As a result, quartz grains with mineral associations were more abundant on the surface than in the entrained samples. This trend could vary by season in line with suggestions by Bullard et al. (2011) who indicate that early season surfaces differ significantly from end of season surfaces in supply limited systems.

Analysis of quartz mineral association could reveal the sample origin, feldspar values for single mineral grains remained consistent between surface and trap samples (17% to 19%) although were noticeably higher in the frisbee sample (27%). Thenardite was found to be a single mineral 53% of the time on the surface, decreasing to 48% in the traps, with the co-incident detection of a thenardite-quartz grain greater in the traps than on the surface. The preferential entrainment of single mineral could be in response to both the lack of cementing (Nickling & Ecclestone, 1981) and the difference in mineral density (Claquin et al., 1999). While the densities of all these minerals vary slightly, with pyroxene the densest (ρ ~3.2); mica, thenardite, feldspar and quartz all have similar densities (ρ 2.6 - ρ 2.7); and halite least dense at ρ 2.16. Therefore, mineral density alone could not be a determinant of the difference between surface and trap chemistry, as the densest mineral (pyroxene) was found to be more abundant in the traps than on the surface.

A further proposal for the observed distribution was noted by Speirs et al. (2008) who observed that grains >125 µm display little change in mineralogy with height, while smaller grains experienced greater variability, indicating that these fine grains are less well mixed with height. Goossen (2007) additionally presents that sampling efficiency is influenced strongly by particle size, proposing that smaller particles may leave the collector more easily in the absence of an appropriate trap device, which is less likely to affect the larger grains as a function of grain inertia. The authors suggest that the process by which particles are transported in suspension is crucial in understanding the traps efficacy as fine particles will follow the air flow and may be disproportionately affected by trap induced turbulence. This could also be a determinant in the relatively better match between surface conditions and the trap samples in the 75 µm to 106 µm range when compared with the two finer sizes. These proposals advocate for the inclusion of boundary layer turbulence, vertical shear and stability when interpreting the chemistry, morphology and mineralogy of samples. These variables

will also aid in understanding the precise transport mechanics of grains, however, it remains possible to consider the likely transport range of grains derived through this study using simple assumptions of a mixed boundary layer and sufficient wind speed to result in local to regional transport.

4.4.4 Likely Aerosol Composition

Through chemical analysis of both surface and airborne samples, as well as a sample collected through dry deposition, it becomes possible to determine the possible aerosol load from this site. Lawrence and Neff (2009) propose that the relationship between clay, silt and sand can be an indicator of how far the aerosol has travelled. The authors suggest that for sediments transported between 0 and 10 km from the source region, clay, silt, and sand ratios will be approximately 20%, 50%, 30% (*Table 4.11*). As clay, silt and sand ratios for the samples collected in the BSNE traps are ~1%, 20%, 80% to ~1%, 30%, 70% this presents that there is a considerably greater contribution of sand and therefore this sample is likely to be highly locally derived and not representative of significant transport. This serves further to confirm the source of sediment as fluff from I4. Additionally, the relatively angular nature of the sediments suggests the grains have not been exposed to significant aeolian transport. However, this angular nature of Makgadikgadi sediments was found to be largely unaffected by transport as Resane et al. (2004) note the characteristic angularity of the mineral grains from the Makgadikgadi Pans after significant aeolian transport.

Table 4.11 General physical characteristics of three distinct classes of aeolian deposition: local, regional, and global. Regional is further divided by source region strength although similar particle size distribution classifications were considered for both (Lawrence and Neff, 2009). Results for the four airborne samples from the BSNE traps have been included.

Deposition Class	Distance from source km	Deposition rate gm-2yr-1 (mean)	Particle size %clay	%silt	%sand
Local	0-10	50 -500 (200)	20	50	30
Regional	100 -1000	1-50 (20)	25	60	15
Primary		25-50			
Secondary		1-25			
Global	>1000	0-1 (0.4)	30	70	0
Makgadikgadi Sediments					
SD200			1	20	80
SD201-SD203			1	30	70

While grain shape is proposed to be less affected with transport, increased distance from source region is proposed to result in significant fining. Assuming minimal changes in mineralogy occur during local transport, the most likely sediment to be transported can be associated with the mineralogy of the finer two size fractions as determined through QEMSCAN analysis. This will provide sediment finer than 75 µm which includes clays, silts and very fine sands with the potential to travel hundreds of kilometres from the source region.

Assuming that the pan surrounding I4 is suitably emissive or at least mineralogically representative of an emissive pan surface, the mineralogy of the BSNE trap samples 0 – 53 µm size ranges are the likely supply of long distance regional aerosols in a minimal deposition environment. The addition of the 53 – 75 µm range likely gives an indication of the local and regional transport as defined by Lawrence and Neff (2009). Given these values, it is possible to determine the mineralogy of sub-local deposition as a function of the 75 – 106 µm. Thus it is proposed that there will be similarity in chemical composition between the frisbee sample and the 75 – 106 µm range with the addition of regionally deposited aerosols.

It can be proposed that a significant amount of coarse, single grained quartz is likely to be deposited locally due to its relative abundance in the coarse size fraction. This is confirmed through the high percentages of quartz observed in the frisbee sample (~44%). However, this does not correspond to regionally and locally depleted quartz values in airborne samples as, by volume, quartz contributes approximately 40% of the overall sample and a considerable proportion is likely to be transported. This high percentage of quartz is in agreement with the values proposed by Lawrence and Neff (2009) who present local and regional aerosols (*Table 4.12*). The authors suggest that when quartz contributed below 30% of the sample, clay minerals dominate and the aerosol sample is likely further than 1000 km from its source region.

Table 4.12 The range of mineral abundances observed for dust of different deposition types (as defined in Lawrence and Neff, 2009). Pyhllosilicates include most clays but are typically dominated by illite and kaolinite.

Deposition Type	Quartz	Feldspar	Carbonates	Phyllosilicates	Other
Local	50 - 60+%	5 - 30 %	0 - 25%	5 - 30%	0 - 12%
Regional	30 - 50 %	5 - 35%	0 - 25%	5 - 40%	0 - 12%
Global	15 - 30%	20 - 40%	0 - 25%	20 - 60%	0 - 12%

While globally feldspar was determined to be a significant aerosol by volume, the results presented here suggest that even assuming the significance of the finest size fraction, feldspar only contributed 5% and is therefore unlikely to be important from this source. Silicates like feldspar and quartz while important by aerosol load volume, have very little impact on terrestrial ecosystems largely due to the abundance of crustal silica globally (Turekian & Wedepohl, 1961; Reynolds et al., 2001; Lawrence & Neff, 2009).

Unlike silicates which are nutrient deficient and largely ecologically un-reactive (Krueger et al., 2004; Soderberg & Compton, 2006), calcite which was indicated by Kruger et al. (2004) to be the most reactive of carbonates, can influence the bioavailability of Na, P, K and Mg. Within the sample, concentrations of calcite were found to be low and largely stable, which further confirms the empirical relationship proposed to exist between grain size and total calcite concentration (Claquin et

al., 1999). The relationship proposes that for increased clay or silt sized components within the sample the relative abundance of $CaCO_3$ will increase. This relatively small but significant contribution of calcite in the aerosol load from Sua, is confirmed by Resane et al. (2004) who verify the presence of calcite in samples even with considerable transport distance and necessitate its consideration on downwind systems. Reynolds et al. (2001) comment that, in high pH soils, the addition of carbonates can decrease the bioavailability of phosphorus, which is a known limiting factor in dry ecosystems, while increasing the bioavailability in low pH environments. Due to the slightly acidic nature of Kalahari sediments (Wang et al., 2007) calcite is likely to be ecologically beneficial (Reynolds et al., 2001; McTainsh & Strong, 2007). As Sua sediments contain between 4% and 6% calcite in the finest size fraction, such low values may have some influence on K and Mg ratios important for ecosystem development. However, the relatively low concentrations together with the alkaline nature of salt will likely reduce the efficacy of calcite, and as such the addition to downwind ecosystems is unlikely to result in the widespread ecological impacts proposed for significant transport of carbonate minerals.

While silicates and carbonates are frequently found in terrestrial ecosystems, halite is more commonly associated with marine conditions (Bullard, 2010) although increasingly understood as an important continental mineral in light of the significance of aerosols produced on global salt pans. Samples from the I4 surface and trap samples were all observed to contain significant concentrations of halite, with values observed to vary with height and between samples. Additionally, the top BSNE trap contained more coarse halite than fine halite; this is however likely the result of re-crystallisation with the other three traps containing a considerably higher percentage (~10% more) of fine grained halite then coarse. Despite this, the frisbee sample contained 20% coarse grained halite, which suggests that halite is transported and deposited within the system locally. This process of in-system recycling is considered to be important for mineral transport within systems (Gillette et al., 2004).

Much of the frisbee trap halite was considerably longer and thinner as well as more angular than any other sample, which indicated active crystallisation within the frisbee post sample capture. Therefore, while some halite is locally precipitated, the presence of halite in the BSNE traps along with the associations of halite in the finer size fractions suggests that there is a considerable amount of halite that has the potential to travel significant distances from source. This is confirmed in a study by Resane et al. (2004) who present the results of a wet deposition event in which halite rich Makgadikgadi sediments were found in Johannesburg over 700 km away.

Thenardite was another significant soluble salt in the fine size fraction, the ecological effects of which are poorly discussed in literature. Additionally, thenardite was found in the greatest concentration in the frisbee sample existing in similar concentrations in all size fractions. This therefore suggests that, like halite transport, there is a degree of local transport of thenardite. While Resane et al. (2004) did

not detect thenardite, results present the detection of the elemental components of thenardite with specific mention of a weak sulphur signature which is likely attributable to the sulphate ion in thenardite.

As significant concentrations of both halite and thenardite are observed to be transported within the system and as a function of their grain size proposed to be transported regionally, their impact is proposed to be noteworthy. McTainsh et al. (1999) note that quantitative process evidence of soluble salt entrainment is only available from a limited number of locations and consequently the ecological impacts are not well understood. The majority of saline aerosol studies are focussed on marine salt aerosols (e.g. Gong et al., 1997) despite the identified importance of highly erodible saline clay pans (Prospero et al., 2002; Mahowald et al., 2003; McTainsh & Strong, 2007). In a continental based study, McTainsh et al. (1999) present the soluble salt concentration of Australian dust with values ranging from 2.7% to 9.3%, while Sua sediments present values in excess of these values with between 9.0% and 10.4% in the 0-53 µm size fraction and 15.2% to 19.6% in the 53-75 µm size fraction. Therefore, as McTainsh and Strong (2007) indicate that Australian salt rich aerosols have widespread ecosystem impacts, they are proposed to be significantly higher for Sua sediments. Further, Dare-Edwards and McTainsh (1989 in McTainsh & Strong, 2007) add that in recent geological time, the saline dust may have contributed to increased leaching and soil horizon differentiation. Therefore, the potential ecological impact of these highly saline sediments is great, with Goudie and Middleton (2006) adding that the deposition of salt rich aerosols may contribute to ground water salinity. This necessitates the study and inclusion of salty continental aerosols in circulation and ecological modelling of southern Africa.

Despite the high transport potential of fine grained sediments which include silicates and evaporite salts, the concentration of all these is all assumed to be greatest within the pan boundaries and on the pan margin, in line with findings by Reheis (1997) at Owens Lake. This localised mineral cycling is particularly noticeable when considering the similarities between the frisbee and the surface fluff sample, however there were significant morphological differences. The relative enrichment in the contribution of quartz in the frisbee sample is unlikely to be sourced from outside the pan margin due to their relatively large grain size and associated wind speed velocities required to transport such large grains. Therefore, it is more likely these grains are associated with preferential deposition post localised entrainment. This serves to support both the representative nature of the surface sample in the aerosol load, together with the assumption that that much of the dry deposition is from regionally and locally derived aerosols. Regionally, the pan system can be considered to be closed with respect to nutrient input with groundwater evaporation the most likely source of the observed mineralogy.

While local systems and boundary layer conditions will help to predict the local distribution of aerosols and the recycling of minerals within the pan boundary, large scale circulation will be

responsible for the regional to global scale transport of aerosols. The following chapter (Chapter 5) will consider synoptic controls on emissions and the large scale impact and likely depositional footprint of the system.

4.5 Summary and Concluding Remarks

The primary goal of this study was to evaluate the chemical variations and trends in physical and chemical properties with transport from a localised source area in the Makgadikgadi Pans through the use of QEMSCAN. Analysis of surface sediments and airborne samples from within the Sua Pan using QEMSCAN has identified trends in both grain size, mineralogy and most importantly, the preferential entrainment.

While this study has attempted to quantify the possible aeolian load from the Sua Pan, the nature of dust storms and the understanding that individual dust events are highly variable, result in the necessity to consider these results as transient and season specific. Additionally, mineral dust plumes are a complex mixture of grains, which evolve spatially and temporally as a function of wind speed and through the atmospheric column. Studies such as this provide valuable insight into entrainment and transport processes occurring at both the pan surface and within the boundary layer. Further, the results presented here are indicative of a local transport event due to the lack of identifiable plume on MODIS imagery and the relatively coarse nature of sediments as outlined. This could significantly influence the both the nature of the sediment that was transported and the representative nature of these samples when viewed in the context of a larger, greater magnitude event. Therefore, while these results cannot be directly transferred into a large emission event it does support the proposal that the surface fluff is the likely sediment source for the aeolian load from this region. The relatively low magnitude of this event however can result in increased sampling efficiency as Sow et al. (2006) suggest that passive samplers have decreased efficiency with increased wind speed. Therefore, it can be proposed that the trapped sediment is a valid representation of transport material.

The key findings of this chapter can be summarised as follows:

i. QEMSCAN is an effective and efficient means for multi-parameter analysis of aeolian samples. Further, this method allowed for quick determination of multiple grain attributes requiring only a small sample mass.
ii. The ability of QEMSCAN to determine grain morphology revealed that, despite the angularity of the samples, they remained largely rounded in shape which justifies the use of Malvern for the determination of grain size and adds validity to the results produced.
iii. QEMSCAN revealed that the sampled dust is a function of the surface from which it was entrained, due to the similarity in bulk chemistry. Confirming the link between surface chemistry and dust chemistry.

iv. However, the dominance of coarse grained sediments is not consistent with results presented for well travelled dust (Zender et al., 2003; Lawrence & Neff, 2009), which is dominated by comparatively finer textured material. Therefore, it can be interpreted that the samples captured in the BSNE and frisbee are locally derived.

v. Statistical analysis of sorting confirmed the locally derived nature of sediments, with the distribution of skewness indicating that saltation was unlikely to be a mechanism for entrainment.

vi. A wide range of grain size were captured including a high proportion of coarse sediments, in this setting, this is likely a function of pan surface crusting and aggregation.

vii. Consideration of mineral association revealed that, for quartz grains, mineral association was indicative of entrainment through the cementing effect associated with evaporites and the resultant increase in grain size experienced.

viii. Analysis of the frisbee sample revealed a strong similarity to the bulk chemistry of the surface, strongly suggesting that the pan surface is likely the dominant source of aerosol in the region, thereby excluding Kalahari sands as a significant source of aerosol load. Additionally, the coarse nature of the deposition in the frisbee trap, suggests significant mineral transport within the system by local entrainment and deposition.

ix. The results of the PI-SWERL experiment can give an indication of the likely material to be entrained, however, the morphology of the sample was significantly altered during the sample collection through collisions between particles and within the internal wall of the sampling device.

Despite the number of caveats and limitations identified above, QEMSCAN has revealed significant insight into the nature of the pan surface and a sized analysis of grains shape and associated mineralogy. This has revealed that, similar to global studies, quartz, feldspar, calcite and mica are components of the aerosol load predicted for this region. Additionally, important mineral evaporites including halite and thenardite, are likely to be transported significant distances from the source region. In order to understand the transport potential of this site and therefore the likely distribution of impact, the contextualisation the mineralogy within the large scale synoptic features, which will transport the aerosols, is needed. The following chapter will consider the synoptic states which will result in significant entrainment and transport from the Makgadikagdi Pans.

Chapter 5: Synoptic drivers and the Makgadikgadi Pans as a source (2006 to 2012)

5.1 Introduction and Literature review

In order to achieve the fourth objective of this study, which set out to characterise the seasonal, annual and multi-annual emission character of the Makgadikgadi Pans, satellite technology was utilised to visually detect dust plumes emanating from source. This data was then integrated into meteorological data to determine the synoptic drivers responsible for large scale transport from the Makgadikgadi.

5.1.1 Detecting Dust Sources and the Identification of Pans as Emissive Surfaces

Remote sensing has been instrumental in the detection of dust sources globally (Prospero et al., 2002; Washington et al., 2003); additionally, it has permitted for the identification of the emission behaviour of systems. Global aerosol indexed products, including the Total Ozone Mapping Spectroradiometer (TOMS) have produced both global and regional dust maps. However, these produce maps of aerosol dispersion patterns, rather than pointing at source activity. More recently, Engelstaedter and Washington (2007b) made a significant advance on the foundational TOMS based studies by Prospero et al. (2002) and Washington et al. (2003). Through the use of a surface gustiness component in their analysis, Engelstaedter and Washington (2007b) produced a map containing 131 global hotspots, 6 of which lie in southern Africa. Despite this, the coarse nature of the resolution provided by TOMS and similar AI products result in the sources being attributed largely to unspecified domains with little geomorphologic context. Advances in satellite technology have provided higher resolution products, however, these remain at a global scale. For example, Ginoux et al. (2012) present global-scale high-resolution (0.1°) dust source locations, based on Moderate Resolution Imaging Spectroradiometer (MODIS) Deep Blue aerosol measurements. While this study was a significant advance in large global source regions, the product revealed no further insight into the smaller and discrete sources within southern Africa's vast drylands. While not increasing the understanding of source location, these studies improved our understanding of the activation frequency, timing and seasonality of dust sources (e.g. Prospero et al., 2002; Bryant, 2003; Zender et al., 2003; Washington et al., 2003; Bryant et al., 2007; Mahowald et al., 2007; Engelstaedter & Washington, 2007a; Bullard et al., 2011; Shao et al., 2011; Ginoux et al., 2012; Ashpole & Washington, 2012). Nevertheless, it has presented us with the ability to detect spatially discrete and intermittent sources using moderate resolution polar-orbiting satellite data, using platforms such as, SeaWiFS (Sea-viewing Wide Field-of-view Sensor) (Eckardt & Kuring, 2005), MODIS (Bullard et al., 2008; Baddock et al., 2009), and a combination of GOES (Geostationary Operational Environmental Satellite) and MODIS (Lee et al., 2009; Rivera Rivera et al., 2010; Vickery & Eckardt, 2013).

These studies have revealed that there are a number of surface typologies associated with dust emissions. Despite the assumption that dry, unprotected sediments in any environment can be blown into the atmosphere (Goudie & Middleton, 2006), the main sources of soil-derived mineral dust are located in desert regions where rainfall is below 250 $mm.yr^{-1}$. Further, these regions are most commonly associated with large inland drainage basins (e.g. Livingstone & Warren, 1996; Prospero et al., 2002; Washington et al., 2003). Such regions are often extensive, and contain a wide range of surface characteristics and sedimentary environments, including stone pavements, unconsolidated aeolian deposits, endorheic depressions, fluvial, alluvial and groundwater dominated systems, and consolidated or sealed surfaces such as evaporite crusts, duricrusts or bedrock (Bullard et al., 2011). All of these surfaces have differing dust potential, with consolidated or crusted surfaces commonly associated with the lowest dust potential (Gillette et al., 2001). The complexity of surfaces and sediment availability of geomorphological characteristics is associated with active sources, and results in a high degree of spatial and temporal emission variability. These availability limitations were considered by Bullard et al. (2011) to be broadly classified by the following definitions:

i. supply limited - lack of suitable sediment,
ii. availability limited - where sediment is available but not readily entrainable, and
iii. transport capacity limited - insufficient wind capacity to result in entrainment.

These definitions are based on the principal assumption that, with increased aridity, sediment production decreases while sediment exposure increases. However, these classifications are by no means mutually exclusive, but do provide a base upon which emission characteristics can be based (e.g. Zender & Kwon, 2005; Mahowald et al., 2007).

When compared with the large expanses of Chinese loess (Mei et al., 2004) and Saharan sand sea (e.g. Schepanski et al., 2007; Washington et al., 2009; Crouvi et al., 2012), which are assumed to contain an abundant supply of sediment, pans are considered to be relatively small features. Further, it is proposed that these are often limited by, one or more factors, as outlined by Bullard et al. (2011). Despite this, these vegetation-free expanses of flat, fine-sediment dominated ephemeral basins have been identified as important sources of dust both in terms of their intensity and magnitude (e.g. Reheis, 1997; Prospero et al., 2002; Mahowald et al., 2003; Washington et al., 2003; Goudie & Middleton, 2006; Reheis, 2006a; Bullard et al., 2008; Bullard et al., 2011).

Early observations by Pye (1987), amongst others, noted the highly active nature of pan landscapes, noting the importance of water, despite the perceived arid nature of their location. Shaw and Thomas (1997) confirm the importance of water, suggesting that the extent and seasonality, as well as frequency and duration of inundation, result in these features being "…among the most ephemeral of geomorphological phenomena…lasting no longer than the interval between one rainfall event and the

next." (Shaw & Thomas, 1997: 309). Additionally, Shaw and Thomas (1997) and Prospero et al. (2002) suggest that such environments are prominent sources of dust due to their nature as receptacles of sediments just as the Bodélé, Taoudenni, Tarim, Eyre, Etosha, Makgadikgadi, Uyuni and the Great Salt Lake are (Washington et al., 2003). These sediments are deposited and then exposed through the annual, cyclic nature of inundation leading to deposition, followed by deflation through aeolian processes as the waters recede. The periodic renewal of sediments, through ephemeral flood inundation events, imposes an aspect of supply control on these sources, resulting in a reliance on the flood events to provide the sediment (Shaw & Thomas, 1997).

Chemically, pans are often salt rich (Saint-Amand et al., 1987), and inundation periods, combined with the effects of direct rainfall onto the pan surface, affect crystal growth and dissolution. The authors add that the temperature dependence on mineral formation and state, necessitate the need to view the climatological and hydrological regimes of the region. Shaw and Thomas (1997) elaborate further that moisture and mineral variations on the pan surface can serve both to inhibit and promote dust deflation, arguing that the development of evaporite and clay crusts can protect surfaces from deflation. The lack of protective vegetation cover, high sodium concentrations, the development of wind-susceptible clay desiccation curls and pellets, as well as the presence of fine sediments, all favour the operation of deflation from playa and pan floors when they are not inundated by water (Shaw & Thomas, 1997). Shaw and Thomas (1997) add that the relationship between these systems and their larger environment is essential for context, as transport of coarse grains from the basin margin into the basin is proposed (Bullard et al., 2011), to result in significant saltation and increased emission.

This dynamic nature of pan surfaces identifies their importance, further enforcing the prominence of large basins of internal drainage as global dust sources (Prospero et al., 2002; Washington et al., 2003). This inference is confirmed globally as basin and pan surfaces occupy the 6th through to 9th positions amongst the most important sources. The Makgadikgadi Pans rank 9th, below the large and extensive Taklamakan Basin in China and the Lake Eyre Basin in Australia, as well as the similarly sized Etosha Pans in Namibia (Washington et al., 2003). These four large basin systems are all proposed to be subject to extensive seasonal inundation, resulting in both supply and source associated limitations to these sites (Bullard et al., 2011). The expression of such variability can be observed on the Makgadikgadi Pans, where discrete areas of the pan proved to be consistent sources, while others that theoretically should be, did not result in detectable plumes. Bullard et al. (2008) goes further to suggest that the current gap in understanding of source regions is at the sub-basin scale, and that global understanding fails to quantify and provide parameters for the physical characteristics, variability and dynamics of source areas.

A study by Vickery et al. (2013) identified the value of the Makgadikgadi system within southern Africa in terms of emission frequency. Additionally, the Vickery et al. (2013) study revealed notable variability in both emission characteristics and source locations over a four year time period. In order to understand this system better in the context of seasonal and inter-annual variability, a longer time period was required. This chapter serves to extend the data set derived by Vickery et al. (2013), and determine the meteorological drivers that result in emission from the Pan. Through linking the seasonal, annual and multi-annual emission character of the Makgadikgadi with the spatial and temporal variations detected for the pans, it attempts to provide possible explanations for the observed trends in emission.

5.2 Atmospheric Circulation over Southern Africa

The climate of southern Africa is influenced by its location in the sub-tropics, with perturbations coming from both the tropics to the north and the temperate latitudes to the south (Tyson & Preston-Whyte, 2000) (*Figure 5.1*). The mean circulation over the sub-continent is dominated by a semi-permanent, sub-tropical, high-pressure cell, resulting in anti-cyclonic circulation (Tyson & Preston-Whyte, 2000). This anti-cyclonic circulation dominates at mid and high-latitude throughout the year, intensifying and shifting northwards during the winter months (Tyson, 1987).

The presence and persistence of the south Atlantic and south Indian high pressure systems dominate during the summer months, changing by March (Tyson & Preston-Whyte, 2000) to make way for a central continental, high pressure system during winter. This shift results in the circulation of warm, moist, tropical air into the interior during winter, providing additional dry, inter-seasonal months, when the influences of tropical easterlies and mid-latitude westerlies dominate. With the associated changes in isobaric pressure and system dominance, the greatest interior wind speeds are expected between April and July, decreasing towards October, while the lowest wind speeds regionally are observed in February and March (Tyson & Preston-Whyte, 2000).

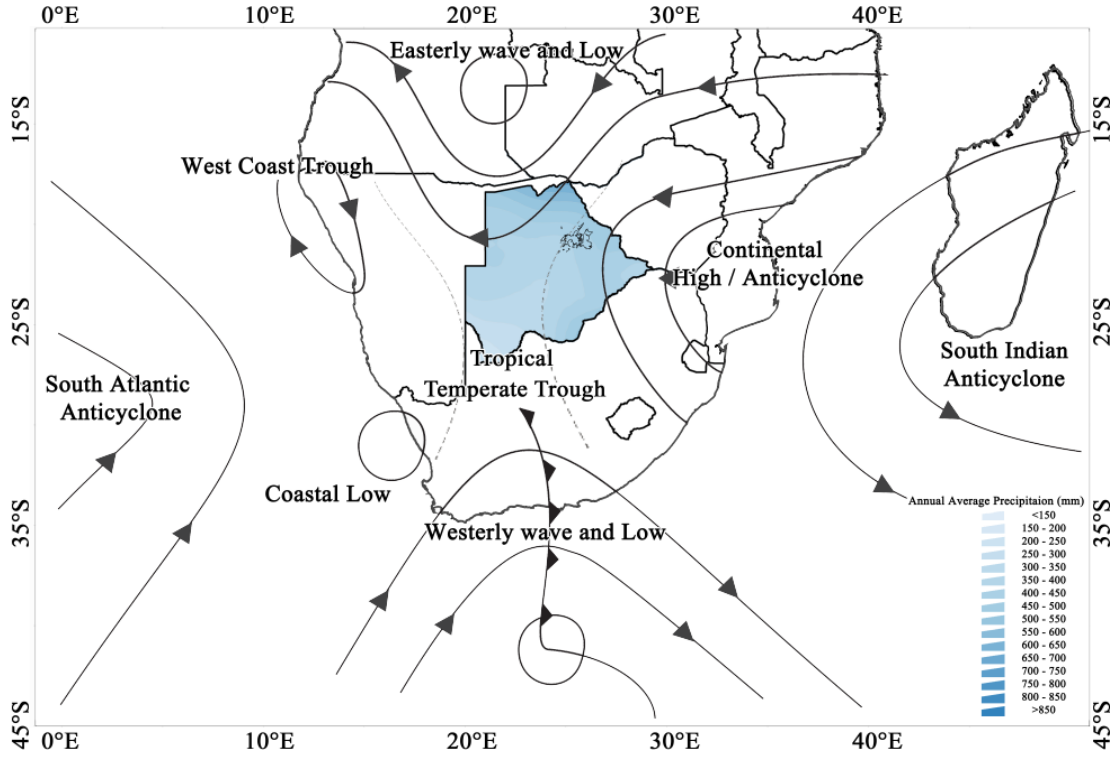

Figure 5.1 Mean circulation features in southern Africa with annual isohyets for Botswana (modified after Tyson and Preston-Whyte (2000).

Tyson et al. (1996b) present five major circulation types affecting southern Africa, which are driven by the circulation features presented in (*Figure 5.1*). These include the (i) continental anti-cyclone, (ii) ridging anti-cyclone, which follows a (iii) westerly wave/low, (iv) a cut-off low, and finally a (v) tropical easterly disturbance. Tyson and Preston-Whyte (2000) present additional features characterised as functions of the five Tyson et al. (1996a) circulations, suggesting that various circulation features tend to occur together, resulting in composite situations, which are often difficult to classify. The ten composite features as identified by Tyson and Preston-Whyte (2000) are: (i) fine-weather and mildly disturbed: continental high pressure, coastal low and berg winds, (ii) tropical disturbances in the easterlies: easterly wave, easterly low, (iii) temperate disturbances in the westerlies: westerly wave/trough, cut off-low, southerly meridional flow, ridging anticyclone, west-coast trough and cold snap (*Table 5.1*). These composite features were used to determine the synoptic states on which emission occurred. The final system noted by Tyson and Preston-Whye (2000), and further analysed by Ratna et al. (2013), is the tropical temperate trough (for further details on synoptic states, see Appendix 8).

Table 5.1 Summary of synoptic states presented by Tyson et al (1996b) and Tyson and Preston-Whyte (2000) indicating the system origin and the number of systems proposed by each study.

Circulation Classification	Circulation Type	
	Tyson et al. (1996b)	Tyson and Preston-Whyte (2000)
Fine and mildly disturbed conditions		coastal low and berg winds
	continental anti-cyclone	continental high pressure
Tropical easterly disturbances	tropical easterly disturbance	easterly wave
		easterly low
Temperate Westerly Systems	ridging anticyclone	ridging anticyclone
		west coast trough
	westerly wave/low	westerly wave/trough
	cut off low	cut off low
		southerly meridional flow
		cold snap
Composite Disturbance		tropical temperate trough (TTT)

5.3 Methods

There are a number of methods used for dust detection, ranging from early observations to modern satellite based composites. The Total Ozone Monitoring Spectrometer (TOMS) onboard the Nimbus-7 satellite provided the foundation upon which much of the modern aerosol literature is based (Bryant et al., 2007; Washington et al., 2003; Kaufman et al., 2002; e.g. King et al., 1999). The TOMS product was succeeded by the OMI product (Ozone Monitoring Instrument) onboard the NASA Aura satellite. However, both of these products are limited to daily resolution, with detection further restricted by the height of the plume, cloud cover and contamination, along with transport time sampling biases (Zhang et al., 2008). The requirement presented itself to provide a higher spatial and temporal resolution of dust source and emission characteristics. While Vickery et al. (2013) used a multisensor approach, the higher resolution provided by MODIS resulted in the selection of this product for further analysis and to create a longer time period of analysis on the dynamic and highly variable Makgadikgadi system. In light of this information, this chapter focuses on true colour imagery from MODIS Terra and Aqua. These satellites provide images twice daily at 250 m resolution, which allows for the detection and attribution of plumes at a high temporal and spatial resolution. The detection of plumes is contextualised through synoptic analysis of events and within the context of regional circulation features (Vickery & Eckardt, 2013).

5.3.1 Moderate Resolution Imaging Spectroradiometer

The Moderate Resolution Imaging Spectroradiometer (MODIS) flies onboard NASA's Aqua and Terra satellites as part of the NASA-centred international Earth Observing System (Vermote & Vermeulen, 1999). Both satellites orbit the Earth from pole to pole with a near total (95%) daily coverage (Chu et al., 2003). MODIS Terra (morning) and Aqua (afternoon) images, with approximate

equatorial crossing times of ≈10:30 and ≈13:30 respectively, provided good spatial resolution (Bullard et al., 2008), with each image representing a true colour composite of a single Level-1B daytime five minute granule of MODIS data.

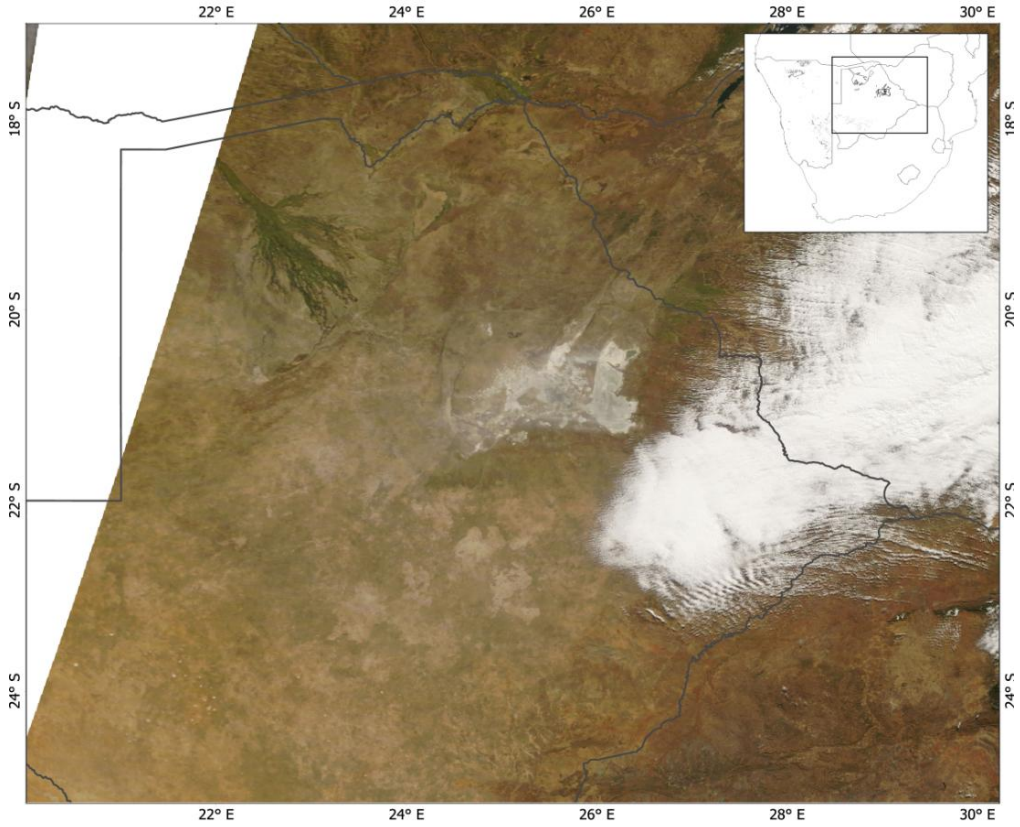

Figure 5.2 Domain of SERVIR Africa South Central Tile used for analysis of emission frequency and characteristics of dust from the Makgadikgadi Pans. This image shows a dust plumes from northern Sua on the 2nd of July 2007. Inset figure shows the domain of the tile covering much of Botswana and Zimbabwe.

For this study, the true colour composite images were analysed for the presence of dust as well as used for validation of signal through correlation with the rapid fire product. The colour composites, available online through the Rapid Fire website (http://rapidfire.sci.gsfc.nasa.gov/) at differing resolutions (2 km, 1 km, 500 m and 250 m), provide a time series of images which can be analysed for dust activity. True-colour images were produced from attributing the red (channel 1: 620-670 nm), green (channel 4: 540-570 nm) and blue (channel 3: 460-480 nm) bands to the red, green and blue channels, respectively. This true colour composite, which is available for multiple domains over southern Africa, was selected for use in this study. The SERVIR Africa South Central Tile was selected as it presented a good spatial coverage of the pan, as well as good coverage around the pans to allow for the detection of plumes in transport (Figure 5.2) (SERVIR is a joint venture between USAID and NASA to provide satellite-based earth observation to developing countries. The tile is therefore a sub-set derived for the initiative covering most of Botswana).

5.3.2 Detecting Dust Sources using MODIS

Typically, the visible spectrum has been reserved for detecting and tracking dust as it is transported over the ocean, where the pale dust contrasts strongly against the dark background (King et al., 1999; Prospero, 1999; Eckardt & Kuring, 2005; Schepanski et al., 2007). From Figure 5.3, which shows dust plumes over various surfaces and source locations, highlights the clear contrast between plumes and the ocean (a, c and d) while less defined over land (b). According to Prospero (1999), dust plumes are one of the most prominent and commonly visible atmospheric constituent features in satellite imagery, due to their potential to cover large areas.

Due to airborne dust having similar reflective properties as the underlying land, Lee (1989) discusses the limitations of using visible images over land concluding that alone they are generally not suitable for detection, and best used in combination with other products. However, developments in algorithms and the knowledge of band combinations have led to algorithms based on visible wavelengths being developed (e.g. Landsat-5 - Kaufman et al., 2000; MODIS - Hsu et al., 2004; Meteosat - Brindley & Ignatov, 2006).

While the majority of studies of dust in the visible spectrum, using true colour images, are focussed on detection over the ocean, in this study MODIS images are used to detect terrestrial plumes identified as emanating from the Makgadikgadi Pan. Despite the limitations proposed by Lee (1989), sequential viewing of images was found to permit successful detection of plumes, which, due to the pale nature of pan sediments, contrasted against the base Kalahari sediments. Further, the dust in transport distorted surface features which, when viewed in sequence and in combination with synoptic charts, could give an indication of transport direction, with the head of the plume being associated with the furthest upwind location of detected dust while being the least dispersed. The level of dispersion was further used as an indicator of active emission, with poorly dispersed plumes often associated with close proximity to the emitting source, while increased dispersion was observed further from source.

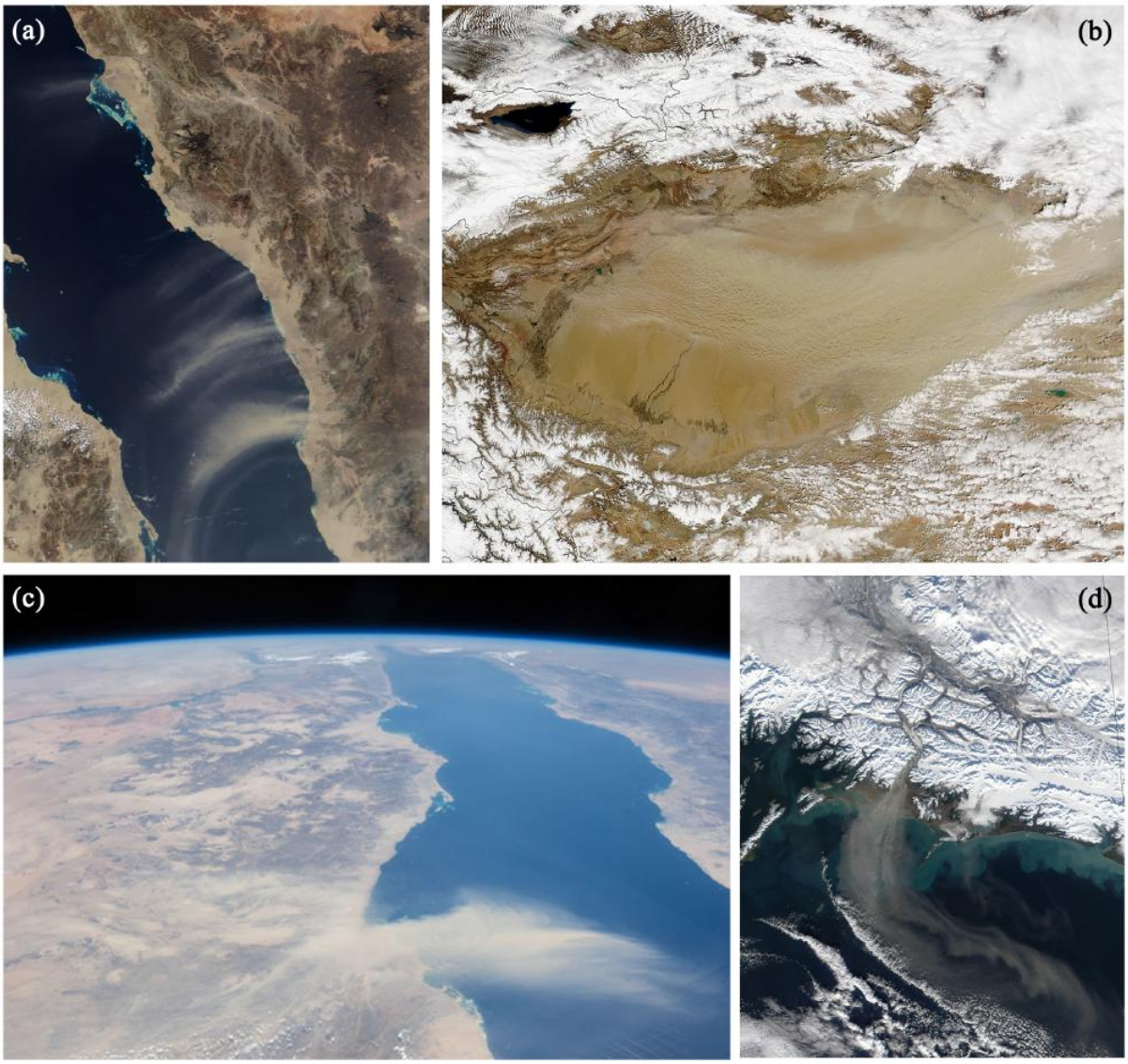

Figure 5.3 Visible images of dust storms globally from multiple sensors. (a) February 8, 2004 dust from the Arabian Peninsula in transport over the Red Sea captured on MODIS Terra (Image courtesy NASA/GSFC, MODIS Rapid Response). (b)March 26, 2004 dust from the Tian Shan Mountains and across the Taklimakan Desert basin in western China captured on MODIS Aqua. Image courtesy NASA/GSFC, MODIS Rapid Response). (c) June 22, 2013 dust plume over the Sudan in transport towards the Arabian Peninsula. The image is a photograph taken by the crew onboard the International space station (Image courtesy of the Image Science & Analysis Laboratory, NASA Johnson Space Centre). (d) October 26, 2001 glacial dust along the Copper River in Alaska in transport over the Gulf of Alaska captured on the MODIS Terra (Image courtesy NASA/GSFC, MODIS Rapid Response).

There are several caveats involved in the detection of dust plumes. The first involves the timing of emission and the timing of the overpass, with Ashpole and Washington (2013 Accepted) noting that it is possible for some transport to have occurred before detection becomes possible. Secondly, by the time of detection, multiple plumes could have combined to result in a single plume mass and the method of detection fails to identify all emissive sources. This favours the detection of the furthest

upwind source as noted by amongst others, Bullard et al. (2011) and Baddock et al. (2009). Finally, detection assumes the source is visible from the satellite and as such plumes beneath clouds associated with thunderstorm downdrafts and frontal systems (Huang et al., 2007) are often obscured and therefore remain undetected (Prospero, 1999). Through the visual detection and sorting of imagery, it is thought that learning and repeat observation of plume characteristics, allows for the use of personal judgement to determine plume age and the nature of transport. Therefore, visual detection, while laborious, can further inform the precise detection and attribution of source regions. This laborious approach allowed for point source detection and additional metrics associated with plume timing, direction and length to be extracted (sensu Schepanski et al., 2007; Bullard et al., 2008). This, through correlation with synoptic data and trajectory analysis, allowed for monthly, annual and inter-annual dust plume frequency and transport trends to be determined (Vickery et al., 2013).

5.3.3 HYSPLIT

The Hybrid Single-Particle Lagrangian Integrated Trajectory (HYSPLIT) product was used in this study and is available online through NOAA ARL (Air Research Laboratory - http://www.ready.noaa.gov/ready/open/hysplit4.html). For this study, HYSPLIT Trajectory modelling utilising NCEP Reanalysis data, was used to plot trajectories (Wang et al., 2011). NCEP Reanalysis data was used to ensure consistency with the geopotential surfaces created for synoptic state analysis. The trajectories were determined for all plumes and run for 24 hours to ascertain the dominant transport pathways of aerosols emitted from the Makgadikgadi Pans.

HYSPLIT forward trajectory analysis plots of days on which plumes were detected were also created. The approximate time of emission using timings of Terra or Aqua overpasses were used, and the trajectories were calculated for 24 assuming an emission height of 10 m above ground level. These were compared with the mapped trajectories from the true colour imagery and set in the context of the 1000 hPa, 850 hPa and 500 hPa surfaces to determine the effects of large scale circulation on trajectory and recirculation. Additionally, the identification of 24 hours of transport can indicate the extent of the downwind impact of entrained material.

5.3.4 Synoptic Circulation and Climatological Analysis

For all days on which plumes were detected, gridded climate data representing the 500 hPa, 850 hPa and 1000 hPa surfaces were created using NCEP Reanalysis data available online from the NOAA ESRL (National Oceanic and Atmospheric Administration, Earth Science Research Laboratory) website (http://www.esrl.noaa.gov/psd/data/gridded/). Monthly mean circulation and historic monthly means were also downloaded, against which event days were compared. In accordance with studies by Tyson et al. (1996b) archetypal conditions were linked to all events to summarise findings into existing literature. Eight circulation features were determined to be drivers for emission, which are

broadly grouped into: i) Fine weather and mildly disturbed conditions (coastal low and continental anticyclone), ii) Tropical Easterly disturbances (easterly wave low and TTT), iii) Temperate Westerly disturbances (ridging anticyclone, west coast trough, westerly wave low and trough, cut off low, TTT). Strong et al. (2011) highlight the difficulties involved in synoptic classification, revealing that systematic and statistical classification of systems does not scale down to identifying daily events within weather systems easily. Therefore, the authors propose that visual classification of events consider days preceding and after the event to provide context, result in the best identification.

5.4 Results

5.4.1 Six Year Sub-basin Variability within the Makgadikgadi Pan

From within the Makgadikgadi Basin, 123 dust plumes were detected, occurring between January 1st 2006 and December 31st 2012 (*Table 5.2*). This time period was analysed using 4803 images which represent 2371 aqua images (93% of all days) and 2432 terra images (95% of all days). The 123 plumes were detected to have occurred on 50 days between April and November, with an average of just over 2 plumes per dust day. Of all plumes, 90% were detected on Terra (111 dust plumes), while 10% were detected on Aqua (12 dust plumes).

Table 5.2 Number of emissions and number of emission days for the Makgadikgadi Pans for the time period 2006 to 2012 inclusive. Monthly and annual counts and cumulative totals are presented for the region.

Years		Months												
		January	February	March	April	May	June	July	August	September	October	November	December	**TOTAL**
2006	Plumes	0	0	0	0	0	2	3	0	0	0	0	0	**5**
	Emission Days	0	0	0	0	0	1	3	0	0	0	0	0	**4**
2007	Plumes	0	0	0	1	2	3	2	1	0	1	1	0	**11**
	Emission Days	0	0	0	1	1	2	1	1	0	1	1	0	**8**
2008	Plumes	0	0	0	0	2	4	3	5	0	1	0	0	**15**
	Emission Days	0	0	0	0	1	2	1	3	0	1	0	0	**8**
2009	Plumes	0	0	0	0	1	0	26	27	4	1	0	0	**59**
	Emission Days	0	0	0	0	1	0	5	4	2	1	0	0	**13**
2010	Plumes	0	0	0	0	3	5	4	8	3	0	0	0	**23**
	Emission Days	0	0	0	0	1	2	3	3	1	0	0	0	**10**
2011	Plumes	0	0	0	0	0	1	5	0	0	0	0	0	**6**
	Emission Days	0	0	0	0	0	1	2	0	0	0	0	0	**3**
2012	Plumes	0	0	0	0	0	0	1	2	1	0	0	0	**4**
	Emission Days	0	0	0	0	0	0	1	2	1	0	0	0	**4**
TOTAL	**Plumes**	**0**	**0**	**0**	**1**	**8**	**15**	**44**	**43**	**8**	**3**	**1**	**0**	**123**
	Emission Days	**0**	**0**	**0**	**1**	**4**	**8**	**16**	**13**	**4**	**3**	**1**	**0**	**50**

July and August were the dustiest months with 16 and 13 dust days, producing 44 and 43 dust plumes respectively. June was the third dustiest month producing 15 plumes on eight days (*Table 5.2*). Analysis of inter-annual trends revealed that 2009 was the dustiest year, producing 59 dust plumes on 13 days. For 2009, single plumes in May and October start and end the season, with 5 days in July producing 26 plumes and a further 27 plumes on four days in August. The remaining four plumes were produced on two days in September. Following an emissive 2009, 2010 was the second dustiest

year producing 23 dust plumes on 10 days. A single day in May produced three plumes, with 5 in June on two separate days, 4 in July on three days, 8 plumes on three days in August and three plumes on one day in September. The remaining years all produced dust, with 2008 resulting in 15 plumes on 8 days, while 2007 saw 11 plumes on eight days, 2011 produced 6 plumes on three days with five of the plumes occurring on two days in July. Five plumes were produced on four days in 2006, while 2012 saw four plumes on four separate days, two of which occurred in August and one in each of July and September.

Of the 123 dust plumes, all attributed to the surface of the Makgadikgadi Pan, 73 plumes were detected to have originated from Ntwetwe Pan, with the remaining 50 from Sua Pan (*Table 5.3*).

Table 5.3 Count of number of plumes from the Ntwetwe and Sua Pans per year.

	Ntwetwe	Sua	**TOTAL**
2006	5	0	**5**
2007	4	7	**11**
2008	11	4	**15**
2009	34	25	**59**
2010	17	6	**23**
2011	1	5	**6**
2012	1	3	**4**
TOTAL	**73**	**50**	**123**

From Table 5.2 and Table 5.3 it can be observed that there is significant variability between years and in the emissive nature of the pan surface.

5.4.2 Synoptic Results

The plume lengths varied significantly between years, with an average length of 72 km, although a standard deviation of 64 km. Plume lengths were marked according to the maximum extent of the plume, as identified on the last image on which it was clearly visible. Plume origins were marked by the furthest upwind location discernable as a plume, while the furthest downwind point was noted by the last coherent definable structure of the plumeThe longest plume detected was 326.5 km occurring on the 13th of November 2007; the plume travelled in a south westerly direction (243°). The shortest detected plume was only 6.5 km in length occurring on the 8th of July 2009 and was one of 14 plumes all travelling off the pan in a westerly direction (274°). Analysis of Figure 5.4 reveals that plumes are most commonly between 0 km and 50 km in length, with only 10% of all plumes exceeding 175 km in length.

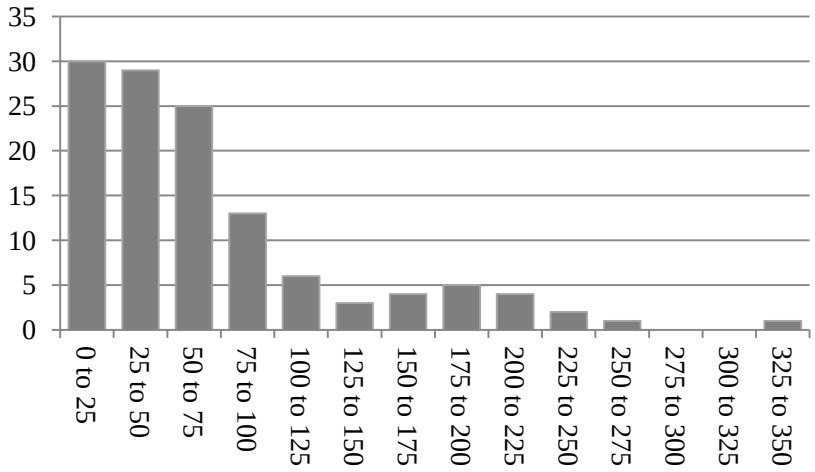

Figure 5.4 Histogram of plume length for all plumes detected from 2006 to 2012. Plumes lengths calculated as maximum extent of coherent plume on single or multiple images and represented by length in kilometres.

Plume lengths in 2009 and 2011 were notably shorter than the other years; however plume transport direction remained consistent. The average plume direction was south westerly off the pan, with a mean bearing of 252° and a standard deviation of 43°. The only major departure from south westerly transport occurred in 2012, where plumes were detected to travel with a mean bearing of 167°, representing south south easterly transport off the pan surface. This result is, however, skewed by 2012 only resulting in 4 plumes, with a single plume detected to travel in a north easterly direction (46°) while the remaining three plumes had an average trajectory of 207° which is in a south westerly direction.

Table 5.4 Statistical Results for plume length and direction as calculated for all plumes from 2006 to 2012

	Plume Length				Plume Bearing	
	Average	Standard Deviation	Minimum	Maximum	Average	Standard Deviation
2006	151.7	27.3	122.4	184.8	235.9	20.7
2007	189.7	67.1	65.2	326.5	237.4	29.3
2008	127.7	65.4	67.5	260.5	252.7	10.3
2009	34.2	21.2	6.5	96.5	251.8	40.4
2010	71.6	46.7	21.9	206.8	269.9	44.6
2011	34.1	13.7	20.7	51.2	271.9	16.9
2012	72.1	14.9	55.0	91.2	167.2	85.0
Average	72.5	64.5			251.6	42.6

Correlation of synoptic states on the day of emission revealed trends in weather systems responsible for deflation from the pan surface (*Table 5.5*). A ridging anticyclone to the south of the continent accounted for 55 plumes on 18 days, which was responsible for the most emissions in all years with

the exception of 2006. The development stage, location and strength of this system within the temperate westerlies, and the associated response of the easterlies, resulted in a wide range of plume bearings from south (~180°) to north (360°), with an average plume travelling in a south westerly direction (259°). The dominance in plume frequency of this system was largely derived through a single day (7th August 2009), which resulted in 17 plumes. A similarly high number of plumes were observed on the 8th of July 2009, when an intensified continental high pressure system with the centre of the high at ~26°S produced 14 plumes. In total, the fine weather continental anticyclone was responsible for 28 plumes on 7 days, between 2006 and 2010. Plumes were found to be transported in a south westerly direction (mean 266°) with little variation in trajectory experienced (minimum 230° and maximum 280°) primarily driven by the location of the centre of the high pressure system. The west coast trough, produced 17 plumes on 7 days, with the location and development stage of the trough, creating highly variable plumes from north east (41°) through to south west (270°) with south westerly plumes dominating on average (226°). Similarly, the remaining three temperate westerly disturbances produced highly variable plume trajectories, with the development of tropical temperate troughs producing the most stable plume trajectory (246° to 266°) and the longest average plume length at just less than 120 km.

Table 5.5 Summary of circulation features resulting in plumes. The number of days and the total count of plumes along with the minimum and maximum bearings as well as mean bearings have been included.

Circulation Classification	Circulation type	Bearing (°)		Mean	Mean	Plumes	Days
		Min	Max	(°)	Length (km)		
Fine weather and mildy disturbed conditions	Coastal Low	215		215	65	1	1
	Continental Anticyclone	230	280	266	68	28	7
Tropical Easterly Disturbance	Easterly Wave/ Low	198	221	211	98	3	3
Temperate Westerly Disturbance	Ridging Anticyclone	184	360	259	74	55	18
	West Coast Trough	41	270	226	45	17	7
	Westerly wave/trough	218	263	244	98	9	6
	Cut off low	46	305	207	54	4	4
Composite Disturbance	TTT	243	266	250	119	6	4

The ridging anticyclone was found to produce the highest number of plumes on a single day producing 17 plumes on one occasion and 8 on another, while the continental anticyclone was found to produce two high plume count days, one of 14 and one of 5. A deepening west coast trough resulting in a ridging anticyclone produced 6 plumes in August 2009, with the remaining features largely resulting in one (25), two (14) and three (4) plumes per circulation feature per day.

5.4.3 HYSPLIT Trajectory Analysis

Trajectory analysis revealed similar trends to those observed from manual mapping of plumes using the true colour imagery. The difference between the emission bearing of HYSPLIT modelled and

physically mapped plumes is 8° on average. While mean plume lengths determined from MODIS imagery were observed to be less than 200 km, using forward trajectory analysis and considering the distance the air-parcel would travel in the 24 hours following the emission, it was observed that there was significant advance on the area over which the plume travelled. From Figure 5.5, it can be seen that air parcels were mainly observed to travel between 200 and 400 km from the central point on the pan in 24 hours. After 24 hours, 105 plumes or 85% of all emission had travelled more than 400 km, while the remaining 18 plumes (15% on 8 days) were between 500 km and 1000 km from source within 24 hours.

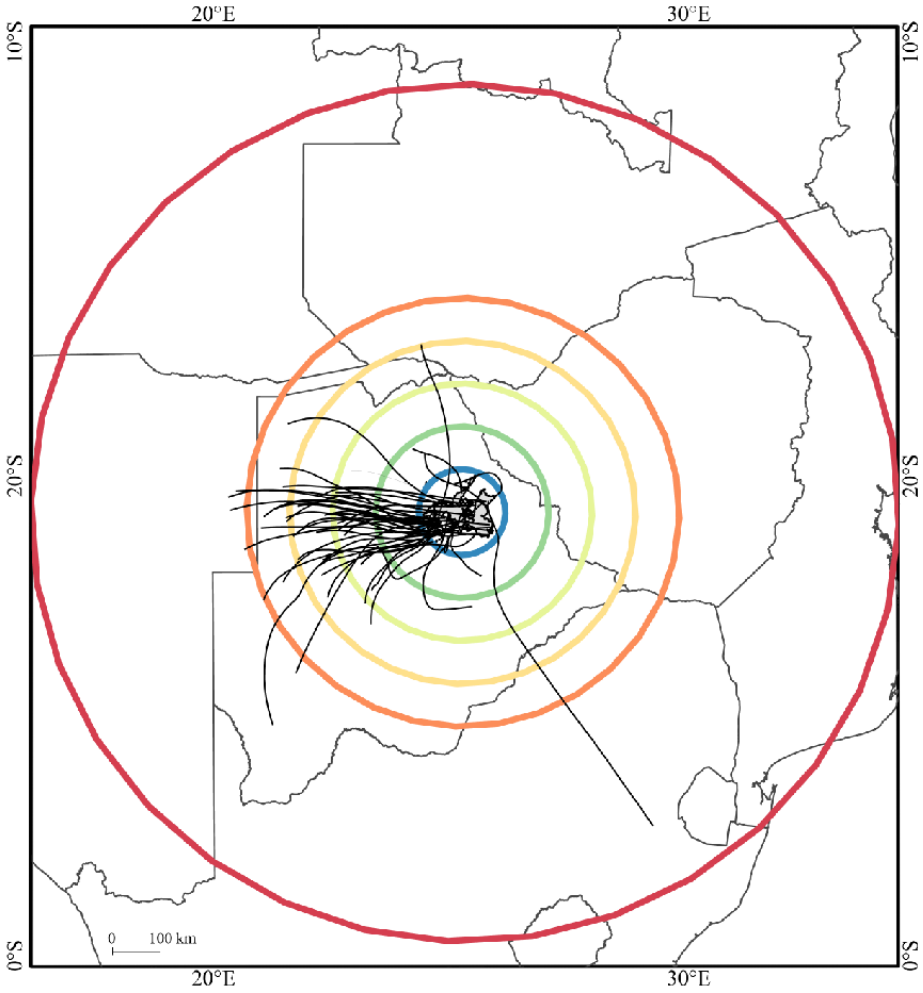

Figure 5.5 HYSPLIT modelled plumes run for 24 hours from time of emission. Each trajectory represents an air parcel leaving the determined point of emission modelled from a point 10 m above ground level. Due to the resolution of the model, days on which multiple plumes occurred are represented by a single trajectory as minor differences in source location were not resolved. Geographic circles were drawn with radii 100 km wider than the previous circle, with the first of radius 100 km, increasing incrementally to 500 km with the largest representing a 1000 km radius from a central point on the Makgadikgadi Pan surface.

5.4.4 Results Summary

This study has provided seven year analysis true colour (MODIS) imagery to determine the spatial and temporal characteristics of dust plumes from within the Makgadikgadi Pans. This section has presented the data coverage, plume length and direction as well as variability of source location as derived from MODIS. The results confirm the spatial and temporal variability of dust emission experienced from the Makgadikgadi Pans, while reaffirming its importance as a dust producing region (Prospero et al., 2002; Washington et al., 2003; Bryant et al., 2007; Vickery et al., 2013).

Due to the availability of multiple images per day, events could be analysed for persistence and the temporal dominance of emissions, with MODIS Terra identified as the dominant sensor for detection which is associated with morning coverage. Analysis of plume length and trajectory revealed that plumes were emitted by eight dominant circulation types with south westerly transport off the pans dominating largely irrespective of the synoptic system. Additionally, with increased time and through the use of forward trajectory analysis, it can be assumed that, within 24 hours, plumes were likely to be between 200 and 400 km away from the pans, largely to the west and south west.

5.5 Discussion

Ideally, studies of climate patterns and dust activity should cover extended time periods in order to truly capture inter-annual variability (Strong et al., 2011). However, historical archives of data are often poor (McGowan & Clark, 2008) requiring the use of reanalysis data. As a result studies are often limited to individual events (Resane et al., 2004; McTainsh et al., 2005), or only cover a few years (Offer & Goossens, 2001; Bullard et al., 2008; Cattle et al., 2009) at a time. The seven year time period analysed in this study presented the ability to determine both spatial and temporal variations experienced in the emission character of the Makgadikgadi basin. Through the analysis of MODIS imagery, 123 dust plumes occurring on 50 days were detected to have originated from the Makgadikgadi Pans between 2006 and 2012. Generally, these emissions were clustered both seasonally and spatially on the pan surface, although presented some noteworthy variation. The following discussion will first present the sub-basin emission from the Makgadikgadi Pans examining spatial and temporal variability. It will then discus synoptic drivers responsible for emission.

5.5.1 Sub-basin Scale Emissions from the Makgadikgadi Pans

5.5.1.1 Temporal Variability

Temporal variability was experienced at source on daily, seasonal and annual scales. On a daily scale, plumes were most frequently detected on Terra (am), with only 10% observed on Aqua. This equates to morning emissions, which is in agreement with Vickery et al. (2013). At the time of overpass, plumes were on average 72 km in length. This confirms both morning uplift and suggests that

entrainment occurred earlier than satellite overpass, as notable transport had already occurred. Terra overpass occurs at approximately 10:30 local time (08:30 GMT), which is in confirmation of a morning wind speed peak as proposed by Krishna (1968). This morning wind speed peak was theorised by Krishna (1968) to be associated with boundary layer diurnal variations, which are controlled by latitude such that at mid-latitudes wind speeds peak at midnight, while peaking at sunrise at 17°N/S becoming later towards the equator. The author suggests that the amplitude of diurnal range is at a maximum at 30° decreasing to the north and south. Therefore, the location of the Makgadikgadi at approximately 20°S would indicate that there would be an early morning wind speed peak with a strong diurnal signature to the wind speeds. This could be a prominent large scale influence on emission timing, as Washington et al. (2003) indicate that the location of the Makgadikgadi Pan is situated in a region where topographic channelling of the wind is unlikely to produce significant acceleration. Therefore, despite the limitations of only two images per day, it can be assumed that through diurnal fluctuations in wind speed and an understanding of synoptic scale drivers, this trend is in fact representative of emission from the region.

While it can be confirmed that morning emission dominates in the Makgadikgadi Basin, there also appeared to be a strong seasonal signature to emissions on the pan. Figure 5.6 presents a dust season which starts in April and ends in November, which is consistent with observations by Bryant et al. (2007). The peak in emission is observed to occur in July and August, which coincides with winter drying in the region (Thomas & Shaw, 1991), and is further associated with a peak in interior wind speed (Tyson & Preston-Whyte, 2000).

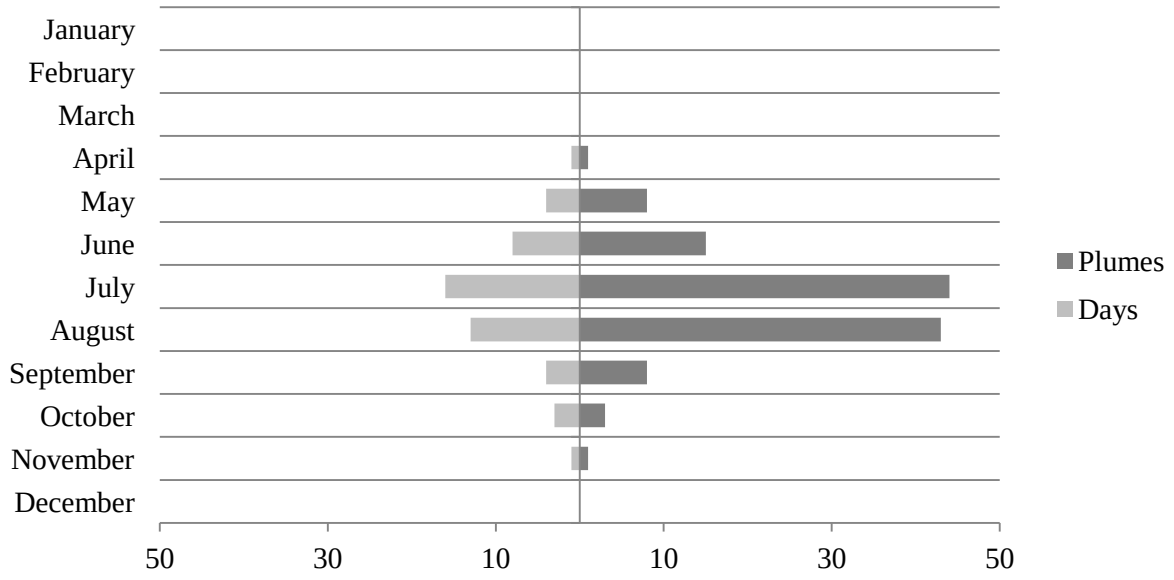

Figure 5.6: Plot presenting number of days on which emissions occurred by month to the left and the number of plumes that were produced to the right. This presents that, in the peak season, single days produce multiple plumes, while on the fringes of the dust season it is likely that only single plumes are produced on a given day.

Figure 5.6 also reveals that during the peak of the dust season, multiple plumes occur on a single day. This presents the proposal that despite the variable nature of the pan surface, given sufficiently strong surface winds multiple emissions will occur.

While there was a dominant dust season between July and August, there was also a detectable inter-annual variability, with 2007 experiencing the longest season starting in April and ending in November, while 2011 only saw plumes in June and July. Figure 5.7 reveals the spatial variability associated with the inter-annual trend, showing the emissive character of the pan surface for the seven years of study.

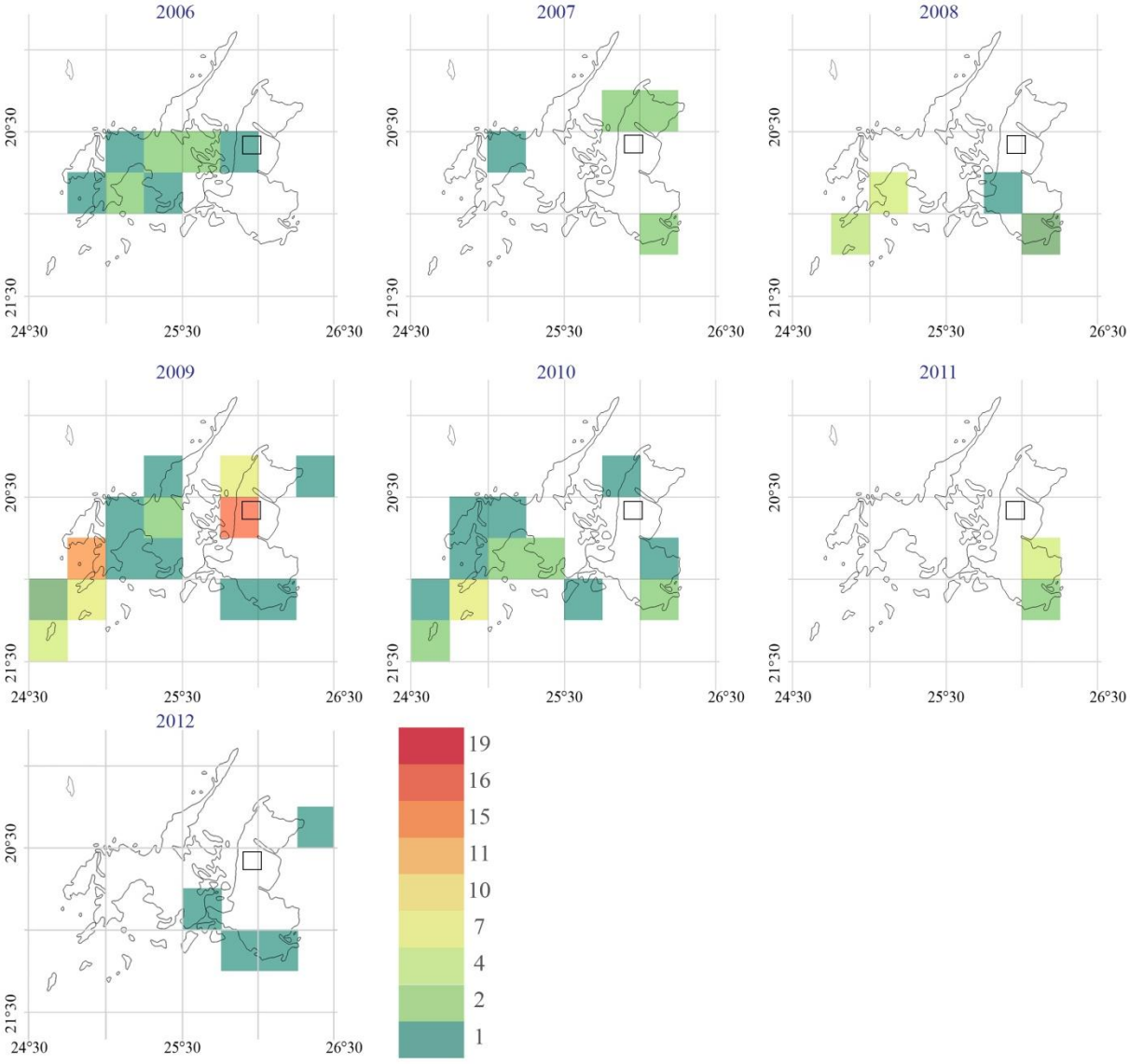

Figure 5.7: Emission frequency by year for the Makgadikgadi Pans. Figures represent a calendar year (January to December) for each year as indicated. A 0.15 resolution surface has been used to reveal trends in emission.The location of the DO4 grid, has been included for reference.

Despite this study not being unable to attribute precise drivers for the inter-annual trends, from Figure 5.7 it is evident that there is considerable inter-annual variability. Such variability was attributed by Bryant et al. (2007) to be in response to hydrologic controls. Viewing Figure 5.7 within the hydrologic context of the system, as well as seasonal rainfall statistics (*Figure 5.8*), river flow and climatic controls from ENSO, could reveal why 2009 was the dustiest year. Additionally, viewing the dust activity on an inter-annual scale reveals that, following a very dusty 2009, 2010 was another dusty year. This would serve to discount the proposal that the system is supply limited, as indicated by Washington et al. (2003), as the absence of significant sediment input following a dusty year, would suggest that a less active year would follow. It is more likely, therefore, that the limitation is associated with a complex set of surface conditions including moisture (Bryant et al., 2007) roughness (Laurent et al., 2008), crusting (Gillette et al., 2001; Langston & McKenna Neuman, 2005) and saltation (Cahill et al., 1996), which serve to promote or inhibit an abundant supply of sediment.

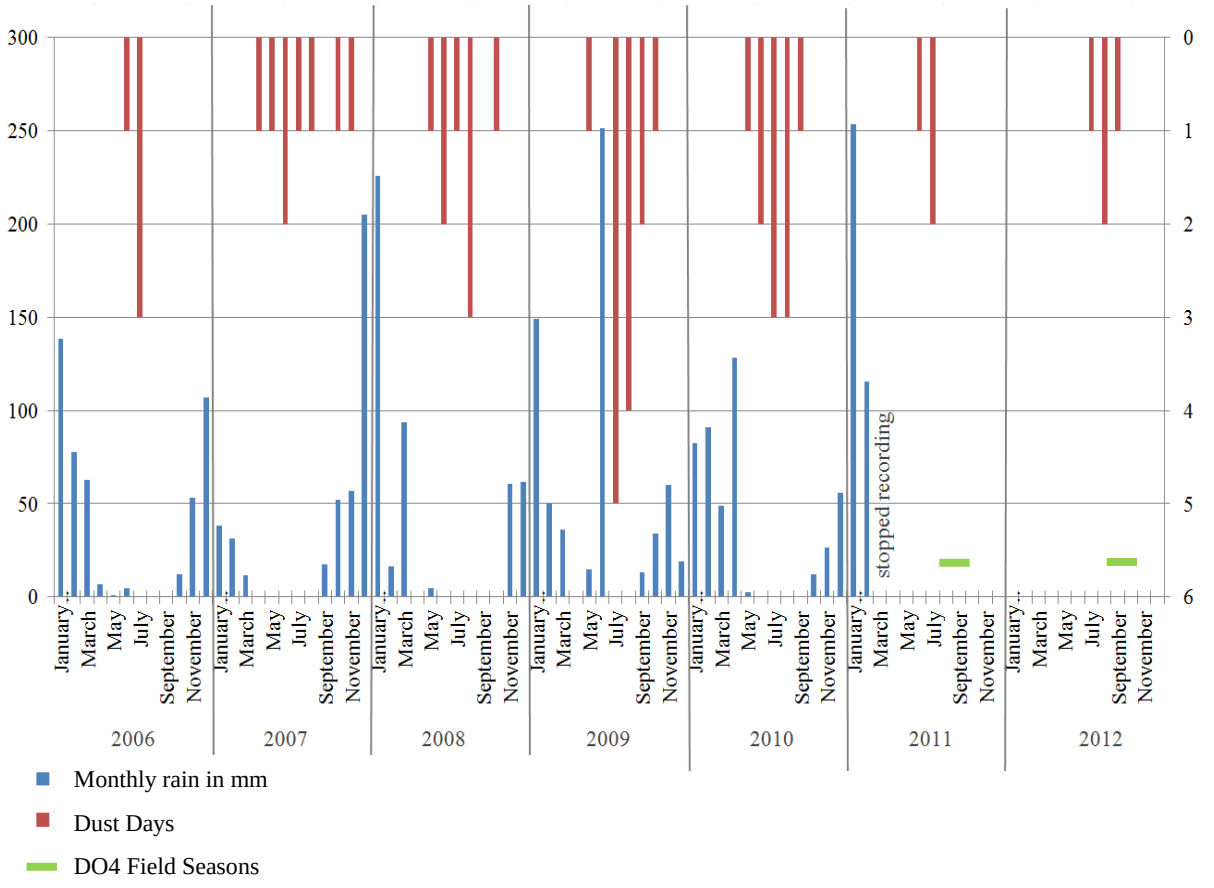

Figure 5.8 Plot of rainfall in mm and count of dust days for 2006 to 2012. Rainfall data from weather station on Sua spit, the station ceased recording in this location in March of 2011.

Strong et al. (2011) indicate that the temporal correlation between dust storm occurrence and annual climate likely shows system response to lag seasons. As this study only covers seven years, information is needed on how these years fit into the longer term climate patterns and dust activity trends. This would reveal the context of the dusty years and could highlight further associations

between ENSO cycles as proposed by Bryant et al. (2007) and which were revealed to be decisive for Australian sources by Strong et al. (2011).

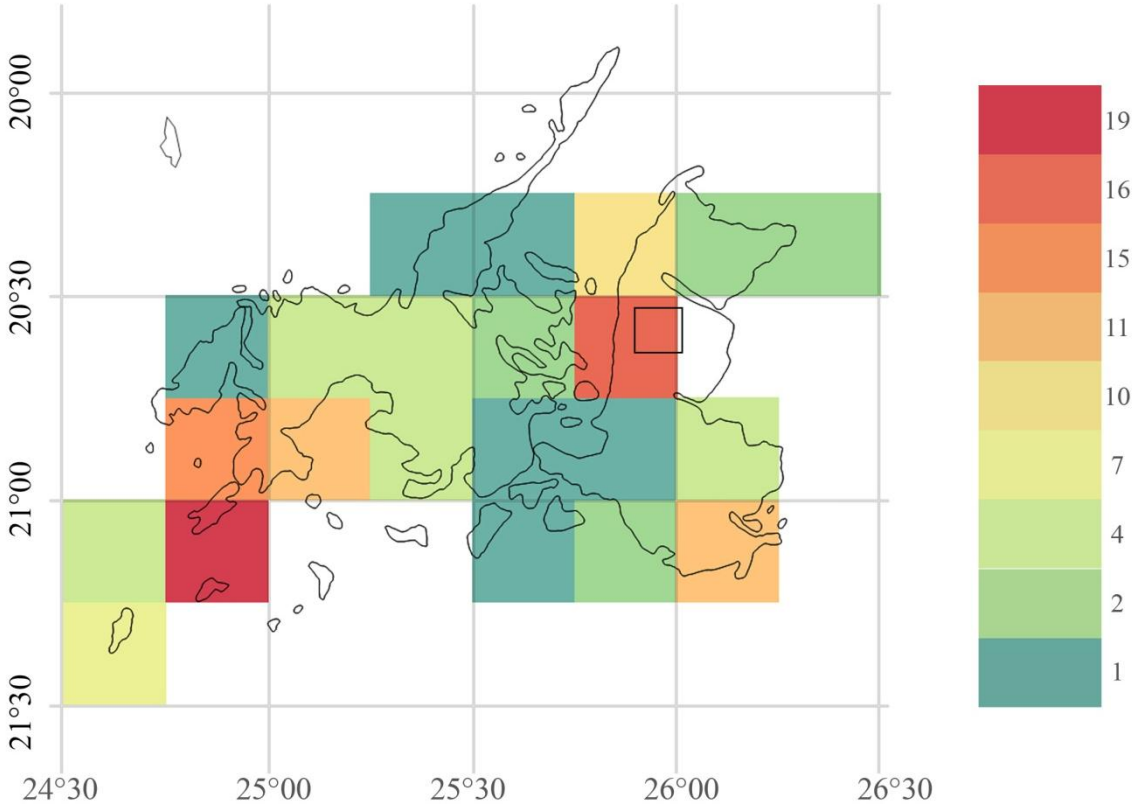

Figure 5.9: Emission frequency for the Makgadikgadi Pans, representing the 2006 to 2012 composite, a 0.15° surface has been used which reveals trends in actively emissive areas. The location of the DO4 grid, has been included for reference.

5.5.1.2 Spatial Variability

Similar to the temporal variability, a high degree of spatial variability was observed for the Makgadikgadi Pans (*Figure 5.9*). This variability is not unexpected as this large pan complex contains a number of emissive surface environments as defined by Middleton (1997). These surfaces were ranked by Middleton (1997) as a function of deflation potential and susceptibility for entrainment or inhibition, with the resulting rankings being (from most erodible to least): disturbed soils; sand dunes; alluvial and aeolian sand deposits; disturbed playa soils; skirts of playas; playa centres and desert pavements. As the higher resolution provided by MODIS has permitted for the identification of sub-basin scale source regions, it was possible to attribute emissions to both the pan margin, pan centre and pan surrounds, further identifying sub-clusters within the large pan complex (*Figure 5.10*).

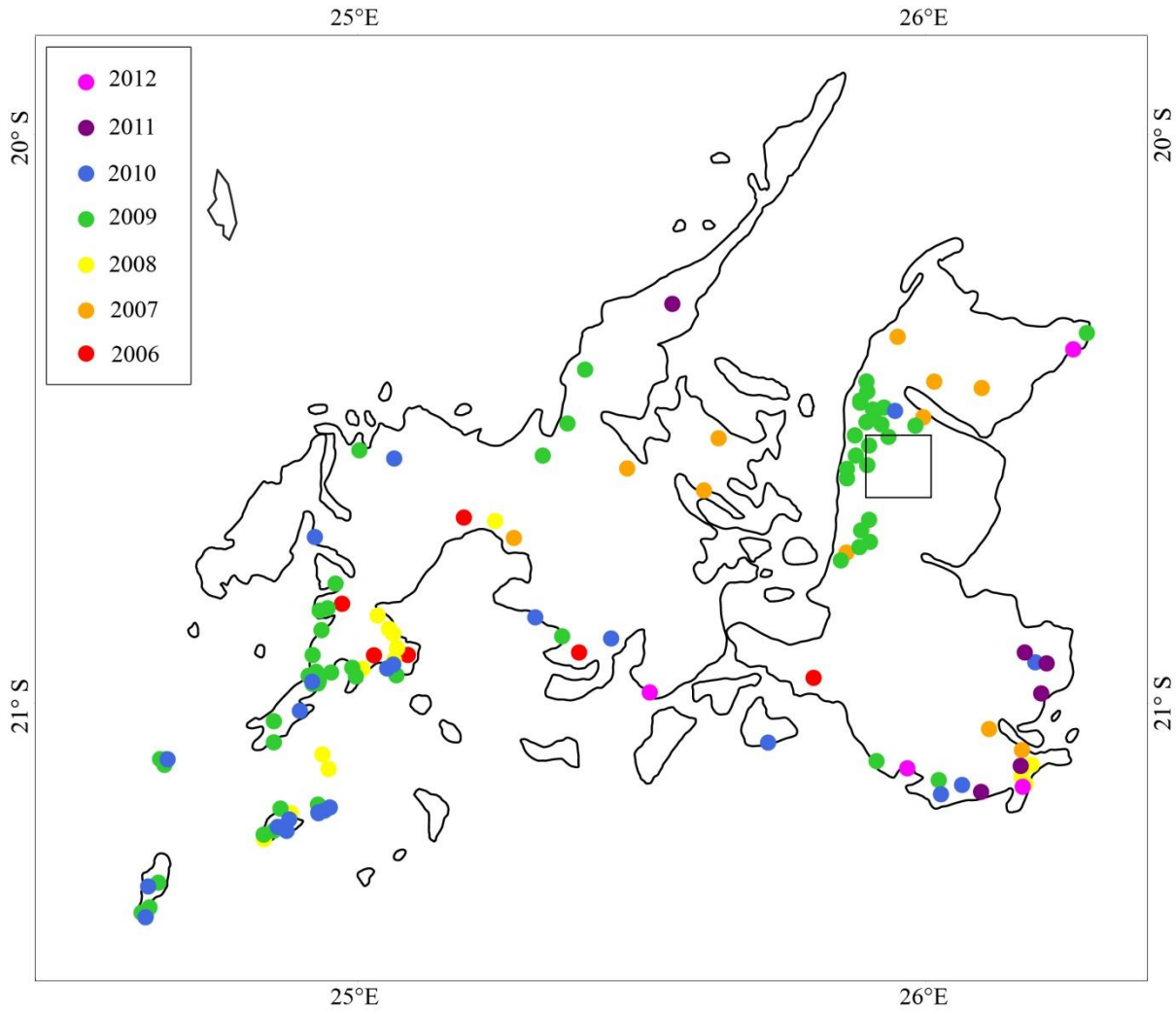

Figure 5.10 Plot of emission sources from the Makgadikgadi Pans for 2006 to 2012. Clusters of emission hot spots can be seen on the pan margins of both Sua and Ntwetwe Pans consistent between years. The location of the DO4 grid, has been included for reference.

As emission occurred in discrete areas of the pan margins, this confirms the higher propensity of emissions from the margins compared to the interior of the pan in line with the findings of Middleton (1997). This most likely indicates the faster response of the margin to seasonal wetting and drying, combined with the effects of turbidity of the wind system at the transition between the pan surface and grassy pan margins. Therefore, while these pan margin hot spots are likely representative of emission characteristics, there is the additional caveat that plumes are harder to detect when the pale dust is transported over the pale pan surface, and that it is only once transport occurs over the pan margins which are spectrally different, is detection possible. However, despite this caveat, this trend was observed in all years, and with plumes travelling in a number of directions from the pan; suggesting that, despite the limitations of detection, the pan margins are indeed the most prolific source of dust from the pans.

The finding that a number of discrete surfaces are responsible for emission, is in line with findings by Bullard et al. (2008) who present that there are sub-basin scale geomorphological controls in the Lake Eyre Basin. Similarly, this large ephemeral basin revealed that a range of localised geomorphological units were associated with emission. Unlike the Lake Eyre basin which contained sands, gibber, alluvial deposits and ephemeral pans, on the Makgadikgadi the divisions could be summarised as pan margin, pan centre and smaller satellite pans. Interestingly, 2009, which was the dustiest year, also saw the greatest number of pan centre emissions. This could indicate that the pan surface was drier and therefore experienced a lower soil moisture content to inhibit emission (Fecan et al., 1999). However, this does not necessarily indicate the nature of the 2008/2009 wet/dry season as Bullard et al. (2008) note that the response of clay and salt pans to rainfall and drying is complex.

Although this study does not attempt to include hydrologic and climatic controls for emission, Bryant (2014, *pers. comm.,* 7 February) developed an indicator for the surface wetness of the pan (*Figure 5.11*). While there was potential for the false identification of moisture through the detection of hydrated salts, the trend clearly reveals wetter eastern margins, drier interiors and a good correlation between the location of dust hot spots and areas devoid of surface moisture. This trend of a wetter eastern margin is proposed to be in response to Sua Pan, notably the eastern margin, being the lowest part of the Makgadikgadi complex (Hulsmans et al., 2006). Additionally, 5 rivers sourced in the wetter eastern catchments flow intermittently into the eastern margin of the pan during the wet season. This introduction of moisture, to both the surface and ground water, can be assumed to be significant for ground water recharge and sediment moisture content. While the relationship indicated in Figure 5.11, appears to reveal strong correlation between dry surfaces and dust emission, the timings and seasonality of when the pan was detected to be wet is not included. Despite this, it indicates that dust emission is strongly controlled by surface moisture inhibiting emission and would propose that areas that are seasonally dry would be appreciable sources of dust emission. However, the link between surface moisture, rainfall and river through flow has not been considered.

Bullard et al. (2008) propose the simplified relationship such that emissions decreases with increasing rainfall and then following a seasonal lag, the dust flux will then increase. Bryant (2003) and Bryant et al. (2007) analysed this relationship, demonstrating that atypically large inundation events had both a rapid and lingering effect on dust emission. The authors presented that inundation initially suppressed emission, however following surface drying, emission increased. This suggests that inundation and surface moisture changes the timing of emission, suppressing emission in the early dust season and delaying peak emissions towards the end of the season sometimes even into the following season. Reynolds et al. (2009) add that in highly saline environments where a large proportion of the surface sediment if composed of evaporite minerals, sustained aridity can further impede dust emission through increased drying and the development of a hardened salt crusted surface. Reynolds et al. (2009) propose that the nature and origin of the moisture input, and the

duration and speed of surface drying, are vital considerations in determining whether hard crusted or soft emissive surfaces result at the end of the wet season. Therefore the nature and source of inundation needs to be considered for mechanisms involved in sediment input and ground water recharge. For the Makgadikgadi, river inflow leading to surface inundation is not proposed to be vital as river flow is noted to be sporadic and rarely results in surface flow on the pan (McCulloch et al., 2008). Much of the inundation can be proposed to be the result of summer rainfall in the region, with the addition of ground water through flow recharging the system.

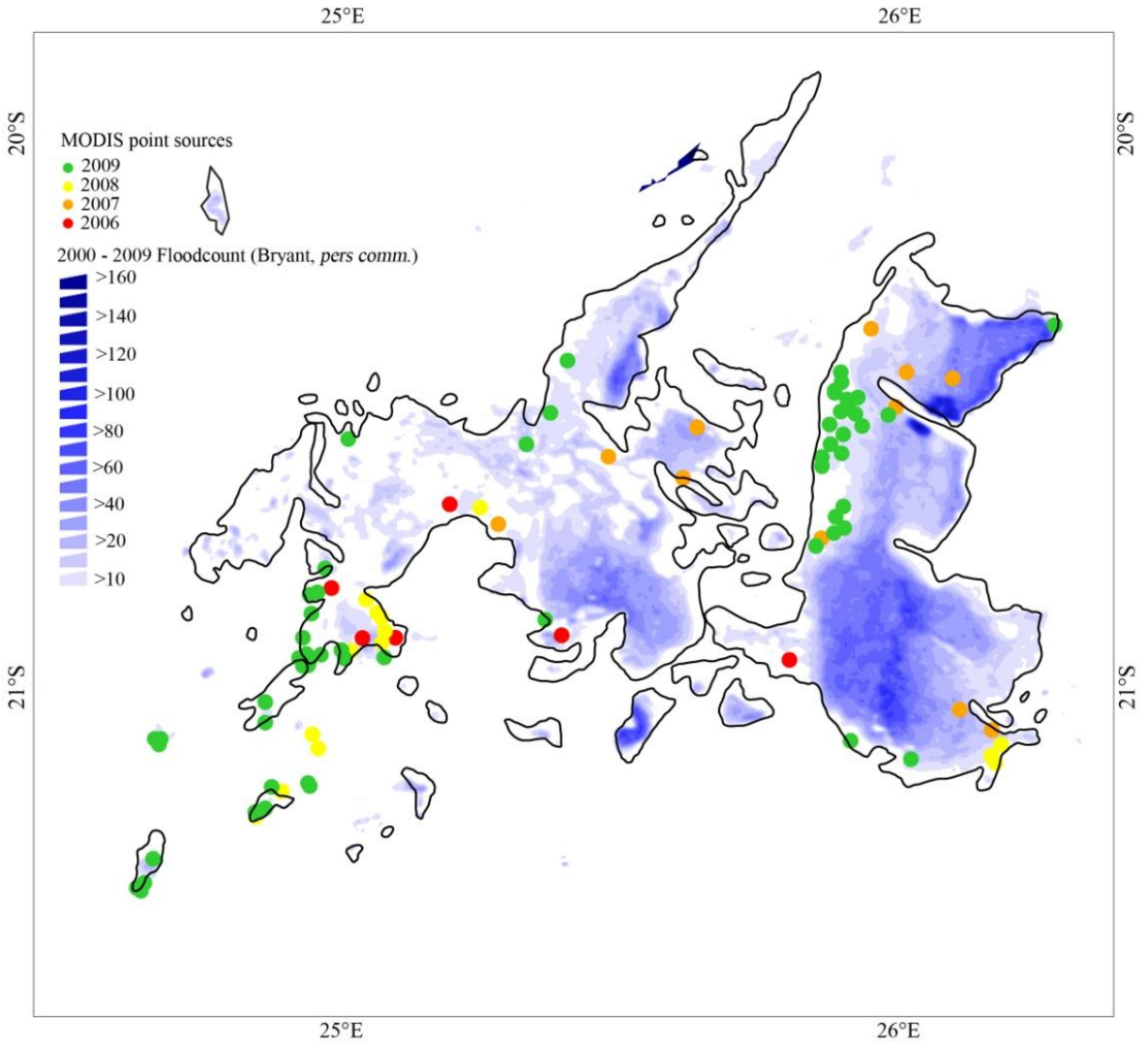

Figure 5.11 Map of the number of days on which surface water is proposed to have occurred between 2000 and 2009. Dust emissions from 2006 to 2009 have been included to reveal the correlation between surface moisture and emission. (Surface moisture data courtesy of Dr Robert Bryant)

The relationship between surface rainfall and emission was analysed by Natsagdorj et al. (2003). In their study in Mongolia, the authors attempted to correlate the number of rain days and dust days including seasonality; finding a weak negative correlation. The authors found that in addition to this trend, much of the signal was explained by population changes, land use change and the increase in

livestock movements through hot spots. A similar mechanism could possibly account for the observed variability in the Makgadikgadi Pans. However, as the country is carved up by livestock fences to contain disease (Perkins & Thomas, 1993), the large scale migration of animals through the regions is limited. In spite of this, animals have been observed on the pans, although activity is largely focused on the grassy margins (Cooke, 1979). While livestock movements may be negligible, Setlhogile et al. (2011) present land use and population statistics for the region, noting that about 72% and 56% of households living around the Makgadikgadi wetland area (population approximately 51 000 to 57 000 (Setlhogile et al., 2011) are engaged in crop and livestock farming respectively. These practices could present additional mechanisms for dust activity through degradation of crusts and changes in land state, vegetation cover and surface roughness.

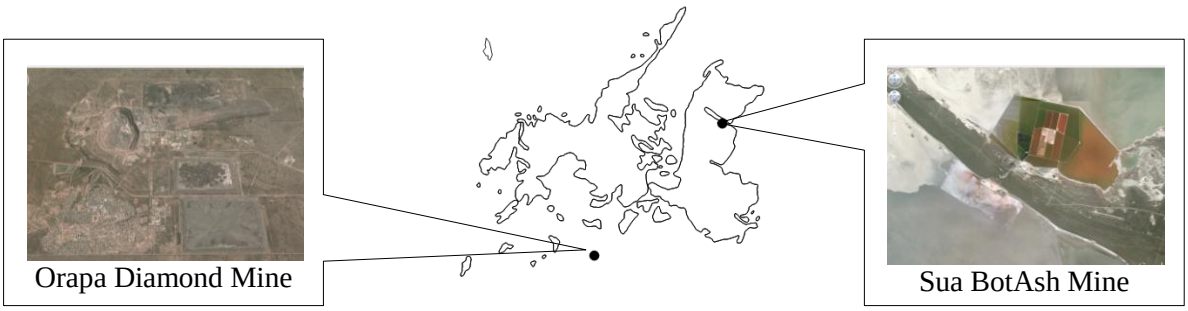

Figure 5.12 Map indicating the location of the large two industrial operations within the Makgadikgadi Basin.

Human influence in the region is not limited to crop and live stock farming, with two large mining activities located within close proximity to the pan (Setlhogile et al., 2011). The primary influence of these industries on the pan is through the extraction of ground water. Ground water extraction has been widely considered in the response to dust activity (Saint-Amand et al., 1986; Reheis & Kihl, 1995; Reheis, 1997). While large expanses of the pan are mostly undisturbed (Setlhogile et al., 2011), sub-surface brine extraction occurs at two locations in the Makgadikgadi Basin.

The first, a soda ash mine (BotAsh) located on the Sua spit is a significant anthropogenic influence on the system (Coakley, 2003) (*Figure 5.12*). This industrial setup includes over 100 well points located on the surrounding pan, which pump approximately 2400 m^3 of sub-surface brine per hour (Coakley, 2003). The cluster of dust sources to the west and south west of the spit could be in response to the changes in ground water and salinity and could be responsible for increasing the emissivity of the region.

The second, the Orapa diamond mine, has two well fields located within the Makgadikgadi wetland system (Setlhogile et al., 2011). Despite being further away, Setlhogile et al (2011) indicate that the mine extracts more than double the volume extracted by BotAsh, with similar estimated recharge

values. Therefore, despite being located further from the pan complex, activities at Orapa could be affecting the ground water and hydrological state of the southern margin of the pan system.

Four key influencing factors have been presented for the trend observed in spatial emission characteristics, while not exhaustive of the possible drivers, they include:

i. naturally occurring trends in seasonality of wet and dry cycles including surface moisture,
ii. variations in pan surface chemistry and sediment supply,
iii. human alteration of pan surface through agricultural and pastoral impact, and finally
iv. ground water extraction from the local industry.

It is likely that these factors in combination explain much of the observed spatial variability. Further, as many of these factors will be spatially discrete and seasonally dependant, it is proposed that regions will have individual responses on seasonal, annual and inter-annual scales. Regardless of all the spatial variability, the system produced dust with a clear peak dust season (*Figure 5.6*). As dust emission is controlled by both surface and climatic drivers, the following section will consider the synoptic scale features responsible for emission from the pan surface.

5.5.2 Climate Drivers of the Makgadikgadi System

Despite the relative infrequency of dust events, the duration of the study, and the assumption that the 7 year time period reflects a range of seasonal and inter-annual cycles, allows for the analysis of weather systems responsible for emission. Understanding the circulation features associated with emission makes it possible to determine the local and regional transport and regional impact.

The following discussion will present an analysis of the circulation features identified on all days on which plumes were detected. While earlier work by Tyson et al. (1996b), viewed regional circulation features as a function of five systems, all of these were found to result in dust. Therefore, as this level of classification does not eliminate the potential of any circulation to produce dust, an additional number of synoptic states needed to be considered. Consequently, in order to try and refine the understanding of systems responsible for plumes, the ten states as outlined by Tyson and Preston-Whyte (2000) will be used for further discussion. Using these 10 states, it was observed that dust plumes were emitted on eight of the ten dominant circulation features. With southerly meridional flow and the cold snap circulation features, the only two not to be attributed to a dust event. The following discussion will consider the synoptic setting for each event (as discussed in section 5.2) in accordance with Tyson and Preston-Whyte's (2000) classifications of features of southern Africa.

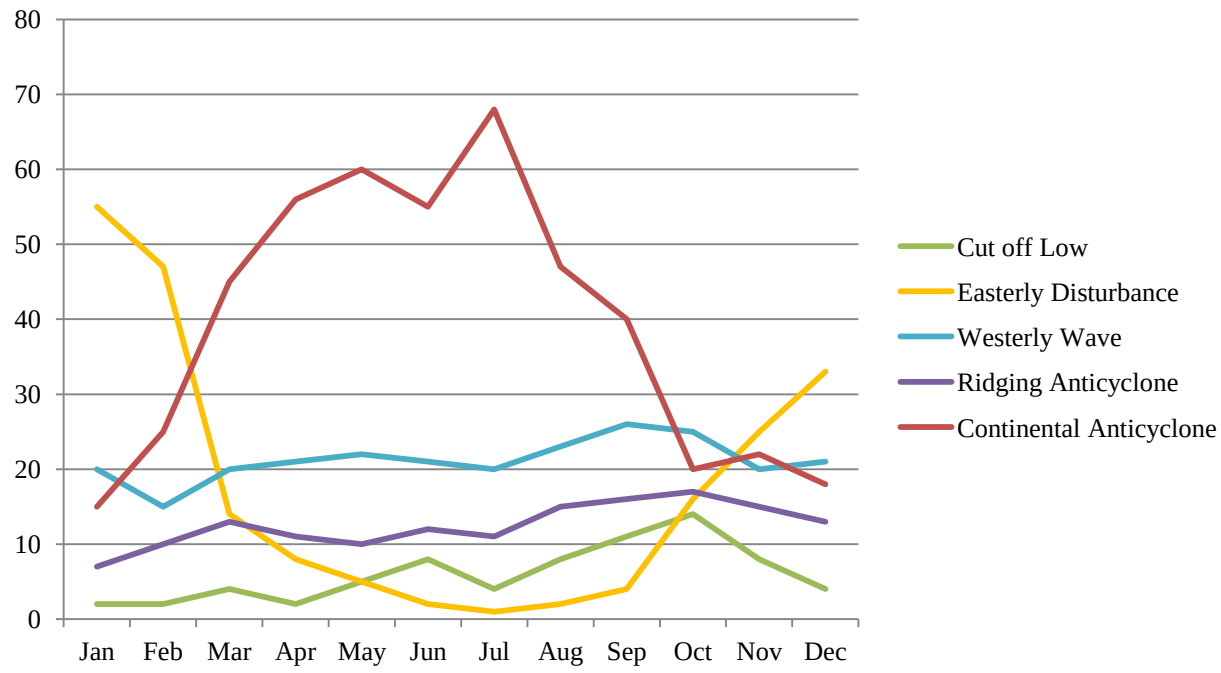

Figure 5.13 Monthly frequency of occurrence of major circulation features affecting southern Africa, for the five year period 1988-1992. Modified after Tyson 1996b.

The dust season was observed to peak between June and August, which from Figure 5.13 can be seen to be months associated the continental anticyclone with the lesser influence from westerly waves; ridging anticyclones; cut off lows; and towards the end of the season tropical easterly disturbances. Additionally, these months are associated with the peak average wind speed over the region as identified by Tyson and Preston-Whyte (2000). These accelerated wind speeds are associated with the continental anti-cyclone, which dominates circulation over the interior during the dusty (Bryant et al., 2007; Vickery et al., 2013) winter months (Tyson et al., 1996a; Tyson et al., 1996b; Piketh et al., 2000) (*Figure 5.13*). Due to its persistence in these months, it would be assumed that the presence of this feature would commonly be associated with dust emission. However, this was not confirmed in this study with the continental anticyclone only producing 28 plumes on 7 days. This circulation feature was proposed by Tyson et al. (1996b) and Tyson and Preston-Whyte (2000) to occur on between 65% and 70% of days between July and September (*Figure 5.13*). Assuming the frequency proposed by Tyson et al. (1996b) a possible 581 days were dominated by the continental anticyclone between 2006 and 2012, only 7 of these produced dust which equates to 1%. Tyson and Preston-Whyte (2000) indicate that this system is most commonly associated with surface divergence and strong subsidence. However, periodically localised within the system upward motion can dominate. This periodic reversal could be responsible for dust emission from this otherwise stable subsidence dominated system. Alternatively, regional intensification of the high pressure could produce sufficiently strong surface winds required to entrain dust from the highly crusted surface (Gillette et al., 2001) (see Chapter 3 for further information on crusts). Despite the relative infrequency of emission, the plumes that were transported by the continental anticyclone were associated with west

to south west trajectories, with plumes averaging 68 km in length in the satellite imagery, extending to over 300 km following 24 hours of transport.

Additionally, the nature and seasonal persistence of the anticyclone has been proposed to be an important air quality determinant for southern Africa. Tyson and D'Abreton (1998) and later Piketh et al. (2000) analysed the patterns of aerosol recirculation over southern Africa during the austral spring. While much of the focus of this research was on industrial and biomass burning derived aerosols (Abel et al., 2005), mapping of air transport trajectories revealed that the high pressure system resulted in recirculation of air masses over periods of 10 to 21 days (Tyson & Preston-Whyte, 2000). Tyson and Gatebe (2001) analysed the composition of the re-circulated aerosols revealing that, in the coarse fraction, almost 85% was composed of soil derived dust, decreasing to 36% in the fine fraction. Through analysis of the southern Africa domain (Vickery et al., 2013), the Makgadikgadi Pans are the most prominent source of soil derived dust in the interior and are the likely contributor of much of this aerosol load. Conversely, industrial sulphur was dominant in the fine fraction, with biomass burning and marine aerosols completing the detected load. This highlights that, despite the relative paucity of emissions associated with the anticyclone, the recirculation of aerosols within the system can increase the transport and range of influence that Makgadikgadi sediments can have in southern Africa. The fine to coarse ratio observed at Ben MacDhui (Tyson & Gatebe, 2001) reveals that, similar to surface conditions (Chapter 2), Makgadikgadi aerosols occupy a relatively coarse mode despite significant transport from source. The authors add that the recirculation of aerosols has an impact on regional biogeochemical cycles, including the delivery of nutrients to the Okavango Delta. This assumption of regional chemical recycling associated with the continental anticyclone confirms that through transport and subsidence within the system wet and dry deposition must be present.

Therefore, despite the persistence of this circulation feature during the dust season, it is not this system alone, but rather the changing dominance between this system and others, or possibly the intensification of the continental high, that produces dust. Additionally, recirculation associated with the continental anticyclone can increase the impact of entrained aerosols through prolonged transport duration and through recirculation increase the area over which aerosols may be deposited.

The second most frequently detected synoptic state associated with dust days was the ridging anticyclone. This feature occurs on between 10% and 17% of days between May and October (Tyson et al., 1996b) (which equates to between 3 and 5 days monthly), however only 18 days produced dust (*Table 5.5*) between 2006 and 2012. Therefore, out of a potential almost 24 days per year (168 days between 2006 and 2012) approximately 10% of days with this feature resulted in an emission. However, the importance of this system is not only viewed by the number of days on which emission occurred; through this system 55 plumes were emitted between May and October of 2007 to 2012 making this system responsible for the greatest number of plumes. Additionally plumes were detected

to be approximately 75 km long on satellite imagery, extending to on average almost 400 km in 24 hours. As this system is experienced year round at approximately the same frequency (*Figure 5.13*) surface controls must be present to result in a strong seasonal signature to the emission frequency.

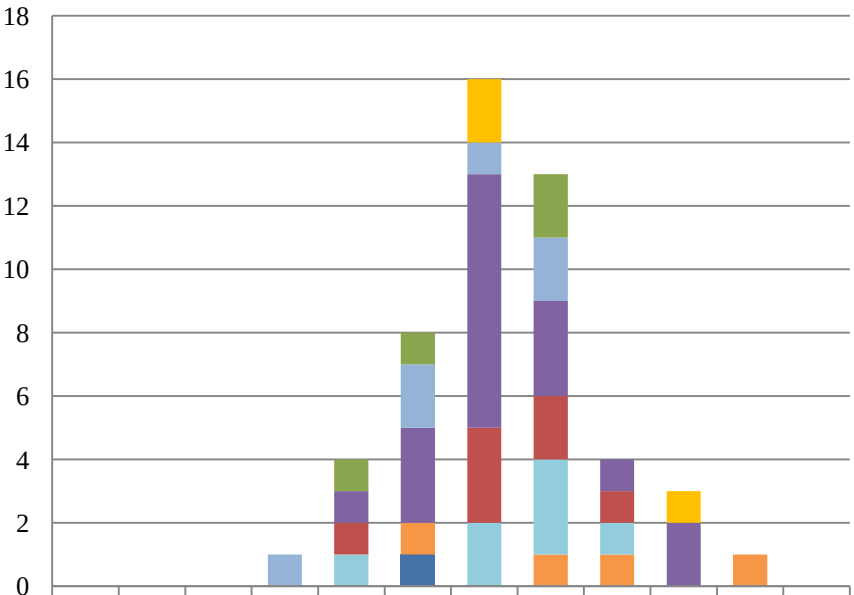

	Jan	Feb	Mar	Apr	May	Jun	Jul	Aug	Sep	Oct	Nov	Dec
Cut off low					1	1		2				
Easterly Wave low							2			1		
Westerly wave low / trough				1		2	1	2				
Ridging Anticyclone					1	3	8	3	1	2		
Continental Anticyclone					1		3	2	1			
West Coast Trough					1		2	3	1			
TTT						1		1	1		1	
Coastal Low						1						

Figure 5.14 Plot of circulation features responsible for dust emission by month.

Tyson and Preston-Whyte (2000) classify the ridging anticyclone as a temperate disturbance in the westerlies, which highlights the importance of activity in the temperate latitudes for dust emission from the Makgadikgadi Pans. However, despite its origin in the westerlies, its circulation extends into the interior and is recognised by Tyson and Preston-Whyte (2000) to be a greater contributor of sub-continental aerosols to the Atlantic than the continental anti-cyclone, through both recirculation and percentage frequency. Therefore, both the continental and the ridging anticyclone are recognised to be important for recirculation and transport of aerosols to both the Atlantic and Indian oceans; with the presence of either circulation alone not prescriptive of a dust event.

The temperate latitudes also introduce westerly wave lows and troughs, which influence the circulation of southern Africa. These cyclonic westerly wave disturbances bring rain to the south of the continent blocked by the continental high pressure which dominates the sub-continent (Tyson &

Preston-Whyte, 2000). However, on occasion they have the potential to extend into the interior with extreme and dramatic effects (Tyson & Preston-Whyte, 2000). This was confirmed through an observation at case study level by Resane et al. (2004) who identified that a westerly wave low was associated with a particular event referred to as 'The day of the white rain', which saw an unusually strong westerly wave low extending over the interior. The associated transport was in a strong southerly direction, resulting in the deposition of sediment over Johannesburg. This sediment, deposited through wet deposition, was determined through chemical analysis, to be sourced from the Makgadikgadi Pans (Resane et al., 2004). A similar synoptic scale event was observed on the 26th of October 2006. Although the influence of the westerly wave low was not experienced as far north, with the centre of the systems low pressure being located at approximately 18°S. This is noticeably further north than all other events identified from this source in this study which averaged at approximately 25°S. These westerly wave disturbances were determined to be important as combined 26 plumes were produced on 13 days. While the westerly wave low/troughs produced 9 plumes on 6 days, the plumes were notably longer in extent than the 17 plumes on 7 days produced by the west coast trough.

The final circulation feature classified as a temperate westerly disturbance is a cut off low (Taljaard, 1982). Cut off lows are more intense forms of the westerly wave trough with biannual peaks in late summer (March to May) and late winter (August to November) (Tyson & Preston-Whyte, 2000). These characteristically inter-seasonal features are known to experience high inter-annual variability. While travelling anti-clockwise along the coast, these systems often produce widespread floods and extreme weather throughout southern Africa (Taljaard, 1982). On four occasions in 2009 – 2012, cut off lows produced short plumes (40 km to 70 km on satellite imagery), which travelled in a southerly direction in 2011 and 2012 (212 ° and 221°) while travelling north in 2009 and 2010 (305° and 46°). These two pathways are in response to the location of the low. In 2009 and 2010 the centre of the low was on the west and south west coast of South Africa with the continental high pressure remaining dominant over the interior. However, in 2011 and 2012 the coastal low was further up the east coast in the Mozambique Channel. This resulted in the circulation associated with the low pressure and cyclonic circulation and northerly transport off the pan. As the peak of these systems coincides with the end of the wet season, and then again at the start of the wet season in Botswana, they are not commonly associated with dust emission due to the presence of moisture on the surface controlling emission.

The location of southern Africa and the seasonal cycle of the ITCZ results in strong seasonal signatures to circulation (Nicholson, 2009). Therefore, westerly waves were observed to produce dust in the early dust season, while their effects drop off towards the end of the dust season (early austral summer), as easterly circulation dominates again blocking the effect of these systems (Tyson et al., 1996a; Tyson et al., 1996b; Tyson & Preston-Whyte, 2000). Therefore, the influence of the five

temperate dust producing disturbances in the westerlies have limited windows in which their influence can occur.

While westerly waves disturbances are a feature of the early dust season, easterly wave disturbances are commonly associated with summer circulation over the region and therefore the wet season in the interior (Lindesay, 1998; Tyson & Preston-Whyte, 2000). Despite this, easterlies are known to occur "...rarely between April and October..." (Tyson & Preston-Whyte, 2000: 195) and it is these atypical easterlies that produced three dust days, two in July of 2006 and one in October of 2009 each with a single plume. These dust plumes, which travelled in a south westerly initial trajectory, were entrained in the anti-cyclonic flow associated with the low pressure easterly wave (Tyson et al., 1996b).

Another circulation feature not explicitly identified by Tyson and Preston-Whyte (2000), is the tropical temperate trough (TTT). This system connects the disturbances between the tropics and the mid-latitudes (Ratna et al., 2013) and while it is more typically associated with rainfall over the interior (Todd & Washington, 1999), here it was identified as being associated with six dust plumes on four days. Ratna et al. (2013) present the annual frequency of TTT events to be between zero and four per year between 1980 and 2009 with an average of two per year. The authors additionally present that in 2007 there were two TTT events, of which one was associated with a plume; similarly, two TTT events in 2009 saw a further dust day with two plumes. While four TTT events in 2008 saw only one dust day with two plumes. The presence of these troughs in the early stages to the east of the basin results in an intensification and south east shift of the high pressure system over the interior. The associated anti-cyclonic circulation of the shifting high results in a larger southerly component, while the approaching trough increases the westerly component of transport. As TTTs are typically dominant during the summer months and therefore occur later in the dust season; the events described here were observed to occur later in the dust season, with a 300 km long defined plume in November of 2007. The six TTT plumes were associated with transport from the shifting high with south to south-westerly transport observed. The relatively infrequent occurrence of these systems combined with the high association between a TTT event and a dust event highlights the importance of these systems for dust transport for the Makgadikgadi Pans.

The final noteworthy circulation system associated within this region is the presence of a coastal low to the west of the pan complex. Like the cut off low, the effect of the coastal low, while indirect to the pan system, influences of the location of the main continental pressure systems. This was observed through the west-east location of this system influencing plume bearing, with a greater southerly component expected with a greater westward location of the low. During this period of study, only a single coastal low was determined to produce a dust event; this produced similar circulation features to the westerly wave trough, although a more intensified version of this feature (Tyson et al., 1996b). The location of this system to the west of the domain suggests that it is the perturbation in circulation

to the east that is imposed by this system, rather than the system itself, which is responsible for dust emission.

Table 5.6 Results of number of plumes by circulation feature as per Tyson and Preston-Whyte (2000) by year.

	Year							
Circulation Feature	**2006**	**2007**	**2008**	**2009**	**2010**	**2011**	**2012**	**TOTAL**
Coastal Low		1						1
Continental Anticyclone	1	1	1	1	3			7
Cut off low				1	1	1	1	4
Easterly Wave low	2			1				3
Ridging Anticyclone		3	6	5	1	2	1	18
TTT		1	1	1			1	4
West Coast Trough		1		2	3		1	7
Westerly wave low / trough	1	1		2	2			6

The discussion above has presented that significant inter-annual variability between dust producing synoptic features was observed (*Table* 5.6). Moreover, no single feature was observed to produce dust in all years, with the dust production of most years reliant on multiple features. With the exception of the coastal low and a plume associated with a west coast trough, all systems resulted in a largely southerly to westerly transport (*Table 5.5*). The resultant plume trajectories ranged from southerly to northerly in a clockwise direction. This is represented by a mean bearing of 252° identified in this study. This confirms the findings presented by Bryant et al. (2007) and Washington et al. (2003) who observed an AI maximum (derived through the TOMS product) to lie to the south west of the Makgadikgadi Pans.

Therefore, despite the earlier assumptions that it is the continental anti-cyclone which dominates emission, it is in fact a number of systems which result in emissions. It was also found that regardless of the system into which the dust was entrained, transport appeared to be consistently in a south westerly direction, remaining within the large scale upper air circulation as determined through HYSPLIT trajectory analysis. This confirms that, once entrained, continental scale circulation and recirculation determines the trajectory of the aerosols. Ryder et al. (2013) observed that Saharan aerosols larger than 20 µm had an airborne life time in the order of 12 hours. This suggests that a large percentage of the detected silt and clay sized particles could be associated with great transport and therefore results in a relatively large downwind footprint. HYSPLIT plots which ran for 24 hours indicated that the air parcel is likely between 200 and 400 km from the pans, therefore even in just 12 hours the air parcel and entrained aerosols are likely further than 100 km from source. Additionally Mahowald et al. (2013) suggest that these coarse aerosols become preferential cloud condensation nuclei, produce the largest short wave radiative effect per unit mass and due to the chemistry of the coarse fraction have high biogeochemical impact.

Correlating the proposed frequency of circulation features as per Tyson et al. (1996b) with dust emission, it is revealed that the region was not satisfactorily active. Easterly and westerly wave disturbances and the continental anti-cyclone produce dust far less frequently than they occur, suggesting that the presence of the system alone is not sufficient to result in dust. However, tropical temperate troughs, as well as cut off and coastal lows, which are stronger deeper features, often associated with extreme weather throughout the domain (Tyson et al., 1996b; Resane et al., 2004), result in few but potentially stronger events. Therefore, it can be surmised that it is intensifications or perturbations to the dominant systems which are responsible for dust events during this period of the year. Additionally, due to the limitation of detection beneath clouds, dust plumes associated with thunderstorm downdrafts, which have been determined to be globally significant (Offer & Goossens, 2001; Strong et al., 2011), and are associated with localised interior disturbance, are not detected.

The seven year duration of this study has identified the variable nature of both atmospheric circulation and pan surface conditions. This is evident in the number of systems which produce dust and the inter-annual significance of differing systems. Despite this variability, through the correlation of events to the synoptic circulations dominant on the day and days preceding the event, it can be determined that for the Makgadikgadi Pans, a set of synoptic controls can be considered to be conducive to dust events. However, as only a fraction of the days on which these circulations occurred dust was produced, it can be proposed that an element of transport capacity limitation (Bullard et al., 2011) maybe be experienced at site. Additionally, through an understanding of surface chemistry and hydrological controls as presented by Bryant et al. (2007) availability limitations can be proposed for this system. Combined, these factors produce a highly variable system in terms of emission characteristics and inter-annual trends (*Figure 5.9*, *Figure 5.10*).

5.6 Conclusion

This study provided a seven year analysis of the Makgadikgadi Pan using true colour MODIS imagery. Due to the high resolution used in this study, it was possibly to derive a sub-basin scale emission signature for the region. Additionally, the resolution provided by Terra and Aqua allowed for the identification of specific source areas, which provided the potential to link to micro-scale erodible features and surface controls. Within the basin at half a degree resolution, three regions were identified to be dominant occurring on both the southern margins of the Ntwetwe and Sua Pans and the final on the central-western region of Sua Pan. Analysis of sub-basin scale chemistry confirms the variability in pan surface chemistry (see Chapter 3) with similarly variable results presented for grain size (see Chapter 2). Additionally, ground water and surface moisture controls were considered, which, when viewed with anthropogenic influences, could explain the highly variable spatial and temporal signature of the pan.

Despite this variability, there appears to be a set of synoptic drivers which are conducive to dust entrainment and associated transport over southern Africa at both regional and more local scales. However, analysis of individual events and the correlation with the proposed frequency as determined by Tyson et al. (1996b) (*Figure 5.13* and Figure 5.14 and *Table* 5.6), revealed that the system was not suitably emissive. As analysis of pan sediment revealed that there was an abundance of fine grained sediment within the profile, it cannot be supply limitations controlling emissivity. This therefore suggests that either transport capacity or availability limitations are controlling emission.

Chemical analysis (Chapter 3) confirms the presence of salt within the system and therefore the potential for surface crusting. This was observed to cap the available fluff which presents an availability limitation for the system. However, as synoptic states were observed to repeat within a short period, with dust plumes resulting on one day and not on another, it suggests that the system must also be limited by transport capacity. This transport capacity limitation is particularly important in the context of the Makgadikgadi, since the large pan system is located in an area devoid of major topography. Therefore, unlike acceleration of the low level jet in the Bodélé Depression, in response to the regional topography (Engelstaedter & Washington, 2007a), here it is the strength of the wind as driven by the synoptic system alone that is required to produce dust. This proposed limitation of transport capacity confirms earlier proposals by Washington et al. (2003) and indicates why viewing synoptic controls in isolation did not determine the potential for dust events.

While synoptically the system remains largely unpredictable, due to the availability of two images per day it was possible to determine the temporal response of the system. It was observed that there was morning dominance in the emissions from the pans. With 111 of the plumes identified occurring on the Terra platform, while only 12 occurred on Aqua. As plumes were mapped to be most commonly between 0 and 50 km averaging just over 70 km, this indicated that emission was earlier than the satellite overpass, and that at time of detection, transport had already occurred. The character of the plumes showed that the head of the plume was the most concentrated, with increased dispersion detected with transport. However, very little can be inferred from the plume length as timing of initial emission cannot be determined. Despite this, mapping of plumes can be compared with the dominant circulation, and reveal that plume trajectories mapped closely with the dominant circulation. Therefore, while satellite derived plume length does not provide great insight into the nature of dispersion and large scale circulation, the addition of trajectory analysis resulted in the possibility of determining air parcel transport. This revealed that, within 24 hours of emission, aerosols were 400 – 500 km from source to the south west of the pan regardless of synoptic state for emission.

Due to the links between transport direction (mapped plumes) and large scale circulation (HYSPLIT air parcel trajectory analysis) it can be confirmed that once entrained aerosols from this region are

transported, the dominant synoptic scale circulation and associated recirculation occurs (Tyson & D'Abreton, 1998).

Finally, this study has allowed for the potential to attribute aerosol load to specific circulation features, and through this, the potential to revise aerosol loads in the southern African haze layer. This has been particularly visible through HYSPLIT, which has provided a significant advancement through our ability to understand where aerosols are transported once entrained, as well as increasing our ability to predict dust storms and attribute aerosol load to a set of synoptic drivers.

5.7 Concluding Remarks

The results of this chapter provide direct links between the different weather systems driving dust emission, quantitatively confirming south westerly transport off the pan, while presenting that a number of synoptic states are responsible for emission. The analysis of the synoptic scale circulation and dust events indicates that a 7-year period may be long enough to detect cyclicity. For a more complete picture, especially with respect to possible effects of climate cycles, multi-decadal data is required. Additionally, correlating the synoptic state with local wind speeds and within the context of the seasonal and annual rainfall trends would reveal important context to both surface and sub-surface moisture conditions and important hydrologic controls (see Bryant et al., 2007) (*Figure 5.11*). The main conclusions of this chapter can be summarised as follows:

i. No single factor or condition could explain the pattern, frequency or distribution of dust emission from this source. Reynolds et al. (2009) confirm that understanding controls on dust emissions remains challenging due to the highly variable response to seasonal and inter-annual climate. This is proposed to be further complicated by the size of the basin (Goudie & Wells, 1995; Shaw & Bryant, 2011) and the variability observed within large systems. Therefore, additional investigation of local wind strength, mineral crusts and hydrological context are all required to assist in understanding this system.
ii. There was a high degree of both spatial and temporal variability to emissions. Inter-annual variability revealed that 2009 was the dustiest year with 59 plumes on 13 days, while 2006 and 2012 were the least dusty years with 4 and 5 plumes on 4 days each respectively.
iii. Dust plume activity from the Makgadikgadi Pans peaks in July, with the dust season occurring between April and November. The highest frequency of dust days occurs between June and August. Bryant et al. (2007) suggest that hydrologic controls are the main determinant of this seasonal signature.
iv. Emission timing showed morning dominance, with 90% of plumes detected on Terra overpass images. This confirms findings by Krishna (1968) who suggests a morning wind speed peak at mid-latitudes in the absence of local topographic forcing.

v. Despite the seasonal persistence of the continental anticyclone, it was the ridging anticyclone that produced the most dust days and plumes in the time period.
vi. Although dust was emitted through a number of systems, transport was consistently from the north east resulting in south westerly plumes, consistent with earlier findings by Bryant et al. (2007) and Washington et al. (2003) are inferred through the location of AI maximum to the south west of the pan complex.
vii. Spatially, Ntwetwe was the dustier of the two pans within the Basin producing 73 plumes, while Sua only produced 50 plumes in the time period. Additionally, both pans produced regions which were dustier than others, and these occurred largely on the pan margins.

While dust activity from the Makgadikgadi Pans is not a new finding, as it has been previously identified (Prospero et al., 2002; Washington et al., 2003; Resane et al., 2004; Bryant et al., 2007; Wood et al., 2011; Vickery et al., 2013); that understanding the synoptic controls and revealing the sub-basin scale emission characteristics over an extended time period has the potential to reveal further insight into the nature of this highly variable yet important mineral aerosol source.

Chapter 6: The Makgadikgadi Pan as a Dust Source

6.1 Introduction

The need for better understanding of the role of atmospheric dust in the global climate system has led to research in the causes of dust variability in space and time (Engelstaedter et al., 2006). Developments of satellite products and global models have increased our understanding of source region and transport pathways, while simulating patterns of distributions and impacts. Despite the many advances, Bullard (2010) indicates that modern global models of earth-atmosphere-ocean processes are becoming increasingly sophisticated but still require validation against empirical data and observations (Bullard, 2010: 496). A recent field campaign has improved our understanding of processes and surface conditions on the Makgadikgadi Pans. Multiple *in situ* measurements, together with a suite of chemical and morphological analysis of both surface and entrained samples, has dramatically increased our understanding of this important yet variable emissive surface. With a focus on the Makgadikgadi Pans, the degree to which the dust emissions are controlled by spatial variations and temporal controls was investigated through the use of physical and chemical analysis of surface conditions and set in the context of a seven year emission frequency study.

6.2 Conceptual Model of the Pan as a System

Earlier chapters have considered various aspects of the pan system; however, in order to understand the processes which control the emission and state of the system fully, we need to consider: grain size and surface texture (Chapter 2); chemistry (Chapters 3 and 4); and spatial and temporal characteristics leading to limitations and chemistry, grain size and transport induced controls (Chapters 3,4,5). This chapter will discuss the pan environment within the general literature of pans as dust sources and contextualise the role of the Makgadikgadi Pans within a global context.

Similar studies on dust source regions have considered much larger producers where there is an abundant supply of sediment (e.g. Sahara) or multiple geomorphological units Lake Eyre Basin (LEB) (Baddock et al., 2009). Therefore, unlike other large dust producing regions globally – e.g. LEB (Australia), Chihuahuan Desert, (North America – USA and Mexico) (e.g. Rivera Rivera et al., 2010), and the Taklamakan Desert (China) (e.g. Okada & Kai, 2004) – the Makgadikgadi pan surface at a first glance can largely be classified as a single relatively homogenous geomorphic unit.

However, it is apparent that emissions from the pan surface are subject to considerable spatial and temporal variability, with Gillette et al. (2001) confirming that variability can even occur within a single playa or source region. These have been determined to be a function of:

i. the solute movement through the capillary zone,
ii. the introduction of fresh water,
iii. salinity balance,
iv. flood and draught cycles,
v. climate change and anthropogenic activity.

Such a high degree of variability can be attributed largely to the interplay between surface properties and the hydrogeochemistry, particularly with respect to the precipitation of different types of salts as well as crust strengths (Reynolds et al., 2007).

6.3 The Pans as a Dust Source

Any terrestrial surface with a supply of suitably sized sediment and an appropriate wind regime can be a dust source (Bullard, 2010). However, within this definition, a classification of preferential sources (Bullard et al., 2011) can be derived such that surfaces can be differentiated into a number of geomorphic units of differing importance (*Table 6.1*). These are driven largely by factors including:

i. surface roughness,
ii. climate,
iii. setting,
iv. topography and
v. sediment availability (Prospero et al., 2002; Washington et al., 2003; Bullard, 2010; Bullard et al., 2011).

6.3.1 Emission Source/ System Typology

The Makgadikgadi has been classified as a large inland ephemeral basin (Cooke, 1979; Helgren, 1984; Thomas & Shaw, 1991) although these studies have used this classification largely in terms of a geomorphic unit, rather than a surface characterisation considering variable dust emission potential. In general, arid inland basins have been identified to be important emissive geomorphological units due to their ability to act as sediment receptacles (Pye, 1987; McTainsh et al., 1999; Prospero et al., 2002; Washington et al., 2003; Reheis, 2006b; Bullard et al., 2011; Bryant, 2013). This classification is further sub-divided to represent the differences and possible emission controls as experienced at source to include: wet lake; ephemeral lake; dry, consolidated; and dry, non-consolidated. This differentiation between wet and dry corroborates the theory discussed by Reynolds et al. (2007) who stress the role of shallow ground water in shaping the pan surface. An earlier paper by Reheis (2006b) also indicated that studies on dust generation needed to differentiate between wet and dry systems, noting that this difference affected both dust generation and dust depositions. Reheis (2006b) expounded that dry pans respond by emitting dust in dry periods after major storm events

deliver fresh sediment and (or) destabilise the surface crust, while wet pans emit dust as a response to capillary rise and surface evaporation.

The ephemeral Makgadikgadi can be classified as type 1b lake system. Therefore, it produces dust in response to seasonal rainfall, capillary zone transport, surface crusting and desiccation (*Table 6.1*).

Table 6.1: Identification of surface geomorphologies (preferential types), their soil texture and limitations resulting in their contribution and relative importance in dust emission schemes (Adapted from Bullard 2011).

	Preferential Type	Emission Sources	Soil Texture	Limitation	Importance
1a	Lakes	Wet	Sand, Silt, Clay	Availability - limited	Low
1b		Ephemeral	Silt, Clay	Supply - limited	High
1c		Dry, consolidated	Silt, Clay	Availability - limited	Low
1d		Dry, non consolidated	Silt, Clay	Transport capacity limited	High
2a	High relief alluvial systems	Armored, incised	Mega-gravel, Gravel, Sand	Availability - limited	Low
2b		Armored, unincised	Mega-gravel, Gravel, Sand	Availability - limited	Low
2c		Unarmored, incised	Gravel, Sand, Silt, Clay	Supply - limited	Medium
2d		Unarmored, unincised	Sand, Silt, Clay	Supply - limited	Medium
3a	Low relief alluvial systems	Armored, incised	Gravel, Sand	Availability - limited	Low
3b		Armored, unincised	Gravel, Sand, Silt, Clay	Supply - limited	Medium
3c		Unarmored, incised	Sand, Silt, Clay	Transport capacity limited	Low
3d		Unarmored, unincised	Sand, Silt, Clay	Supply - limited	Medium
4	Stony Surfaces	Stony surfaces: low angle surfaces not connected to fluvial source of fines	Gravel, Sand, Silt, Clay	Availability - limited	Low
5a	Aeolian systems	Sand sheet	Sand	Supply - and/or availability - limited	Medium
5b		Aeolian sand dunes	Sand	Supply - and/or availability - limited	Medium
6		Loess	Silt, Clat	Availability limited	Low
7	Low emission surfaces	Low emission surfaces: bedrock, rocky slopes, duricrust (snow/ice permanant cover)	Mega-gravel, Gravel, Sand, Silt, Clay	Supply - limited	Low

The following discussion will examine the functioning of the Makgadikgadi Pans within the framework outlined in Bullard et al. (2011), determining the applicability of associating the source with the classification of an ephemeral lake.

6.3.2 Textural Soil Type / Material Characterisation

The Makgadikgadi has been ranked among the top ten dustiest places on earth (Washington et al., 2003), with no reference being made to the surface conditions, sediment supply or budget. The pan complex has further been identified as an un-vegetated ephemeral pan with a supply of fine sediment. Due to the known importance of pans, they have been considered extensively in dust literature (Prospero et al., 2002; Mahowald & Luo, 2003; Washington et al., 2003; Bullard et al., 2008), however, their emissivity is often poorly quantified. This is often associated with the lack of textural surface characteristic data, including size distribution and surface roughness for such regions. In light of this, determining the nature of these variables is essential in characterising a region. Bullard (2010) reveals that textural information for dust models was traditionally derived through global databases

which did not correlate well with actual surface conditions (Bullard, 2010). Furthermore, Chatenet et al. (1996) add that the soil texture data commonly refers to particle sizes determined from dispersed or disaggregated sediments, which may not reflect particle sizes in the field.

Throughout the DO4 field campaign, measurements of surface crusts, texture, strength and emissivity were taken. The results of these field tests suggest the natural state of surface conditions would not be obtained through sampling dispersed or disaggregated sediments. Therefore subsequent laboratory testing (Chapter 2) using conservative ethanol processing presented a surface dominated by sand (~80%) and silt (~20%) sized grains with minimal contribution of clays ~2%. However, through digestion a surface with high emissive potential (6% clay, ~50% silt and ~44% sand) is revealed. Furthermore, Chapter 2 revealed that the fine clay and silt size particles detected following digestion occurred as coarser sand size aggregates in the undigested (natural) sample; a phenomenon observed in other salt rich environments globally.

While these digested results allow for direct comparison with other source regions, as classification schemes largely adopted methods of digestion in quantifying results for surface modelling (Chatenet et al., 1996), they do not present the natural state of the pan surface. Furthermore, the digested results present a dominantly silty system, which is notably coarser than other dust producing regions elsewhere, with much of the sediment above the threshold proposed for aeolian transport. Similarly, the ethanol processed undigested sample presented a sand, silt, and clay dominated system. The inclusion of sand reveals a coarser grain size distribution than indicated by Bullard et al. (2011) for an ephemeral system, although makes reference to the chemistry of the system. Therefore, it can be proposed that regardless of the method of grain size determination, the pans contain a relatively coarse sediment supply

In addition to this coarse nature, the vertical structure of the pan presents a crust capped surface. Similar crusts have been extensively considered in literature (see section 3.3.2.1 in Chapter 3) particularly as limiting factors to emission. The following section will consider limitations acting at the source.

6.3.3 Limiting Factors

In determining the emissive nature of a system, sediment supply and transport are the key parameters. For lake systems, as proposed by Bullard et al. (2011), these parameters are all important and these surfaces can further be associated with all three limitations; source, supply and transport.

i. supply limited - lack of suitable sediment,
ii. availability limited - where sediment is available but not readily entrainable, and
iii. transport capacity limited - insufficient wind capacity to result in entrainment.

The following section will consider the applicability of these limitations to the Makgadikgadi.

6.3.3.1 Wind Regime and Transport Capacity

In line with findings by Bullard et al. (2011), the ephemeral character of the pan surface would not likely present transport capacity limitations. On a regional scale, this was confirmed in Chapter 5, through the identification of numerous synoptic scale features which resulted in emission. However, on a local scale transport capacity limitations occur as a result of the surface crusting and high salt content. Field observation identified a near continuous surface crust occupying much of the pan surface, which introduces transport capacity limitations (Nickling & Ecclestone, 1981; Gillette et al., 1982; Cahill et al., 1996; Rice et al., 1996; Gillette et al., 2001; Langston & McKenna Neuman, 2005).

Consequently, it can be proposed that on a basin wide scale, the Makgadikgadi is associated with a wind and climate regime that, in most years, appeared to be sufficient to erode sediment from discrete areas on the pan surface. Large scale circulation and thermally driven local winds are likely to exert greatest control on the flat pan surface, which is unlikely to experience accelerated wind speeds due to the absence of topographic channelling.

Textural and material characteristics of the pan sediments, as presented in section 6.3.2 and Chapter 2, reveal that there is an abundance of sediment on site. While all results indicate that these are largely coarser than the definitions of dust, selective entrainment of the fines present suggest that supply limitations would be not commonly associated with this source. This largely eliminates supply as a controlling factor for the Makgadikgadi Pans. Therefore, the spatial and temporal variations in emission could be better attributed to changes in sediment availability driven by diurnal, decadal and multi-decadal changes in soil moisture and associated availability. Consequently, it can be proposed that surface crusting and soil moisture along with transport capacity provide greater limitations then sediment supply.

6.3.3.2 Crusts Leading to Availability Limitations

Chapter 3 provided a comprehensive review on the chemistry of the pan and crust characteristics, presenting a salt rich environment composed of halite, thenardite, mirabilite, trona and calcite. Rice et al. (1996) acknowledge crusts as major structural features of surface soils and sediments, with the degree of crusting being an important factor in the release/inhibition of fine particles from desert surfaces. Through both chemical analysis (Chapters 3 and 4) and field observation, the salt aggregates were found to be largely concentrated in the surface crust and below that in the highly emissive fluff. Chapter 4 identified that this emissive fluff was the most likely source of the dust load. However, as the crust was capping the emissive fluff, identifying the crust characteristics was an important factor in determining the emission potential of the region, with McTainsh and Strong (2007) suggesting that

biological crusts are more emissive than physical crusts in both the presence and absence of saltation. Buck et al. (2011) indicate that salt rich surfaces with the highest emissive potential are those that are associated with salts in both the hydrous and anhydrous phases in combination with seasonally fluctuating shallow sub-surface water. This is particularly relevant on this ephemeral surface with the co-incident detection of thenardite and mirabilite. These minerals are also presented to produce emissive surfaces as a result of their prismatic crystalline structure (Buck et al., 2011). Additionally, combined with carbonate and sulphate structures and diurnal temperature fluctuations such conditions promote salt heaving, which reduces the cementing effects of the salt producing thrust broken and ridged crusts. Therefore, despite the extensive crust that was observed to occur on the pan surface, conditions similar to those described above were present, which modified the crusts to produce broken ridges which exposed the finer fluff. This was particularly evident on the dryer surface sections of the study site. Reynolds et al. (2007) indicate that these natural processes, together with human activity and high winds, result in the mobilisation of aggregated sediments which act to disaggregate the crusted surface, resulting in emission. These high winds are noted by King et al. (2011) who comment on the increased sheer velocity (u*) required for transport on crusted surfaces, thereby suggesting that consolidated surfaces are subject to transport capacity limitations, in addition to availability limitations.

Analysis of emission frequency in Chapter 5 identified a number of discrete plumes at the beginning and end of the dust season. These plumes, following shoulder seasonal rains, are in line with observations by Reheis (2006b) who proposed that these rains destabilise the crusted surface, thus producing a dry system response. During the dry, dusty winter months, the capillary derived crusts break exposing sediment in line with proposed wet systems responses. Reheis (2006b) adds that the nature of salts which crystallise (recrystallise) on the pan surface have different effects on the emissive potential of the system, to salts which are drawn through the capillary zone; thus revealing that rain is an integral control in determining the nature and state of the surface (Rice et al., 1996). Elmore (2008) states that ephemeral crusts are more prone to dust generation than older developed crusted surfaces. Therefore, in determining the emissive nature of the system, both the state of the crust and wet and dry pan controls need to be considered.

In addition to the modification of the surface through seasonal rains, salt thrusting and heaving, and strong winds, crusts have been considered to be particularly vulnerable to disturbance by stock trampling (McTainsh & Strong, 2007) and human activity (Reynolds et al., 2007). With Leys and Eldridge (1998) indicating that disturbed crusts may lead to increased wind erosion rates, and that once initiated, saltation impact during wind erosion can itself break up crusts

6.3.3.3 Saltation as a limiting factor for availability

The introduction of saltation to the suite of mechanisms which can be relevant for predicting emission potential is well considered. With Wang and Jia (2011) stating that: "The basic mechanisms of dust emission is well understood; wind stresses impart momentum to sand size particles, which then saltate and release dust through surface sandblasting." (Wang & Jia, 2011: 1). With Kok (2011) adding that the cohesive forces between PM_{20} grains is often larger than the aerodynamic forces, such that saltation is an essential mechanism in promoting liberation of finer grains.

Piezoelectric saltation sensors (Sensits) were deployed to monitor the occurrence of saltation activity on the surface of the pan. However, data suggests that saltation is not a major contributor to the deflation process on the pan (Wiggs, G.F.S. 2013, *pers. comm.*, 31 December). This therefore introduces the concept of lack of saltation being a limiting factor in the destruction of crusts and liberation of the emissive material. However, the absence of saltation on the interior of the pan, does not exclude the potential of saltation on the pan margin. Unlike the pan centre, the pan margins are exposed to the Kalahari sands which are an abundant supply of sand sized grains with transport potential. This could be an additional driving factor for the increased dust potential observed on the pan margin. A further control which could explain the increased activity from the pan margins is rivers transporting sediments into the pan. The eastern margins of Sua could be indicative of this, as the Nata, Semowane, Mosetse Lepashe and Mosupe Rivers flow intermittently during the summer months into the basin (Hulsmans et al., 2006).

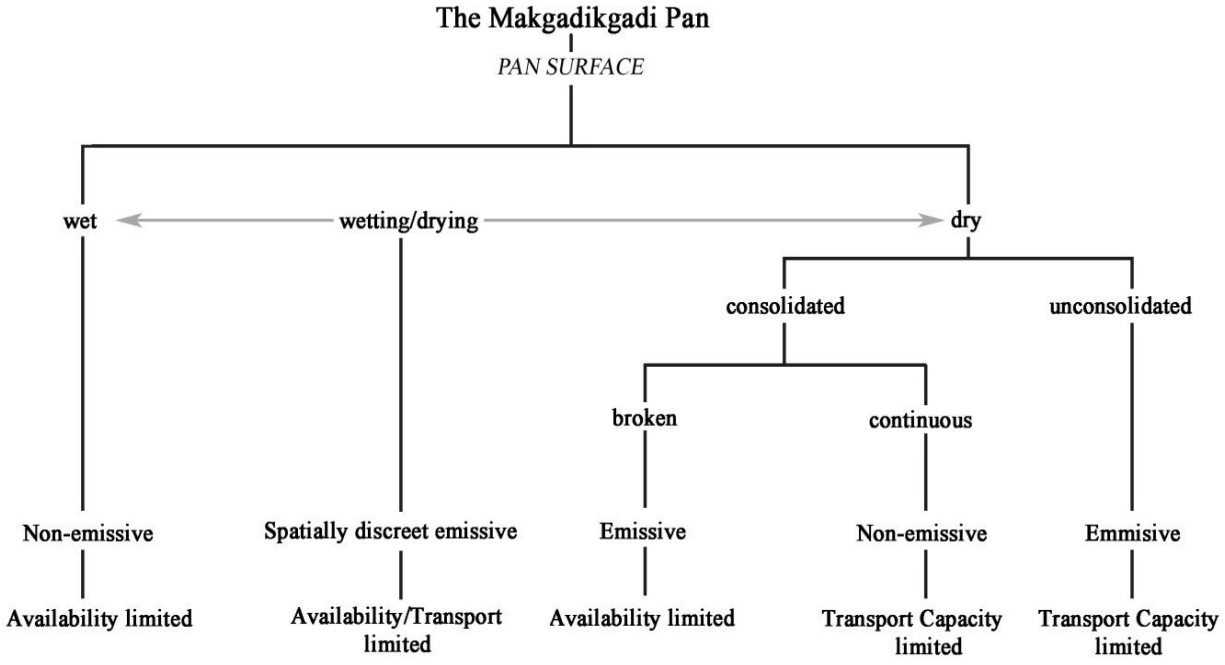

Figure 6.1: Representation of the controls which lead to determining the emissive nature of the Makgadikgadi Pans, considering the wet and dry controls proposed for the ephemeral pans.

So far, an ephemeral pan which emits as a function of seasonal limitation has been considered. Therefore, the definition provided by Bullard et al. (2011) that lake surfaces are classified to be either wet, ephemeral, dry consolidated or dry unconsolidated can be viewed as too simplistic. It can be presented that the Makgadikgadi Pans are better represented by both availability and transport capacity limitations, as a function of wet summers and dry winters (*Figure 6.1*). With the addition of wetting and drying during the shoulder seasons (beginning and end of the dust season) providing spatially discrete emissions as a function of both availability and transport limitations.

6.4 Classifying Characteristics of the Pan

The above discussion has considered various aspects of the pan, from simple geomorphic classification through to the various limitations that are considered for the surface. Due to the seasonal coverage of water, the Makgadikgadi conforms to the classification of an ephemeral pan. This has determined the supply of fine grained material derived through ground water, biogenic origin and fluvial controls (Bullard et al., 2011). In an ephemeral (Type 1b) system, the surface winds and soil moisture are known to be important controls on dust emission rates (Engelstaedter et al., 2003). Additionally, it is noted that surface water is reliably detected using remote sensing (Bullard et al., 2011), while soil moisture is better detected through field monitoring and as such there remains the need for empirical data and surface validation (Bullard, 2010). Therefore, during the DO4 field campaign on the Makgadikgadi Pans, soil moisture and surface winds were monitored and analysed, revealing that surface soil moisture accounted for much of the variation in emission and erosion thresholds (King et al., 2013). This study has shown that soil texture and chemistry may also exert additional emission controls on the pan surface.

While this study did not consider the analysis of soil moisture, characteristics of textural soil type and chemical analysis revealed the signature of the pan surface structure. These indicated that wet system processes driven by proximity to ground water (Reynolds et al., 2007) are also important drivers here. Additionally, direct surface wetting as well as groundwater recharge may enhance the subsequent evaporative concentration of salts at and just below the surface, which in turn is likely to increase the susceptibility to wind erosion as long as the water table remains below the surface – although this is largely dependent on salt chemistry (Eugster, 1980).

Therefore, in addition to wet systems processes that are particularly responsive to local wet or dry years, as well as long-term precipitation change in the system catchment, the ephemeral nature can produce surfaces that are better represented by dry system responses. These are particularly observed to occur during the shoulder seasons, when spring or autumn rains fall causing the destruction of crusts and promotion of salt phase change and further crust ridging which can expose sediment. The trends observed in Chapter 5 confirm this through the detection of single day, single plume emissions towards at the beginning of the dust season responding to spatially discrete drying, or crust

destruction and therefore the availability of sediment. These emissions are considered to be transport capacity limited, while multiple emissions that occur during the long dry dust season when the system has a dry system response are limited by the consolidated surface. This transition between different limitations and controls could explain the highly variable nature of early season dust storms responding to inter-annual conditions, while more predictable summer storms respond to the high magnitude wind events.

6.4.1 Temporal Patterns

All atmospheric constituents including dust are subject to variations in space and time. Consequently, the existence and identification of dust emission provides the opportunity to establish trends and possible controls to this variability. Furthermore, due to the nature of dust sources, much of the variability and underlying controls are better presented over a number of time scales, from diurnal to decadal and even multi-decadal scales. While this variability is known to affect large sources with abundant supplies of sediment including large expanses of North Africa (e.g. Engelstaedter et al., 2006), the same can be observed for the smaller Makgadikgadi Pans. In this study it was demonstrated (in Chapter 5) that similar to global sources, seasonal, annual and inter-annual time scales are clearly acting on the system, while Chapters 3 and 4 discussed the importance of diurnal chemical changes on the surface and sub-surface of the pan.

While this study has extended the record for the pan to include the years between 2006 and 2012, identifying trends in the cyclicity is likely to be found over longer, multi-decadal scales. This was revealed by Bryant et al. (2007) utilising satellite products, who observed over a time period from 1980 to 2005 that the system responded to both ENSO cycles (e.g. Nicholson & Kim, 1997; Nicholson et al., 2001; Nicholson, 2009) and Indian Ocean indices (e.g. Landman & Mason, 1999; Reason, 2002; Washington et al., 2003; Washington & Preston, 2006). In line with these findings, there was noteworthy inter-annual variability (see chapter 5 for further discussion), which did not appear to correlate strongly with the rainfall record and is therefore likely to be responding to other climatic cycles.

The connections between rainfall and emission have been studied elsewhere, with Reheis (2006b) presenting that alluvial sources in the Mojave are the primary dust sources during lengthy drought periods, while wet playas are the primary dust source during high rainfall years. Similarly, Littmann (1991) observed that dust emission in the Sahel was a seasonal phenomena linked closely to soil moisture deficits in dry years. A study by Bryant et al. (2007) on the Makgadikgadi linked atypically wet periods with prolonged suppression of emission followed by increased activity after a lag period. Reheis (2006b) additionally states that the nature of the pan is important in considering response to seasonal and annual cycles indicating that dry playas with hard silt-clay surfaces and relatively deep water tables, behave similarly to alluvial sources with an abundant sediment supply. Dry pans are

likely to have a more variable dust flux due to the localised nature of storms, with the period of transition from wet to dry affecting the water table and the associated mobilisation of subsurface salts which results in the pan responding more like a wet pan (*Figure 6.1*). Reheis (2006b) elaborates that following a particularly wet year, the dry system produced a greater dust flux behaving more like a wet system in response to the higher ground water. This could be a possible cause for the highly active 2009 dust year following above average rains and a raised water table (Chapter 5).

Therefore, understanding the conditions at the site (Reheis, 2006b) and which limitations are determining the response of the system (Bullard et al., 2011) can help predict the systems response to seasonal, annual and inter-annual cycles.

6.5 Anthropogenic Influence

There is much uncertainty regarding the anthropogenic influence on dust producing regions and their regional setting, through both direct and indirect consequences e.g. disturbing soils, removing vegetation cover, desiccating water bodies and changing climate and hydrological cycles (Ginoux et al., 2012). Therefore, in addition to the ephemeral nature of this system and associated lack of predictability, considering aspects of anthropogenic influence compounds the challenges of predicting the emissive nature of the pan. Zender et al. (2004) identify two ways in which humans can alter the dust load. Firstly by altering land use, which affects soil conditions thereby modifying dust potential, and secondly through indirect and direct climatic modification. One of the most widely considered anthropogenic dust examples is the American 'Dust Bowl' years in the 1930's (Worster, 1982; Svobida, 1986; Cook et al., 2009).

While the Bullard et al. (2011) classification scheme did not include anthropogenically modified surfaces, global studies have identified substantial changes in the magnitude and frequency of dust emissions. The Sahel has been subject to investigation of the effects of anthropogenic emissions, with Engelstaedter et al. (2006) indicating that dust emissions here have increased significantly, particularly during the drought periods of the last decades in response to population expansion, resulting in a growing demand for food leading to over cultivation, overgrazing, deforestation and ultimately mismanagement of irrigation and desertification. Mahowald et al. (2002) presented that these mechanisms have resulted in increased soil disturbance and therefore increased dust emission.

Human population growth, and livestock access on the pan margins can be determined to affect the system, primarily through changes to vegetation regimes, seasonal burning and livestock grazing. The proximity of the BotAsh plant on the Sua spit potentially has a more direct effect through both the settling pond and the sub-surface brine pumping on changing the dynamics and solute load of the ground water. The structural components of the pan have presented a highly saline environment, with strong similarities presented between the ground water chemistry (Eckardt et al., 2008) and surface

chemistry. Significant drawdown associated with water extraction from the BotAsh mine could be causing a decrease in the salinity of near surface waters to the north and south of the spit (*Figure 6.2*).

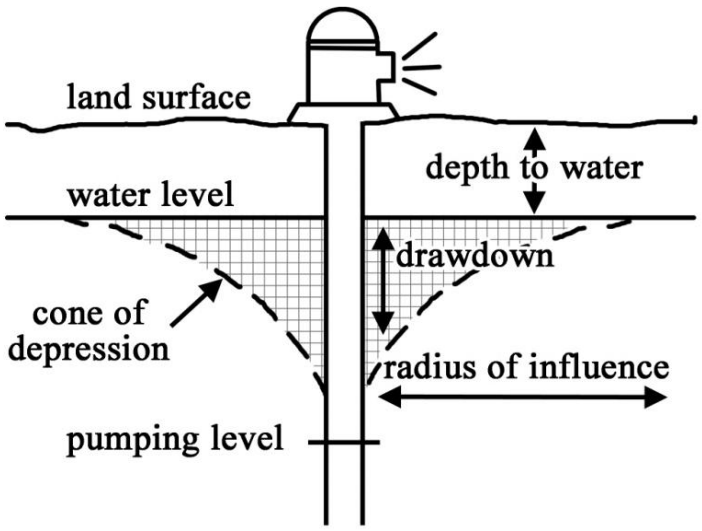

Figure 6.2 Schematic representation of the effects of sub-surface pumping on water level indicating the drawdown with associated cone of depression. The radius of influence can be seen to extend in both directions from the surface pump head.

Buck et al. (2011) elaborate on the importance of a continuous supply of subsurface brines not only for surface conditions, but for capillary zone interactions. Indicating that, through changes in both ground water depth and freshwater input, salts will precipitate in potentially lower horizons, leaving a silicate rich mineral surface. These surfaces, which under certain conditions could be emissive, may in fact be less emissive than the salt rich environment. Additionally, through ground water freshening, a surface salinity decrease is predicted; this could provide suitable environments for vegetation migration onto the pan surface. An increase in vegetation would affect both the availability of fine grained sediment and the transport capacity of the surface through changing surface roughness and thus entrainment thresholds. Further, Engelestaedter et al. (2003) considered the role of vegetation in determining the dust storm frequency for regions, concluding that there is a good correlation between different vegetation regimes and emission frequency. Thus the proposed changes to ground water has the potential to produce both a more emissive surface and a less emissive surface over a range of temporal scales.

6.6 Global Importance of the Makgadikgadi Pans

A number of factors need to be considered when determining the true global importance of the Pans, including emission frequency, scale of system, ecological and biological effects and the longevity of emission from the region. Additionally, these factors need to be viewed in the context of global dust source regions.

While early classification was largely based on TOMS or similar products, which determine aerosol optical depth, ecological and biological implications of the sources were not considered. However, Washington et al. (2003) produced the following classifications which ranked the top 10 dust sources globally based on optical depth.

Table 6.2 Maximum Mean Aerosol Index (AI) Values for Major Global Dust Sources Determined from TOMS (Washington et al., 2003).

Location	Mean AI Value
Bodélé Depression of south central Sahara	> 3.0
West Sahara in Mali and Mauritania	> 2.4
Arabia (southern Oman/Soudi border)	> 2.1
Easter Sahara (Libya)	> 1.5
Southwest Asia (Makran coast)	> 1.2
Taklamakan/Tarim Basin	> 1.1
Etosha Pan (Namibia)	> 1.1
Lake Eyre Basin (Australia)	> 1.1
Makgadikgadi Basin (Botswana)	> 0.8
Salar de Uyuni (Bolivia)	> 0.7
Great Basin of the United States	> 0.5

The resultant classifications in Table 6.2 largely agree with subsequent findings by Bullard et al. (2011), presenting large inland depressions without supply and availability limitations as high importance, the Bodélé Depression and the expanses of fine sediments in the Sahara as well as the Taklamakan/Tarim Basin - rankings 1,2,3,4 and 5. While smaller limited systems, Salar de Uyuni and the Etosha and Makgadikgadi Pans were associated with moderate to low importance as a function of both scale and systematic limitations at the source, rankings 6-10. Additionally, this classification based on size was acknowledged by Washington et al. (2003) who suggest that aerial extent can be used to determine the importance of the system.

Therefore, in terms of scale, the Makgadikgadi warrants consideration within the global context confirmed through current and historical emission frequencies. Thus, in addition to scale and persistence, including both biological and ecological measures would conclusively confirm the status of the pans. Early studies indicated that the ecological effects of dust storms had the potential to produce significant health hazards depending on the type of dust, with Saint-Amand et al. (1986: 33) adding that "…although little is known about the health effects of the dust, a report cited by Lundholm [(Lundholm, 1977)] states that the Kalahari area of Botswana, which is very overgrazed in parts, has the highest death rate from lung disease in the world". Subsequent studies on ecological and human health associated with the airborne transport of sediments from the Makgadikgadi and greater Kalahari are largely absent in the literature.

However, through this research the addition of chemical and morphological data has the potential to add substantial context. While such analysis is beyond the scope of this study, early statements by Lundholm (1977) indicates the possibly hazardous consequence of sediment transport while a review by Goudie (2014) considers the effects of dust globally on human health. Morman and Plumlee (2013) consider the implications of both urban and naturally occurring mineral aerosols, adding that inhalation of silica can lead to the development of pneumoconiosis or desert lung syndrome. This under diagnosed disease was detected to be prevalent in communities living in North Africa, China and the Middle East and was recognised as a significant ailment in troops deployed in the Persian Gulf in Operation Desert Storm in 1991. The potential population impact expected from Sua Pan is less, due to the relatively low population density observed in the down wind direction from the source. However, this number is not negligible and the associated circulation features result in the recirculation of these aerosols with the potential to impact a large population – further due to the fining that is associated with transport the impact is proposed to increase. Therefore studies like this have the potential to advance not only our understanding of the links between surface conditions and aerosol load, but can increase our understanding of the human health impacts such transport could cause.

Studies by Cahill et al. (1996), Reheis (1997) and Gill et al. (2002) indicate that salt rich sediments transported from the much smaller (280 km^2) Owens Lake (USA) travel hundreds of kilometres from source resulting in concern about potential human health effects and environmental impacts downwind, not only from the transported salts but also the metals which may be present in the dust (Gill et al., 2002). While Young and Evans (1986), Baath et al. (1992) and Farmer (1993) comment on the effects of salt transport downwind on soils and vegetation, indicating that long-term downwind depositions of salts can raise the pH of soils, affect photosynthesis, respiration and transpiration of vegetation communities; thereby reducing productivity and community structure, leading to the dominance of salt-tolerant plants. For the Makgadikgadi, studies are limited although Humpries et al. (2013) consider the role of Makgadikgadi dust on tree island growth in the Okavango delta. Such findings were in line with work by McCarthy et al. (2012) who confirm that the Makgadikgadi sediments dominate both the surface and subsurface material of Okavango Islands. While earlier work by Wood et al. (2011) suggested that over three million metric tons of sodium, chloride and bicarbonate were transported off the Makgadikgadi annually infiltrating ground water as far as 150 km downwind. Therefore the effects of Makgadikgadi aerosols have been confirmed to affect both humans and vegetation communities, thus recognising the regional influence of this system.

6.7 Concluding Remarks

Through controls discussed above both natural (wind, crusts and saltation) and anthropogenic, the preferential nature of this site as a dust source has been considered. Such systems were attributed by Bullard et al. (2011) to range in importance from low to high with a multitude of possible controls determining such classification. However, the multiple controls and lack of spatial homogeneity detected on the Makgadikgadi propose a system which may in fact have moderate dust potential. This classification has potential for considerable change even under the current anthropogenic influences on pan. Additionally, Bryant et al. (2007) indicated that the system was highly variable and responded to climatic and long term seasonal cycles. Thus, combined with the anthropogenic impacts considered above, the pans have the potential to be much dustier for a finite length of time, before supply limitations come into play as a result of limited recharge through capillary drawing, or availability limitations through increased vegetation cover.

Despite the considered changes above to the current state of the system, the Makgadikgadi is unlikely to be upgraded to high importance when compared with the large expanses of Chinese loess (Mei et al., 2004) and Saharan sand sea (e.g. Schepanski et al., 2007; Washington et al., 2009; Crouvi et al., 2012). These are assumed to contain an abundant supply of sediment, while the Makgadikgadi Pans are considered to be relatively small features. Further, unlike the Lake Eyre basin and Chihuahuan Deserts, which are mapped by Bullard et al. (2011) revealing discrete areas of high, medium and low emissive potential, the surfaces of the Makgadikgadi basin can largely be considered a single geomorphic unit (type 1b) within which there are discrete sources associated with preferential emission.

This discussion has considered the multiple controls currently acting on the pan, together with suggestions of possible future conditions. Intrinsic to understanding this system is the salinity and nature of the ground water level and recharge and any associated changes in the hydrology of the Makgadikgadi basin. It is these conditions which determine the nature of the surface, which we propose force the spatial variability that it detected from the pan surface.

Therefore, the importance of the Makgadikgadi is both a function of dust emission and frequency, combined with the downwind effects of the system. Upon considering all these factors and the scale of the system, this chapter has largely confirmed the applicability of the Bullard et al. (2011) preferential dust sources classifications. Consequently, the relevance of geological units in terms of emission potential and representing the chemical signature of both the dust and source can be seen to be an advance on classical methods of classifying dust sources.

Chapter 7: Conclusion

This study set out to characterise the chemical and morphological nature of sediments from the Makgadikgadi Pans. Additionally, it sought to evaluate how the conditions observed on the surface serve to promote or inhibit emission, and therefore determine the limitations controlling emission characteristics of the Pans. The relevant aeolian literature presents two general scales of inquiry. Firstly the micro scale perspective, derived through ground based studies and laboratory analysis with focus on particle properties. Secondly, the regional scale, generated through the use of remotely sensed imagery and climate products, with focus on emission events and actual transport. These two scales were addressed through answering the following questions:

1. What is the particle size distribution of sediments on the surface and sub-surface on the Makgadikgadi Pans?
2. What is the chemistry of these sediments and what can the vertical stratifications in chemistry reveal about the processes acting on the pans?
3. What are the seasonal, annual and multi-annual macro scale controls acting on the pans?
4. What are the climatic drivers on controlling emission from the Makgadikgadi?
5. How does the micro state of the pan surface, mineralogy and morphology, link with dust emission at the macro scale?

In considering the first four questions above, three key themes were considered, namely:

i. Grain Size: Evaluate methods of determining and presenting grain size of salt rich samples (Chapter 2).
ii. Chemistry: Determine the chemical nature of sediments and consider their role in surface emisivity (Chapters 3 and 4).
iii. Limitations: Characterise the seasonal, annual and inter-annual emission signature of the pan and consider the role of surface, source and climate as limiting factors (Chapters 5 and 6).

These three themes were then integrated to evaluate the pans within global dust source literature answering the fifth and final question. Combining the three themes, through addressing the five questions above, pan sediments and meteorological controls on dust emission were evaluated. Review of Aims and Objectives

This study set out to chemically and morphologically examine pan surface sediments and synoptic controls on dust emission on Sua Pan. In order to achieve this key methodological and process based objectives were identified.These three objectives followed three themes, which were determined to be; the determining of grain size and particule size distribution of sediments, the evaluation of the

chemistry of surface, sub-surface and airborne samples and finally determining the limitations (availability, supply and transport capacity) acting on the pan surface. The following section will consider each chapter, evaluating the outcomes and key findings in light of the aims and objectives of this study.

Through the literature review in Chapter 1 the critical role dust plays in global radiative feedback systems was presented, and the concept of dust was defined, while the Makgadikgadi as a large ephemeral pan was contextualised within global dust source typologies.

The second chapter considered both traditional dry sieving and modern laser methods to determine the particle size distributions of 41 samples collected at 12 locations during the DO4 field campaign between August and October 2011, demonstrating that non-destructive, conservative (undigested) preparation of the samples and associated analyses provided fast, reproducible results which most closely depicted the natural state of the pan sediments at the surface. The micro scale analysis of such undigested samples alongside digested samples revealed a link between chemistry and particle size distributions. This was primarily through the agglomerating effects of salts, which produce a surface crust and fluff consisting of silt size grains which may be presented as sand size conglomerates in the case of fluff and crust. Results further indicated that, regardless of the method, samples from the Makgadikgadi were consistently larger than those presented for other dust producing regions elsewhere. On average, soil samples were the finest, with a mean of 183 µm (fine sand) and then the fluffs with a mean of 261 µm (medium sand) the crusts was the coarsest with a mean of 328 µm (medium sand), while the average second crusts had a mean of 305 µm (medium sand). All samples were dominated by sand ≈ 80%, with < 1% clays. Site variability revealed that I4 was the finest site with all values below the grid mean, while I8 was the coarsest with all samples above the mean. Digestion changed the composition of the samples and consequently the particle size distributions. Following digestion, fluff samples were the finest, with a mean grain size of 53 µm (silt), while crusts and soils had means of 63 µm and 75 µm respectively (very fine sand), while second crust had mean of 188 µm and therefore fine sand. This shift from sand dominated to silt dominated ≈ 50% of the sample was accompanied by an average mass loss of 68% with an average of 80% loss experienced by the crusts. These findings confirm the importance of considering chemistry in the method. The results presented in Chapter 2, reveal that the first objected was achieved through the identification of trends in grain size and in the development of a methodology for the efficient and effective analysis of grain size for salt rich sediments.

Chapter 3 utilised both ICP and XRD to determine the chemistry of pan surface sediments. Twenty two fluff and crust samples from 12 sites were analysed for ICP analysis, while fluff, crust and second crust from three sites were considered for XRD analysis. The results of XRD presented a pan surface mineralogy dominated by common evaporite salts, including halite, thenardite, mirabilite, and trona,

in line with general observation by Eugster (1980), which produces the agglomeration described above. The suite of minerals detected by XRD, highlighted the role of shallow ground water in controlling the evaporite mineralogy and crusting, and in turn the emissive nature of the pan. On the micro-scale the relative contributions of the different minerals and their locations within the vertical structure revealed a very heterogeneous pan environment which could result in chemistry controlled spatially discrete emissions. Therefore, the bulk mineralogy was predictable as it conformed to a Eugster (1980) type and was observed to link to the geochemistry, however on the micro-scale there was variation both between sites and sampling horizons which was less predictable and showed variation. ICP analyses added little to understanding the nature of the Makgadikgadi Pan surface with the 16 identified minerals including sodium, silicon and calcium failing to account for more than 50% of the sample. Silica appears to be present in an amorphous state which was also confirmed using SEM.

In Chapter 4, QEMSCAN provided unprecedented high resolution morphological and mineralogical data on the nature of surface and airborne sediments, and identified selective entrainment of surface sediment, by comparing the potential aerosol load collected from a BSNE trap with the corresponding surface material. Seven samples representing 4 BSNE samples, one surface fluff sample, one sample combined from two frisbee traps, and the exhaust from a PI-SWERL run, were analysed counting 27 000 grains over three size fractions, attributing the grains to composite or single minerals from an extensive 255 mineral list. Event based observations revealed that, not only was the pan surface surrounding the BSNE trap the dominant source of trapped aeolian sample, but that locally derived sediment dominated the mineralogical signature of the frisbee sample suggesting the pans as the dominant source of the local aerosol load. QEMSCAN results here represented a significant advance in morphological and mineralogical sediment classification, but only represent a single event from a single location. Nevertheless, QEMSCAN validated the use of laser diffraction of the morphology results presented through as a method of grain size determination through confirming that the sediments were relatively round. Additionally, QEMSCAN detected all minerals identified by XRD and confirmed many of the elements detected through ICP analysis, further identifying a number of undetected minerals through the more comprehensive suite of minerals analysed in QEMSCAN (255 in QEMSCAN compared with 16 in XRD).

Chapters 3 and 4 achieved the second and third objectives of this study which were to determine the elemental and chemical nature of surface and sub-surface sediments, and their role in the emission process, and evaluate QEMSCAN as a tool for the mineral and morphological classification of dust in aerosols studies.

While the three previous chapters examined the micro scale nature of Makgadikgadi Pans surface sediments, Chapter 5 linked dust events to their actual synoptic states and considered seasonal and

interannual emission characteristics. A number of circulation features were associated with dust plumes, suggesting that the mean circulation was sufficient for transport and that surface conditions imposed the greater control. This can be concluded as almost all synoptic states that are experienced over the domain produced dust during the period of analysis, while emission could have occurred on an intensified version of the system, but on the whole the mean is sufficient. This study also identified the dominance of south westerly transport trajectories from the pan, regardless of the emission timing and location. It was further established that there is a peak in dust plume activity in July, with 90% of the plumes being active in the morning and therefore visible on the Terra overpass. It was also noted that local rainfall may either enhance or suppress dustiness depending on both the nature of the rainfall, its timing and the state of the pan surface. Consequently, Chapter 5 contextualised the emission characteristics of the pan within spatial and temporal scales and considered the possible controls at the source, achieving the fourth aim of this study.

The following section will present the limitations encountered through analysis, this will be followed by future research directions which have arisen through meeting all the aims and objectives set out in this study.

7.1 Limitations

Firstly, samples collected and analysed in this study which were proposed to be representative of the conditions present on the pan surface, were taken from an undisturbed 144 km^2 site within Sua Pan. Identification of emission from the pan presented in Chapter 5, indicates that this sampling location may not represent the full character of the pan surface. Additionally, these samples are also only representative of the mineralogical conditions of the 2011 field season, which are known to vary as a function of both temperature and moisture. Furthermore, samples were not analysed *in situ* which has the potential to impact their nature. This therefore highlights the necessity of additional field sampling extending beyond the DO4 grid. Additionally, sampling of the wider pan environment, including sampling on both Ntwetwe and Sua and smaller satellite pans, together with the pan margin, and both upwind and downwind of the source, would better determine the spatial extent of emissive material and the footprint of Makgadikgadi sediments on local and regional biogeochemical cycles. Additionally, such monitoring could quantify the degree to which the Pans are affected by human activities through identification of crust conditions and evaporite horizons as a function of ground water depth and salinity

Secondly, in determining the emission response of the pans not all MODIS images were present in the archive. Consequently it is possible that dust events were not observed and was therefore not even catalogued. Furthermore, the scale of MODIS may preclude the detection of local dust transport as in the case of the event discussed in Chapter 5. These shortcomings suggest that the emission signature

of the region may not be fully resolved. In line with this, synoptic states associated with emission may not have been considered nor the precise context of rainfall identified as an inhibiting and initiating factor. While no sensor with a higher spatial resolution currently exists, increased temporal resolution offered through alternative sensors, including the geostationary Meteosat Second Generation (MSG), could add detail in the timing of emission and persistence of the plume. Such detail could confirm the role of synoptic drivers and increase our understanding of diurnal controls.

Despite the above limitations, this study has highlighted the importance of timing and sampling conditions in presenting the state of the surface.

7.2 Future Research Directions

This work emerged through discussion and analysis performed as part of the Dust Observation for Climate (DO4) project. The full list of instrumentation which was employed for two seasons as part of the project is presented in Chapter 1, including equipment to monitor wind, temperature, crust strength, solar radiation and ambient atmospheric aerosol concentration. Therefore, there is considerable scope for contextualising the data presented in this study within the data collected from the project. This includes the potential for increasing our understanding of emission characteristics through measurements of surface and sub-surface moisture, surface roughness, vertical shear and wind speed and direction data, together with quantifiable data on crust strength. These measurements were all identified to be important, through both literature review and personal observation during the field season.

In addition, the sampling of sediments from outside the pan margins would allow for a greater geochemical context for the pan complex. Similarly, the roles of the Nata and Boteti rivers for transporting sediments and solutes into the pans also needs to be considered, as the link between ground water chemistry and evaporite conditions appear to show strong correlation.

Throughout this analysis the question of the nature of the sediments as a limiting factor was considered. The relatively coarse nature of the grains, combined with the high salt content and the absence of saltation, complicated the understanding of simple entrainment. Despite these limitations, emissions were and have been detected from the region, which indicates that mechanisms are acting on the pan surface to produce dust. These could include sufficiently strong winds which blow across the large, flat pan with the large fetch assisting in accelerating the winds, increasing capacity and increasing the capability of the wind to entrain sand sized grains. Surface roughness from the crusted surface may also act to change the wind shear and turbidity and therefore increase the potential for entrainment. Additionally, observations of conditions on the pan confirmed a high number of dust devils, which have been considered as potential mechanism for breaking crusts and transporting sediments, which may later be entrained and impart further momentum of surface grains. Increasing our understanding of these mechanisms may reveal insight into the emissive character of the pan

surface. Through considering these intermediate controls it could be possible to contextualise the case study presented in Chapter 5, within an understanding of additional erodibility controls including surface roughness, crust coverage, wind shear, turbitity and the physical setting of the moisture content. This event, which was below satellite detection limits, was an important emission event, resulting in airborne sediment capture. Therefore, adding detail of synoptic and measured surface winds and shear into the nature of the event, and linking the observed transport with thresholds and sample mass and size distribution, could reveal the intermediate controls on emission from the salt rich pan.

Crusts have been consistently identified as a crucial control in emission from the region, with the DO4 project utilising the capabilities of terrestrial laser scanning to determine the role of moisture in crust conditions (Nield et al., 2014) and crusts in aerodynamic roughness (Nield et al., 2013). The results of these studies, and those derived here, have advanced the understanding of this ephemeral pan significantly.

7.3 Summary

Despite the size of the pan surface, the depth of fine grained sediment and the frequency of suitable wind regimes, dust events occur more sporadically than one would have anticipated, given the insight gained from the micro and macro scale examination of the system. Controls which cause the pan surface to be less productive in general, and even specifically during the observational record produced during the DO4 field campaign, require examination. Understanding the controls on dust emissions from ephemeral basins has been identified as a considerable challenge (e.g. Reynolds et al., 2009) which rests in particular at the intermediate scale (e.g. Thomas & Wiggs, 2008). This was demonstrated here, considering the Makgadikgadi which revealed key aspects of variability - including spatial and temporal, at both the micro and macro scales. Chapter 6 placed the Makgadikgadi Pans within the context of established dust sources worldwide (Bullard et al., 2011) with the added emphasis on intermediate scale considerations around issues of dust emission controls and thresholds. Further, disturbances to the natural pan environment were considered, including the proximity and influence of mining at Sua and increased livestock movements throughout the region, particularly on the pan margins. Anthropogenic activities have been identified as a cause for increased emission frequency including the effects of animal disturbances to surfaces. Such observations could account for the detected increase in dust activity.

To understand the system, it was necessary to consider the three central themes, which can be developed to include the morphology and mineralogy, the synoptic setting and the nature of the geomorphic unit.

- In terms of size characteristics, Makgadikgadi sediments were found to have a uni-modal distribution centred at medium sand, although changing dispersants revealed that much of this was a function of evaporite induced clay/silt to sand agglomeration. This indicated that the description of size characteristics of Makgadikgadi Pan sediments (in space and time) are strongly influenced by surface and sub-surface chemistry.
- Chemically, the suite of minerals observed to dominate the pan surface and sub-surface is in line with studies on the hydrochemistry of the region (Eckardt et al., 2008) confirming the depth to ground water as an important control for surface conditions (e.g. Reynolds et al., 2007). A mix of evaporites and carbonates was determined to be important for the prediction of the emissive nature of the surface, with such minerals found to respond to diurnal and seasonal changes in temperature and moisture conditions. These minerals created a vertically stratified pan surface, with the role of chemical crusting determined to be an important limiting factor in controlling the availability of the emissive fluff to winds.
- Synoptically, through extending the record for the Pans this study has confirmed earlier studies by Bryant et al. (2007) and Vickery et al. (2013) which identified south westerly transport off the pan driven by a number of synoptic states with emission peaking in July. Analysis revealed that large scale circulation was not a limiting factor.
- Geomorphologically, this study has confirmed this large ephemeral basin as a persistent dust source contributing to the aerosol load in southern Africa. It has also confirmed the controls proposed for both wet and dry systems (Bullard et al., 2011) to be applicable to the ephemeral Makgadikgadi. The proposal that this system could be considered as a potential analogue for large ephemeral dust producing systems globally was challenged. Investigation indicated that dust frequency was determined by responses to seasonal and inter-annual climate together with pan setting - which was influenced by drainage systems, river flow and land use. Such variability suggests that, at the intermediate scale, these systems cannot be considered to be analogues of one another, although the relevance of considering dust sources as geomorphological units, or as preferential dust source units, can be seen as a significant advance on classical methods of classifying dust sources.

Importantly, the identification of the Makgadikgadi Pans as a persistent dust source in southern Africa is not a new finding, nor is the identification of a highly variable emission signature. In addition, many studies have considered both natural and anthropogenic dust sources, indicating the highly sensitive nature of natural source to minor perturbations. Through this study, spatial and temporal emission signatures as a function of both naturally occurring variability and anthropogenic disturbances have been identified, as have the mineralogical and morphological context of these.

Many authors indicate the importance of including mineralogy and morphology in global models, which can advance our current understanding of the role of aerosols within the global dust cycle. The data presented here can be used to inform models to constrain the chemical and physical, and therefore optical, properties of the aerosols included in regional climate models for southern Africa. The synoptic states and transport pathways derived through HYSPLIT and NCEP reanalysis data, can be used to better attribute transport routes. Similarly, the suite of minerals presented can be utilised by biologists and ecologists to determine the downwind impacts such transport could have.

This study has considered the micro and macro scale of dust research and attempted to consider the effects of these two scales on the intermediate systematic response of the Makgadikgadi. This revealed the complexity involved in understanding dust emissions from the pans providing a base from which, and into which, further research can be conducted.

Chapter 8: Reference list

Abel, S.J., Highwood, E.J., Haywood, J.M. & Stringer, M.A. 2005. The direct radiative effect of biomass burning aerosols over southern Africa. *Atmospheric Chemistry and Physics.* 5:1999-2018.

Afeti, G.M. & Resch, F.J. 2000. Physical characteristics of Saharan dust near the Gulf of Guinea. *Atmospheric Environment.* 34(8):1273-1279.

Allen, J.R.L. 1985. *Principles of physical sedimentology.* First ed. London: George Allen & Unwin.

Allen, T. 1975. *Particle Size Measurements.* Second ed. London: Chapman and Hall Ltd.

Alpert, P., Kaufman, Y.J., Shay-El, Y., Tanre, D., da Silva, A., Schubert, S. & Joseph, J.H. 1998. Quantification of dust forced heating of the lower troposphere. *Nature.* 398:367-370.

Amato, J.A. 2000. *Dust: a history of the small and invisible.* University of California Press.

Arimoto, R. 2001. Eolian dust and climate: relationships to sources, tropospheric chemistry, transport and deposition. *Earth-Science Reviews.* 54(1-3):29-42.

Ashpole, I. & Washington, R. 2012. An automated dust detection using SEVIRI: A multiyear climatology of summertime dustiness in the central and western Sahara. *Journal of Geophysical Research: Atmospheres.* 117(D8)

Ashpole, I. & Washington, R. 2013 Accepted. A new high-resolution central and western Saharan summer time dust source map from automated satellite dust plume tracking. *Journal of Geophysical Research: Atmospheres.* :n/a-n/a.

Ayling, B., Rose, P., Petty, S., Zemach, E. & Drakos, P. 2012. QEMSCAN (Quantitative Evaluation of Minerals by Scanning Electron Microscopy): Capability and application to fracture chatacterisation in geothermal systems. *PRECEEDINGS, Thirty-Seventh Workshop on Geothermal Reservoir Engineering Stanford University.* January 30 - February 1, 2012. Stanford, California: .

Baath, E., Frostegarda, A. & Fritze, H. 1992. Soil bacterial biomass, activity, phospholipid fatty acid pattern, and pH tolerance in an area polluted with alkaline dust deposition. *Applied Environmental Microbiology.* 58:4026-4031.

Baddock, M.C., Bullard, J.E. & Bryant, R.G. 2009. Dust source identification using MODIS: A comparison of techniques applied to the Lake Eyre Basin, Australia. *Remote Sensing of the Environment.* 113(7):1511-1523.

Baddock, M.C., Wiggs, G.F.S. & Livingstone, I. 2011. A field study of mean and turbulent flow characteristics upwind, over and downwind of barchan dunes. *Earth Surface Processes and Landforms.* 36:1435-1448.

Bagnold, R.A. 1941. *The Physics of wind blown sand and desert dunes.* First ed. London: Methuen.

Baillieul, T.A. 1979. Makgadikgadi pans complex of central Botswana . *Geological Society of America Bulletin.* 90(Part II):289-312.

Barth, H.G. & Sun, S.T. 1985. Particle size analysis. *Analytical Chemistry.* 57(5):151-175.

Belnap, J. & Warren, S.D. 2002. Patton's tracks in the Mojave Desert, USA: An ecological legacy. *Arid Land Research and Management.* 16:245-258.

Bennion, P., Hubbard, R., O'Hara, S., Wiggs, G., Wegerdt, J., Lewis, S., Small, I., van der Meer, J. & Upshur, R. 2007. The impact of airborne dust on respiratory health in children living in the Aral Sea region. *International Journal of Epidemiology.* 36(5):1103-1110.

Berner, R.A. 1975. The role of magnesium in the crystal growth of calcite and aragonite from sea water. *Geochimica Et Cosmochimica Acta.* 39(4):489-504.

Beuselinck, L., Govers, G., Poesen, J., Degraer, G. & Froyen, L. 1998. Grain-size analysis by laser diffractometry: comparison with the sieve-pipette method. *Catena.* 32:193-208.

Bhalotra, Y.P.R. 1987. *Climate of Botswana: Part II. Elements of climate, rainfall.* Gaborone, Botswana: Department of Meteorological Services Ministry of Works and Communication.

Bing, C., Hiroyuki, K., Ke, H., Dongmei, J.I.E., Junpeng, Y. & Jingmin, L. 2009. Element and mineral characterization of dust emission from the saline land at Songnen Plain, Northeaster China. *Journal of Environmental Science.* 21:1363-1370.

Blanco, A., Dee Tomasi, F., Filippo, E., Manno, D., Perrone, M.R., Serra, A., Tafuro, A.M. & Tepore, A. 2003. Characterization of African dust over southern Italy. *Atmospheric Chemistry and Physics.* 3(6):2147-2159.

Blank, R.R., Young, J.A. & Allen, F.L. 1999. Aeolian dust in a saline playa environment, Nevada, U.S.A. *Journal of Arid Environments.* 41(4):365-381.

Blott, S.J. & Pye, K. 2001. GRADISTAT: a grain size distribution statistics package for the analysis of unconsolidated sediments. *Earth Surface Processes and Landforms.* 26:1237-1248.

Brindley, H.E. & Ignatov, A. 2006. Retrieval of mineral aerosol optical depth and size information from Meteosat Second Generation SEVIRI solar reflectance bands. *Remote Sensing of the Environment.* 102:344-363.

Brindley, H.E., Knippertz, P., Ryder, C. & Ashpole, I. 2012. A critical evaluation of the ability of the Spinning Enhanced Visible and Infrared Imager (SEVIRI) thermal infrared red-green-blue rendering to identify dust events: Theoretical analysis. *Journal of Geophysical Research: Atmospheres.* 117(D7):D07201.

Brooks, N. & Legrand, M. 2000. Dust variability and rainfall in the Sahel. In *Linking climate change to land-surface change.* S. McLaren & D. Kniveton, Eds. First ed. Dordrecht: Kluwer Academic Publishers. 1-25.

Bryant, R.G. 2003. Monitoring Hydrological Controls on dust emissions: Preliminary observations from Etosha Pan, Namibia. *The Geographical Journal.* 169(2):131-141.

Bryant, R.G. 2013. Recent advances in our understanding of dust source emission processes. *Progress in Physical Geography.* 37(3):397-421.

Bryant, R.G., Bigg, G.R., Mahowald, N.M., Eckardt, F.D. & Ross, S.G. 2007. Dust emission response to climate in southern Africa. *Journal of Geophysical Research.* 112(D09207)

Buch, M.W. & Rose, D. 1996. Mineralogy and geochemistry of the sediments of the Etosha Pan Region in northern Namibia: a reconstruction of the depositional environment. *Journal of African Earth Sciences.* 22(3):355-378.

Buck, B.J., King, J. & Etyemezian, V. 2011. Effects of salt mineralogy on dust emissions, Salton Sea, California. *Soil Science Society of America Journal.* 75(5):1971-1985.

Buck, B.J., Wolff, K., Merkler, D.J. & McMillan, N.J. 2006. Salt Mineralogy of Las Vegas Wash, Nevada. *Soil Science Society of America Journal.* 70(5):1639-1651.

Bullard, J., Baddock, M., McTainsh, G.H. & Leys, J. 2008. Sub-basin scale dust source geomorphology detected using MODIS. *Geophysical Research Letters.* 35(15):L15404.

Bullard, J.E. 2010. Bridging the gap between field data and global models: current strategies in aeolian research. *Earth Surface Processes and Landforms.* 35(4):496-499.

Bullard, J.E., Harrison, S.P., Baddock, M.C., Drake, N., Gill, T.E., McTainsh, G. & Sun, Y. 2011. Preferential dust sources: A geomorphological classification designed for use in global dust-cycle models. *Journal of Geophysical Research: Earth Surface.* 116(F4):- F04034.

Bullard, J.E. & Livingstone, I. 2002. Interactions between aeolian and fluvial environments in dryland environments. *Area.* 34(1):8-16.

Bullard, J.E. & McTainsh, G.H. 2003. Aeolian-fluvial interactions in dryland environments: examples, concepts and Australia case study. *Progress in Physical Geography.* 27(4):471-501.

Burrough, S.L., Thomas, D.S.G. & Bailey, R.M. 2009. Mega-Lake in the Kalahari: A Late Pleistocene record of the Palaeolake Makgadikgadi system. *Quaternary Science Reviews.* 28(15–16):1392-1411.

Buurman, P., Pape, T. & Muggler, C.C. 1997. Laser grain-size determination in soil genetic studies 1. Practical problems. *Soil Science.* 162(3):211-218.

Buurman, P., Pape, T., Reijneveld, J.A., de Jong, F. & van Gelder, E. 2001. Laser-diffraction and pipette-method grain sizing of Dutch sediments: correlations for fine fractions of marine, fluvial and loess samples. *Netherlands Journal of Geosciences.* 80:49-57.

Cahill, T.A., Gill, T.E., Reid, J.S., Gearhard, E.A. & Gillette, D.A. 1996. Saltating particles, playa crusts and dust aerosols at Owen (dry) Lake, California. *Earth Surface Processes and Landforms.* 21(7):621-639.

Carslaw, K.S., Boucher, O., Spracklen, D.V., Mann, G.W., Rae, J.G.L., Woodward, S. & Kulmala, M. 2010. A review of natural aerosol interactions and feedbacks with the Earth system. *Atmospheric Chemistry and Physics.* 10(4):1701-1737.

Castillo, S., Moreno, T., Querol, X., Alastuey, A., Cuevas, E., Herrmann, L., Mounkaila, M. & Gibbons, W. 2008. Trace element variation in size-fractionated African desert dusts. *Journal of Arid Environments.* 72(6):1034-1045.

Cattle, S.R., McTainsh, G.H. & Elias, S.. 2009. Eolian dust deposition rates, particle-sizes and contributions to soils along a transect in semi-arid New South Wales, Australia. *Sedimentology.* 56(3):765-783.

Chatenet, B., Marticorena, B., Gomes, L. & Bergametti, G. 1996. Assessing the microped size distributions of desert soild erodible by wind. *Sedimentology.* 43(5):901-911.

Chiapello, I., Prospero, J.M., Herman, J.R. & Hsu, N.C. 1999. Detection of mineral dust over the North Atlantic Ocean and Africa with Nimbus 7 TOMS. *Journal of Geophysical Research.* 104(D8):9277-9291.

Chu, D.A., Kaufman, Y.J., Chern, J.D., Mao, J., Li, C. & Holben, B.N. 2003. Global monitoring of air pollution over land from the Earth Observing System-Terra Moderate Resolution Imaging Spectroradiometer (MODIS). *Journal of Geophysical Research.* 108(D21):4661.

Chudnovsky, A., Ben-Dor, E., Kostinski, A.B. & Koren, I. 2009. Mineral content analysis of atmospheric dust using hyperspectral information from space. *Geophysical Research Letters.* 36(15):- L15811.

Claquin, T., Schulz, M. & Balkanski, Y.J. 1999. Modeling the mineralogy of atmospheric dust sources. *Journal of Geophysical Research: Atmospheres (1984–2012).* 104(D18):22243-22256.

Clarke, M.L. & Rendell, H.M. 1998. Climate change impacts on sand supply and the formation of desert sand dunes in the southwest USA. *Journal of Arid Environments.* 39:517-531.

Coakley, G.J. 2003. The mineral industry of Botswana. *USGS Minerals Yearbook.* :5.1-5.4.

Compton, J.S., White, R.A. & Smith, M. 2003. Rare earth element behavior in soils and salt pan sediments of a semi-arid granitic terrain in the Western Cape, South Africa. *Chemical Geology.* 201(3–4):239-255.

Cook, B.I., Miller, R.L. & Seager, R. 2009. Amplification of the North American "Dust Bowl" drought through human-induced land degradation. *Proceedings of the National Academy of Sciences.* 106(13):4997-5001.

Cooke, H.J. & Verstappen, B.T. 1984. The Landforms of the western Makgadikgadi basins of northern Botswana, with a consideration of the chronology of Lake Palaeo-Makgadikgadi. *Zeitschrift Für Geomorphologie.* NF28:1-19.

Cooke, R.U. & Warren, A. 1973. *Geomorphology in deserts.* 394p ed. London: Batsford Ltd.

Cooke, R.U., Warren, A. & Goudie, A.S. 1993. *Desert Geomorphology.* London: UCL Press.

Cooke, H.J. 1979. The Origin of the Makgadikgadi Pans. *Botswana Notes and Records.* 11:37-42.

Crouvi, O., Schepanski, K., Amit, R., Gillespie, A.R. & Enzel, Y. 2012. Multiple dust sources in the Sahara Desert: The importance of sand dunes. *Geophysical Research Letters.* 39(13):- L13401.

D'Almeida, G.A., Koepke, P. & Shettle, E.P. 1991. *Atmospheric aerosols. Global climatology and radiative characteristics.* Hampton, Virginia: Deepak Publishing.

Daniels, R.B. & Hammer, R.D. 1992. *Soil Gomorphology.* United States of America: John Wiley & Sons Inc.

Darwin, C. 1889. *Journal of Researches into the Natural History and Geology of the Countries Visited During the Voyage of the H.M.S. Beagle Round the World.* Ward Lock and Co.

Di Stefano, C., Ferro, V. & Mirabile, S. 2010. Comparison between grain-size analyses using laser diffraction and sedimentation methods. *Biosystems Engineering.* 106(2):205-215.

Doornkamp, J.C. 1974. Analysis of the Surface Texture of Selected Quartz Grains From Southern Africa Using a Scanning Electron Microscope. *South African Geographical Journal.* 56(2):121-127.

Durán, O., Claudin, P. & Andreotti, B. 2011. On aeolian transport: Grain-scale interactions, dynamical mechanisms and scaling laws. *Aeolian Research.* 3(3):243-270.

Eckardt, F.D., Bryant, R.G., McCulloch, G., Spiro, B. & Wood, W.W. 2008. The hydrochemistry of a semi-arid pan basin case study: Sua Pan, Makgadikgadi, Botswana. *Applied Geochemistry.* 23(6):1563-1580.

Eckardt, F.D. & Kuring, N. 2005. SeaWiFS identifies dust sources in the Namib Desert. *International Journal of Remote Sensing.* 26(19):4159-4167.

Edwards, G.V. & Butcher, A.R. 1999. *A new application for QEMSCAN – quantifying the mineralogy of drill cuttings from oil and gas exploration and production wells.* CSIRO Report.

Eitel, B., Dieter Blümel, W., Hüser, K. & Mauz, B. 2001. Dust and loessic alluvial deposits in Northwestern Namibia (Damaraland, Kaokoveld): sedimentology and palaeoclimatic evidence based on luminescence data. *Quaternary International.* 76–77(0):57-65.

Elmore, A.J., Kaste, J.M., Okin, G.S. & Fantle, M.S. 2008. Groundwater influences on atmospheric dust generation in deserts. *Journal of Arid Environments.* 72(10):1753-1765.

Engelbrecht, J.P. & Derbyshire, E. 2010. Airborne Mineral Dust. *Elements.* 6:241-246.

Engelstaedter, S., Kohfeld, K.E., Tegen, I. & Harrison, S.P. 2003. Controls of dust emissions by vegetation and topographic depressions: An evaluation using dust storm frequency data. *Geophysical Research Letters.* 30(6):1294.

Engelstaedter, S., Tegen, I. & Washington, R. 2006. North African dust emissions and transport. *Earth Science Reviews.* 79:73-100.

Engelstaedter, S. & Washington, R. 2007a. Atmospheric controls on the annual cycle of North African dust. *Journal of Geophysical Research.* 112(D03103)

Engelstaedter, S. & Washington, R. 2007b. Temporal controls on global dust emissions: The role of surface gustiness. *Geophysical Research Letters.* 34(L15805)

Eugster, H.P. & Hardie, L.A. 1978. Saline Lakes. In *Chemistry, Geology and Physics of Lakes.* A. Lerman, Ed. New York: Springer Verlag. 237-239.

Eugster, H.P. 1980. Geochemistry of evaporitic lacustrine deposits. *Annual Review of Earth and Planetary Sciences.* 8:35.

Evans, R.D., Jefferson, I.F., Kumar, R., O'Hara-Dhand, K. & Smalley, I.J. 2004. The nature and early history of airborne dust from North Africa; in particular the Lake Chad basin. *Journal of African Earth Sciences.* 39(1-2):81-87.

Farmer, A.M. 1993. The effects of dust on vegetation- A review. *Envrionmental Pollution.* 79(1):63-75.

Fecan, F., Marticorena, B. & Bergametti, G. 1999. Parameterisation of the increase of the aeolian erosion threshold wind friction velocity due to soil moisture for arid and semi arid areas. *Annales Geophysicae.* 17:149-157.

Field, J.P., Belnap, J., Breshears, D.D., Neff, J.C., Okin, G.S., Whicker, J.J., Painter, T.H., Ravi, S., Reheis, M.C. & Reynolds, R.L. 2010. The Ecology of Dust. *Frontiers of Ecolology and the Environment.* 8(8):423-430.

Folk, R.L. 1966. A review of grain-size parameters. *Sedimentology.* 6(2):73-93.

Folk, R.L. & Ward, W.C. 1957. Brazos River bar: a study in the significance of grain size parameters. *Journal of Sedimentary Petrology.* 27(3):26.

Frostick, L. & Reid, I. 1990. Structural control of sedimentation patterns and implication for the economic potential of the East African Rift basins. *Journal of African Earth Sciences (and the Middle East).* 10(1):307-318.

Fryberger, S.G. 1979. Dune forms and wind regime. In *A Study of Global Sand Seas.* E.D. Mckee, Ed. 137-169.

Fryrear, D.W. 1986. A field dust sampler. *Journal of Soil Water Conservation.* 41:117-120.

Gill, T.E. 1996. Eolian sediments generated by anthropogenic disturbance of playas: human impacts on the geomorphic system and geomorphic impacts on the human system. *Geomorphology.* 17(1):207-228.

Gill, T.E., Gillette, D.A., Niemeyer, T. & Winn, R.T. 2002. Elemental geochemistry of wind-erodible playa sediments, Owens Lake, California. *Nuclear Instruments and Methods in Physics Research Section B: Beam Interactions with Materials and Atoms.* 189(1–4):209-213.

Gillette, D., Ono, D. & Richmond, K. 2004. A combined modeling and measurement technique for estimating windblown dust emissions at Owens (dry) Lake, California. *Journal of Geophysical Research: Earth Surface.* 109(F1):- F01003.

Gillette, D.A. 1979. Environmental factors affecting dust emission by wind erosion. In *Saharan Dust.* C. Morales, Ed. Scope 14 ed. New York: J . Wiley and Sons. 71-94.

Gillette, D.A., Adams, J., Muhs, D.R. & Kihl, R. 1982. Threshold friction velocities and rupture moduli for crusted desert soils for the input of soil particles into the air. *Journal of Geophysical Research: Oceans.* 87(C11):9003-9015.

Gillette, D.A., Niemeyer, T.C. & Helm, P.J. 2001. Supply-limited horizontal sand drift at an ephemerally crusted, unvegetated saline playa. *Journal and Geophysical Research.* 106(NO. D16):18085-18089.

Ginoux, P., Prospero, J.M., Gill, T.E., Hsu, N.C. & Zhao, M. 2012. Global-scale attribution of anthropogenic and natural dust sources and their emission rates based on MODIS Deep Blue aerosol products. *Reviews of Geophysics.* 50(3):- RG3005.

Gong, S.L., Barrie, L.A. & Blanchet, J.-. 1997. Modeling sea-salt aerosols in the atmosphere: 1. Model development. *Journal of Geophysical Research: Atmospheres.* 102(D3):3805-3818.

Goodall, W.R., Scales, P.J. & Butcher, A.R. 2005. The use of QEMSCAN and diagnostic leaching in the characterisation of visible gold in complex ores. *Minerals Engineering.* 18(8):877-886.

Goossens, D. 2001. The Aeolian Dust Accumulation Curve. *Earth Surface Processes and Landforms.* 26:1213-1219.

Goossens, D. 2008. Techniques to measure grain-size distributions of loamy sediments: a comparative study of teninstruments for wet analysis. *Sedimentology.* 55(1):65-96.

Goossens, D. 1985. The granulometrical characteristics of a slowly-moving dust cloud. *Earth Surface Processes and Landforms.* 10(4):353-362.

Goossens, D. & Buck, B. 2011. Gross erosion, net erosion and gross deposition of dust by wind: field data from 17 desert surfaces. *Earth Surface Processes and Landforms.* 36(5):610-623.

Goossens, D. 2006. Aeolian deposition of dust over hills: the effect of dust grain size on the deposition pattern. *Earth Surface Processes and Landforms.* 31(6):762-776.

Goossens, D. 2007. Bias in grain size distribution of deposited atmospheric dust due to the collection of particles in sediment catchers. *Catena.* 70(1):16-24.

Gottlieb, P., Wilkie, G., Sutherland, D., Ho-Tun, E., Suthers, S., Perera, K., Jenkins, B., Spencer, S., Butcher, A. & Rayner, J. 2000. Using quantitative electron microscopy for process mineralogy applications. *Journal of Mineralogy.* 52(4):24-27.

Goudie, A.S. 1983. Dust storms in space and time. *Progress in Physical Geography.* 7:502-530.

Goudie, A.S. 2009. Dust storms: Recent developments. *Journal of Environmental Management.* 90:89-94.

Goudie, A.S. 2013. *Arid and Semi-Arid Geomorphology.* First ed ed. New York, United States of America: Cambridge University Press.

Goudie, A.S. 2014. Desert dust and human health disorders. *Environment International.* 63(0):101-113.

Goudie, A.S., Anderson, M., Burt, T., Lewis, J., Richards, K., Whalley, B. & Worsley, P. 1990. Part Three: Material Properties. In *Geomorphological Techniques: British Geomorphological Research Group.* W.B. Whalley, Ed. Second ed. London: Unwin Hyman Ltd. 109-144.

Goudie, A.S. & Middleton, N.J. 2001. Saharan dust storms: nature and consequences. *Earth-Science Reviews.* 56:179-204.

Goudie, A.S. & Middleton, N.J. 2006. *Desert Dust in the global system.* London: Springer.

Goudie, A.S. & Thomas, D.S.G. 1985. Pans in southern Africa with particular reference to South Africa and Zimbabwe. *Zeitschrift Für Geomorphologie.* NF29:1-19.

Goudie, A.S. & Wells, G.L. 1995. The nature distribution and formation of pans in arid zones. *Earth Science Reviews.* 38:1-69.

Grousset, F.E. & Biscaye, P.E. 2005. Tracing dust sources and transport patterns using Sr, Nd and Pb isotopes. *Chemical Geology.* 222:149-167.

Gumbricht, T. & McCarthy, T.S. 2003. Spatial Patterns of Islands and Salt Crusts in the Okavango Delta, Botswana. *South African Geographical Journal.* 85(2):164-169.

Haberlah, D., Williams, M.A.J., Halverson, G., McTainsh, G.H., Hill, S.M., Hrstka, T., Jaime, P., Butcher, A.R. & Glasby, P. 2010. Loess and floods: High-resolution multi-proxy data of Last Glacial Maximum (LGM) slackwater deposition in the Flinders Ranges, semi-arid South Australia. *Quaternary Science Reviews.* 29(19–20):2673-2693.

Hadi, K.M. & Al-Ruwaih, F.M. 2008. Geochemical evolution of the fresh groundwater in Kuwait Desert. *Emirates Journal of Engineering Research.* 13:1-9.

Hardie, L.A., Smoot, J.P. & Eugster, H.P. 1978. Saline lakes and their deposits: a sedimentological approach. In *Modern and Ancient Lake Sediments.* A. Matter & W. Tucker, Eds. Special Publication 2 ed. International Association of Sedimentologists. 7-41.

Hardy, M. & Cornu, S. 2006. Location of natural trace elements in silty soils using particle-size fractionation. *Geoderma.* 133(3–4):295-308.

Harrison, S.P., Kohfeld, K.E., Roelandt, C. & Claquin, T. 2001. The role of dust in climate changes today, at the last glacial maximum and in the future. *Earth-Science Reviews.* 54(1-3):43-80.

Haywood, J.M. & Boucher, O. 2000. Estimates of the direct and indirect radiative forcing due to tropospheric aerosols: A review. *Reviews of Geophysics.* 38(4):513-543.

Helgren, D.M. 1984. Historical Geomorphology and Geoarchaeology in the Southwestern Makgadikgadi Basin, Botswana. *Annals of the Association of American Geographers.* 74(2):298-307.

Herman, J.R., Bhartia, P.K., Torres, O., Hse, C., Seftor, C. & Celarier, E. 1997. Global distribution of UV-absorbing aerosols from Nimbus 7/TOMS data. *Journal of Geophysical Research.* 102(D14):911-196.

Hesse, P.P. & McTainsh, G.H. 2003. Australian dust deposits: Modern processes and the Quaternary record. *Quaternary Science Reviews.* 22(18-19):2007-2035.

Hobbs, P.V. 2000. *Introduction to Atmospheric Chemistry.* First ed. USA: Cambridge University Press.

Holben, B.N., Tanre, D., Smirnov, A., Eck, T.F., Slutsker, I., Abuhassan, N., Newcomb, W.W., Schafer, J.S., Chatenet, B. & Lavenu, F. 2001. An emerging ground-based aerosol climatology: Aerosol optical depth from AERONET. *Journal of Geophysical Research: Atmospheres (1984–2012).* 106(D11):12067-12097.

Hsu, N.C. 2007. Global retrieval of aerosol properties from sources to sinks by MODIS. *Developments in Earth Surface Processes.* 1:23.

Hsu, N.C., Tsay, S.C. & King, M.D. 2004. Aerosol Properties Over Bright-Reflecting Source Regions. *IEEE Transactions on Geoscience and Remote Sensing.* 42(3)

Hsu, N.C., Tsay, S.C., King, M.D. & Herman, J.R. 2006. Deep blue retrievals of Asian aerosol properties during ACE-Asia. *Geoscience and Remote Sensing, IEEE Transactions On.* 44(11):3180-3195.

Huang, J., Ge, J. & Weng, F. 2007. Detection of Asia dust storms using multisensor satellite measurements. *Remote Sensing of the Environment.* 110:186-191.

Hulsmans, A., Bracke, S., Moreau, K., Riddoch, B.J., De Meester, L. & Brendonck, L. 2006. Dormant egg bank characteristics and hatching pattern of the Phallocryptus spinosa (Anostraca) population in the Makgadikgadi Pans (Botswana). *Hydrobiologia.* 571(1):123-132.

Humphries, M.S., McCarthy, T.S., Cooper, G.R.J., Stewart, R.A. & Stewart, R.D. 2013. The role of airborne dust in the growth of tree islands in the Okavango Delta, Botswana. *Geomorphology.* (0)

Ichoku, C., Remer, L.A., Kaufman, Y.J., Levy, R., Chu, D.A., Tanre, D. & Holben, B.N. 2003. MODIS observation of aerosols and estimation of aerosol radiative forcing over southern Africa during SAFARI 2000. *Journal of Geophysical Research.* 108(D13):8499.

Jickells, T.D. *et al.* 2005. Global Iron Connections Between Desert Dust, Ocean Biogeochemistry, and Climate. *Science.* 308(1 April 2005):67-71.

Joeckel, R.M. & Clement, B.A. 1999. Surface features of the Salt Basin of Lancaster County, Nebraska. *Catena.* 34(3–4):243-275.

Kaufman, Y.J., Karnieli, A. & Tanre, D. 2000. Detection of Dust Over Deserts Using Satellite Data in the Solar Wavelengths. *IEEE Transactions on Geoscience and Remote Sensing.* 38(1)

Kaufman, Y.J., Tanre, D. & Boucher, O. 2002. A satellite view of aerosols in the climate system. *Nature.* 419:215-225.

Khalaf, F. 1989. Textural characteristics and genesis of the aeolian sediments in the Kuwaiti desert. *Sedimentology.* 36(2):253-271.

Kidson, F. & Gregory, J. 1930. Australian Origin of Red Rain in New Zealand. *Nature.* 125:410-411.

Kiefert, L. 1994. Characteristics of wind transported dust in Eastern Australia. PhD Thesis, Faculty of Environmental Science, Griffith University, Brisbane, Australia.1-340

King, J., Wiggs, G.F.S., Thomas, D.S.G. & Washington, R. 2013. *The Role of Moisture on Controlling Dust Emissions from Crusted Supply-Limited Surfaces.* Abstract from EGU General Assembly 2013, Held 7-12 April, 2013 in Vienna, Austria, ID. EGU2013-12332.

King, M., Kaufman, Y., Tanre, D. & Nakajima, T. 1999. Remote sensing of tropospheric aerosols from space: past, present and future. *Bulletin of the American Meteorological Society.* 80:2229-2259.

King, J., Etyemezian, V., Sweeney, M., Buck, B.J. & Nikolich, G. 2011. Dust emission variability at the Salton Sea, California, USA. *Aeolian Research.* 3(1):67-79.

Kjelgaard, J., Sharratt, B., Sundram, I., Lamb, B., Claiborn, C., Saxton, K. & Chandler, D. 2004. PM10 emission from agricultural soils on the Columbia Plateau: comparison of dynamic and time-integrated field-scale measurements and entrainment mechanisms. *Agricultural and Forest Meteorology.* 125(3–4):259-277.

Klüser, L. & Schepanski, K. 2009. Remote sensing of mineral dust over land with MSG infrared channels: A new Bitemporal Mineral Dust Index. *Remote Sensing of Environment.* 113(9):1853-1867.

Knippertz, P. & Todd, M.C. 2012. Mineral dust aerosols over the Sahara: Meteorological controls on emission and transport and implications for modeling. *Reviews of Geophysics.* 50(1).

Kocurek, G.A. 1996. Desert aeolian systems. In *Sedimentary Environments: Processes, Facies and Stratigraphy*. H.G. Reading, Ed. Third Edition ed. Oxford: Blackwell Science. 125-153.

Kohlfeld, K.E. & Tegen, I. 2007. The Record of Soil Dust Aerosols and Their Role in the Earth System. In *Treatise on Geochemistry* . H.D. Holland & K.K. Turekian, Eds. Update 1 v 4.13 ed. Oxford: Elsevier Ltd. 1-26.

Kok, J.F. 2011. A scaling theory for the size distribution of emitted dust aerosols suggests climate models underestimate the size of the global dust cycle. *Proceedings of the National Academy of Sciences of the United States of America.* 108(3):1016-1021.

Komar, P.D. 1987. Selective grain entrainment by a current from a bed of mixed sizes; a reanalysis. *Journal of Sedimentary Research.* 57(2):203-211.

Kommalapati, R.R. & Valsaraj, K.T. 2009. Atmospheric Aerosols and Their Importance. In *Atmospheric Aerosols: Characterization, Chemistry, Modeling, and Climate.* K.T. Valsaraj & R.R. Kommalapati, Eds. USA: American Chemical Society, Oxford University Press. 1-12.

Konert, M. & Vandenberghe, J.E.F. 1997. Comparison of laser grain size analysis with pipette and sieve analysis: a solution for the underestimation of the clay fraction. *Sedimentology.* 44(3):523-535.

Kriews, M. & Schrems, O. 1998. Aerosol sampling depending on precipitation at Spitsbergen. *Journal of Aerosol Science.* 29(Supplement 2):S685-S686.

Krishna, K. 1968. A numerical study of the diurnal variation of meteorological parameters in the planetary boundary layer. *Monthly Weather Review.* 96:269-276.

Krueger, B.J., Grassian, V.H., Cowin, J.P. & Laskin, A. 2004. Heterogeneous chemistry of individual mineral dust particles from different dust source regions: the importance of particle mineralogy. *Atmospheric Environment.* 38(36):6253-6261.

Kunze, G.W. & Dixon, J.B. 1986. Pretreatment for mineralogical analysis. In *Methods of soil analysis. Part 1: Physical and mineralogical methods.* A. Klute, Ed. SSSA Book Series 5, 2nd ed. ed. Madison, WI: American Society of Agronomy-Soil Science Society of America. 91-100.

Landman, W.A. & Mason, S.J. 1999. Operational long-lead prediction of South African rainfall using canonical correlation analysis. *International Journal of Climatology.* 19(10):1073-1090.

Langston, G. & McKenna Neuman, C. 2005. An experimental study on the susceptibility of crusted surfaces to wind erosion: A comparison of the strength properties of biotic and salt crusts. *Geomorphology.* 72(1–4):40-53.

Laurent, B., Marticorena, B., Bergametti, G., Léon, J.F. & Mahowald, N.M. 2008. Modeling mineral dust emissions from the Sahara desert using new surface properties and soil database. *Journal of Geophysical Research: Atmospheres.* 113(D14):- D14218.

Lawrence, C.R. & Neff, J.C. 2009. The contemporary physical and chemical flux of aeolian dust: A synthesis of direct measurements of dust deposition. *Chemical Geology.* 267(1-2):46-63.

Lawrence, C.R., Painter, T.H., Landry, C.C. & Neff, J.C. 2010. Contemporary geochemical composition and flux of aeolian dust to the San Juan Mountains, Colorado, United States. *Journal of Geophysical Research: Biogeosciences.* 115(G3):- G03007.

Lee Black, D., McQuay, M.Q. & Bonin, M.P. 1996. Laser-based techniques for particle-size measurement: A review of sizing methods and their industrial applications. *Progress in Energy and Combustion Science.* 22(3):267-306.

Lee, J.E., Gill, T.E., Mulligan, K.R., Acosta, M.D. & Perez, A.E. 2009. Land use/land cover and point sources of the 15 December 2003 dust storm in southwestern North America. *Geomorphology.* 105(1-2):18-27.

Lee, T.F. 1989. Dust tracking using composite Visible/IR images: A Case Study. *Notes and Correspondance in Weather and Forcasting.* 4:258-263.

Leys, J.F. & Eldridge, D.J. 1998. Influence of cryptogamic crust disturbance to wind erosion on sand and loam rangeland soils. *Earth Surface Processes and Landforms.* 23(11):963-974.

Leys, J.F. & McTainsh, G.H. 1996. Sediment fluxes and particle grain-size characteristics of wind-eroded sediments in southeastern Austrailia. *Earth Surface Processes and Landforms.* 21(7):661-671.

Lindesay, J.A. 1998. Present Climates of southern Africa. In *Climates of the Southern Continents: Past, Present and Future.* J.E. Hobbs, J.A. Lindesay & H.A. Bridgman, Eds. Chichester: John Wiley & Sons. 5-62.

Littmann, T. 1991. Rainfall, Temperature and Dust Storm Anomalies in the African Sahel. *The Geographical Journal.* 157(2):136-160.

Livingstone, I. & Warren, A. 1996. *Aeolian Geomorphology: An Introduction. Longman.* Longman.

Loizeau, J., Arbouille, D., Santiago, S. & Vernet, J. 2006. Evaluation of a wide range laser diffraction grain size analyser for use with sediments. *Sedimentology.* 41(2):353-361.

Lowenstein, T.K. & Hardie, L.A. 1985. Criteria for the recognition of salt-pan evaporites. *Sedimentology.* (32):627-644.

Lu, H. 1999. An integrated wind erosion modelling system with emphasis on dust emission and transport. PhD (Mathematical Science). School of Mathematics, The University of New South Wales, Sydney, Australia.

Lundholm, B. 1977. Chapter 3: Ecology and Dust Transport. In *Saharan Dust.* C. Morales, Ed. New York: John Wiley and Sons. 297.

Ma, Z., Merkus, H.G., de Smet, J.G.A.E., Heffels, C. & Scarlett, B. 2000. New developments in particle characterization by laser diffraction: size and shape. *Powder Technology.* 111(1–2):66-78.

Ma, Z., Merkus, H.G. & Scarlett, B. 2001. Extending laser diffraction for particle shape characterization: technical aspects and application. *Powder Technology.* 118(1–2):180-187.

Maher, B., Prospero, J.M., Mackie, D., Gaiero, D., Hesse, P.P. & Balkanski, Y. 2010. Global connections between aeolian dust, climate and ocean biogeochemistry at the present day and at the last glacial maximum. *Earth Science Reviews.* 99(1-2):61-97.

Mahowald, N. 2011. Aerosol indirect effect on biogeochemical cycles and climate. *Science.* 334(6057):794-796.

Mahowald, N.M., Albani, S., Kok, J.F., Engelstaeder, S., Scanza, R., Ward, D.S. & Flanner, M.G. Corrected Proof. The size distribution of desert dust aerosols and its impact on the Earth system. *Aeolian Research.* (0)

Mahowald, N.M., Ballantine, J.A., Feddema, J. & Ramankutty, N. 2007. Global trends in visibility: implications for dust sources. *Atmospheric Chemistry and Physics.* 7(12):3309-3339.

Mahowald, N.M., Bryant, R.G., del Corral, J. & Steinberger, L. 2003. Ephemeral lakes and desert dust sources. *Geophysical Research Letters.* 30(2):1074.

Mahowald, N.M. & Luo, C. 2003. A less dusty future? . *Geophysical Research Letters.* 30(17):1903.

Mahowald, N.M., Muhs, D.R., Levis, S., Rasch, P.J., Yoshioka, M., Zender, C.S. & Luo, C. 2006. Change in atmospheric mineral aerosols in response to climate: Last Glacial period, preindustrial, modern, and doubled carbon dioxide climates. *Journal of Geophysical Research - Atmospheres.* 111(D10202).

Mahowald, N.M., Ward, D.S., Kloster, S., Flanner, M.G., Heald, C.L., Heavens, N.G., Hess, P.G., Lamarque, J. & Chuang, P.Y. 2011. Aerosol Impacts on Climate and Biogeochemistry. *Annual Review of Environment and Resources.* 36(1):45-74.

Mahowald, N.M., Zender, C.S., Luo, C., Savoie, D., Torres, O. & Del Corral, J. 2002. Understanding the 30-year Barbados desert dust record. *Journal of Geophysical Research.* 107(D21):4561.

Malvern Instruments Limited 2012. *A Basic Guide to Particle Characterization: Inform white paper.* Grovewood Road, Malvern, Worcestershire, UK: Malvern Instruments.

Malvern Instruments Limited. March 2007. *Mastersizer 2000 User Manual.* Malvern Instruments, Malvern, Worcestershire, United Kingdom: .

Marticorena, B., Bergametti, G., Gillette, D., Gillette, D.A. & Belnap, J. 1997. Factors controlling threshold friction velocity in semiarid and arid areas of the United States. *Journal of Geophysical Research: Atmospheres (1984–2012).* 102(D19):23277-23287.

Martin, R.S., Mather, T.A., Pyle, D.M., Power, M., Allen, A.G., Aiuppa, A., Horwell, C.J. & Ward, E.P.W. 2008. Composition-resolved size distributions of volcanic aerosols in the Mt. Etna plumes. *Journal of Geophysical Research.* 113:D17211-D17228.

McCarthy, T.S., Humphries, M.S., Mahomed, I., Le Roux, P. & Verhagen, B.T. 2012. Island forming processes in the Okavango Delta, Botswana. *Geomorphology.* 179(0):249-257.

McCave, I., Bryant, R., Cook, H. & Coughanowr, C. 1986. Evaluation of a laser-diffraction-size analyzer for use with natural sediments. *Journal of Sedimentary Research.* 56(4):561-564.

McCulloch, G.P. 2003. The Ecology of Sua Pan and its flamingo populations. PhD thesis. University of Dublin Trinity College and Ministry of Environment, Wildlife and Tourism.

McCulloch, G.P., Irvine, K., Eckardt, F.D. & Bryant, R.G. 2008. Hydrochemical fluctuatiuons and crustacean community composition in an ephemeral saline lake (Sua Pan, Makgadikgadi Botswana). *Hydrobiologia.* 596:31-46.

McFadden, L.D., Wells, S.G. & Jercinovich, M.J. 1987. Influences of eolian and pedogenic processes on the origin and evolution of desert pavements. *Geology.* 15(6):504-508.

McFarlane, M.J., Coetzee, S.H., Kuhn, J.R., Vanderpost, C.H.M. & Eckardt, F.D. 2007. In situ rounding of quartz grains within an African surface weathering profile in North West Ngamiland, Botswana. *Zeitschrift Für Geomorphologie.* 51(3):269-286.

McGowan, H. & Clark, A. 2008. Identification of dust transport pathways from Lake Eyre, Australia using Hysplit. *Atmospheric Environment.* 42:6915-6924.

McKenna-Neuman, C. & Gilbert, R. 1986. Aeolian processes and landforms in glaciofluvial environments of southeastern Baffin Island, NWT, Canada. *Aeolian Geomorphology.* :213-235.

McTainsh, G., Chan, Y., McGowan, H., Leys, J. & Tews, K. 2005. The 23rd October 2002 dust storm in eastern Australia: characteristics and meteorological Conditions. *Atmospheric Environment.* 3(7):1227-1236.

McTainsh, G. & Strong, C. 2007. The role of aeolian dust in ecosystems. *Geomorphology.* 89(1-2):39-54.

McTainsh, G.H., Leys, J.F. & Nickling, W.G. 1999. Wind erodibility of arid lands in the Channel Country of western Queensland, Australia. *Zeitschrift Für Geomorphologie.* 116:113-130.

McTainsh, G.H., Livingstone, I. & Strong, C.L. 2013. Fundamentals of Aeolian sediment transport: Aeolian sediments. In *Treatise on Geomorphology, Volume 11: Aeolian Geomorphology.* J.F. Shroder, Ed. Oxford: Academic Press. 23-42.

Mees, F. 2001. An occurrence of lacustrine Mg-smectite in a pan of the southwestern Kalahari, Namibia. *Clay Minerals.* 36(547):556.

Mees, F. 2003. Salt mineral distribution patterns in soils of the Otjomongwa pan, Namibia. *Catena.* 54(3):425-437.

Mei, F., Zhang, X., Lu, H., Shen, Z. & Wang, Y. 2004. Characterization of MASDs of surface soils in north China and its influence on estimating dust emission. *Chinese Science Bulletin.* 49(20):2169-2176.

Middleton, N.J. 1997. Desert Dust. In *Arid Zone Geomorphology.* D.S.G. Thomas, Ed. Second Edition ed. Chichester: John Wiley and Sons. 413-436.

Middleton, N.J. & Goudie, A.S. 2001. Saharan dust: sources and trajectories. *Transactions of the Institue of British Geographers.* 26:265-171.

Mishchenko, M.I., Travis, L.D., Kahn, R.A. & West, R.A. 1997. Modeling phase functions for dust-like tropospheric aerosols using a shape mixture of randomly oriented polydisperse spheroids. *Journal of Geophysical Research.* 102:16831-16847.

Moreno, T., Querol, X., Castillo, S., Alastuey, A., Cuevas, E., Herrmann, L., Mounkaila, M., Elvira, J. & Gibbons, W. 2006. Geochemical variations in aeolian mineral particles from the Sahara–Sahel Dust Corridor. *Chemosphere.* 65(2):261-270.

Morman, S.A. & Plumlee, G.S. 2013. The role of airborne mineral dusts in human disease. *Aeolian Research.* (9):203-212.

Muhs, D.R. 2013. The geologic records of dust in the Quaternary. *Aeolian Research.* 9:3-48.

Nash, D.J., Thomas, D.S.G. & Shaw, P.A. 1994. Siliceous duricrusts as palaeoclimatic indicators: evidence from the Kalahari desert of Botswana. *Palaeogeography, Palaeoclimatology, Palaeoecology*. 112(3–4):279-295.

Natsagdorj, L., Jugder, D.J. & Chung, Y.S. 2003. Analysis of dust storms observed in Mongolia during 1937 - 1999. *Atmospheric Environment.* 37:1401-1411.

Neff, J.C., Ballantyne, A.P., Farmer, G.L., Mahowald, N.M., Conroy, J.L., Landry, C.C., Overpeck, J.T., Painter, T.H., Lawrence, C.R. & Reynolds, R.L. 2008. Increasing eolian dust deposition in the western United States linked to human activity. *Nature Geoscience - Advanced Online Publication.* 1:185-189.

Nicholson, S.E. 2009. A revised picture of the structure of the "monsoon" and land ITCZ over West Africa. *Climate Dynamics.* 32(7-8):1155-1171.

Nicholson, S.E. & Kim, J. 1997. The relationship of the El Nino–southern oscillation to African rainfall 117–135. *International Journal of Climatology.* 17:117-135.

Nicholson, S.E., Leposo, D. & Grist, J. 2001. The relationship between El Nino and drought over Botswana. *Journal of Climate.* 14:323-335.

Nickling, W.G. 1983. Grain-size characteristics of sediment transported during dust storms. *Journal of Sedimentary Petrology.* 53(3):1011-1024.

Nickling, W.G. 1984. The stabilizing role of bonding agents on the entrainment of sediment by wind. *Sedimentology.* 31(1):111-117.

Nickling, W.G. & Ecclestone, M. 1981. The effects of soluble salts on the threshold shear velocity of fine sand. *Sedimentology.* 28(4):505-510.

Nield, J.M., King, J. & Jacobs, B. 2014. Detecting surface moisture in aeolian environments using terrestrial laser scanning. *Aeolian Research.* 12:9-17.

Nield, J.M., King, J., Wiggs, G.F.S., Leyland, J., Bryant, R.G., Chiverrell, R.C., Darby, S.E., Eckardt, F.D., Thomas, D.S.G., Vircavs, L.H. & Washington, R. 2013. Estimating aerodynamic roughness over complex surface terrain. *Journal of Geophysical Research: Atmospheres.* 118(23):12948-12961.

Nield, J.M., Wiggs, G.F.S., King, J., Bryant, R.G., Eckardt., F.D., Thomas, D.S.G., Washington, R. & Coetzee, S.H. in prep. Salt crust and moisture interactions on an emissive sodic playa. *Earth Surface Processes and Landforms.* :1-37.

O'Neill, N.T., McArthur, J.L.B. & Strawbridge, K.B. 2005. Recent Progress in the Remote Sensing of Aerosols. *Physics in Canada.* September/October:93-99.

O'Loingsigh, T.O., McTainsh, G.H., Tews, E.K., Strong, C.L., Leys, J.F., Shinkfield, P. & Tapper, N.J. 2014. The Dust Storm Index (DSI): A method for monitroing broadscale wind erosion using meteorological records. *Aeolian Research. 12:29-40*

Offer, Z.Y. & Goossens, D. 2001. Ten years of aeolian dust dynamics in a desert region (Negev desert, Israel): analysis of airborne dust concentration, dust accumulation and the high-magnitude dust events. *Journal of Arid Environments.* 47(2):211-249.

Okada, K. & Kai, K. 2004. Atmospheric mineral particles collected at Qira in the Taklamakan Desert, China. *Atmospheric Environment.* 38(40):6927-6935.

Okin, G.S., Baker, A.R., Tegen, I., Mahowald, N.M., Dentener, F.J., Duce, R.A., Galloway, J.N., Hunter, K., Kanakidou, M. & Kubilay, N. 2011a. Impacts of atmospheric nutrient deposition on marine productivity: Roles of nitrogen, phosphorus, and iron. *Global Biogeochemical Cycles.* 25(2):GB2022.

Okin, G.S., Bullard, J.E., Reynolds, R.L., Ballantine, J.A., Schepanski, K., Todd, M.C., Belnap, J., Baddock, M.C., Gill, T.E. & Miller, M.E. 2011b. Dust: Small-Scale Processes With Global Consequences. *EOS Transactions: (American Geophysical Union).* 92:241-248.

Olesik, J.W. 1991. Elemental analysis using ICP-OES and ICP/MS. *Analytical Chemistry.* 63(1):12A-21A.

Painter, T., Barrett, A., Landry, C.C., Neff, J.C., Cassidy, M.P., Lawrence, C.R., McBride, K.E. & Farmer, G.L. 2007. Impact of disturbed desert soils on duration of mountain snow cover. *Geophysical Research Letters.* 34(12):L12502.

Perkins, J.S. & Thomas, D.S.G. 1993. Spreading deserts or spatially confined environmental impacts? land degradation and cattle ranching in the kalahari desert of botswana. *Land Degradation & Development.* 4(3):179-194.

Petit, J.R., Briat, M. & Royer, A. 1981. Ice age aerosol content from East Antarctic ice core samples and past wind strength. *Nature.* 293(5831):391-394.

Piketh, S.J., Annegarn, H.J. & Tyson, P.D. 1999. Lower Tropospheric aerosol dust loadings over South Africa: The relative contribution of aeolian dust industrial emissions and biomass burning. *Journal of Geophysical Research.* 104:1597-1607.

Piketh, S.J., Tyson, P.D. & Steffen, W. 2000. Aeolian Transport from southern Africa and iron fertilisation of marine biota in South Indian Ocean. *South African Journal of Science.* 96:244-246.

Powers, M.C. 1953. A new roundness scale for sedimentary particles. *Journal of Sedimentary Petrology.* 23(2):117-119.

Prospero, J.M., Charlson, R.J., Mohnen, V., Jaenicke, R., Delany, A.C., Moyers, J., Zoller, W. & Rahn, K. 1983. The Atmospheric Aerosol System: An overview. *Reviews of Geophysics.* 21(7):1607-1629.

Prospero, J.M. 1999. Long-range transport of mineral dust in the global atmosphere: Impact of African dust on the environment of the south eastern United States. *Proc.National Academy of Science, USA.* 96:3396-3403.

Prospero, J.M., Ginoux, P., Torres, O., Nicholson, S.E. & Gill, T.E. 2002. Environmental characterization of global sources of atmospheric soil dust identified with the nimbus 7 Total Ozone Mapping Spectrometer (TOMS) absorbing aerosol product. *Review of Geophysics.* 40(1):1002.

Prospero, J.M., Nees, R.T. & Uematsu, M. 1987. Deposition rate of particulate and dissolved aluminum derived from Saharan dust in precipitation at Miami, Florida. *Journal of Geophysical Research - Atmospheres.* 92(D12):14723-14731.

Pye, K. 1987. *Aeolian dust and dust deposits.* First ed. London: Academic Press.

Ramanathan, V., Crutzen, P.J., Kiehl, J.T. & Rosenfeld, D. 2001. Aerosols, Climate, and the Hyrdological Cycle. *Science.* 294:2119-2124.

Ramaswamy, V., Boucher, O., Haigh, J., Hauglustine, D., Haywood, J., Myhre, G., Nakajima, T., Shi, G.Y. & Solomon, S. 2001. Radiative forcing of climate change. In *Climate Change 2001: The Scientific Basis.* J.T. Houghton, and others, Ed. Cambridge: Cambridge University Press. 349-416.

Ratna, S.B., Behera, S., Ratnam, J.V., Takahashi, K. & Yamagata, T. 2013. An index for tropical temperate troughs over southern Africa. *Climate Dynamics.* 41:421-441.

Ravi, S., D'Odorico, P., Breshears, D.D., Field, J.P., Goudie, A.S., Huxman, T.E., Li, J., Okin, G.S., Swap, R.J., Thomas, A.D., Van Pelt, S., Whicker, J.J. & Zobeck, T.M. 2011. Aeolian processes and the biosphere. *Reviews of Geophysics.* 49(3):n/a-n/a.

Reason, C.J.C. 2002. Sensitivity of the southern African circulation to dipole sea-surface temperature patterns in the south Indian Ocean. *International Journal of Climatology.* 22:377-393.

Reason, C.J.C., Engelbrecht, F., Landman, W.A., Lutjeharms, J.R.E., Piketh, S., de Wet, C.J., Rautenbach, W. & Hewitson, B.C. 2006. A review of South African research in atmospheric science and physical oceanography during 2000-2005. *South African Journal of Science.* 102:35-45.

Reheis, M.C. 1997. Dust deposition downwind of Owens (dry) Lake, 1991-1994: Preliminary findings. *Journal of Geophysical Research.* 102(D22):25999-26008.

Reheis, M.C. 2006a. USA: Controls on dust generation and accumulation. *Journal of Arid Environments.* 67:487-520.

Reheis, M.C. & Kihl, R. 1995. Dust deposition in southern Nevada and California, 1984?1989: Relations to climate, source area, and source lithology. *Journal of Geophysical Research: Atmospheres.* 100(D5):8893-8918.

Reheis, M.C. 2006b. A 16-year record of eolian dust in Southern Nevada and California, USA: Controls on dust generation and accumulation. *Journal of Arid Environments.* 67(3):487-520.

Reheis, M.C., Budahn, J.R. & Lamothe, P.J. 2002. Geochemical evidence for diversity of dust sources in the southwestern United States. *Geochimica Et Cosmochimica Acta.* 66(9):1569-1587.

Reid, I. & Frostick, L.E. 1985. Beach orientation, bar morphology and the concentration of metalliferous placer deposits: a case study, Lake Turkana, N Kenya. *Journal of the Geological Society.* 142(5):837-848.

Reid, J.S., Jonsson, H.H., Maring, H.B., Smirnov, A., Savoie, D.L., Cliff, S.S., Reid, E.A., Livingston, J.M., Meier, M.M. & Dubovik, O. 2003. Comparison of size and morphological measurements of coarse mode dust particles from Africa. *Journal of Geophysical Research.* 108(D19):8593-8620.

Resane, T., Annegarn, H. & Freiman, T. 2004. The day of the white rain: origin of unusual dust deposition in Johannesburg, South Africa. *South African Journal of Science.* 100(9-10):483-487.

Retsch GmbH. 31 July 2012. *Operating Instructions - AS200 Analytical Sieve Shakers.* Haan, Retsch-Allee 1-5, Federal Republic of Germany: Retsch Technical Document.

Reynolds, R.L., Belnap, J., Reheis, M.C., Lamothe, P. & Luiszer, F. 2001. Aeolian dust in Colorado Plateau soils: nutrient inputs and recent change in source. *Proceedings of the National Academy of Sciences.* 98(13):7123-7127.

Reynolds, R.L., Neff, J.C., Reheis, M.C. & Lamothe, P. 2006. Atmospheric dust in modern soil on aeolian sandstone, Colorado Plateau (USA): Variation with landscape position and contribution to potential plant nutrients. *Geoderma.* 130(1–2):108-123.

Reynolds, R.L., Bogle, R., Vogel, J., Goldstein, H.L. & Yount, J.C. 2009. Dust Emission at Franklin Lake Playa, Mojave Desert (USA): Response to Meteorological and Hydrologic Changes 2005-2008. *Natural Resources and Environmental Issues.* 15(Article 18):105-115.

Reynolds, R.L., Yount, J.C., Reheis, M.C., Goldstein, H., Chavez, P., Fulton, R., Whitney, J., Fuller, C. & Forester, R.M. 2007. Dust emission from wet and dry playas in the Mojave Desert, USA. *Earth Surface Processes and Landforms.* 32(12):1811-1827.

Rice, M.A., Willetts, B.B. & McEwan, I.K. 1996. Wind erosion of crusted soil sediments. *Earth Surface Processes and Landforms.* 21(3):279-293.

Ridgwell, A.J. 2002. Dust in the Earth System: The Biogeochemical Linking of Land, Air and Sea. *Philosophical Transactions: Mathematical, Physical and Engineering Sciences.* 360(1801, Astronomy and Earth Science):pp. 2905-2924.

Ringrose, S., Huntsman-Mapila, P., Basira Kampunzu, A., Downey, W., Coetzee, S., Vink, B., Matheson, W. & Vanderpost, C. 2005. Sedimentological and geochemical evidence for palaeo-environmental change in the Makgadikgadi subbasin, in relation to the MOZ rift depression, Botswana. *Palaeogeography, Palaeoclimatology, Palaeoecology.* 217(3–4):265-287.

Ringrose, S., Downey, B., Genecke, D., Sefe, F. & Vink, B. 1999. Nature of sedimentary deposits in the western Makgadikgadi basin, Botswana. *Journal of Arid Environments.* 43(4):375-397.

Rivera Rivera, N.I., Gill, T.E., Bleiweiss, M.P. & Hand, J.L. 2010. Source characteristics of hazardous Chihuahuan Desert dust outbreaks. *Atmospheric Environment.* 44:2457-2468.

Rodríguez, S., Alastuey, A. & Querol, X. 2012. A review of methods for long term in situ characterization of aerosol dust. *Aeolian Research.* 6(0):55-74.

Ryder, C.L., Highwood, E.J., Lai, T.M., Sodemann, H. & Marsham, J.H. 2013. Impact of atmospheric transport on the evolution of microphysical and optical properties of Saharan dust. *Geophysical Research Letters.* 40(10):2433-2438.

Saint-Amand, P., Gaines, C. & Saint-Amand, D. 1987. Owens Lake, an ionic soap opera staged on a nitric playa. *Geological Society of America - Centennial Field Guide.* Cordilleran Section:113-118.

Saint-Amand, P., Mathews, L.A., Gaines, C. & Reinking, R. 1986. Dust storms from Owens and Mono Valleys, California. *Naval Weapons Center Technical Document 6731.* :83.

Schepanski, K., Tegen, I., Laurent, B., Heinold, B. & Macke, A. 2007. A new Saharan dust source activation frequency map derived from MSG-SEVIRI IRchannels. *Geophysical Research Letters.* 34(L18803)

Schulze, M.R. 1972. South Africa. In *Climates of Africa. World Surveys of Climatology.* J.F. Griffiths, Ed. Volume 10 ed. Amsterdam: Elsevier. 501-586.

Setlhogile, T., Arntzen, J., Mabiza, C. & Mano, R. 2011. Economic valuation of selected direct and indirect use values of the Makgadikgadi wetland system, Botswana. *Physics and Chemistry of the Earth, Parts A/B/C.* 36(14–15):1071-1077.

Shahidzadeh-Bonn, N., Desarnaud, J., Bertrand, F., Chateau, X. & Bonn, D. 2010. Damage in porous media due to salt crystallization. *Physical Review E.* 81(6):066110.

Shang, C. & Zelanzy, L.W. 2008. Selective dissolution techniques for mineral analysis of soils and sediments. In *Methods of soil analysis. Part 5: Mineralogical Methods.* A.L. Ulery & L.R. Drees, Eds. SSSA Book Series 5 ed. Madison, WI: Soil Science Society of America. 33-80.

Shao, Y. 2000. *Physics and modelling of wind erosion.* Dordrecht: Kluwer.

Shao, Y., Wyrwoll, K.H., Chappell, A., Huang, J., Lin, Z., McTainsh, G.H., Mikami, M., Tanaka, T.Y., Wang, X. & Yoon, S. 2011. Dust cycle: An emerging core theme in Earth system science. *Aeolian Research.* 2(4):181-204.

Shao, Y., McTainsh, G., Leys, J. & Raupach, M. 1993. Efficiencies of sediment samplers for wind erosion measurement. *Soil Research.* 31(4):519-532.

Shaw, P.A. & Bryant, R.G. 2011. Pans, Playas and Salt Lakes. In *Arid Zone Geomorphology: Process, Form and Change in Drylands.* D.S.G. Thomas, Ed. 3rd Edition ed. Chichester, UK: John Wiley & Sons, Ltd. 373-401.

Shaw, P.A. & Thomas, D.S.G. 1997. Pans playas and salt lakes. In *Arid Zone Geomorphology: Processes, Form and Change in Drylands.* D.S.G. Thomas, Ed. John Wiley and Sons. 293-318.

Shi, Z., Krom, M.D., Jickells, T.D., Bonneville, S., Carslaw, K.S., Mihalopoulos, N., Baker, A.R. & Benning, L.G. 2012. Impacts on iron solubility in the mineral dust by processes in the source region and the atmosphere: A review. *Aeolian Research.* 5(0):21-42.

Soderberg, K. & Compton, J.S. 2006. Dust as a Nutrient Source for Fynbos Ecosystems, South Africa. *Ecosystmes.* 10:550-561.

Sokolik, I.N. & Toon, O.B. 1996. Direct radiative forcing by anthropogenic airborn mineral aerosols. *Nature.* 381(6584):681-683.

Solomon, S. et al. 2007. Technical Summary . In *Climate Change 2007: The Physical Science Basis. Contribution of Working Group I to the Fourth Assessment Report of the Intergovernmental Panel on Climate Change.* . Solomon, S.,Qin, D., and others, Ed. Cambridge, United Kingdom and New York, NY, USA.: Cambridge University Press.

Soukup, D.A., Buck, B.J. & Harris, W. 2008a. Preparing soils for mineralogical analyses. In *Methods of Soil Analysis, Part 5: Mineralogical Methods.* A.L. Ulery & L.R. Drees, Eds. Volume 5 of Soil Science Society of America Book Series ed. Madison, WI, USA: ASA-CSSA-SSSA. 13-31.

Soukup, D.A., Drees, L.R. & Lynn, W.C. 2008b. Sampling soils for mineralogical analyses. In *Methods of Soil Analysis, Part 5: Mineralogical Methods.* A.L. Ulery & L.R. Drees, Eds. Volume 5 of Soil Science Society of America Book Series ed. Madison, WI, USA: ASA-CSSA-SSSA. 1-11.

Sow, M., Goossens, D. & Rajot, J.L. 2006. Calibration of the MDCO dust collector and of four versions of the inverted frisbee dust deposition sampler. *Geomorphology.* 82(3-4):360-375.

Speirs, J.C., McGowan, H.A. & Neil, D.T. 2008. Polar Eolian Sand Transport: Grain characteristics determined by an Automated Scanning Electron Microscop (QEMSCAN). *Arctic, Antarctic, and Alpine Research.* 40(4):731-743.

Stout, J.E., Warren, A. & Gill, T.E. 2009. Publication trends in aeolian research: an analysis of the Bibliography of Aeolian Research. *Geomorphology.* 105:6-17.

Strong, C.L., Parsons, K., McTainsh, G.H. & Sheehan, A. 2011. Dust transporting wind systems in the lower Lake Eyre Basin, Australia: A preliminary study. *Aeolian Research.* 4(2):205-214.

Sun, J. & Ariya, P.A. 2006. Atmospheric organic and bio-aerosols as cloud condensation nuclei (CCN): A review. *Atmospheric Environment.* 40(5):795-820.

Svobida, L. 1986. *Farming the Dust Bowl: A First-Hand Account from Kansas.* First ed. Kansas, USA: University Press of Kansas.

Swap, R., Garstang, M., Greco, S., Talbot, R. & Kallberg, P. 1992. Saharan dust in the Amazon Basin. *T.* 44(2):133-149.

Sweeney, M., Etyemezian, V., Macpherson, T., Nickling, W., Gillies, J., Nikolich, G. & McDonald, E. 2008. Comparison of PI-SWERL with dust emission measurements from a straight-line field wind tunnel. *Journal of Geophysical Research: Earth Surface.* 113(F1):- F01012.

Swineford, A. & Frye, J.C. 1945. A mechanical analysis of wind-blown dust compared with analyses of loess. *American Journal of Science.* 243(5):249-255.

Taljaard, J.J. 1982. Cut-off lows and heavy rain over the Republic. *South African Weather Bureau Newsletter.* No. 403:155-156.

Tanner, W.F. 1958. The zig-zag nature of Type I and Type IV curves. *Journal of Sedimentary Research.* 28(3):372-375.

Tegen, I. 2003. Modelling the mineral dust aerosol in the climate system. *Quaternary Science Reviews.* (22):1821-1834.

Tegen, I. & Fung, I. 1995. Contribution to the atmospheric mineral aerosol load from land surface modification. *Journal of Geophysical Research: Atmospheres.* 100(D9):18707-18726.

Tegen, I., Hollrig, P., Chin, M., Fung, I., Jacob, D. & Penner, J. 1997. Contribution of different aerosol species to the global aerosol extinction optical thickness: Estimates from model results. *Journal of Geophysical Research: Atmospheres.* 102(D20):23895-23915.

Thomas, D.S.G. 1987. Discrimination of depositional environments using sedimentary characteristics in the Mega Kalahari, central southern Africa. In *Desert Sediments: Ancient and Modern.* L.E. Frostick & I. Reid, Eds. Geological Society of London Special Publication. 293-306.

Thomas, D.S.G. & Shaw, P. 1991. *The Kalahari Environment.* Cambridge University Press.

Thomas, D.S.G. & Wiggs, G.F.S. 2008. Aeolian system responses to global change: challenges of scale, process and temporal integration. *Earth Surface Processes and Landforms.* 33(9):1396-1418.

Thomas, D.S. 2011. *Arid zone geomorphology: process, form and change in drylands.* Wiley.

Tinke, A.P., Carnicer, A., Govoreanu, R., Scheltjens, G., Lauwerysen, L., Mertens, N., Vanhoutte, K. & Brewster, M.E. 2008. Particle shape and orientation in laser diffraction and static image analysis size distribution analysis of micrometer sized rectangular particles. *Powder Technology.* 186(2):154-167.

Todd, M.C. & Washington, R. 1999. Circulation anomalies associated with tropical-temperate troughs in southern Africa and the south west Indian Ocean. *Climate Dynamics.* 15:937-951.

Torres, O., Bhartia, P.K., Herman, J.R., Sinyuk, A., Ginoux, P. & Holben, B. 2002. A long-term record of aerosol optical depth from TOMS observations and comparison to AERONET measurements. *Journal of the Atmospheric Sciences.* 59(3):398-413.

Tsoar, H. & Pye, K. 1987. Dust transport and the question of desert loess formation. *Sedimentology.* 34(1):139-153.

Turekian, K.K. & Wedepohl, K.H. 1961. Distribution of the elements in some major units of the earth's crust. *Geological Society of America Bulletin.* 72(2):175-192.

Turner, J. & Colbeck, I. 2008. Physical and Chemical Properties of Atmospheric Aerosols. In *Environmental Chemistry of Aerosols.* I. Colbeck, Ed. First ed. Oxford, UK: Blackwell Publishing. 1-25.

Tyson, P.D. 1987. *Climate Change and Variability in southern Africa.* Oxford University Press.

Tyson, P.D. & D'Abreton, P.C. 1998. Transport and recirculation of aerosols off southern Africa - macroscale plume structure. *Atmospheric Environments.* 32(9):1511-1524.

Tyson, P.D., Garstang, M. & Swap, R. 1996a. Large-Scale Recirculation of Air over Southern Africa. *Journal of Applied Meteorology.* 35:2218-2236.

Tyson, P.D., Garstang, M., Swap, R.J., Edwards, S. & Kallberg, P. 1996b. An air transport climatology for subtropical southern Africa. *International Journal of Climatology.* 16:365-291.

Tyson, P.D. & Gatebe, C.K. 2001. The atmosphere, aerosols, trace gases and biogeochemical change in southern Africa: a regional integration. *South Africa Journal of Science.* 97:106-118.

Tyson, P.D. & Preston-Whyte, R.A. 2000. *The Weather and Climate of Southern Africa.* Oxford University Press.

Udden, J.A. 1898. The Merchanical Composition of Wind Deposits. *Augustana Library Publications.* (1):69.

Udden, J.A. 1914. Mechanical composition of clastic sediments. *Bulletin of the Geological Society of America.* 25:655-744.

Vermote, E. & Vermeulen, A. 1999. Atmospheric correction algorithm: spectral reflectances (MOD09). *ATBD Version.* 4

Vickery, K.J. & Eckardt, F.D. 2013. Dust emission controls on the lower Kuiseb River valley, Central Namib. *Aeolian Research.* 10:125-133.

Vickery, K.J., Eckardt, F.D. & Bryant, R.G. 2013. A sub-basin scale dust plume source frequency inventory for southern Africa, 2005–2008. *Geophysical Research Letters.* 40(19):5274-5279.

Viles, H.A. & Goudie, A.S. 2007. Rapid salt weathering in the coastal Namib desert: Implications for landscape development. *Geomorphology*. 85(1):49-62.

Wang, H. & Jia, X. 2011. Field observations of windblown sand and dust in the Taklimakan Desert, NW China, and insights into modern dust sources. *Land Degradation & Development.* 24(4):323-333.

Wang, L., D'Odorico, P., Ringrose, S., Coetzee, S. & Macko, S.A. 2007. Biogeochemistry of Kalahari sands. *Journal of Arid Environments.* 71(3):259-279.

Wang, Y., Stein, A.F., Draxler, R.R., de la Rosa, J.D. & Zhang, X. 2011. Global sand and dust storms in 2008: Observation and HYSPLIT model verification. *Atmospheric Environment.* 45(35):6368-6381.

Warren, A., Chappell, A., Todd, M.C., Bristow, C., Drake, N., Engelstaedter, S., Martins, V., M'bainayel, S. & Washington, R. 2007. Dust-raising in the dustiest place on earth. *Geomorphology*. 92(1–2):25-37.

Washington, R., Bouet, C., Cautenet, G., Mackenzie, E., Ashpole, I., Engelstaedter, S., Lizcano, G., Henderson, G.M., Schepanski, K. & Tegen, I. 2009. Dust as a tipping element: The Bodélé Depression, Chad. *Proceedings of the National Academy of Sciences.* 106(49):20564-20571.

Washington, R. & Preston, A. 2006. Extreme wet years in southern Africa: the role of the Indian Ocean. *Journal of Geophysical Research: Atmospheres.* 111(D15104).

Washington, R., Todd, M.C., Engelstaedter, S., Mbainayel, S. & Mitchell, F. 2006. Dust and the low-level circulation over the Bodele Depression Chad: Observations from BoDEx 2005. *Journal of Geophysical Research.* 111(D03201)

Washington, R., Todd, M.C., Middleton, N.J. & Goudie, A.S. 2003. Dust-Storm source areas determined by the Total Ozone Monitoring Spectrometer and Surface Observations. *Annals of the Association of American Geographers.* 93(2):297-313.

Wentworth, C.K. 1922. A scale of grade and class terms for clastic sediments. *The Journal of Geology.* 30(5):377-392.

White, K. & Eckardt, F. 2006. Geochemical mapping of carbonate sediments in the Makgadikgadi basin, Botswana, using moderate resolution remote sensing data. *Earth Surface Processes and Landforms.* 31(6):665-681.

Wood, W.W., Eckardt, F.D., Kraemer, T.F. & Eng, K. 2011. Quantitative eolian transport of evaporite salts from the Makgadikgadi Depression (Ntwetwe and Sua Pans) in northeastern Botswana: Implications for regional ground-water quality. In *Sabkha Environments, Volume III: Africa and Southern Europe.* M. Ozturk, and others, Ed. London: Springer. 27-38.

Worster, D. 1982. *Dust bowl: the southern plains in the 1930s.* Oxford University Press.

Wright, E.P. 1978. Geological Studies in the Northern Kalahari. *The Geographical Journal.* 144(2):235-249.

Yang, Y.Q., Hou, Q., Zhou, C.H., Liu, H.L., Wang, Y.Q. & Niu, T. 2008. Sand/dust storm processes in Northeast Asia and associated large-scale circulations. *Atmospheric Chemistry and Physics.* 8:25-33.

Yechieli, Y. & Wood, W.W. 2002. Hydrogeologic processes in saline systems: playas, sabkhas, and saline lakes. *Earth-Science Reviews.* 58(3–4):343-365.

Young, J.A. & Evans, R.A. 1986. Erosion and deposition of fine sediments from playas. *Journal of Arid Environments.* 10:103-115.

Zender, C.S., Bian, H. & Newman, D. 2003. Mineral Dust Entrainment and Deposition (DEAD) model: Description and 1990s dust climatology. *Journal of Geophysical Research.* 108(D14):4416.

Zender, C.S. & Kwon, E.Y. 2005. Regional Contrasts in Dust Emission Responses to Climate. *Journal of Geophysical Research.* 110(D13201)

Zender, C.S., Miller, R.L. & Tegen, I. 2004. Quantifying mineral dust mass budgets: Terminology, constraints, and current estimates. *Eos, Transactions American Geophysical Union.* 85(48):509-512.

Zender, C.S. & Talamantes, J. 2006. Climate controls on valley fever incidence in Kern Country, California. *International Journal of Biometeorology.* 50:174-182.

Zhang, B., Tsunekawa, A. & Tsubo, M. 2008. Contributions of sandy lands and stony deserts to long-distance dust emission in China and Mongolia during 2000–2006. *Global and Planetary Change.* 60(3-4):487-504.

Zobler, L. 1986. *A world soil file for global climate modeling.* New York, N.Y: NASA Goddard Institute for Space Studies.

Appendix 1. Vertical Structure of the Pan Surface and Sampling Conditions.

Crust samples represent the hardened pan surface crust that was found at most sites with varying thickness from a few millimetres to over a centimetre in thickness. Below this, was found a dry powdery layer of varying thickness from zero to almost 8 centimetres, this represents the fluff. At some sites a second hardened layer was found between the fluff and the wet sediment layer below again in the order of a few millimetres to a centimetre in thickness, this is described by the second crust or horizon crust. The wet sediment which represents the lowest sampling horizon, extended relatively homogenously over a meter below the pan surface, has been classed as soil.

Fluff samples were then given the suffix F, which crust samples were given the suffix C, Soil was given S, which the secondary crust layer which lay beneath the primary crust (C) was given the suffix H, representing the horizon crust.

Samples were collected from the each site on the DO4 grid, sites were located centrally within each 1 km^2 grid. Samples were collected into zip lock bags and labelled according the naming procedure presented in Table B 1.1. Samples were collected between August and Octover before being stored at Sua lodge until being transported to Cape Town in late October of 2011. All samples were analysed in various laboratories at the University of Cape Town.

Table B 1.1: Table listing sample ID as used in this study as per naming procedure of site ID as developed for the DO4 Project with latitude and longitude co-ordinates of site presented.UTM co-ordinates also shown, samples not present are indicated by a '-'.

	Co-ordinates				Sample ID			
Site ID	Longitude	Latitude	Lon E (UTM 35S)	Lat S (UTM 35S)	Crust	Fluff	H-Crust	Soil
B3	25.9112	-20.5480	386500	7727500	B3C	B3F	-	B3S
B7	25.9109	-20.5841	386500	7723500	B7C	B7F	-	B7S
D2	25.9304	-20.5391	388500	7728500	D2C	D2F	D2H	D2S
D5	25.9303	-20.5662	388500	7725500	D5C	D5F	D5H	D5S
D10	25.9299	-20.6113	388500	7720500	D10C	D10F	D10H	D10S
G2	25.9592	-20.5392	391500	7728500	G2C	G2F	G2H	G2S
G6	25.9590	-20.5754	391500	7724500	G6C	G6F	-	G6S
I4	25.9783	-20.5574	393500	7726500	I4C	I4F	I4H	I4S
I8	25.9780	-20.5936	393500	7722500	I8C	I8F	I8H	I8S
J3	25.9879	-20.5484	394500	7727500	J3C	J3F	-	J3S
J11	25.9875	-20.6207	394500	7719500	J11C	-	J11H	J11S
L5	26.0070	-20.5666	396500	7725500	L5C	-	-	L5S

Appendix 2. Glossary of Statistical Terms as Defined by Folk (1966)

A2.1 Median

The diameter which has half the grains (by weight) finer and half coarser. Can be found graphically by finding the intercept of the 50^{th} percentile with the cumulative curve

A2.2 Mode

This is the most frequently occurring grain diameter – can have more than one modal class (bimodal/multimodal) in which case the most abundant is often termed the primary mode (Folk, 1966)

A2.3 Mean

The best measure of overall average size of the sediment as influenced by source supply, environment of deposition etc. – all sample values added and divided by the number included – not the best representation of samples with more than one modal value.

A2.4 Sorting

Sorting is the ratio between successive classes on a histogram as a function of total spread of histogram. Using the spread of the standard deviation from the mean on a normal distribution as an expression of the level of 'sortedness' of the sample

A2.5 Skewness

Skewness is the measure of non-normality of a distribution – geometrically independent of sorting. A dominant fine population with a subdominant course population results in negative skewness, while a dominant course population with subdominant fine population will result in a positive skewness. These skewed distributions of one dominant and one subdominant population will result in leptokurtic or excessively skewed distributions.

A2.4 Kurtosis

The measure of peakedness or kurtosis looks at the spread of the central distribution with respect to the spread of the tails. A normal curve with have a kurtosis value of 1. A bimodal curve is described as platykurtic – when it has two equally and widely separated modes (equal contributions of course and fine modes) or when or a curve with has low, wide peak. While leptokurtic describes a distribution which has an acute peak about the mean

Appendix 3. Full details of Digestion Method

A3.1 Removal of Soluble Salts and Gypsum

The sample was placed in plastic test tube before being suspended in 20ml de-ionised distilled water and thoroughly mixed using a vortex genie for 2 minutes. The sample was then placed in a swing bucket centrifuge for 5 minutes spinning at 1500 rpm. The supernatant fluid was poured off and the process repeated 6 times upon which a sample of the supernatant was tested with an equal volume of acetone. The absence of a white precipitate indicated that there was no gypsum present in the solution.

The sample was decanted into pre-labelled and weighed glass test tubes. The test tube was rinsed with distilled de-ionised water to ensure all precipitate was transferred from the plastic test tube into the glass. The glass test tube was then transferred to an oven set at 80°C for 12-18 hours until sample was dry and desiccated. The warm sample was weighed to determine mass loss.

A3.2 Removal of Carbonates

The method of HCl was used as no soluble salts were proposed to be present following the first stage of digestion and therefore the caution of Kunze and Dixon (1986) in which HCl may remove soluble salts was not of concern. The use of HCl is further discussed as effective in Shang and Zelaszy (2008).

The sample was then decanted using de-ionsed distilled water back into their original plastic test tube. The sample was topped up to 20 ml with distilled water and thoroughly mixed for 2 minutes using the vortex genie. Samples were then placed in a water bath set to 40°C with the sample and solution submerged.

To this, 5ml of 15% HCl was then added and the temperature increased to 70°C at a rate of 10°C per 10 minutes. The samples were left at 70°C for 30 minutes to ensure as much reaction took place at the higher temperature. The samples were then centrifuged for 5 minutes at 1500 rpm. The supernatant was decanted, neutralised and discarded.

The sample was then replaced in the water bath (at 70°C) and the samples were topped up with de-ionsed distilled water to 10 ml before being treated with 15 ml of 15% HCl, centrifuged and decanted a further two times. Confirmation that all reaction had occurred was tested using three drops of 30% HCl which produced no effervescence and therefore all carbonates were assumed to have been removed.

The sample was decanted into pre-labelled and weighed glass test tubes. The test tube was rinsed with distilled de-ionised water to ensure all precipitate was transferred from the plastic test tube into the glass. The glass test tube was then transferred to an oven set at 80°C for 12-18 hours until sample was dry and desiccated. The warm sample was weighed to determine mass loss.

A3.3 Removal of Organics

The final stage involved the removal of organics (*Figure A* 3.1); the sample was again decanted using de-ionsed distilled water back into their original plastic test tube. The sample was topped up to 20 ml with distilled water and thoroughly mixed for 2 minutes using the vortex genie. The sample was then placed in a water bath set to 30°C with the sample and solution submerged.

Five millilitres of 30% H_2O_2 was then added 1ml at a time to the sample to ensure the sample did not react too violently, when the frothing has stopped the next ml increment was added. Once all 5ml had been added, the temperature was then increased to 60°C at a rate of 10°C per 10 minutes. The samples were left at 60°C for 30 minutes to ensure maximum reaction. The sample was then centrifuged for 5 minutes at 1500 rpm. The supernatant was decanted, neutralised and discarded.

The sample was replaced in the water bath (at 60°C) and the sample was topped up with de-ionsed distilled water to 10 ml before being treated with 25 ml of H_2O_2, centrifuged and decanted a further two times. Confirmation that all reaction had occurred was tested using three drops of 40% H_2O_2 which produced no effervescence and therefore all organics were assumed to have been removed.

The sample was decanted into pre-labelled and weighed glass test tubes. The test tube was rinsed with distilled de-ionised water to ensure all precipitate was transferred from the plastic test tube into the glass. The glass test tube was then transferred to an oven set at 80°C for 12-18 hours until sample was dry and desiccated. The warm sample was weighed to determine mass loss. This value represented the final mass loss associated with removal of the soluble salts, carbonates and organics.

Figure A 3.1 Pre-labelled and weighted glass test tubes with samples following the loss of organics in preparation for drying.

Appendix 4. Results of Grain Size for Undigested Samples run in Ethanol Determined by Laser Diffraction

A4.1 Full Results of Crust Samples:

Table A 4.1 Results of laser diffraction for all undigested, ethanol run crust samples analysed. Results indicate the contribution of the sample to the various grain sizes as defined by Blott and Pye (2001) using the Folk and Ward method as well as statistical descriptors derived through the geometric methods.

Sample ID	B3C	B7C	D2C	D5C	D10C	G2C	G6C	I4C	I8C	J3C	J11C	L5C
Grain size	% Contribution to each grain size range											
clay	1.47	0.89	0.74	0.77	0.64	0.10	0.61	0.30	0.03	0.81	0.57	0.26
very fine silt	2.16	1.12	1.12	1.19	1.06	0.48	1.03	0.74	0.25	1.67	1.01	0.92
fine silt	3.44	1.93	1.77	1.94	1.73	0.78	1.70	1.14	0.64	2.57	1.69	1.40
medium silt	5.16	3.88	3.22	3.25	2.92	1.23	2.82	1.91	1.28	3.56	2.90	2.07
coarse silt	8.40	7.53	6.77	5.60	5.64	2.25	4.38	3.70	1.90	5.36	4.23	3.69
very coarse silt	11.14	11.53	11.05	8.12	9.58	3.48	7.99	7.98	2.53	7.53	5.96	7.29
very fine sand	11.97	11.88	14.32	10.75	12.78	4.89	13.55	16.55	4.60	9.68	8.68	15.16
fine sand	11.90	7.88	13.48	10.06	12.94	5.45	18.63	23.29	6.92	11.47	12.65	21.70
medium sand	11.79	2.69	11.48	13.76	10.58	3.09	22.06	23.75	10.05	15.67	19.30	24.96
coarse sand	15.91	7.78	17.30	29.88	19.17	30.58	12.26	14.44	30.08	22.70	18.85	20.69
very coarse sand	16.66	42.88	18.75	14.68	22.96	47.66	14.96	6.21	41.72	19.00	24.16	1.87
	Statistical Description											
Mean	160.0	324.0	206.7	257.0	248.8	632.3	230.0	199.8	642.2	246.8	308.3	206.8
Sorting	6.2	5.7	5.0	4.6	4.9	3.2	4.3	3.2	2.9	5.2	4.5	3.2
Skewness	-0.2	-0.6	-0.1	-0.5	-0.2	-0.6	-0.1	-0.1	-0.5	-0.4	-0.3	-0.2
description	Fine Skewed	Very Fine Skewed	Fine Skewed	Very Fine Skewed	Fine Skewed	Very Fine Skewed	Fine Skewed	Fine Skewed	Very Fine Skewed	Very Fine Skewed	Very Fine Skewed	Fine Skewed
Kurtosis	0.81	0.67	0.81	0.89	0.80	2.07	1.10	1.10	1.41	0.93	0.98	1.04
description	Platykurtic	Platykurtic	Platykurtic	Platykurtic	Platykurtic	Very Leptokurtic	Mesokurtic	Mesokurtic	Leptokurtic	Mesokurtic	Mesokurtic	Mesokurtic

A4.2 Full Results of Fluff Samples:

Table A 4.2 Results of laser diffraction for all undigested, ethanol run fluff samples analysed. Results indicate the contribution of the sample to the various grain sizes as defined by Blott and Pye (2001) using the Folk and Ward method as well as statistical descriptors derived through the geometric methods.

Sample ID	B3F	B7F	D2F	D5F	D10F	G2F	G6F	I4F	I8F	J3F
Grain size	% Contribution to each grain size range									
clay	0.00	0.62	0.00	0.60	0.08	0.00	0.29	0.00	0.16	0.00
very fine silt	0.18	0.75	0.25	1.09	0.49	0.26	0.82	0.29	0.61	0.20
fine silt	0.51	1.27	0.53	1.66	0.87	0.57	1.41	0.54	1.06	0.40
medium silt	1.20	2.81	0.12	2.61	1.77	1.06	2.39	0.95	1.79	0.62
coarse silt	3.89	7.48	0.00	4.90	4.76	2.51	4.34	2.10	2.76	1.03
very coarse silt	9.96	15.12	0.00	7.83	10.79	6.82	7.80	7.43	3.90	2.14
very fine sand	17.37	21.29	6.87	10.60	17.94	17.84	13.93	20.72	7.07	5.20
fine sand	18.31	22.19	31.04	11.26	22.37	28.54	20.69	30.91	14.19	14.38
medium sand	14.24	19.30	36.59	12.78	19.51	25.75	19.91	21.58	26.76	23.59
coarse sand	19.18	9.05	22.89	26.78	13.44	14.04	17.50	9.11	30.29	26.04
very coarse sand	15.15	0.13	1.72	19.89	7.97	2.61	10.92	6.37	11.41	26.39
	Statistical Description									
Mean	243.72	121.99	307.86	289.77	187.43	204.61	223.49	191.76	345.95	500.21
Sorting	3.60	3.16	1.89	4.48	3.41	2.57	3.78	2.65	3.07	2.63
Skewness	-0.01	-0.11	-0.01	-0.44	-0.04	-0.09	-0.14	0.04	-0.36	-0.19
description	Symmetrical	Fine Skewed	Symmetrical	Very Fine Skewed	Symmetrical	Symmetrical	Fine Skewed	Symmetrical	Very Fine Skewed	Fine Skewed
Kurtosis	0.79	0.95	0.86	0.89	0.99	1.03	1.03	1.17	1.26	0.94
description	Platykurtic	Mesokurtic	Platykurtic	Platykurtic	Mesokurtic	Mesokurtic	Mesokurtic	Leptokurtic	Leptokurtic	Mesokurtic

A4.3 Full Results of Second Crust Samples:

Table A 4.3 Results of laser diffraction for all undigested, ethanol run second crust samples analysed. Results indicate the contribution of the sample to the various grain sizes as defined by Blott and Pye (2001) using the Folk and Ward method as well as statistical descriptors derived through the geometric methods.

Sample ID	D2H	D5H	D10H	G2H	I4H	I8H	J11H
Grain size	% Contribution to each grain size range						
clay	0.00	0.78	0.35	0.46	0.74	0.00	0.28
very fine silt	0.22	1.12	0.70	0.88	1.07	0.07	0.59
fine silt	0.40	1.53	1.12	1.36	1.59	0.19	0.95
medium silt	0.88	2.57	1.87	2.35	2.84	0.41	1.68
coarse silt	2.51	5.32	3.84	4.49	5.71	1.01	3.25
very coarse silt	5.98	10.52	7.39	8.09	11.28	2.07	6.47
very fine sand	10.35	18.62	12.30	12.65	19.43	3.96	12.41
fine sand	14.96	24.59	14.37	14.75	31.69	6.78	18.06
medium sand	18.86	17.21	12.53	16.07	19.59	5.57	23.55
coarse sand	22.69	7.89	20.98	20.18	5.38	27.46	20.80
very coarse sand	23.14	9.85	24.56	18.73	0.68	52.48	11.97
	Statistical Description						
Mean	369.95	162.77	316.79	267.15	125.54	787.87	268.93
Sorting	3.36	3.85	4.09	4.24	2.94	2.45	3.42
Skewness	-0.24	-0.06	-0.28	-0.23	-0.30	-0.55	-0.21
description	Fine Skewed	Symmetrical	Fine Skewed	Fine Skewed	Fine Skewed	Very Fine Skewed	Fine Skewed
Kurtosis	0.88	1.23	0.83	0.89	1.18	1.64	1.04
description	Platykurtic	Leptokurtic	Platykurtic	Platykurtic	Leptokurtic	Very Leptokurtic	Mesokurtic

A4.4 Full Results of Soil Samples:

Table A 4.4 Results of laser diffraction for all undigested, ethanol run soil samples analysed. Results indicate the contribution of the sample to the various grain sizes as defined by Blott and Pye (2001) using the Folk and Ward method as well as statistical descriptors derived through the geometric methods.

Sample ID	B3S	B7S	D2S	D5S	D10S	G2S	G6S	I4S	I8S	J3S	J11S	L5S
Grain size	% Contribution to each grain size range											
clay	0.59	0.64	0.24	0.39	0.74	0.78	0.45	0.68	0.48	1.24	0.93	0.76
very fine silt	1.56	1.24	0.64	1.03	1.35	1.51	1.28	1.43	1.32	2.50	1.82	1.72
fine silt	2.45	1.99	1.05	1.52	2.02	2.38	1.87	2.18	1.96	3.44	2.64	2.45
medium silt	3.93	3.73	1.62	2.32	3.40	3.98	2.84	3.39	2.75	4.59	4.11	3.52
coarse silt	7.52	8.67	3.63	4.35	8.01	9.60	4.88	6.11	4.34	7.51	6.98	6.51
very coarse silt	14.06	15.36	7.11	7.57	13.82	17.85	7.68	10.58	6.80	11.53	9.56	10.46
very fine sand	20.11	17.85	9.50	11.70	15.48	20.07	10.64	15.74	10.54	15.52	11.75	14.70
fine sand	20.30	16.56	12.07	12.16	15.42	23.41	14.44	21.00	14.53	15.24	11.49	15.55
medium sand	22.20	19.88	14.68	11.86	23.36	18.82	33.48	24.80	22.94	12.30	16.52	18.02
coarse sand	7.26	7.58	21.20	25.32	15.37	1.59	22.24	13.26	25.30	21.04	26.18	17.65
very coarse sand	0.00	6.51	28.26	21.78	1.03	0.00	0.19	0.85	9.04	5.11	8.02	8.67
	Statistical Description											
Mean	113.51	122.05	358.73	306.92	137.50	92.44	201.28	146.21	241.21	134.75	183.65	167.85
Sorting	3.51	4.04	4.02	4.30	3.82	3.20	3.44	3.64	3.98	5.17	4.88	4.61
Skewness	-0.20	-0.06	-0.37	-0.40	-0.23	-0.20	-0.52	-0.30	-0.38	-0.17	-0.37	-0.20
description	Fine Skewed	Symmetrical	Very Fine Skewed	Very Fine Skewed	Fine Skewed	Fine Skewed	Very Fine Skewed	Fine Skewed	Very Fine Skewed	Fine Skewed	Very Fine Skewed	Fine Skewed
Kurtosis	0.98	0.99	0.86	0.87	0.86	0.95	1.04	1.03	1.06	0.89	0.87	0.96
description	Mesokurtic	Mesokurtic	Platykurtic	Platykurtic	Platykurtic	Mesokurtic	Mesokurtic	Mesokurtic	Mesokurtic	Platykurtic	Platykurtic	Mesokurtic

Appendix 5. Results of Grain Size for Digested Samples run in Water determined by Laser Diffraction

A5.1 Full Results of Crust Samples:

Table A 5.1 Results of laser diffraction for all digested, water run crust samples analysed. Results indicate the contribution of the sample to the various grain sizes as defined by Blott and Pye (2001) using the Folk and Ward method as well as statistical descriptors derived through the geometric methods.

Sample ID	B3C	B7C	D2C	D5C	D10C	G2C	G6C	I4C	I8C	J3C	J11C
Grain size	% Contribution to each grain size range										
clay	5.97	5.90	2.93	5.57	3.84	2.50	5.08	4.32	5.35	4.21	4.02
very fine silt	7.68	8.07	4.68	7.51	5.69	3.44	7.22	6.41	8.57	5.98	6.50
fine silt	10.75	11.02	6.38	9.37	7.91	4.57	9.80	8.64	11.90	7.02	9.21
medium silt	15.76	13.58	6.67	11.11	9.85	6.05	13.50	10.48	14.85	7.04	11.32
coarse silt	20.30	15.78	5.30	11.81	9.51	7.63	14.82	9.65	15.41	6.60	11.05
very coarse silt	15.11	17.56	3.69	10.55	6.67	7.58	9.83	6.22	10.38	6.45	7.99
very fine sand	8.31	14.84	5.87	8.69	6.55	7.03	5.88	5.64	6.21	8.26	6.32
fine sand	5.02	7.21	10.74	7.81	6.38	7.70	4.58	7.13	5.82	11.05	4.50
medium sand	6.93	4.76	22.63	11.59	6.42	22.82	7.98	17.90	7.17	25.40	12.24
coarse sand	4.14	1.27	26.57	12.27	18.80	27.33	13.37	19.39	8.04	17.95	21.61
very coarse sand	0.04	0.00	4.52	3.72	18.39	3.35	7.95	4.22	6.32	0.03	5.24
	Statistical Description										
Mean	23.42	23.18	125.45	46.80	97.74	144.00	47.30	73.86	35.65	85.96	63.68
Sorting	5.34	4.78	7.12	8.13	9.44	6.13	8.91	8.02	8.27	7.08	8.27
Skewness	0.08	-0.08	-0.59	0.03	-0.19	-0.58	0.21	-0.26	0.24	-0.50	-0.03
description	Symmetrical	Symmetrical	Very Fine Skewed	Symmetrical	Fine Skewed	Very Fine Skewed	Coarse Skewed	Fine Skewed	Coarse Skewed	Very Fine Skewed	Symmetrical
Kurtosis	1.14	0.95	0.79	0.73	0.65	0.82	0.70	0.67	0.84	0.73	0.65
description	Leptokurtic	Mesokurtic	Platykurtic	Platykurtic	Very Platykurtic	Platykurtic	Platykurtic	Very Platykurtic	Platykurtic	Platykurtic	Very Platykurtic

A5.2 Full Results of Fluff Samples:

Table A 5.2 Results of laser diffraction for all digested, water run fluff samples analysed. Results indicate the contribution of the sample to the various grain sizes as defined by Blott and Pye (2001) using the Folk and Ward method as well as statistical descriptors derived through the geometric methods.

Sample ID	B3F	B7F	D2F	D5F	D10F	G2F	G6F	I4F	J3F
Grain size	% Contribution to each grain size range								
clay	3.75	4.33	5.40	4.53	5.17	6.04	5.51	8.57	5.85
very fine silt	5.29	5.37	7.54	6.37	6.81	8.66	7.62	13.09	9.14
fine silt	7.03	7.33	9.97	8.06	8.70	11.41	10.53	19.65	11.26
medium silt	8.15	10.69	11.39	8.70	9.90	13.22	13.45	25.69	10.59
coarse silt	9.69	16.97	12.36	7.46	11.25	14.01	13.43	22.44	8.75
very coarse silt	11.01	18.03	10.95	5.69	11.82	11.68	9.21	9.37	6.38
very fine sand	10.74	10.96	9.69	5.71	10.89	7.35	4.49	1.17	4.40
fine sand	10.98	4.82	8.29	6.17	7.99	4.74	2.11	0.02	1.53
medium sand	17.52	5.04	11.18	12.63	12.52	6.54	2.47	0.00	18.16
coarse sand	13.73	9.75	9.71	17.31	13.33	10.06	7.86	0.00	23.75
very coarse sand	2.11	6.72	3.51	17.36	1.60	6.29	23.33	0.00	0.20
	Statistical Description								
Mean	69.14	52.09	43.07	107.30	50.81	38.63	56.29	9.15	49.42
Sorting	6.82	7.53	7.75	9.91	7.62	8.81	11.11	2.84	8.62
Skewness	-0.20	0.15	0.05	-0.35	-0.04	0.20	0.25	-0.14	-0.05
description	Fine Skewed	Coarse Skewed	Symmetrical	Very Fine Skewed	Symmetrical	Coarse Skewed	Coarse Skewed	Fine Skewed	Symmetrical
Kurtosis	0.77	1.08	0.77	0.67	0.74	0.82	0.59	0.94	0.59
description	Platykurtic	Mesokurtic	Platykurtic	Very Platykurtic	Platykurtic	Platykurtic	Very Platykurtic	Mesokurtic	Very Platykurtic

A5.3 Full Results of Second Crust Samples:

Table A 5.3 Results of laser diffraction for all digested, water run second crust samples analysed. Results indicate the contribution of the sample to the various grain sizes as defined by Blott and Pye (2001) using the Folk and Ward method as well as statistical descriptors derived through the geometric methods.

Sample ID	D2H	D5H	D10H	G2H	I4H	I8H	J11H
Grain size	% Contribution to each grain size range						
clay	4.55	4.72	0.84	4.32	4.61	8.64	5.08
very fine silt	6.83	7.66	1.47	6.97	6.82	12.88	7.41
fine silt	8.77	9.98	1.90	9.24	8.24	16.03	10.47
medium silt	8.77	10.13	2.11	9.74	8.27	16.29	14.14
coarse silt	7.26	7.88	2.25	8.87	7.13	13.23	14.99
very coarse silt	5.50	5.24	1.67	7.00	5.51	8.05	10.94
very fine sand	6.16	4.95	1.71	5.95	3.75	4.73	7.85
fine sand	8.58	5.22	1.86	7.45	3.78	3.69	6.19
medium sand	22.06	10.56	1.32	22.31	11.72	7.82	10.83
coarse sand	19.97	16.13	38.39	17.91	20.21	8.30	11.19
very coarse sand	1.55	17.53	46.48	0.24	19.95	0.34	0.90
	Statistical Description						
Mean	79.63	85.14	897.30	65.99	124.43	21.90	38.70
Sorting	7.84	10.44	2.80	7.53	10.29	7.71	7.35
Skewness	-0.44	-0.19	-0.49	-0.28	-0.49	0.31	0.16
description	Very Fine Skewed	Fine Skewed	Very Fine Skewed	Fine Skewed	Very Fine Skewed	Very Coarse Skewed	Coarse Skewed
Kurtosis	0.66	0.62	3.46	0.65	0.64	0.96	0.77
description	Very Platykurtic	Very Platykurtic	Extremely Leptokurtic	Very Platykurtic	Very Platykurtic	Mesokurtic	Platykurtic

A5.4 Full Results of Soil Samples:

Table A 5.4 Results of laser diffraction for all digested, water run soil samples analysed. Results indicate the contribution of the sample to the various grain sizes as defined by Blott and Pye (2001) using the Folk and Ward method as well as statistical descriptors derived through the geometric methods.

Sample ID	B3S	B7S	D2S	D5S	D10S	G2S	G6S	I4S	I8S	J3S	J11S	L5S
Grain size	% Contribution to each grain size range											
clay	4.33	3.65	4.14	5.83	1.66	3.65	3.68	4.35	5.69	4.54	6.50	3.27
very fine silt	5.95	4.75	5.52	7.71	2.50	4.94	5.16	6.10	8.01	6.74	9.60	4.91
fine silt	8.40	6.86	7.51	10.45	3.41	7.07	6.98	8.53	10.25	7.70	12.34	6.11
medium silt	11.61	11.09	9.77	13.87	4.20	9.53	8.61	11.08	11.77	7.06	13.55	6.49
coarse silt	15.86	19.98	14.18	16.63	5.07	15.89	9.89	13.82	11.98	6.94	13.34	6.85
very coarse silt	18.94	25.13	17.55	16.18	5.14	22.50	10.32	17.07	10.66	6.75	11.57	6.29
very fine sand	15.67	16.23	13.11	11.84	4.68	13.99	9.07	13.78	7.76	6.10	8.14	6.59
fine sand	7.33	5.47	8.78	5.92	3.05	3.86	6.17	6.85	4.83	1.72	3.53	7.71
medium sand	7.80	3.94	12.56	6.61	8.38	7.95	14.76	10.41	9.79	19.96	8.51	23.77
coarse sand	4.11	2.74	6.88	4.48	33.96	10.51	19.82	7.89	14.50	31.77	10.40	25.65
very coarse sand	0.00	0.16	0.00	0.47	27.94	0.12	5.55	0.12	4.77	0.72	2.52	2.36
	Statistical Description											
Mean	33.32	30.64	46.12	25.94	286.62	49.36	78.56	42.78	45.83	107.63	33.64	118.46
Sorting	5.05	3.96	5.94	5.53	6.30	6.02	7.59	6.21	8.70	7.98	8.19	6.95
Skewness	-0.06	-0.10	-0.03	0.02	-0.68	0.06	-0.15	0.00	0.10	-0.70	0.19	-0.60
description	Symmetrical	Fine Skewed	Symmetrical	Symmetrical	Very Fine Skewed	Symmetrical	Fine Skewed	Symmetrical	Coarse Skewed	Very Fine Skewed	Coarse Skewed	Very Fine Skewed
Kurtosis	1.07	1.30	0.92	1.03	1.01	1.21	0.72	0.96	0.68	0.66	0.86	0.77
description	Mesokurtic	Leptokurtic	Mesokurtic	Mesokurtic	Mesokurtic	Leptokurtic	Platykurtic	Mesokurtic	Platykurtic	Very Platykurtic	Platykurtic	Platykurtic

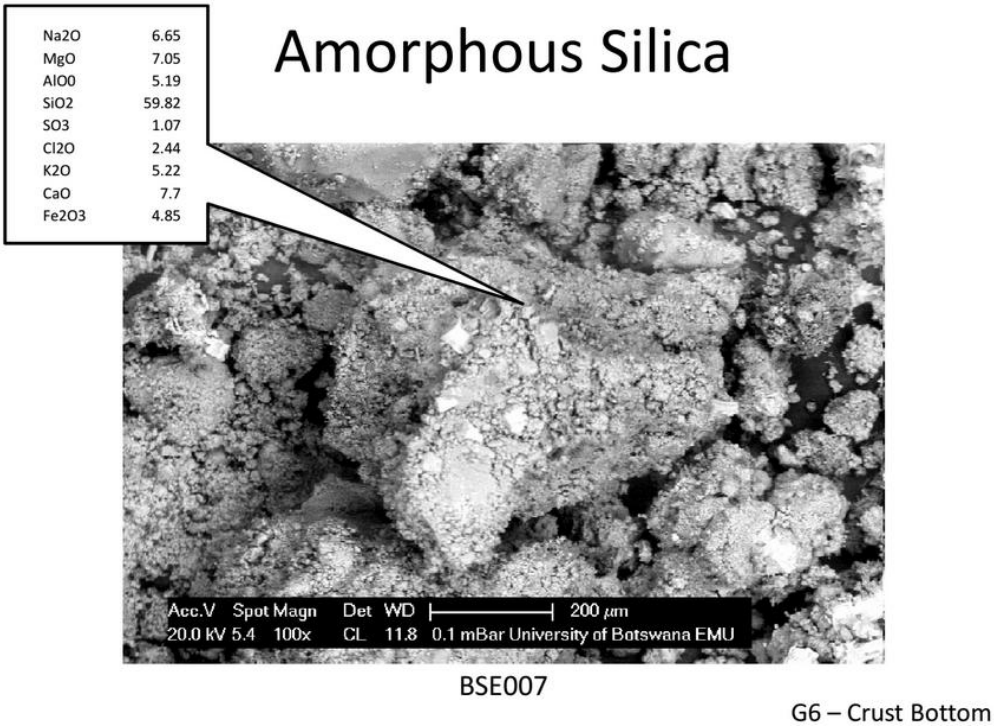

Figure A 6.1 Amorphous silica as identified through SEM analysis performed at the University of Botswana. The sample taken from the underside of a crust sampled from G6 during the 2011 field season.

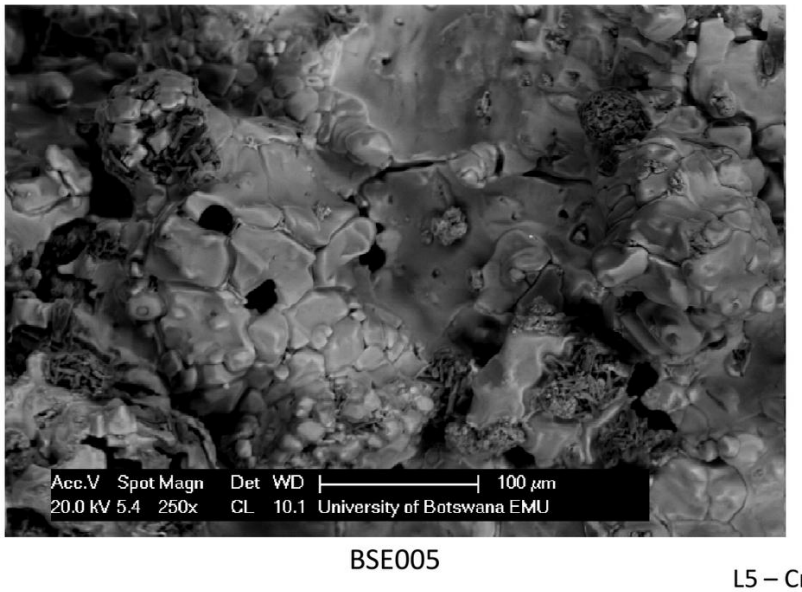

Figure A 6.2 Halite and trona formed on silica balls, image confirms trends observed through QEMSCAN analysis of a high association between these three minerals. Figure 7.3 in the appendix confirms this trend. This image was taken of a sample from the crust at L5, representing the top of the crust,

Appendix 7. QEMSCAN Method

A7.1 Laboratory Procedure:

Approximately 0.1 g of sample was split using a rotary microriffler and premade QEMSCAN disc labelled. The discs were covered on one side with a layer of double sided tape while labels were placed on the other side. Three discs were prepared per size fraction (*Figure A 7.1*) they were labelled A, B, and C.

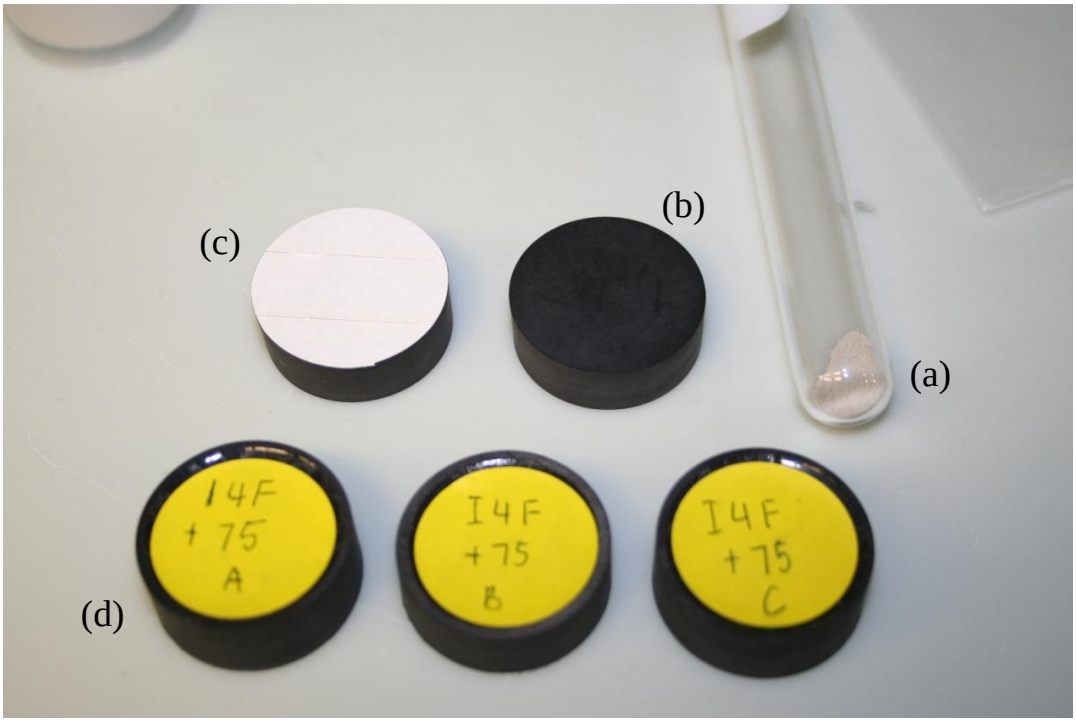

Figure A 7.1 QEMSCAN preparation, (a) shows the approximately 0.1 g of the I4F 75 µm to 106 µm sample, (b) shows the disc before the layer of double sided tape is added. While in (b) the layer of tape can be seen, (d) shows the labels on the three discs prepared for each size fraction of each sample.

The 0.1 g of sample was then carefully sieved – using a screen one size greater than the sample being used - over the exposed sticky disc ensuring a total coverage (Figure A 7.2).

Figure A 7.2 (a) screening the sample onto the disc, (b) insufficient coverage, (c) total coverage of disc before mechanical removal using compressed air.

The remaining sample was captured and the re-sieved over the second disc for that size fraction. Once all particles were assumed to be representatively affixed to the sticky disc, poorly adhered particles were mechanically removed using compressed air. The resultant single layer of sample on the disc was then places in a sample jar to ensure to airborne contaminants do not land on the disc. The discs were then coated with a thin layer of graphite pre-analysis.

The discs are places in a 40°C oven before being run to ensure that ambient moisture is not drawn onto the samples.

A7.2 Machine Conditions:

The discs are placed in the QEMSCAN machine and the vacuum set up – the machine is then calibrated to a Faraday cup, a quartz grain and a gold standard to calibrate the machine. The beam returns to the faraday cup every 30 minutes to ensure calibration remains consistent. 3000 grains per disc were counted, resulting in 9000 grains for each size fraction. Only full grains were counted starting from the centre of each disc working concentrically outwards.

A7.3 QEMSCAN Post Processing:

A comprehensive 255 mineral list was created; specific minerals identified through XRD and from existing mineralogical studies in southern and central Africa were added. In identifying minerals, a pre-selected threshold level for elemental ratios were set, grains were then classified as belonging to one of the set minerals or classed as other if no elemental ratio condition was met.

In addition to elemental and mineralogical classification, QEMSCAN permits for the analysis of morphology through a number of measurement based queries. In this study the following three morphological classifications were considered:

A7.3.1 Area

This was calculated using the diameter of a circle with the same area. This morphological classification assumed a high degree of sphericity for the sample, using only one measurement. This was not considered to be representative of conditions and therefore not further analysed.

A7.3.2 Aspect Ratio

Aspect ratio is calculated using the smallest length divided by the largest length (perpendicular to it). The numbers vary between 0 and 1, with things closest to 0 being long and thin, getting rounder or more equal towards 1.

A7.3.3 Shape

Shape Factor was used to determine shape using the grain perimeter squared, divided by the grain area. Values were determined relative to a perfect circle (and sphere) which has a value 12.56 or 4π, therefore a grain with a shape factor <15 was termed well-rounded, 15-16 as rounded, 16-17 as subrounded, 17-18 as subangular, 18-19 as angular, and >19 as very angular, with these values corresponding to classes as per those considered by Powers (1953).

In addition to these selected morphological classification of the sediments, the mineral associations of grains were considered.

A7.3.4 Mineral Association

The QEMSCAN software analyses each grain counting at a predetermined distance, isolating the elemental ratio at each step. Following the attribution of mineralogy from elemental ratio, grains can be analysed to determine the number of minerals present on each grain. The boundaries between minerals are counted with the resultant classification representing mineral associations. Minerals with low counts of associations are relatively pure grains, while minerals with high counts suggest the minerals form composite grains with other minerals.

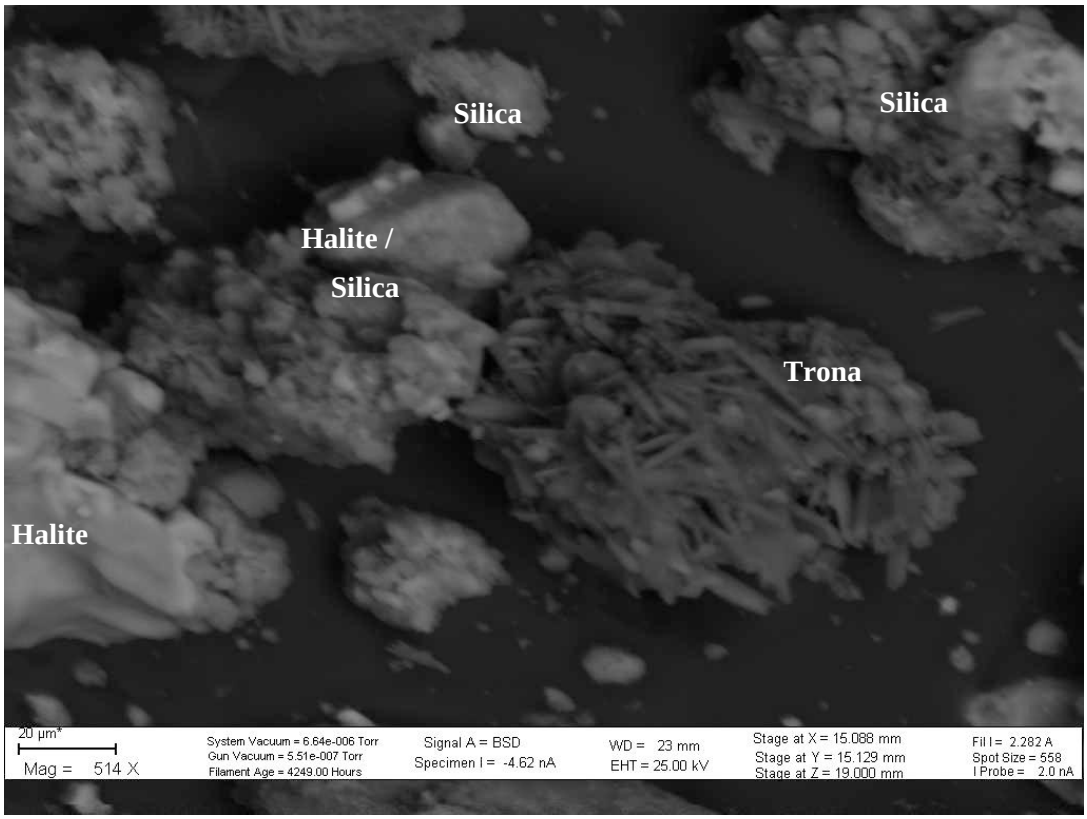

Figure A 7.3 Screen capture from a QEMSCAN visualisation of SD200 looking at the 75-106 µm size fraction on disk A. Needlelike trona can be clearly seen as a largely single grain, while halite/silica grains and further silica populate the remainder of this image.

Appendix 8. Explanation of Synoptic States

All states are described as per Preston-Whyte and Tyson (2000) with the exception of Tropical Temperate Troughs which are described by Todd and Washington (1999).

A8.1 Coastal lows

Coastal lows occur frequently along the South African coast. Coastal low travel along the coast of southern Africa and are marked by change in both wind direction and speed. The lows are generated by cyclonic vorticity with eastward movement of air off the high interior plateau. Occasionally, coastal lows are associated with an increase in wind speed, which may cause damage to property and are potentially hazardous to aviation and shipping. Coastal lows are commonly associated with a berg winds which may be associated with pre-frontal divergence and further warming of offshore moving air. Current global scale numerical weather prediction models do not forecast the intensity of these mesoscale systems well. These systems are largely confined to coastal regions, rarely extending onto the plateau. As such their influence on climatic conditions in the interior and further north is more a result of perturbations to interior circulation. Occurrence of the system peaks from August to December.

A8.2 Continental Anticyclone

The continental anticyclone is associated with fine and mildly disturbed conditions over much of the sub-continent. The deep systems are characterised by strong subsidence and near surface divergence. Such conditions produce largely fine weather with little rainfall. Anticyclones reach a maximum frequency over the interior in June and July, rarely occurring during December. During June and July the system may dominate for extended periods, often lasting up to a week resulting in severe heat waves. While the system is dominated by subsidence, rare occurrences of upward motion to occur although this is largely localised within the system creating variable weather.

A8.3 Cut off low

Cut off lows are forms of the westerly trough, forming through the intensification and deepening of these troughs, which develop into a closed circulation. Cut off lows are associated with strong convergence extending higher than the 500 hPa surface. The systems are frequently linked with flood producing rains typically occurring between March and May and then again between September and November.

A8.4 Easterly Wave and Low

The easterly wave low is proposed to originate through instability in the African easterly jet. The waves are semi-stationary, have a typical period of 3 to 4 days are associated with the Inter-Tropical Convergence Zone (ITCZ). The warm, humid easterly winds are confined between the ITCZ and the

sub-tropical high pressure belt. Low level convergence associated with upper air divergence results in strong uplift and sustained rainfall in the absence of pronounced instability.

The easterly low is associated with surface convergence occurs to the east of the low with divergence in the upper troposphere. Both the easterly wave and the easterly low are associated with rainfall and northerly airflow, and occur throughout the year although peak during the summer months between December and February. The occurrence and frequency of these systems are considered to control summer rainfall and can be used to distinguish abnormally wet years from dry years.

A8.5 Ridging Anticyclone

The ridging anticyclone associated with a westerly wave in the upper atmosphere. The system is commonly associated with widespread rainfall over the eastern parts of southern Africa as warm moist air is advected from the Indian Ocean inland. Orographic uplift can bring further rain to the eastern region in response to the ridging anti-cyclone and the steep pressure gradients promoting the transport of moist unstable air. While the anti-cyclone brings rain to the east; clear, fine and hot weather to the west often accompanied by strong south easterly winds. These conditions are most common during December and February, although can occur from October to May.

A8.6 Tropical Temperate Trough

The composite tropical temperate trough feature which was described in depth by Todd and Washington (1998 and 1999). Tropical-temperate troughs, link tropical convection in the easterlies with transient zonal westerlies and have been shown to be important rainfall producing systems for southern African summer rainfall. The joining of the two systems is relatively infrequent although occur during the summer months of November to March, exhibiting marked inter-annual variability.

A8.7 West Coast Trough

The west coast trough is commonly associated with widespread rain over the western and central parts of southern Africa; with these systems common in early summer and autumn. Surface convergence ahead of the trough produces vertical motion, with the cyclonic disturbance following a south easterly trajectory over the continent towards the Indian Ocean. They are associated with periods of active tropical convection, suggesting the easterly convection is integral in their formation.

A8.8 Westerly Wave Low and Trough

The westerly wave low typically has a period of between 2 and 8 days, associated with surface convergence and upper air divergence to the east of the west to east propagating wave. Behind the surface trough cloud and rain are associated with the unstable air. Westerly waves are known to extend into to the interior, extending as far north as the tropics, however the rainfall is rarely experienced on the escarpment. Blocked in their northerly extent by the continental anticyclone in the summer months,

consequently the westerly wave low is typically a winter feature. These fronts frequently link with the equatorial trough, with the eastward movement of these systems affecting circulation over the interior. In front of the front, north easterly flow changes to southerly as the wave passes and the high pressure which lies behind the system covers the sub-continent.

While westerly troughs occur most frequently between October and April, rarely occurring between May and September. They are modulated on a semi-annual showing peak frequencies in early summer and late autumn.